



UNIL | Université de Lausanne

Unicentre

CH-1015 Lausanne

<http://serval.unil.ch>

Year : 2023

Investigating the role of pseudouridine in Drosophila

Stock Michael

Stock Michael, 2023, Investigating the role of pseudouridine in Drosophila

Originally published at : Thesis, University of Lausanne

Posted at the University of Lausanne Open Archive <http://serval.unil.ch>

Document URN : urn:nbn:ch:serval-BIB_8F5FFA2431713

Droits d'auteur

L'Université de Lausanne attire expressément l'attention des utilisateurs sur le fait que tous les documents publiés dans l'Archive SERVAL sont protégés par le droit d'auteur, conformément à la loi fédérale sur le droit d'auteur et les droits voisins (LDA). A ce titre, il est indispensable d'obtenir le consentement préalable de l'auteur et/ou de l'éditeur avant toute utilisation d'une oeuvre ou d'une partie d'une oeuvre ne relevant pas d'une utilisation à des fins personnelles au sens de la LDA (art. 19, al. 1 lettre a). A défaut, tout contrevenant s'expose aux sanctions prévues par cette loi. Nous déclinons toute responsabilité en la matière.

Copyright

The University of Lausanne expressly draws the attention of users to the fact that all documents published in the SERVAL Archive are protected by copyright in accordance with federal law on copyright and similar rights (LDA). Accordingly it is indispensable to obtain prior consent from the author and/or publisher before any use of a work or part of a work for purposes other than personal use within the meaning of LDA (art. 19, para. 1 letter a). Failure to do so will expose offenders to the sanctions laid down by this law. We accept no liability in this respect.



UNIL | Université de Lausanne

Faculté de biologie
et de médecine

Center for Integrative Genomics

Investigating the role of pseudouridine in *Drosophila*

Thèse de doctorat ès sciences de la vie (PhD)

présentée à la

Faculté de biologie et de médecine
de l'Université de Lausanne

par

Michael STOCK

Master en biochimie et biologie moléculaire de l'Université de Bayreuth,
Allemagne

Jury

Prof. Michel Chapuisat, Président
Prof. Jean-Yves Roignant, Directeur de thèse
Prof. Richard Benton, Expert
Prof. Yuri Motorin, Expert

Lausanne, 2023



UNIL | Université de Lausanne

Faculté de biologie
et de médecine

Ecole Doctorale

Doctorat ès sciences de la vie

Imprimatur

Vu le rapport présenté par le jury d'examen, composé de

Président·e	Monsieur	Prof.	Michel	Chapuisat
Directeur·trice de thèse	Monsieur	Prof.	Jean-Yves	Roignant
Expert·e·s	Monsieur	Prof.	Richard	Benton
	Monsieur	Prof.	Yuri	Motorin

le Conseil de Faculté autorise l'impression de la thèse de

Michael Stock

Master of Science in Biochemistry and molecular biology, Universität Bayreuth, Allemagne

intitulée

Investigating the role of pseudouridine in *Drosophila*

Lausanne, le 13 octobre 2023

pour le Doyen
de la Faculté de biologie et de médecine

Prof. Michel Chapuisat

I. Table of Contents

I. Table of Contents	i
II. List of Figures	iii
III. List of Tables	iv
IV. List of Supplementary Figures	iv
V. List of Supplementary Tables	iv
VI. Abbreviations	v
VII. Abstract	viii
VIII. Resumé	ix

1 Introduction	1
1.1 The epitranscriptome as a new regulatory layer in gene expression.	1
1.2 The history of RNA modifications with a focus on Ψ	2
1.3 Transcriptome-wide mapping of RNA modifications reveals novel functions in mRNAs	7
1.4 The knowledge about Ψ gained from 1950-2000	12
1.4.1 Synthesis of Ψ	12
1.4.2 guide-RNA dependent Ψ synthesis	13
1.4.3 Ψ synthesis by standalone synthases	15
1.4.4 Functions of pseudouridine in canonical Ψ sites	20
1.5 Human Ψ synthases with a role in disease	25
1.6 Other indications of Ψ in neuronal function.	29
1.7 Expression of cytoplasmic tRNA genes	30
1.7.1 tRNA transcription and maturation	30
1.7.2 tRNA surveillance mechanisms	32
1.8 The roles of tRNA fragmentation in gene expression	35
1.8.1 Classes of tRNA-derived small RNAs	35
1.8.2 Effects of tRNA fragments on gene expression	36
1.8.3 Effects of tRNA modifications on fragmentation	38
1.9 tRNA expression defects and human disease	39
1.10 The integrated stress response in human disease	43
1.11 Project aim	47
2 Results	48
2.1 Expression patterns of PUS1, PUSL1, PUS3 and PUS7	48
2.2 Characterization of <i>PUS7</i> in <i>Drosophila</i>	49
2.2.1 Evaluation of the <i>PUS7</i> expression pattern	49
2.2.2 Phenotypic characterization of <i>PUS7</i> in <i>Drosophila</i>	50

2.2.3	The role of Pus7 in oogenesis	53
2.2.4	<i>Pus7^{fs}</i> flies lack Pus7 catalytic activity	54
2.2.5	<i>Pus7</i> mutation leads to a reduction of tRNA ^{Asp} levels	57
2.2.6	tRNA ^{Asp} overexpression partially rescues the <i>Pus7^{fs}</i> phenotypes.	58
2.2.7	<i>Pus7</i> mutation leads to translational changes	59
2.2.8	<i>Pus7</i> mutation leads to changes in the metabolome	65
2.2.9	Mitochondrial function is reduced in <i>Pus7^{fs}</i> mutants	67
2.3	PUSL1 mutation in humans causes developmental delay, microcephaly and intellectual disability	70
2.3.1	<i>Drosophila</i> PusL1 is a mitochondrial protein	70
2.3.2	Generation of <i>PusL1</i> mutants in <i>Drosophila</i>	71
2.3.3	Phenotypic characterization of <i>Drosophila PusL1</i>	71
2.3.4	Lack of PusL1 affects activity in <i>Drosophila</i>	73
2.4	Characterization of <i>Pus3</i> in <i>Drosophila</i>	75
2.4.1	<i>Drosophila</i> Pus3 is a cytoplasmic protein	75
2.4.2	Characterization of <i>Pus3</i> phenotypes in <i>Drosophila</i>	76
3	Discussion	81
3.1	Neuronal roles of Ψ synthases	81
3.1.1	Pus mutations as neurodevelopmental diseases	81
3.1.2	The central complex and mushroom body are potentially defective in flies carrying mutations in Pus enzymes	81
3.2	The questionable role of mRNA Ψ sites	83
3.2.1	Challenges in reproducibility	83
3.2.2	Pus7 primarily targets tRNAs	84
3.3	Potential role of Pus7 mRNA Ψ sites in embryogenesis	85
3.4	The Pus7 phenotype is reminiscent of a tRNA disease	86
3.5	Lack of Pus7 causes translational changes	87
3.6	Mitochondrial dysfunction, the glycolytic shift and aggression might be linked in <i>Pus7^{fs}</i> flies	89
3.7	Conclusion	92
	Materials and methods	93
	Contributions	116
	References	118
	Supplementaries	173

II. List of Figures

1	RNA modifications in the three kingdoms of life.	1
2	Detection of bulky modified residues in RNA.	5
3	Chemical structures of RNA modifications characterized in mRNA	7
4	Synthesis of Ψ	13
5	Domain structure and localization of the Pus enzymes.	16
6	Occurrence and functions of Ψ in non-coding and coding RNA.	20
7	Processing and maturation of transfer RNA.	32
8	tRNA surveillance pathways.	33
9	The biogenesis of tsRNAs.	36
10	Mutations in tRNA metabolism cause neurological diseases.	39
11	The integrated stress response.	44
12	Expression patterns of Pus1, PusL1, Pus3 and Pus7.	48
13	<i>Pus7</i> is ubiquitously expressed and localizes to the nucleus.	50
14	<i>Pus7^{fs}</i> mutant flies feature fertility defects, hyperactivity, increased aggression and developmental delay.	52
15	Lack of Pus7 causes ventralization phenotypes in <i>Drosophila</i>	54
16	Pus7 modifies cytoplasmic tRNAs, mRNAs and lncRNAs in <i>Drosophila</i>	56
17	tRNA ^{ASP} is downregulated in <i>Pus7^{fs}</i> mutants.	58
18	tRNA ^{ASP} overexpression partially rescues the <i>Pus7^{fs}</i> phenotypes.	59
19	Lack of Pus7 causes increased ribosome occupancy over aspartate codons <i>in vivo</i>	61
20	Metabolic enzymes are dysregulated in <i>Pus7^{fs}</i> flies.	63
21	Lack of Pus7 leads to a glycolytic shift in <i>Drosophila</i>	67
22	Upregulated glycolysis but not mitochondrial dysfunction causes aggression in <i>Pus7^{fs}</i> flies.	69
23	<i>Drosophila</i> PusL1 localizes to the mitochondria in S2R+ cells.	70
24	Generation of <i>Drosophila PusL1</i> mutants with CRISPR/Cas9.	71
25	A potential role of PusL1 in oxidative stress in mitochondria.	72
26	Flies lacking PusL1 show signs of hyperactivity.	74
27	Pus3 is cytoplasmic in <i>Drosophila</i> S2R+ cells.	75
28	Generation of <i>Drosophila Pus3</i> mutants with CRISPR/Cas9.	76
29	Lack of Pus3 affects the lifespan upon metabolic stress in <i>Drosophila</i>	78
30	<i>Pus3</i> mutation causes reduced activity and developmental delay.	79
31	Regions of the fly brain.	82

III. List of Tables

1.1	Clinical pictures of PUS patients.	28
2.1	Frequency of abnormal embryo phenotypes in <i>Pus7^{fs}</i> flies.	54
2.2	Putative Pus7 substrates in <i>Drosophila</i>	57
2.3	Pus7 mRNA targets in ovaries.	57
2.4	Putative Pus3 substrates in <i>Drosophila</i>	77
4.1	List of gRNAs used for mutagenesis with CRISPR/Cas9.	93
4.2	List of primers used for PCR amplification and sequencing.	93
4.3	List of primers used for qPCR.	93
4.4	List of primers used for generation of T7 PCR templates.	95
4.5	List of oligonucleotides used for site directed mutagenesis.	95
4.6	List of oligonucleotides used for northern blotting.	95
4.7	Probes used for microscale thermophoresis.	95
4.8	List of oligonucleotides used to generate plasmids.	96
4.9	List of plasmids used in this study.	96
4.10	List of antibodies used in this study.	98
4.11	Restriction enzymes used for cloning.	98
4.12	Fly lines used in this study.	99

IV. List of Supplementary Figures

S.1	<i>Pus7</i> expression is affected in <i>EGFP-Pus7</i> and <i>E3R-Pus7</i> flies.	173
S.2	Expression analysis of transgenic Flag-Myc-Pus7 in the <i>Pus7^{fs}</i> background by western blot.	173
S.3	tRNA ^{Asp} is systemically downregulated in <i>Pus7^{fs}</i> males and females.	174
S.4	<i>Pus7</i> knockdown in S2R+ cells is not sufficient to trigger translational defects.	175
S.5	Genes with ribosome pausing sites show higher protein levels in <i>Pus7^{fs}</i>	176
S.6	Potential causes for translational changes in <i>Pus7^{fs}</i> flies.	178
S.7	Amino acids including aspartate are dysregulated in <i>Pus7^{fs}</i> flies.	183

V. List of Supplementary Tables

S.1	Proteins in relevant pathways mentioned in this study.	176
S.2	Dysregulated metabolites in <i>Pus7^{fs}</i> flies.	178
S.3	Protein levels of genes involved in the UPR, JNK, ISR and RQC.	183

VI. Abbreviations

ψ	Pseudouridine
α -KG	α -Ketoglutarate
2-DG	2-Deoxyglucose
2'O-me	2'-O-methylation
A	Adenosine
aaRS	Aminoacyl tRNA synthetase
ac4C	N4-acetylcytidine
ALS	Amyotrophic lateral sclerosis
ANG	Angiogenin
Asp	Aspartate
BS	bisulfite
BSRR	Branch site recognition region
C	Cytosine
cDNA	complementary DNA
circRNA	circular RNA
CMCT	N-cyclohexyl-N'-b-(4-methylmorpholinium) ethylcarbodiimide methyl-p-toluenesulfonate
CMT	Charcot-Marie-Tooth
COXPD	Combined oxidative phosphorylation deficiency
cP	2',3'-Cyclic phosphate
CRC	Colorectal cancer
Cyt c	Cytochrome C
D	Aspartate
DC	Dyskeratosis congenita
DILP	<i>Drosophila</i> insulin-like peptide
DKC1	Dyskerin
EBV-LCL	Epstein-Barr virus transformed lymphoblastoid cell line
EGFP	Enhanced green fluorescent protein
eIF2	Eukaryotic initiation factor
ER	Endoplasmatic reticulum
eRNA	Enhancer RNA
FACS	Fluorescence-activated cell sorting
G	Guanine
GARS	Glycyl-tRNA synthetase gene
GEF	Guanine nucleotide exchange factor
GFP	Green fluorescent protein
Grk	Gurken

GSC	Glioblastoma stem cell
GSEA	Gene set enrichment analysis
heph	Hephaestus
I	Isoleucine
ISR	Integrated stress response
JNK	Jun N-terminal kinase
k	Lysidine
K	Lysine
KO	Knockout
L	Leucine
LC-MS	Liquid chromatography-mass spectrometry
lncRNA	long non-coding RNA
LTR	Long terminal repeat
M	Methionine
m1A	N1-methyladenosine
m1G	N1-methylguanosine
m2G	N2-methylguanosine
m5C	N5-methylcytosine
m5U	N5-methyluridine
m6A	N6-methyladenosine
m6Am	N6,2'-O-dimethyladenosine
mcm5s2U	N5-methoxycarbonylmethyl-2-thiouridine
MD	Multidendritic
miRNA	micro RNA
MLASA	Myopathy, lactic acidosis, and sideroblastic anemia
mRNA	Messenger RNA
MST	Microscale thermophoresis
mt	Mitochondrial
MTD	Met22-dependent RTD
NAD+	nicotinamide adenine dinucleotide
ncRNA	non-coding RNA
NGS	Next-generation-sequencing
Nm	2'-O-methylation
OXPHOS	Oxidative phosphorylation
PERK	PKR-like ER kinase
PH	Pontocerebellar hypoplasia
Pol	RNA polymerase
PPP	Pentose phosphate pathway
PTBP1	Polypyrimidine tract binding protein 1

Pum	PUF RNA-binding protein family
Pus	Pseudouridine synthase
Q	Queuosine
ROS	Reactive Oxygen Species
RQC	Ribosome-associated protein quality control
rRNA	Ribosomal RNA
RT	Reverse transcription
RTD	Rapid tRNA decay
scaRNA	small cajal-body specific RNA
SG	Stress granules
snoRNA	small nucleolar RNA
snRNA	small nuclear RNA
snRNP	Small nuclear ribonucleoprotein
SRA	steroid receptor activator
SRSF3	Serine/arginine-rich splicing factor 3
t6A	N6-threonylcarbamoyladenine
TBP	TATA box binding protein
TCA	Tricarboxylic acid cycle
TE	Translation efficiency
TERC RNA	Telomerase RNA component
TF	Transcription factor
tiRNA	tRNA half
TLC	Thin-layer chromatography
TRAMP	Trf4/Air2/Mtr4 Polyadenylation
tRF	tRNA-derived fragment
tRNA	Transfer RNA
tsRNA	tRNA-derived small RNA
U	Uridine
UPR	Unfolded protein response
UTR	Untranslated region
yW	Wybutosine
yW	Wybutosine

ABSTRACT

Pseudouridine (Ψ) is the most abundant RNA modification and is present in various RNA species including tRNAs, snRNAs, snoRNAs, rRNAs, lncRNAs and more recently in mRNAs. It is synthesized by pseudouridine synthases and is required to stabilize the RNA structure. Patients carrying mutations in different PUS enzymes have been identified in the last decades. In this study, we generated three fly models of diseases caused by mutations in Pus enzymes linked to neurological phenotypes to gain insights into the molecular mechanism of PUS diseases. First, we recently reported about patients harboring deleterious mutations in the *pseudouridine synthase 7* (PUS7) gene, featuring intellectual disability, microcephaly, increased aggression levels and hyperactivity. To gain insight into the underlying mechanisms, we generated a *Drosophila* model carrying loss of function mutations in the *Pus7* fly homolog. The mutants are viable but display behavioral defects including altered orientation, aggressiveness and hyperactivity. We show that the *Pus7* mutation leads to the loss of Ψ at position 13 in several tRNAs, which is associated with reduced level of tRNA^{Asp} and increased ribosome occupancy at Asp codons. Furthermore, multiple metabolic pathways including glycolysis, the leloir pathway, TCA cycle and beta oxidation are dysregulated. Mass-spec analysis of the proteome and metabolome revealed a glycolytic shift in *Pus7^{fs}* mutant flies towards increased levels of glycolysis and reduced TCA cycle activity concomitant with reduced mitochondrial respiration. Overexpression of tRNA^{Asp} completely rescues the mitochondrial dysfunction as well as the aggressive behavior highlighting its importance in the mechanism of disease. Moreover, inhibition of glycolysis is sufficient to rescue the defects in aggression suggesting a causal link between aggression and hyperglycemia. Second, our collaborators have identified patients with mutations in *PUSL1* suffering from microcephaly and developmental delay. Hence, we generated flies mutant for *Drosophila PusL1* which feature reduced lifespan on paraquat indicating a conserved mitochondrial role of PusL1, while mitochondrial respiration is not affected matching the observations made in human patients. Additionally, phenotypic characterizations revealed indications of hyperactivity suggesting neurological defects which require further confirmation. Third, patients with mutations in PUS3 were described to feature microcephaly, developmental delay, intellectual disability and seizures. Thus, we generated flies mutant for the *Drosophila Pus3* homolog. Mapping of Ψ sites confirmed that these flies lack pseudouridine at position 38 and 39 in several tRNAs. Furthermore, survival assays revealed increased lifespan on normal food and during complete starvation while lifespan was reduced in response to amino acid starvation. Moreover, this was corroborated by reduced levels of *Drosophila* insulin like peptides indicating a role of Pus3 in metabolic stress response. Also, *Pus3* mutant flies showed reduced activity and developmental delay, however, seizures could not be reproduced in the *Pus3* fly model. Summed up, we could demonstrate that *Drosophila* constitutes a suitable model to investigate neurological defects observed in human PUS diseases and provide a basis for future research of their pathomechanism. Together, our data provide new insight into the molecular defects associated with the loss of pus enzymes in flies and suggest potential new avenues for therapeutic treatment.

RESUMÉ

La pseudouridine (Ψ) est la modification la plus abondante de l'ARN et est présente dans diverses espèces d'ARN, y compris les ARNt, les ARNs, les ARNsn, les ARNr, les ARNsnc et, plus récemment, les ARNm. Elle est synthétisée par les pseudouridines synthases et est nécessaire pour stabiliser la structure de l'ARN. Des patients porteurs de mutations dans différentes enzymes PUS ont été identifiés au cours des dernières décennies. Dans cette étude, nous avons généré trois modèles de mouches de maladies causées par des mutations dans les enzymes Pus liées à des phénotypes neurologiques afin de mieux comprendre le mécanisme moléculaire des maladies PUS. Tout d'abord, nous avons récemment fait état de patients porteurs de mutations délétères dans le gène de la *pseudouridine synthase 7* (PUS7), présentant une déficience intellectuelle, une microcéphalie, une augmentation de l'agressivité et de l'hyperactivité. Afin de mieux comprendre les mécanismes sous-jacents, nous avons généré un modèle de *drosophile* porteur de mutations dans l'homologue de la mouche *Pus7*. Les mutants sont viables mais présentent des défauts de comportement, notamment une orientation altérée, de l'agressivité et de l'hyperactivité. Nous montrons que la mutation de *Pus7* entraîne la perte de Ψ en position 13 dans plusieurs ARNt, ce qui est associé à un niveau réduit d'ARNt^{ASP} et à une augmentation de l'occupation du ribosome au niveau de l'As et une augmentation de l'occupation des ribosomes au niveau des codons Asp. En outre, plusieurs voies métaboliques, dont la glycolyse, la voie de Leloir, le cycle TCA et la bêta-oxydation sont dérégulées. L'analyse de masse du protéome et du métabolome a révélé un changement glycolytique chez les mouches mutantes *Pus7^{fs}* vers des niveaux accrus de glycolyse et une activité réduite du cycle TCA concomitante à une respiration mitochondriale réduite. La surexpression de tRNA^{ASP} résout complètement le dysfonctionnement mitochondrial ainsi que le comportement agressif, soulignant son importance dans le mécanisme de la maladie. De plus, l'inhibition de la glycolyse est suffisante pour sauver les défauts d'agressivité, ce qui suggère un lien de causalité entre l'agressivité et l'hyperglycémie. Deuxièmement, nos collaborateurs ont identifié des patients présentant des mutations dans *PUSL1* et souffrant de microcéphalie et de retard de développement. Nous avons donc généré des mouches mutantes pour *PusL1* de *drosophile* qui présentent une durée de vie réduite sous paraquat, indiquant un rôle mitochondrial conservé de *PusL1*, alors que la respiration mitochondriale n'est pas affectée, ce qui correspond aux observations faites chez les patients humains. En outre, les caractérisations phénotypiques ont révélé des signes d'hyperactivité suggérant des défauts neurologiques qui doivent être confirmés. Enfin, des patients présentant des mutations dans *PUS3* ont été décrits comme présentant une microcéphalie, un retard de développement, une déficience intellectuelle et des crises d'épilepsie. Nous avons donc généré des mouches mutantes pour l'homologue *Pus3* de *drosophile*. La cartographie des sites Ψ a confirmé que ces mouches manquent de pseudouridine en position 38 et 39 dans plusieurs ARNt. En outre, des tests de survie ont révélé une augmentation de la durée de vie avec de la nourriture normale et pendant une famine complète, tandis que la durée de vie était réduite en réponse à une famine d'acides aminés en réponse à la privation d'acides aminés. En outre, ces résultats ont été corroborés par des niveaux réduits de peptides analogues à l'insuline de la *drosophile*

indiquant un rôle de Pus3 dans la réponse au stress métabolique. En outre, les mouches mutantes *Pus3* ont montré une activité réduite et un retard de développement, mais les crises d'épilepsie n'ont pas pu être reproduites dans le modèle de la mouche *Pus3*. En résumé, nous avons pu démontrer que la *drosophile* constitue un modèle approprié pour étudier les défauts neurologiques observés dans les maladies humaines PUS et fournir une base pour la recherche future sur leur pathomécanisme. L'ensemble de nos données donne un nouvel aperçu des défauts moléculaires associés à la perte des enzymes pus et suggèrent de nouvelles voies potentielles pour le traitement thérapeutique.

Chapter 1: INTRODUCTION

1.1 The epitranscriptome as a new regulatory layer in gene expression.

The field of epitranscriptomics constitutes the study of post-transcriptional modifications of RNA [Saletore et al., 2012]. Similar to post-translational modifications on proteins and DNA-histones, RNA modifications represent an additional dynamic regulatory layer of gene expression [Wolffe and Matzke, 1999]. RNA modifications occur in all kingdoms of life and today more than 170 modifications have been identified which are present on all types of RNA species including non-coding RNA (ncRNA) like ribosomal RNA (rRNA), transfer RNA (tRNA) and small RNA but also messenger RNA (mRNA) [Boccaletto et al., 2022]. Biochemically, RNA modifications comprise different types of chemical modifications of the base or the ribose of an RNA molecule including (de)methylations, acylations and isomerizations among many others. While the synthesis and functions of many RNA modifications are not yet completely understood, their impact on the fate of RNA molecules is

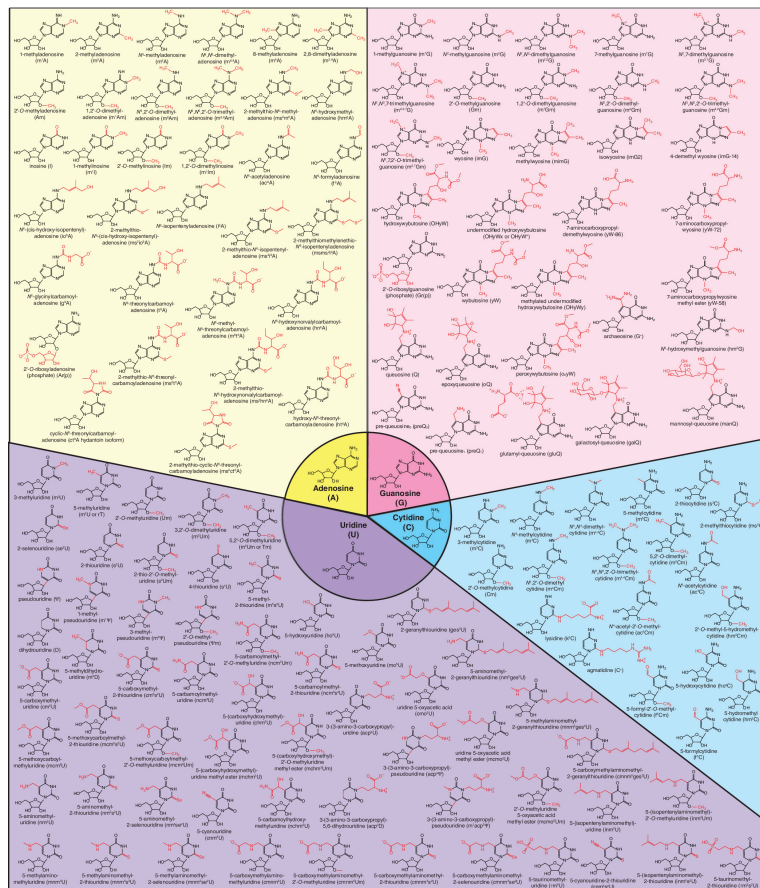


Figure 1: RNA modifications in the three kingdoms of life. Chemical structures of all currently known RNA modifications. Adenosine-derived (yellow), guanosine-derived (pink), uridine-derived (purple), and cytidine-derived (cyan) modifications are classified based on the parent ribonucleoside. Red moieties indicate which portion of the modified ribonucleoside is different from the parent ribonucleoside, whose structures are shown in the central circle. Figure and description from [McCown et al., 2020].

striking as they affect almost all processes of RNA metabolism including splicing and processing [Alarcon et al., 2015, Lence et al., 2016], stability [Shi et al., 2017], structure [Liu et al., 2015], localization [Ma et al., 2018] and translation efficiency [Wang et al., 2015]. After synthesis by dedicated enzymes termed 'writers', these downstream effects are facilitated by the properties of the RNA modification itself or through 'reader' proteins selectively recognizing the modification. Furthermore, 'eraser' proteins have been identified for some RNA modifications which grant them their dynamic and reversible nature [Shi et al., 2019]. As a result, RNA modifications have emerged as a new layer of gene expression greatly increasing the variety of the classical four nucleotides in RNA.

1.2 The history of RNA modifications with a focus on Ψ

The first RNA modification to be identified was pseudouridine (Ψ) which was discovered in 1951 in calf liver [Cohn and Volkin, 1951]. This was facilitated due to its high abundance in total RNA which was estimated to 0.2-0.3% of all nucleotides in yeast RNA [Cohn, 1960]. This led to it being mistakenly labeled as the 'fifth nucleotide' in RNA [Davis and Allen, 1957]. Later, it was correctly identified as 5-ribosyl uracil, an isomer of uridine, and therefore labeled pseudouridine [Cohn, 1960]. Due to technical limitations, the research of RNA modifications at the time was limited to highly abundant RNA modifications in the most abundant RNA species which featured an extensive modification landscape with high modification stoichiometries [Jackman and Alfonzo, 2013, Sloan et al., 2017].

This includes the discovery of 5-methyl cytosine in *E. coli* RNA [Amos and Korn, 1958] and the identification of the first RNA modifying enzyme Trm2 [Fleissner and Borek, 1962] which was later found to catalyze the generation of N5-methyluridine (m5U) on position 54 in the T Ψ loop of almost all tRNAs [Persson et al., 1992]. Shortly after, methylations of the ribose of the four RNA nucleotides (2'-O-methylations or Nm) [Baskin and Dekker, 1967] as well as inosine which is generated by the deamination of adenosine by deaminases were identified in tRNA of *E. coli* [Wagner and Ofengand, 1970]. In fact, already by the end of the 1960s, a plethora of RNA modifications including dihydrouridine, acetylations, isopentenylation of adenosine and thiolations have been discovered in tRNA [Madison, 1968].

The early studies in the field of RNA epigenetics relied mainly on two methods to quantify modification content in non-coding RNA. On the one hand, chromatography-based techniques were used to distinguish nucleotides based on their chemical and physical properties. On the other hand, radioactive labeling of newly synthesized RNA served as an alternative to quantify RNA modifications. This technique was utilized to determine the Ψ content in rRNA of *E. coli* which was estimated to 1.2-3% in the different rRNA fractions [Dubin and Günalp, 1967]. These studies were made possible by the discovery and isolation of a Ψ synthase in extracts of *Agrobacterium tumefaciens* which allowed generation of the labeled nucleotides [Suzuki and Hochster, 1966].

Early evidence for a role of RNA modifications in gene expression was discovered while studying operons regulating the expression of amino acid biosynthesis pathways in bacteria, specifically the *his* operon. This operon contains genes involved in histidine biosynthesis and is itself indirectly regulated by its product histidine which is required to charge tRNA^{His}. The *his* operon contains a leader sequence including a stretch of histidine codons followed by regions capable of forming alternative RNA secondary structures. At high histidyl-tRNA concentrations, translation of the histidine codon stretch by a ribosome changes the secondary structure of the nascent transcript and allows formation of an attenuator stem which acts as a termination signal for RNA polymerase. At low histidyl-tRNA concentrations and thereby slow translation of the histidine codon stretch, the translating ribosome is falling behind and an antiterminator structure is formed instead which allows RNA polymerase to transcribe the operon [Johnston et al., 1980]. Thus, this attenuation control mechanism in *E. coli* and *S. typhimurium* triggers expression of relevant pathway genes when availability of one of their products is low. Consequently, supplementing the culture medium with the histidine analogue triazolalanine inhibits growth in *S. typhimurium* as it is aminoacylated to histidine tRNA [Levin and Hartman, 1963]. [Roth et al., 1966] discovered that strains carrying mutations in the *hisT* gene could escape the inhibitory effect. Later, hisT was identified as a pseudouridine synthase modifying positions 38 and 39 in tRNA^{His} [Singer et al., 1972] which had negative repercussions on the translation speed of the histidine codon stretch in the leader sequence, mimicking a state of low histidyl-tRNA concentration and chronically derepressing the *his* operon [Johnston et al., 1980]. These findings demonstrated a role of RNA modifications in non-coding RNA in the regulation of gene expression both at the translational level and indirectly on the transcriptional level.

Only in the 1970s, the interest in less abundant RNAs was renewed by the discovery of the 5' cap structure of mRNA [Furuichi et al., 1975, Wei et al., 1975, Shatkin, 1976] as well as the description of polyA tails [Edmonds et al., 1971]. Around the same time N6-methyladenosine (m6A) was discovered as the first internal RNA modification by liquid chromatography in cancer cells [Desrosiers et al., 1974], mouse tissues [Perry and Kelley, 1974] and in viruses [Furuichi et al., 1975].

Despite these discoveries the technical limitations remained. Since the exact sites of RNA modifications were mostly unknown, their functional analysis was majorly hindered and the field of RNA modification progressed slowly [Bakin and Ofengand, 1993]. X-ray crystallography of large RNA molecules could serve to map modified sites and solve this issue. However, this method was restricted to employing tRNAs as only those yielded crystals able to diffract at sufficient resolution. Otherwise, NMR studies or neutron scattering were used to study RNA, yet all three mentioned techniques required large mounts of highly purified material [Ehresmann et al., 1987].

An important step forward in RNA modification research occurred in the 1980s with the development of new methods that allowed structural analysis of RNA and exact mapping of individual modified sites [Ehresmann et al., 1987]. In brief, those methods relied on chemical or enzymatic cleavage of RNA molecules at rates of less than one scission per RNA molecule. Modifications resulting from chemical treatment and scissions caused by enzymatic digestion could be mapped at nucleotide resolution using electrophoresis-based systems. The structure of RNA molecules could

be readily inferred by analyzing the fragment patterns caused by enzymes or chemicals specific to paired or unpaired nucleotides in the RNA molecule [Brunel and Romby, 2000]. Similarly, RNA modifications could be mapped by exploiting their unique reactivities or resistances to chemicals and enzymes. The first method, RNA end-labeling, was limited to detecting cleavages in radioactively labeled RNA of molecules containing 200 nucleotides or less followed by visualizing these truncations by electrophoresis or two-dimensional thin-layer chromatography (TLC). One example of its use was the identification of N1-methyladenosine (m1A), m6A, N1-methylguanosine (m1G), m5U and Ψ in human tRNA^{Pro}. This study also suggested the involvement of m1G37 in myopathy [Brule et al., 1998].

The more commonly used method were primer extension assays. In contrast to end labeling, it required the generation of complementary DNA (cDNA) to the input RNA using reverse transcription (RT). Depending on sample availability, either the oligonucleotide primers for RT or alternatively the cDNA were radioactively labeled by elongation in the presence of radioactive ³²P-ATP [Ehresmann et al., 1987]. Chemical or enzymatic treatment of the RNA prior to the RT step lead to nucleotide derivatives or scissions, respectively, causing stochastic truncations in the cDNA which could be mapped at nucleotide resolution using electrophoresis. Using the same approach, certain RNA modifications could be mapped by taking advantage of their unique reactivities with the employed chemicals. For example, four novel Ψ sites were mapped for the first time by primer extension in *E. coli* 23S rRNA in 1993 [Bakin and Ofengand, 1993]. This was achieved by using the chemical N-cyclohexyl-N'-beta-(4-methylmorpholinium) ethylcarbodiimide methyl-p-toluenesulfonate (CMCT) which reacts with Ψ , uridine (U) and guanine (G) but adducts of CMC with U or G are readily cleaved by alkaline conditions whereas Ψ -CMC remains intact (Figure 2) [Gilham and Ho, 1971, Moazed et al., 1986].

Primer extension assays also allowed the mapping of 2'-O-methylations by employing limiting dNTP conditions [Maden et al., 1995, Maden, 2001]. This leads to reduced processivity of the reverse transcriptase causing truncations as a result of pausing or stopping [Motorin et al., 2007]. These methods revealed that with higher organism complexity the amount of modified nucleotides increases (mitochondrial rRNA < bacterial rRNA < eukaryotic rRNA). In higher eukaryotes, rRNAs contain about 100 2'-O-methylated sites and pseudouridines each which depicts a 10-fold enrichment over regular base modifications. Those sites are enriched in conserved core regions whose secondary structure is conserved between prokaryotes and eukaryotes [Maden, 2001, Natchiar et al., 2017, Taoka et al., 2018].

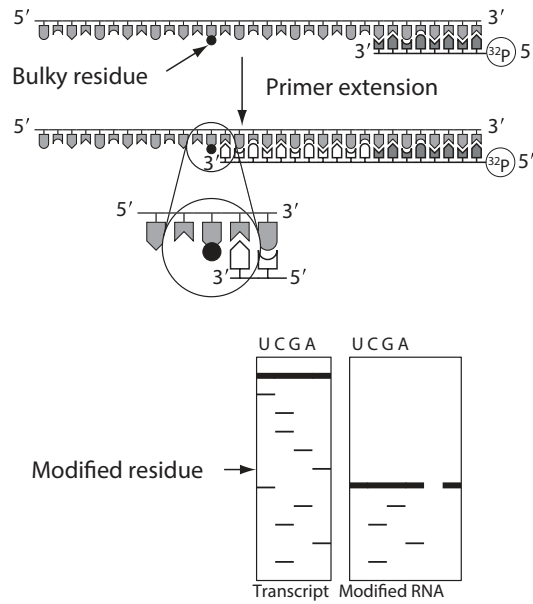


Figure 2: Detection of bulky modified residues in RNA. Some modified nucleotides including CMC- Ψ block primer extension by reverse transcriptase. Figure and description adapted from [Motorin et al., 2007].

Primer extension assays were extensively used by the Ofengand lab which vastly participated in the discovery of Ψ synthases and their RNA targets in *E. coli* (further discussed below). Since these methods allowed quick mapping of Ψ sites, almost all *E. coli* Ψ sites in non-coding RNA were attributed to their respective synthases by the year 2000. This finally allowed functional analysis of these modified sites and yielded considerable insights into their roles in several cellular processes. For example, U2 snRNA was identified to carry a plethora of Ψ sites which were necessary for the assembly of the spliceosome indicating a role of Ψ in splicing [Yu et al., 1998]. Furthermore, it was shown that the deletion of the *E. coli* Ψ synthase RluD which modifies positions 1911, 1915 and 1917 in 23S rRNA causes a growth defect revealing its function in translation [Huang et al., 1998, Raychaudhuri et al., 1998]. Similarly, deletion of RluA which modified U746 in rRNA and 32 in tRNA doesn't affect cell growth, however, presence of the Ψ sites in the *wild type* provided a selection bonus against the mutant highlighting their beneficial effects [Raychaudhuri et al., 1999].

Apart from pseudouridine, further modifications and their functions were revealed. The lysidine modification was identified at position C34 (k2C34) of *E. coli* tRNA^{Ile}. According to its genetic sequence it contains a CAU anticodon which is recognized by MetRS and leads to charging with methionine. Modification with lysidine is necessary to alter the tRNA identity to allow charging by IleRS and decoding of the AUA codon instead of the AUG codon [Muramatsu et al., 1988]. A similar function was observed in tRNAs of marsupials where RNA editing alters the identity of tRNA^{Asp}_{GCC}. Here, the GCC anticodon of tRNA^{Asp}_{GCC} is edited to GUC in approximately half of the transcripts. Since it acts as an identity determinant for the interaction with the Gly and Asp aaRSs, edited tRNA^{Asp} molecules are charged with aspartate while unedited transcripts are charged with glycine. Thereby, RNA editing allows one tRNA species to be charged with different amino acids, adding a layer of complexity to tRNA charging [Börner et al., 1996].

Also, m1A, N2-methylguanosine (m2G), N6-threonylcarbamoyladenine (t6A) and Ψ among other modifications were successfully identified in human mitochondrial (mt.) tRNA^{Lys} and revealed the importance of these modifications for proper tRNA folding [Helm et al., 1998]. This was achieved by a method first described by [Stanley and Vassilenko, 1978] which yields both sequence information as well as modification stoichiometries within an RNA molecule. This is achieved by hydrolysis of the RNA followed by radioactive post-labeling of the 5'-OH groups and resolving of the fragments on a gel to visualize the sequence. Following complete digestion by RNase T1/A, modified and unmodified 5' nucleoside monophosphates can be distinguished in TLC based on their physical properties. While initial approaches employed random fragmentation, later improvements included sequence-specific cleavage with RNase H which allowed mapping of 2'-O-methylation [Yu et al., 1997b], pseudouridine and base methylations [Zhao and Yu, 2004]. This served as the basis for the development of the SCARLET method which included an additional sequence selection step by ligating the 5'-labeled fragment of interest to the 3' end of a DNA oligonucleotide for further purification. This allowed the accurate quantification of m6A and Ψ modification ratios at individual sites to validate high-throughput data [Liu et al., 2013, Li et al., 2015].

Moreover, considerable insights into the roles of RNA editing on tRNA processing were gained. It was shown that RNA editing is essential for both 5' and 3' processing of tRNAs in plant mitochondria. According to the genetic sequence, the acceptor stem of mitochondrial tRNA^{Phe} contains a ⁴C:A⁶⁹ mismatch. It was shown that correction of C to U by RNA editing at position 4 of tRNA^{Phe} is necessary to generate correctly folded pre-tRNA^{Phe}. This step is crucial for the recognition by the 5' and 3' processing machinery in plant mitochondria to generate mature tRNA^{Phe} [Marchfelder et al., 1996, Marechal-Drouard et al., 1996, Kunzmann et al., 1998].

In parallel to the abovementioned studies, mass-spectrometry has been adapted for quantification of RNA modifications for the first time in the 1990s [Kowalak et al., 1993]. A major limitation of the initial methodologies was the fact that prior knowledge regarding the exact RNA sequence of the studied RNA molecule was necessary which was at first limited to well-studied non-coding RNAs or mRNA fragments of model organisms [Wetzel and Limbach, 2016]. For example, mass-spectrometry was successfully employed for the simultaneous discovery and quantification of novel RNA modifications within archaeal tRNA and trypanosomal mRNA [Crain, 1998]. At the turn of the second millennium the advent of genomic sequencing resulted in a growing number of completely sequenced genomes gradually overcoming the initial limitations [Koonin et al., 2003]. Using internal standards [Kellner et al., 2014] or spike-ins [Contreras-Sanz et al., 2012], modern mass-spectrometric approaches allow the detection and quantification of all mass-changing RNA modifications within a single sample [Wetzel and Limbach, 2016] and specific protocols for the quantification of individual RNA modifications like pseudouridine or m6A are being developed for widespread use [Emmerechts et al., 2005, Mathur et al., 2021]. Eventually, combining next generation sequencing and modern liquid chromatography-mass spectrometry (LC-MS) analysis culminated in the generation of a complete map of tRNA modifications in *Lactococcus lactis* showcasing the power of this approach [Puri et al., 2014].

Finally, further examples of RNA modifications affecting translation fidelity were discovered using mass-spectrometry. First of all, modification of position 37 of tRNAs to m1G was found to be ubiquitous to all organisms and necessary for proper growth in both bacteria and eukaryotes where it suppresses +1 frameshift errors [Björk et al., 1989]. In eukaryotes, m1G37 turned out to be a precursor to wybutosine (yW) which is exclusive to tRNA^{Phe} [Björk et al., 2001]. Similar to m1G37, lack of the yW modification at position 37 caused translational frameshifting in HIV, albeit -1 frameshifting, revealing roles in translational fidelity for both modifications [Carlson et al., 1999].

Summed up, substantial knowledge about synthesis, localization and functions of a plethora of RNA modification was gained revealing their importance in various processes including RNA processing, decoding, stability, structure and translation. Furthermore, studies of tRNA modifying enzymes primarily performed in bacteria and yeast yielded valuable insights into their biological relevance.

1.3 Transcriptome-wide mapping of RNA modifications reveals novel functions in mRNAs

Until the 2010s, RNA modifications were thought to be fixed modifications whose only regulatory flexibility consisted in their modification stoichiometry. This impression was refurbished when ALKBH5 and FTO were identified which constituted the first enzymes capable of reversing RNA modifications, specifically m6A [Jia et al., 2011, Zheng et al., 2013]. This discovery conveyed the possibility of dynamic modification landscapes in RNA and renewed the interest in the epitranscriptomics field.

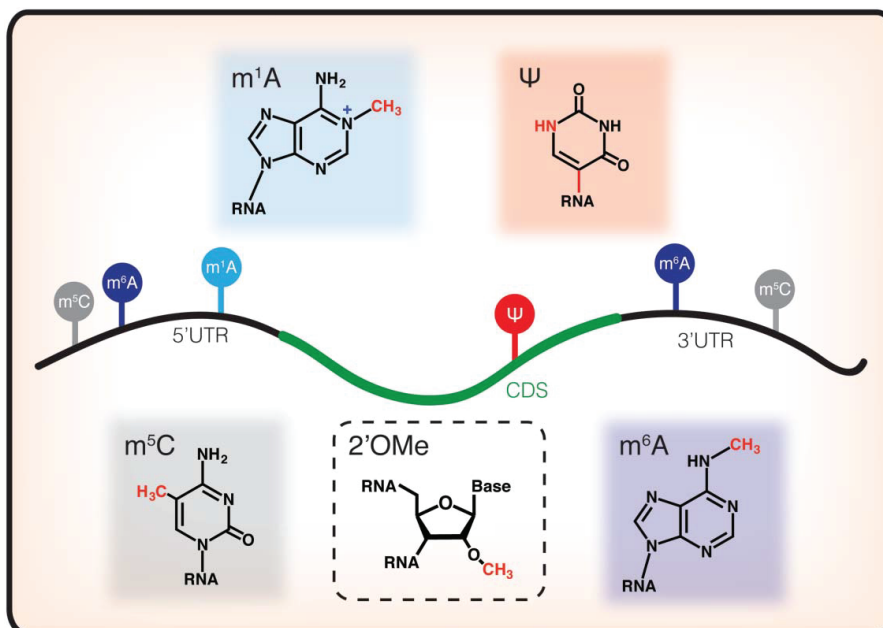


Figure 3: Chemical structures of RNA modifications characterized in mRNA. Figure from [Nachtergaele and He, 2017].

Fortunately, this coincided with great advancements in sequencing technologies as second generation sequencing methodologies with improved sensitivity became commercialized. This led to an advent of next-generation-sequencing (NGS)-based methods which allowed transcriptome-wide mapping of several RNA modifications including m6A, 5-methylcytosine (m5C), N4-acetylcytidine (ac4C), inosine, Nm, m1A and pseudouridine (Figure 3). In the last decade, plenty of studies revealed the impact of RNA modifications on almost every step of RNA processing.

The first RNA modification to be mapped in a transcriptome-wide manner was **m6A** by m6A-seq or meRIP-seq revealing over 10,000 high-confidence m6A sites. The abundance of m6A sites on mRNA is evident since 20-40% of all transcripts are methylated and tend to have multiple sites per transcript [Dominissini et al., 2012, Meyer et al., 2012]. These first methods could, however, not map m6A at nucleotide resolution which was only achieved later by m6A-miCLIP [Linder et al., 2015]. Here, m6A(m) detecting antibodies are covalently linked to bound mRNAs by UV crosslinking. Following m6A pulldown, the antibodies are digested, leaving small peptide fragments at the m6A sites leading to mutations in a subsequent reverse transcription step which are mapped by NGS. Eventually, m6A sites were found on almost all classes of RNA including mRNAs, tRNA, snRNAs, rRNAs, circular RNAs (circRNAs), micro RNAs (miRNAs) and long non-coding (lncRNAs) [Shi et al., 2019]. A plethora of studies followed, linking m6A to functions in almost every step of RNA processing and rendering it the most studied RNA modification to date. First of all, m6A was shown to regulate nuclear export mediated by the m6A reader protein YTHDC1 which delivers methylated RNAs to the splicing factor and nuclear export adaptor protein SRSF3 in HeLa cells [Roundtree et al., 2017].

Second, multiple effects of m6A on splicing have been reported: The most prominent example is the m6A-dependent regulation of alternative splicing by serine/arginine-rich splicing factor 3 (SRSF3). [Xiao et al., 2016] discovered that m6A sites promote the recruitment of SRSF3 through YTHDC1 to mediate exon inclusion. Recently, this mechanism was demonstrated in the regulation of splicing of the lncRNA ANRIL into a longer or shorter isoform based on the presence of m6A sites and provided a functional link between m6A-dependent splicing of lncRNAs and DNA repair [Wang et al., 2022]. Furthermore, METTL4 catalyzes the conversion of internal 2'-O-methyladenosine (Am) of U2 snRNA into N6,2'-O-dimethyladenosine (m6Am), thereby affecting global splicing events [Chen et al., 2020, Gu et al., 2020, Goh et al., 2020]. m6A also affects splicing of transcripts directly by enhancing the binding of the splicing factor SRSF2 to modified transcripts and thereby promoting exon inclusion [Zhao et al., 2014]. Additionally, METTL16 was identified as an m6A writer targeting both pre-mRNAs and position A43 in U6 snRNA which base pairs with 5' splice sites suggesting a dual role in splicing through sites in non-coding RNA [Warda et al., 2017]. Another well studied example is the deposition of m6A on the SAM synthetase Mat2a transcript by METTL16, thereby regulating SAM availability by regulating Mat2a splicing [Pendleton et al., 2017]. The physiological relevance is evident since lack of METTL16 is lethal at the 64 cell blastocyst stage in mouse, likely as a result of the enrichment of the intron-containing unspliced Mat2a transcript which is less stable

resulting in a lack of SAM [Mendel et al., 2018].

Third, further involvements in development were highlighted by the role of m6A in RNA decay: It was shown to be important for development by regulating the transcriptome switch during maternal to zygotic transition through promotion of RNA degradation. Multiple studies highlighted how m6A in mRNAs of certain pluripotency factors regulates their degradation [Geula et al., 2015, Batista et al., 2014, Wang et al., 2014]. As a result, lack of METTL3 is embryonic lethal in mice, likely because mouse embryonic stem cells cannot leave the pluripotency state [Geula et al., 2015, Batista et al., 2014]. m6A was also shown to be required for cortical neurogenesis in mouse where it promotes the decay of certain transcripts in lineage specification [Yoon, 2017, Li et al., 2018].

Fourth, m6A plays a role in regulating mRNA stability by affecting RNA-protein interactions. For example, m6A affects mRNA homeostasis by inhibiting the binding of proteins enhancing mRNA stability (G3BP1) [Edupuganti et al., 2017]. In contrast to that, IGF2BP proteins were identified as m6A readers binding and stabilizing methylated mRNAs under normal conditions and stress conditions [Huang et al., 2018]. Fifth, m6A affects translation both via coding and non-coding RNA. Recently, ZCCHC4 has been discovered as a novel m6A writer specific to 28S rRNA at position A4220. Loss of methylation at this site was revealed to perturb translation globally [Ma et al., 2019] in a codon-specific manner [Pinto et al., 2020]. In coding RNA, m6A was identified in 5' untranslated regions (UTRs) where it regulates translation upon cellular stress. Specifically, m6A sites in 5' UTRs are induced upon DNA damage or heat-shock and promote cap-independent translation via recruiting eIF3 and subsequently the 43S complex [Meyer et al., 2015]. Lastly, m6A also controls the maturation of miRNAs: HNRNPA2B1 was identified as a nuclear m6A reader facilitating the recruitment of the microprocessor complex to methylated pri-miRNAs to generate mature miRNAs [Alarcon et al., 2015].

In 2012 also **m5C**, another highly abundant modification, was mapped for the first time in a transcriptome-wide manner in HeLa cells which revealed more than 10,000 m5C sites in approximately 8500 mRNAs [Squires et al., 2012]. By now, multiple studies identified m5C in mRNAs of several organisms and tissues including human cells [Squires et al., 2012, Yang et al., 2017], mouse [Wei et al., 2018], breast cancer [Huang et al., 2018] and zebra fish [Yang et al., 2019] revealing its presence on RNAs such as tRNA, rRNA, snRNA, miRNA, lncRNA, eRNAs as well as mRNA [Cantara et al., 2010]. These studies uncovered an enrichment of m5C sites in 5' and 3' UTRs of mRNAs as well as about 100 nt downstream of the translation start codon [Yang et al., 2017, Wei et al., 2018]. At these sites, m5C is involved in several processes including pre-mRNA splicing [Young et al., 2005], mRNA export via the m5C reader ALYREF [Yang et al., 2017] and mRNA stability [Yang et al., 2019]. Furthermore, it seems to regulate translational repression when present in the 5' UTR of mRNAs [Tang et al., 2015] but promote translation when near the 3' UTR [Xing et al., 2015, Li et al., 2017a]. Moreover, NSUN2 mediated methylation was implicated in regulating gene expression by promoting the processing of vault RNAs to small RNAs that act analogous to miRNAs [Hussain et al., 2013]. While there are 7 members in the NSUN family of proteins, the predominant methyl

transferases on mRNAs seem to be NSUN2 [Yang et al., 2017] recognizing a $\underline{C}RGGG$ (R=A/G) motif [Huang et al., 2018] and NSUN6 which usually targets C72 in tRNAs [Long et al., 2016] but also a $\underline{C}UCCA$ consensus motif in coding RNA [Selmi et al., 2021]. In contrast, NSUN7 was suggested to target certain enhancer RNAs (eRNAs) to promote their stability. Intriguingly, NSUN7 and NSUN7-dependent methylation are upregulated during starvation suggesting a role in stress response [Aguilo et al., 2016].

Initial transcriptome-wide studies revealed **m1A** sites to be enriched in 5' UTRs and close to start codons and found dynamic changes in m1A patterns upon several cellular stresses [Dominissini et al., 2016, Li et al., 2016b, Li et al., 2017b]. Furthermore, ALKHB3 was identified as a stress-induced m1A eraser emphasizing a potential role during stress response and suggesting that m1A is a dynamic RNA modification similar to m6A [Li et al., 2016b]. Additionally, m1A was shown to improve translation of modified transcripts by regulating translation efficiency [Dominissini et al., 2016]. However, several other studies mapping m1A sites based on misincorporations generated by a highly processive RT instead of antibody-enrichment could not confirm this abundance and suggested m1A to be extremely rare on mRNA [Safra et al., 2017b, Grozhik et al., 2019, Khoddami et al., 2019]. Therefore, the abundance and relevance of m1A on mRNA remain controversial.

Apart from methylations, acylations of RNA have been mapped in a transcriptome-wide manner for the first time in mRNA of HeLa cells in 2018 [Arango et al., 2018]. Here, modification of cytosine to **ac4C** is performed by the nuclear acetyltransferase NAT10 [Ito et al., 2014]. The distribution of ac4C pointed towards an enrichment in the 5' UTR and around the translation start site where acetylations were suggested to increase translation levels by stabilizing transcripts. A follow-up study further showed that ac4C in the 5' UTR can directly inhibit or promote translation initiation depending on the context of the surrounding sequence while ac4C in the CDS generally enhances translation [Arango et al., 2022]. Strikingly, only 6 high confidence sites were identified in yeast with mRNA acetylation increasing drastically upon heat stress, starvation and oxidative stress [Tardu et al., 2019]. The apparent link between acylation and cellular stress was further confirmed on rRNA of archaea by [Sas-Chen et al., 2020] who were unable to find any ac4C sites in mRNA of yeast or HeLa cells under normal conditions.

While **pseudouridine** is one of the most abundant RNA modification in non-coding RNAs, multiple studies have mapped Ψ sites in a transcriptome-manner revealing between 100 and 500 sites in mRNA from yeast and human cells [Schwartz et al., 2014, Carlile et al., 2014, Lovejoy et al., 2014, Dai et al., 2022] while another group utilizing an antibody-based enrichment step identified approximately 2000 sites [Li et al., 2015]. Recently, pseudouridine was mapped in the transcriptome of different mouse tissues revealing thousands of tissue-specific Ψ sites with the highest enrichment in the cerebellum (6617 mRNA sites) [Dai et al., 2022]. While over 4000 highly modified sites ($\Psi/U >50\%$) were identified among twelve mouse tissues, only 500 sites were shared among all

tissues revealing tissue-specific pseudouridylation patterns in mRNA. While functional knowledge about individual Ψ sites is missing, TRUB1-specific Ψ sites generally increased mRNA stability and lifetime. Furthermore, approximately 100 Ψ sites were discovered in stop codons which increased stop-codon readthrough. A role of Ψ in nonsense suppression has been observed before [Karijovich and Yu, 2011] and is likely facilitated by Ψ allowing unusual purine-purine base-pairing between the codon and the anticodon [Fernández et al., 2013]. This was supported by structural studies attesting that Ψ in coding sequences affects ribosome kinetics and triggers amino acid misincorporations at low frequencies ($<1.5\%$) in unstressed cells [Eyler et al., 2019]. Notably, the full extent of recoding might only happen during stress conditions as increasing amounts of evidence indicate a role of pseudouridylation in stress response. First of all, 265 Pus7-dependent Ψ sites have been found to be inducible by heatshock in yeast which was accompanied with a translocation of Pus7 from the nucleus to the cytoplasm [Schwartz et al., 2014]. Inducible pseudouridylation in the transcriptome was further confirmed in human cells where it is regulated by multiple stress signals including heatshock and oxidative stress [Li et al., 2015]. In fact, the heatshock protein HSP90 was recently identified as a binding partner of PUS7 increasing its stability by preventing proteasomal degradation providing further indications for Ψ playing a role in stress response [Song et al., 2021].

Apart from that, multiple studies have indicated a role of Ψ in splicing. First of all, it was postulated that PUS7 could modify pre-mRNA in a cotranscriptional manner as copurification with active RNA polymerase II promoters indicated it to be associated with actively transcribed chromatin [Ji et al., 2015]. Strikingly, a role in splicing was recently confirmed by the Gilbert lab showing that PUS1, PUS7 and RPUSD4 play a role in alternative splicing by modifying pre-mRNA at approximately 2000 intronic sites in cancer cells accounting for 74% of all sites in mRNA [Martinez et al., 2022]. Furthermore, they provided evidence for PUS-dependent alternative polyadenylation and alternative cleavage, foremost by pseudouridines in introns undergoing alternative 5' splicing. Additionally, the binding sites of many RBPs overlapped with detected Ψ sites, many of which are located in introns, suggesting that Ψ could facilitate these functions by affecting RNA-RNA and RNA-protein interactions. This is supported by multiple studies demonstrating that Ψ inhibits the binding of RBPs both indirectly by changing the RNA structure [Chen et al., 2010, deLorimier et al., 2017] and directly when present within the RNA consensus motif of an RBP [Vaidyanathan et al., 2017]. Recently, Ψ sites have been mapped for the first time in mRNA of female *Drosophila* heads [Song et al., 2023]. Interestingly, approximately 1100 mRNA sites were identified which were clustered in transcripts of only 165 genes. Those genes contained numerous ribosomal proteins indicating a possible role of Ψ in translation. Furthermore, this study suggested potential functions of pseudouridine in mitochondria. Almost 100 Ψ sites were discovered in mitochondrially encoded mRNA which could affect translation of the mitochondrially encoded members of the respiratory chain. Additionally, multiple mitochondrial UGA stop codons were modified indicating that Ψ could facilitate recoding to tryptophane at these sites. Finally, almost 25% of the total Ψ sites were accumulated on transcripts of the yolk proteins Yp1, Yp2 and Yp3, accounting for more than 100 Ψ sites each, however, their functions remain mysterious.

Taken together, the transcriptome-wide mapping of RNA modifications yielded vast amounts of information leading to a revitalization of the epitranscriptomics field. While the functions of some abundant RNA modifications like m6A and m5C are being gradually unveiled, revealing roles in almost every aspect of RNA metabolism, the presence and impact of other modifications are still controversial or lack experimental proof. To facilitate the navigation through the extensive quantities of data, multiple databases for sites of RNA modification [Boccaletto et al., 2022] and for RNA modifying enzymes [Nie et al., 2022] as well as several prediction models have been generated [Song et al., 2020a, Chen et al., 2019a].

1.4 The knowledge about Ψ gained from 1950-2000

1.4.1 Synthesis of Ψ

While the structure of pseudouridine was identified early on in 1960 as a C5 glycoside isomer with a C-C glycosidic bond [Cohn, 1960], the synthesis pathway remained unknown for a long time. Even though Ψ synthases were discovered and isolated in extracts of *Tetrahymena pyriformis* as early as 1963 [Heinrikson and Goldwasser, 1963] as well as in extracts of *Agrobacterium tumefaciens* [Suzuki and Hochster, 1966] and later in *E. coli* [Breitman, 1970], no specific gene had been attributed to this activity. Only in 1988 a corresponding gene was identified in *E. coli* with specificity for tRNA positions 38-40. While this gene was already described in 1985, its pseudouridylation activity was unknown until that point [Arps et al., 1985, Kammen et al., 1988]. However, instead of one dedicated enzyme being responsible for the catalysis of all Ψ sites the synthesis pathways turned out to be more complicated. Researchers identified two separate pathways of Ψ synthesis: an evolutionarily younger pathway utilizing a guide RNA dependent mechanism in concert with (snRNP) complex to target the catalytic activity to the substrate RNA by basepairing with it. And an evolutionarily older pathway via standalone Ψ synthases that recognize their targets by RNA structure, sequence or both (Figure 4B).

Even before all enzymes were discovered, the conservation of a presumably catalytic aspartate was observed which was common among all Ψ synthases [Koonin, 1996]. Today, we know that this aspartate is crucial for the mechanism of catalysis which is proposed as a deprotonation of the ribose sugar by the catalytic aspartate resulting in the detachment of the base and the generation of a glycal intermediate [Veerareddy et al., 2016]. Prior to reattachment, the base is rotated by 180° resulting in a C-C glycosidic bond and allowing the N1 atom to serve as an additional hydrogen bond donor. Early NMR studies suggested that this structural rearrangement improves base rotation and therefore RNA stability [Nanda et al., 1974]. Later on, the role of Ψ in RNA stability was confirmed by studies using X-ray crystallography which proposed that pseudouridine interacts with adjacent phosphate residues through a Ψ -coordinated water molecule [Arnez and Steitz, 1994]. Additional investigations using NMR, UV and CD spectroscopy suggested that Ψ improves base-stacking and favors a C3'-endo

conformation of the ribose [Davis, 1995] which increases backbone rigidity [Chen et al., 2010]. While the catalytic mechanism is shared between all Ψ synthases a considerable complexity was uncovered in terms of substrate specificities, subcellular localizations and inducibility by cellular signals.

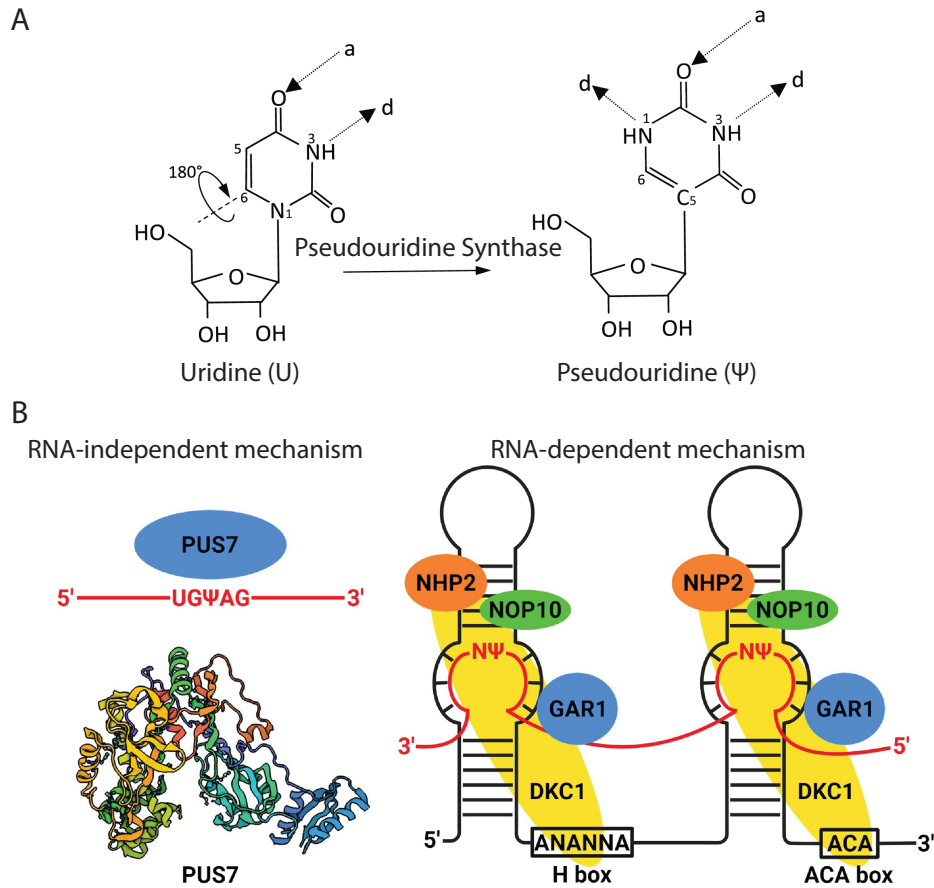


Figure 4: Synthesis of Ψ . Pseudouridine synthases catalyze the isomerization of Uridine to Pseudouridine. The base is detached and rotated by 180°C prior to reattachment resulting in a C-C glycosidic bond and N1 acting as an additional hydrogen bond donor (d) in Pseudouridine. (a) hydrogen bond acceptor. Figure from [Zhao et al., 2018]. (B) RNA-independent catalysis of Ψ by standalone synthases recognizing a consensus motif based on RNA sequence or structure (left). RNA-dependent Ψ formation by dyskerin (DKC1) which forms small ribonucleoproteins (snRNPs) with NHP2, NOP10 and GAR1 as well as H/ACA box snoRNAs which guide specificity to their substrates by base-pairing (right). H/ACA snoRNAs adopt a hairpin-hinge-hairpin structure with a conserved H box between the hairpins and a conserved ACA box at the 3' tail. Figure adapted from [Cerneckis et al., 2022].

1.4.2 guide-RNA dependent Ψ synthesis

The guide RNA dependent pathway of Ψ synthesis is only found in archaea and eukaryotes and was discovered in 1996 around the time as the other Ψ synthases were identified [Kiss-László et al., 1996]. It utilizes small nucleolar RNAs (snoRNAs), a group of small non-coding RNAs that are mainly encoded in introns of coding and non-coding genes, typically localize to the nucleolus of eukaryotic cells and have a length of approximately 60-300 nt [Dieci et al., 2009, Esteller, 2011]. These RNAs act as guide RNAs in small nuclear ribonucleoprotein (snRNP) complexes to target modification to their substrate RNA by basepairing with it. There are three major classes of snoRNAs being H/ACA box snoRNAs, C/D box snoRNAs and small cajal-body specific RNAs (scaRNAs) which

facilitate pseudouridylation, 2'-O-methylation or both, respectively [van der Werf et al., 2021]. They are all transcribed by RNA polymerase II and are cotranscriptionally assembled into snRNP complexes [Liang and Li, 2011].

The main function of **C/D box snoRNAs** is to guide 2'-O-methylation to rRNAs and snRNAs. They contain the conserved boxes C (RUGAUGA) and D (CUGA) which are close to the 5' and 3' termini of the snoRNA, respectively. Of note, some C/D box snoRNAs can contain additional C' and D' boxes [Kiss-Laszlo et al., 1998] which are important for biogenesis and interaction with RBPs [Caffarelli et al., 1996] and can even serve as a second guide for methylation [van Nues and Watkins, 2017]. Usually, C/D box snoRNAs are 60-90 nt long [Balakin et al., 1996] and form a complex with Nop56p, Nop58p, Snu13p and Nop1p (Fibrillarin) as the catalytically active component of the complex [Kiss-Laszlo et al., 1998].

The **H/ACA guide RNAs** are 120-140 nt long [Balakin et al., 1996] and form a snoRNP complex with Nhp2p, Nop10p, Gar1p and Cbf5p (yeast homologe of DKC1) to guide pseudouridylation to rRNAs [Jorjani et al., 2016]. They adopt a conserved structure consisting of two stem loops flanking a hinge region which contains the conserved H box (consensus 5'-ANANNA-3') and an ACA box at the 3' tail [Ganot et al., 1997].

Finally, **scaRNAs** can vary in their sequence containing either C/D boxes or H/ACA boxes or mixtures of both [Enwerem et al., 2014] and can therefore guide both pseudouridylation and 2'-O-methylation. C/D box scaRNAs contain conserved GU repeats which signal their transport to cajal bodies [Marnef et al., 2014] while for H/ACA box scaRNAs this is facilitated by CAB boxes with a UGAG motif in the stem loops [Richard et al., 2003]. There, they modify their main targets being U1, U2, U4, and U5 snRNAs [Marz et al., 2011, Deryusheva and Gall, 2013] whereas U6 snRNA gets modified by both C/D and H/ACA box snoRNAs in the nucleolus [Ganot et al., 1999].

The pseudouridylation of yeast snRNA may mark an evolutionary transition from Ψ being deposited predominantly by standalone synthases in lower eukaryotes towards an increasing reliance on the guide-RNA dependent mechanism in higher eukaryotes. There are six Ψ sites in yeast snRNA [Massenet et al., 1998] while 27 exist in vertebrate snRNA [Borchardt et al., 2020]. Three of the yeast Ψ sites are localized in U2 snRNA at positions 35, 42 and 44 which are modified both by standalone synthases Pus1 and Pus7 and Cbf5 [Ma et al., 2005]. Surprisingly, human PUS1 and PUS7 seem to have lost the ability to modify these sites [Deryusheva and Gall, 2017, de Brouwer et al., 2018]. Instead, most, if not all, Ψ sites in vertebrates are modified by the guide RNA dependent mechanism [Borchardt et al., 2020]. This transition is more evident with the increasing number of modifications accompanying the increase in organism complexity. While there are only eleven Ψ sites in bacterial rRNA which are all modified by standalone synthases, about 50 sites have been identified in yeast [Schattner et al., 2004] and approximately 100 exist in mammalian rRNA [Schat-

tner et al., 2006, Natchiar et al., 2017]. Importantly, the targets of only some snoRNAs are confirmed experimentally, for example U2 snRNA modification at U34 and U44 in *Xenopus* [Zhao et al., 2002] and position 46 of U5 snRNA in mammals [Jády and Kiss, 2001] while the targets of most snoRNAs are predicted by their sequence and lack experimental proof.

1.4.3 Ψ synthesis by standalone synthases

The discovery of multiple *E. coli* Ψ synthases was spearheaded by the Ofengand lab in the 1990s identifying enzymes with different target specificities including tRNA at position 55 by TruB [Nurse et al., 1995], position 746 in 23S rRNA as well as tRNA^{Phe} at position 32 by RluA [Wrzesinski et al., 1995b], 16S rRNA at position 516 by RsuA [Wrzesinski et al., 1995a], positions 955, 2504 and 2580 in 23S rRNA by RluC [Conrad et al., 1998], positions 1911, 1915 and 1917 in 23S rRNA as well as position 13 in tRNA by RluD [Huang et al., 1998, Raychaudhuri et al., 1998, Kaya and Ofengand, 2003]. Finally, the remaining four Ψ synthases in *E. coli* were described being RluB, RluE and RluF targeting positions 2605, 2457 and 2604 in 23S rRNA, respectively, and TruC targeting U65 in tRNA^{Ile} and tRNA^{Asp} [Del Campo Mark and James, 2001]. These discoveries revealed that Ψ synthases featured distinct target specificities which can be restricted to individual sites within the transcriptome.

In spite of differences in sequence between synthases, their conserved structure indicates a common evolutionary origin [Rintala-Dempsey and Kothe, 2017]. Based on sequence similarities, all identified Ψ synthases in *E. coli* were classified into five families being TruA, TruB, TruD, RsuA and RluA (containing TruC) [Hamma and Ferré-D'Amaré, 2006]. Within the following decade, extensive studies revealed all respective homo- and paralogues of pus enzymes in yeast, termed Pus1-10, as well as their target sites in non-coding RNA (Figure 5) [Rintala-Dempsey and Kothe, 2017]. Notably, with increasing organism complexity in eukaryotes including the presence of cellular compartments, mitochondria and gene duplications, an increasing complexity in Ψ synthases was observed. This included the occurrence of the gRNA dependent pathway of Ψ synthesis which assumed many target sites in rRNA [Kiss-László et al., 1996]. Additionally, while RsuA type pus enzymes were only found in bacteria, a novel family comprising Pus10 was identified in archaea and eukaryotes with the exception of yeast [Watanabe and Gray, 2000, Gurha and Gupta, 2008]. While most studies focused on yeast pus enzymes, a growing interest in human PUS enzymes arised with the identification of PUS mutations in human patients revealing a growing evidence for the involvement of Ψ in human diseases including brain and muscle disorders as well as cancer (discussed in 1.5).

In human, twelve standalone PUS enzymes exist with PUS1 and PUS7 having one paralog each being PUSL1 and PUS7L. The structures of five human PUS enzymes have been determined and comparisons with their *E. coli* counterparts revealed the conservation of the core catalytic domain. However, human enzymes can have additional domains which are thought to affect their target specificity [Borchardt et al., 2020]. Compared to the vast knowledge gathered about yeast pus enzymes, comparably little information is available about mammalian PUS enzymes. Therefore, this section

focuses on yeast enzymes unless stated otherwise.

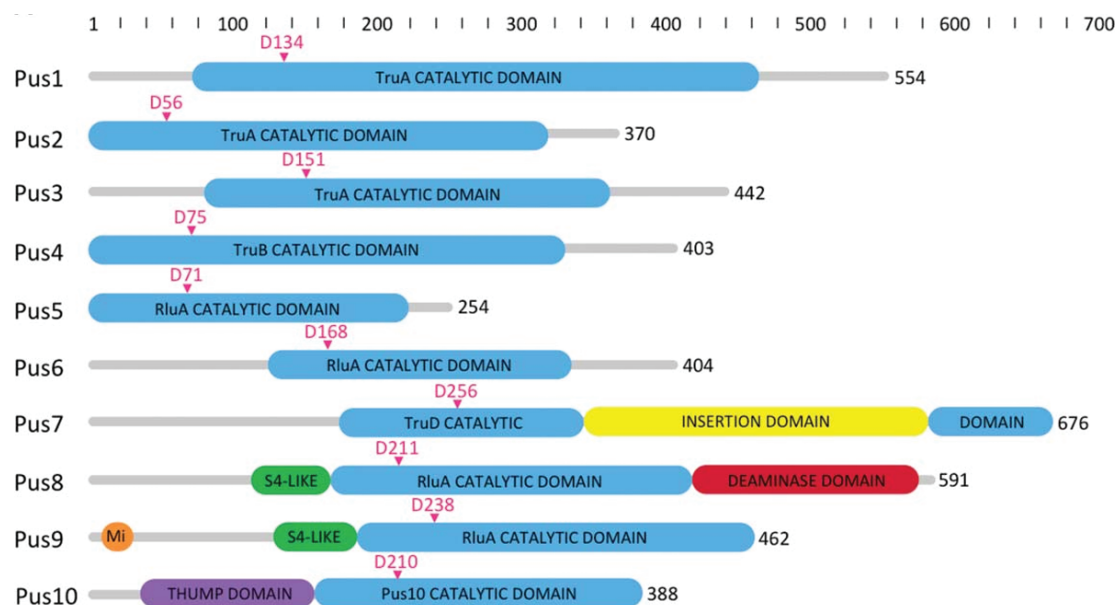


Figure 5: Domain structure and localization of the Pus enzymes. (A) All Pus enzymes share a common catalytic core domain (shown in light blue), with some variations depending on which family of enzymes they belong to. Some of the enzymes have N- or C-terminal extensions beyond the catalytic domains (shown as narrow gray bars), while others have additional domains. Pus7 has an insertion in its catalytic domain (yellow), characteristic of members of the TruD family. Pus8 has an S4-like domain (green) at its N-terminus that aids in binding to RNA and a C-terminal cytidine deaminase domain (red) involved in riboflavin biosynthesis. Pus9 also contains the S4-like domain, but is preceded by an N-terminal mitochondrial targeting sequence (orange). Pus10 contains a THUMP domain (purple). Sequence numbering refers to the yeast proteins with the exception of Pus10 which is not found in yeast; in this case the numbering refers to the *Pyrococcus furiosus* enzyme. The total number of amino acids in each protein is shown (black) and the catalytic aspartate is indicated by an arrow and residue number above the corresponding catalytic domain (magenta). Domain location and sizes have been approximated based on sequence alignments, domain predictions and homologous structures. Figure and description from [Rintala-Dempsey and Kothe, 2017].

TruA family

The TruA family of Ψ synthases in yeast comprises three enzymes. **Pus1** is especially interesting as it is one of the most promiscuous pus enzymes with a broad spectrum of substrates including tRNAs, snRNAs and long-non-coding RNAs. In tRNAs, it targets multiple sites including the first nucleotide U1 in tRNA^{Arg}_{ACG} [Behm-Ansmant et al., 2006] as well as U27, U35 and U36 in intron-containing pre-tRNA^{Ile} [Szweykowska-Kulinska et al., 1994]. Furthermore, an extensive mapping study revealed U27 in cytoplasmic tRNA^{Val}, U27, U28 and U65 in cytoplasmic tRNA^{Trp}, U35 in tRNA^{Tyr} as well as U67 in tRNA^{Ile} as targets of yeast Pus1 [Motorin et al., 1998]. Additionally, it modifies U44 in U2 snRNA, however, how this site might affect splicing remains unknown [Massenet et al., 1999]. Furthermore, a biological role of Pus1 activity was revealed by its involvement in the nuclear export of minor tRNA^{Ile}_{UAU} which was proposed for other tRNAs as well [Großhans et al., 2001]. Another study revealed that Pus1 is upregulated during the filamentous growth program of *S. pombe* which leads to the induced pseudouridylation of U28 in U6 snRNA which is necessary to activate the program [Basak and Query, 2014] revealing a certain flexibility in substrate specificity regulated

by the cellular state. Early studies using recombinant yeast Pus1 and crystal structures of human PUS1 gave possible explanations on the origin of the broad substrate specificity of eukaryotic Pus1. In contrast to *E. coli* TruA, eukaryotic Pus1 contains an additional C-terminal extension domain comprising two helices which prevent oligomerization and renders it to act as a monomer [Arлуison et al., 1999, Czudnochowski et al., 2013]. Furthermore, in vitro studies of the structural requirements of the tRNA and mRNA substrates of yeast Pus1 and human PUS1 revealed that the enzymes recognize their substrates by a structural minimal motif comprised of a bulged stem loop with the targeted U at its 5' base [Carlile et al., 2019]. This confirmed previous investigations in tRNA where a minimal T Ψ C loop was still modified by PUS1 even after replacing all nucleotides except the target U while retaining the correct folding of the anticodon stem loop [Sibert and Patton, 2012]. While one cytoplasmic isoform is expressed in yeast, one shorter isoform localizing to the nucleus and a longer isoform localizing to mitochondria exist in mammals [Fernandez-Vizarra et al., 2006]. In line with this, an expanded set of tRNA targets was discovered for PUS1. For example, U27/28 were found to be modified by PUS1 in vivo in cytoplasmic tRNA^{Ser}_{UGA} and mitochondrial tRNA^{Lys}_{UUU} [Patton et al., 2005]. Furthermore, Ψ sites at U66/67 and U68 were discovered in human mt. tRNA^{Pro} and tRNA^{Ala}, respectively [Suzuki et al., 2020]. While experimental proof is still missing, these sites are likely modified by PUS1, since yeast Pus1 was shown to target U67 in yeast [Motorin et al., 1998].

Pus2 is a paralog of Pus1 but acquired a unique niche in respect to its mitochondrial localization despite lacking a mitochondrial localization signal [Byrne and Wolfe, 2005]. There, it acts on U27 and U28 of mt. tRNA suggesting that the modes of substrate recognition of Pus1 and Pus2 are similar, yet the subcellular localization seems to determine their specificity [Behm-Ansmant et al., 2007].

Pus3 targets U38/39 in cytoplasmic and mitochondrial tRNAs in the anticodon arm. These sites are highly conserved even in bacteria where they are catalyzed by its homologue TruA [Cortese et al., 1974]. A role in facilitating stop-codon readthrough was attributed to the modification of U38/39 since both the natural levels of read-through as well as +1 frameshifting were reduced upon loss of Pus3 suggesting a role in naturally occurring recoding events [Lecoинte et al., 2002]. Another curious finding was the fact that both yeast Pus3 and Pus1 target the long non-coding RNA steroid receptor RNA activator (SRA) [Zhao et al., 2007]. SRA is a ligand for nuclear receptors and their binding can result in changes in gene expression. Both mouse PUS1 and PUS3 were shown to target SRA at different positions serving as nuclear receptor coactivators. However, whether these functionalities lead to a change in gene expression remains to be determined.

TruB family

Pus4 is the sole eukaryotic member of the yeast TruB family and generates the universally conserved Ψ 55 in cytoplasmic and mitochondrial tRNAs despite not containing a mitochondrial localization signal. No other targets have been identified in non-coding RNA illustrating its unique substrate specificity [Becker et al., 1997, Rintala-Dempsey and Kothe, 2017]. Its mode of substrate recognition was proposed to include both sequence and structural information in the form of a GUUCNANNC

consensus motif suggesting a T-loop-type structure in Pus4 substrates [Carlile et al., 2014]. An involvement of both Pus3 and Pus4 in tRNA stabilization was proposed since deletion of any of the enzymes was shown to be lethal in strains lacking the La gene which plays roles in tRNA stabilization, maturation and folding [Copela et al., 2006]. Another study confirmed a pseudouridylation-independent chaperoning function of Pus4/TruB conserved between bacteria and eukarya which is necessary for efficient tRNA maturation [Keffer-Wilkes et al., 2016]. This study highlighted that pus enzymes can adopt dual functions independent of their pseudouridylation activity.

In human, the TruB family comprises two standalone synthases: TRUB1 and TRUB2. TRUB1 localizes to the nucleus, cytoplasm and mitochondria and catalyzes U55 in mitochondrial tRNA^{Asn/Gln/Glu/Pro} [Safra et al., 2017a, Jia et al., 2022]. Here, TRUB1 targets the same consensus motif as yeast Pus4 which forms a 5-bp stem and a 7-bp loop with the Ψ site at the second base in the loop. This indicates that the mode of substrate recognition is conserved between yeast and vertebrate homologues. Also, TRUB1 deficiency was observed to cause defects in oxidative phosphorylation highlighting a role of TRUB1 in mitochondrial function [Jia et al., 2022]. Recently, a pseudouridylation-independent role of TRUB1 in miRNA maturation was identified. [Kurimoto et al., 2020] demonstrated that TRUB1 binds to stem-loops of pri-miRNAs of the let-7 family to recruit DGCR8 and enhance miRNA maturation. Since mature let-7 targets genes involved in cell proliferation [Wang et al., 2013], TRUB1 indirectly suppresses cell growth in human cells. Just like its paralogue, TRUB2 also localizes to mitochondria but no other information is available about it [Antonicka et al., 2016].

Pus10 family

Pus10 depicts a novel Pus family exclusive to archaea and eukarya and targets U54 and U55 in tRNA which overlaps with the target site of enzymes of the TruB family [Gurha and Gupta, 2008]. This raised the question whether a certain level of competition or redundancy might exist between these two families. This idea was further supported by the fact that human PUS10 targets a GUUCA(m1A)AUC consensus sequence highly similar to that of TruB enzymes [Deogharia et al., 2019]. A recent study addressed this and found an intricate interplay between TRUB1 and PUS10 to ensure correct tRNA pseudouridylation [Mukhopadhyay et al., 2021]. It was observed that nuclear TRUB1 primarily modifies tRNAs containing U54U55 at position 55. At the same time, cytoplasmic PUS10 targets certain tRNAs containing U54U55 in some cases both at U54 and U55 while some tRNAs receive only the U54 modification. While all those sites are modified by PUS10, a specific mechanism was set in place to prevent modification of U55 by TRUB1 in the latter group of tRNA species. This is facilitated by a nuclear version of PUS10 which is catalytically inactive and binds those tRNAs containing U54U55 which are supposed to receive only Ψ 54. Thereby, nuclear PUS10 sterically inhibits modification at U55 by TRUB1 in the nucleus to ensure correct tRNA modification [Mukhopadhyay et al., 2021].

Apart from that, nuclear PUS10 is further involved in regulating apoptosis in TRAIL-treated cells [Aza-Blanc et al., 2003, Jana et al., 2017] as well as in miRNA biogenesis [Song et al., 2019]. Here, a lack of PUS10 caused a reduction of miRNA levels by approximately 30% accompanied by an

upregulation of the corresponding mRNA targets. PUS10 was found to play a direct role in miRNA maturation by binding pri-miRNAs and recruiting the miRNA processing machinery for maturation of pri- to pre-miRNAs [Song et al., 2019].

RluA family

Despite representing the largest family of pus enzymes containing Pus5, Pus6, Pus8 and Pus9, relatively few studies have focused on them. In spite of not containing a clear mitochondrial signal like most other mitochondrial pus enzymes, **Pus5** targets position 2819 in 21S mitochondrial rRNA [Ansmant et al., 2000].

Immunostainings of yeast **Pus6** revealed a dual localization to both the cytoplasm and mitochondria where it facilitates the modification of U31 in certain tRNAs [Ansmant et al., 2001].

While **Pus8** modifies U32 of cytoplasmic tRNA [Behm-Ansmant et al., 2004] it distinguishes itself from other pus enzymes by carrying an additional riboflavin domain potentially originating from a gene fusion. While deletion of Pus8 is lethal, this is attributed to its role in riboflavin synthesis and not due to its pseudouridylation activity as supplementing riboflavin into the culture medium restores normal growth [Behm-Ansmant et al., 2004].

Pus9 is the only Pus enzyme to contain an explicit mitochondrial localization signal. Similar to the separate roles of Pus1 and Pus2, Pus8 and Pus9 target the same position 32 in tRNAs, however, Pus9 acts specifically on mitochondrial tRNA [Behm-Ansmant et al., 2004].

In human, the RluA family includes four proteins, RPUSD1-4, which contain a conserved HRLD motif including D as the catalytic aspartate. The exception to this is RPUSD3 which does not carry the catalytic aspartate and is therefore potentially not an active PUS protein [Borchardt et al., 2020]. RPUSD3 and 4 both localize to mitochondria [Antonicka et al., 2016] where RPUSD4 accumulates in RNA granules where it is involved in the biogenesis of the mitoribosome large subunit by binding mitochondrial 16S rRNA [Zaganelli et al., 2017]. Furthermore, RPUSD4 was observed in a localization screen of over 500 human proteins to localize partially to the nucleus, however, no functional analysis was performed [Stadler et al., 2013].

TruD family

While **Pus7** is the only member of the TruD family, it is one of the most studied pus enzymes with a variety of substrates. It targets a variety of tRNAs at position U13 including tRNA^{Asp}, tRNA^{Gly}, tRNA^{Glu}, tRNA^{His}, tRNA^{Pro} and tRNA^{Val} as well as U35 in pre-tRNA^{Tyr} [Decatur and Schnare, 2008]. Furthermore, it modifies 5S ribosomal RNA at position 50 [Decatur and Schnare, 2008], U35 in U2 snRNA [Ma et al., 2003] and was recently found to modify coding RNA as well [Schwartz et al., 2014, Carlile et al., 2014, Lovejoy et al., 2014, Li et al., 2015]. Based on its target sequences, a Pu(G/C)UN Ψ APu (Pu = purine, N = any nucleotide) consensus motif was proposed [Behm-Ansmant et al., 2003] which was later revised to UGUUAR [Schwartz et al., 2014]. Recently, the crystal structure of yeast Pus7 was solved highlighting the requirement of the consensus sequence as well as a preference for less structured substrate RNAs [Purchal et al., 2022]. This study revealed

that Pus7 acts promiscuously on any available RNA that contains its consensus motif which explains its substrate heterogeneity. Moreover, a role of Pus7 in stress response was suggested when it was shown that it inducibly targets U2 snRNA at position 56 upon heatshock or nutrient deprivation [Wu et al., 2011] which is accompanied by a reduction in both Pus7 mRNA and protein levels as well as a relocalization to the cytoplasm [Schwartz et al., 2014]. These inducible sites play a role in pre-mRNA splicing, perhaps by mediating structural changes in U2 snRNA [van der Feltz et al., 2018]. Recently, an additional role of mammalian PUS7 in translational regulation was discovered. [Guzzi et al., 2018] identified a set of 18 nt long tRNA-derived fragments (tRFs) that are modified by PUS7 in their consensus sequence at position 8. tRFs are short regulatory non-coding RNAs that originate from tRNAs and can fulfill several roles as miRNAs, by binding to RBPs or in translational regulation [Yu et al., 2021]. PUS7-modified tRFs were shown to inhibit translation initiation by binding to PABPC1 and thereby displacing the translation initiation factors eIF4A/G and E from the m7G cap of mRNAs. Loss of PUS7 leads to an increase in protein synthesis of genes involved in multiple developmental processes resulting in impaired differentiation [Guzzi et al., 2018]. In addition to positions 13 and 35 in tRNAs, mammalian PUS7 was shown to also modify U50 in several tRNA isoforms, for example tRNA^{Arg}_{CCG-2-1}, in glioblastoma cancer indicating cell type-specific tRNA pseudouridylation [Cui et al., 2021].

1.4.4 Functions of pseudouridine in canonical Ψ sites

The abundance of non-coding RNA in the cell as well as their high density of RNA modifications rendered them an obvious focus point of research in the early days of the epitranscriptomics field. While lots of knowledge has been gathered about RNA modifications in non-coding RNAs in the past decades, surprisingly little is known about their functions. The current knowledge about the functions of pseudouridine in the so-called 'traditional sites' in rRNA, snRNA and tRNA is discussed in this section (Figure 6).

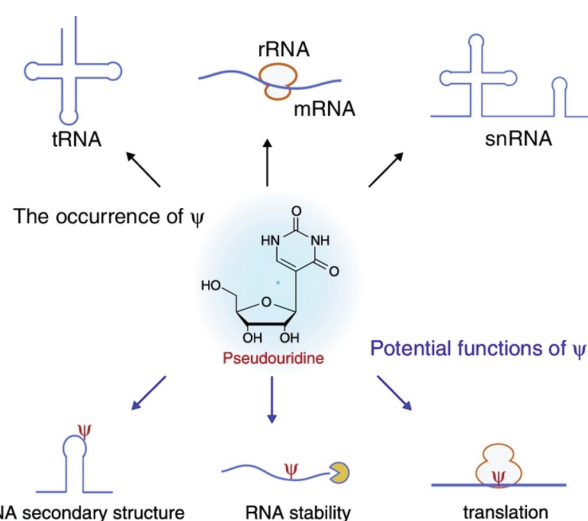


Figure 6: Occurrence and functions of Ψ in non-coding and coding RNA. Figure from [Li et al., 2016a].

Functions of Ψ in rRNA

The structure of ribosomal RNA has been determined approximately two decades ago starting with bacterial rRNA from *T. thermophilis* and eukaryotic rRNA from yeast [Trakhanov et al., 1987, Cate et al., 1999, Yusupov et al., 2001, Decatur and Fournier, 2002]. The enrichment of modified nucleosides in rRNA was abundantly clear with approximately 0.9-1.4% of Us in rRNA of the large ribosomal subunit being modified to Ψ resulting in an approximately 5-fold enrichment compared to total RNA [Charette and Gray, 2000]. Furthermore, it was known from mapping studies that conserved modified sites localized predominantly to functionally important regions like the peptidyl transferase center, the A, P and E sites of tRNA- and mRNA binding, the polypeptide exit tunnel, and sites of subunit-subunit interactions [Brimacombe et al., 1993, Charette and Gray, 2000, Decatur and Fournier, 2002]. However, the limited resolution of early structural studies did not yet allow visualization of atomic details like side chain modifications.

Thanks to technical improvements, by now full structures of bacterial and human rRNA subunits have been resolved at sufficient resolution to allow the identification of rRNA modifications [Polikanov et al., 2015, Natchiar et al., 2017]. This revealed that many RNA modifications are enriched in structurally more flexible regions like bulges, hairpin loops and RNA helices that benefit from modifications adding hydrogen bond donors for stabilization [Natchiar et al., 2017]. The roles of pseudouridine in non-coding RNA have been extensively studied in helix 69. This helix of the large ribosomal subunit is enriched in conserved pseudouridines and performs multiple functions including interactions with the small subunit via the intersubunit bridge B2a [Yusupov et al., 2001]. Also, it interacts with tRNAs [Moazed and Noller, 1989] to ensure tRNA translocation and translation fidelity [Hirabayashi et al., 2006]. Bacterial helix 69 contains three Ψ sites at positions 1911, 1915 and 1917 catalyzed by RluD which are conserved among the three kingdoms [Jiang et al., 2015]. Loss of Ψ at these sites by mutation of RluD causes defects in ribosomal assembly culminating in a growth phenotype in *E. coli* [Gutgsell et al., 2005]. Interestingly, the purpose of Ψ at these sites is not to improve structural stability. It was shown that the three Ψ sites individually stabilize and destabilize the helix depending on their neighbouring sequences and overall do not increase the stability of helix 69 under normal conditions [Meroueh et al., 2000, Sumita et al., 2005]. However, they provide a significant increase in stability at low pH conditions [Jiang et al., 2015] which is likely representing structural conformational changes of the ribosome that are adopted during translation [Abeyasinguwardena and Chow, 2008]. The conservation of these Ψ sites indicates that they might convey a conserved function in structural dynamics of the ribosome in eukaryotes. Furthermore, a role in base-stacking has been attested to these Ψ sites [Desaulniers et al., 2008] which if manipulated by point mutations in the flanking sequences lead to frameshifting indicating the role of helix 69 in translational fidelity [O'Connor and Dahlberg, 1995]. Moreover, at least one of the Ψ sites plays a role in translation termination since lack of all three sites causes drastic increases in readthrough of termination codons [Ejby et al., 2007].

Another role in translation was proposed by [Baudin-Baillieu et al., 2009] who took advantage of the fact that in higher eukaryotes all Ψ sites in rRNA are modified via H/ACA snoRNP complexes.

They separately removed snoRNAs corresponding to certain domains of the rRNA including the E, P and A sites, where loss of Ψ caused reduced translation accuracy or only the A and P sites where it would lead to stop codon readthrough and frameshifting. Finally, pseudouridine is involved in the maturation of 18S rRNA in yeast where U1248 is hypermodified to m¹acp³ Ψ 1248. Removal of the snoRNA responsible for this isomerization caused a drastical slowdown in the final maturation cleavage of 18S rRNA [Liang et al., 2009]. Interestingly, this site is conserved in humans indicating that it could fulfill a similar role in higher eukaryotes [Brand et al., 1978].

Functions of Ψ in snRNA

The amount of modifications in snRNAs increases greatly with increasing organism complexity. While yeast U1, U2, U4, U5 and U6 snRNAs contain only six constitutive Ψ sites and no 2'-O-methylations [Reddy et al., 1988], human snRNAs contain 27 Ψ s, 30 2'-O-methylations, three m6As and one m2G [Borchardt et al., 2020]. Nevertheless, the fact that all modified positions in yeast are strictly conserved in vertebrates suggests conserved functions [Adachi and Yu, 2014]. While the functions of some pseudouridines in snRNA have been described, their exact roles remain mostly mysterious. The effect of pseudouridines in snRNAs on splicing is discussed in this section. The first step in splicing is marked by the interaction of the 5' end of the U1 snRNP with the 5' splice site of the pre-mRNA [Kondo et al., 2015]. Yeast U1 snRNA carries two pseudouridines within the first 10 nucleotides of its sequence at positions 5 and 6 [Massenet et al., 1999]. While vertebrate U1 snRNA contains additionally Am1, Um2 and Am70, the two Ψ sites are strictly conserved indicating important functions [Kiss et al., 2004, Gu et al., 2005]. In fact, these Ψ sites were reported to improve RNA-RNA interactions between U1 snRNA and the pre-mRNA to facilitate splicing of weak atypical 5' splice sites [Roca and Krainer, 2009].

In the next step, U2 snRNP base-pairs with the intron branchpoint sequence of the pre-mRNA forming the so-called complex A together with U1 snRNP [Query et al., 1997]. Yeast U2 snRNA contains three Ψ sites at the branch site recognition region (BSRR) at positions 35, 42 and 44 whose catalysis is shared between standalone and guide RNA dependent pus enzymes [Ma et al., 2003]. These Ψ sites were shown to be directly stabilizing the interaction with the pre-mRNA 5' splice site [Newby and Greenbaum, 2001]. A special role was attested to Ψ 35 of the BSRR catalyzed by Pus7 since deletion mutants featured drastic defects in splicing and growth [Yang et al., 2005]. More importantly, at this position pseudouridine was shown to significantly change and stabilize the structure in the splicosomal branch site to an extrahelical orientation which brings the nucleophilic adenosine into an accessible position allowing the first step of splicing [Newby and Greenbaum, 2001, Newby and Greenbaum, 2002]. In both yeast and vertebrates, U2 snRNA is consistently the most modified snRNA [Borchardt et al., 2020]. In mammals, U2 snRNA is heavily modified with 14 pseudouridines, 10 2'-O-methylations and one m6Am site [Morais et al., 2021]. Moreover, the role of Ψ in pre-mRNA splicing in U2 snRNA was shown to be conserved in vertebrates. First of all, vertebrate U2 snRNA has multiple conserved Ψ sites which are essential for the biogenesis of the spliceosome [Yu et al., 1998]. Notably, almost all Us at the branch site recognition region which interacts with the

pre-mRNA branch site for splicing are modified to pseudouridine. However, not only Ψ but also 2'-O-methylations are strictly required for splicing in vertebrates [Zhao and YI-TAO, 2004, Dönmez et al., 2004] which are not present in yeast U2 snRNA [Morais et al., 2021]. Interestingly, U2 snRNA contains inducible Ψ sites at positions 56 and 93 by Pus7 and snR81, respectively. Both sites can be induced by nutrient deprivation [Wu et al., 2016b] while position 56 can only be induced by heatshock [Wu et al., 2011]. A recent study reported that Ψ at these positions promotes structural changes [van der Feltz et al., 2018] which are potentially aiding pre-mRNA splicing.

In the meantime, the U2 auxiliary factor U2AF recognizes the 3' splice site [Ruskin et al., 1988, Wu et al., 1999] and U4, U5 and U6 snRNPs form the U4/U6.U5 tri-snRNP particle. Here, U4 and U6 snRNAs perform extensive base-pairing [Hashimoto and Steitz, 1984]. Human U4, U5 and U6 snRNAs contain three Ψ sites each at positions 4, 72 and 79 [Zerby and Patton, 1997], 43, 46 and 53 [Krol et al., 1981] as well as at 31, 40 and 86, respectively [Epstein et al., 1980]. In U4 and U6 snRNA these Ψ sites are located in the regions of base-pairing indicating that they could stabilize this interaction, however, experimental proof is lacking. Eventually, the interaction between U4 and U6 snRNA needs to be actively separated by a helicase to progress spliceosome assembly [Raghuathan and Guthrie, 1998]. After unwinding of the U4/U6 snRNA duplex, the U4/U6.U5 tri-snRNP joins complex A to form the fully assembled ribosome called complex B [Boehringer et al., 2004]. Now, U5 snRNA interacts with pre-mRNA at the 5' and 3' splice sites through a conserved loop (GmCCUUmU Ψ ACm Ψ) containing two Ψ sites [Newman and Norman, 1992, Frank et al., 1994, Szkukalek et al., 1995]. While both the Ψ 99 as well as the loop sequence GCCUUU Ψ AC are conserved in U5 yeast snRNA, no clear function has been attributed to these sites.

Before the first step of splicing occurs, U1 and U4 snRNAs leave the spliceosome and U2, U5 and U6 snRNA interact with the pre-mRNA and with each other in the mature spliceosome. U2 and U6 snRNA form three short base-paired duplexes which contain multiple Ψ sites and are part of the catalytic center of the spliceosome [Zhang et al., 2018a]. These Ψ s were proposed to slightly contribute to the dynamics and conformation of the U2-U6 snRNA helices by stabilizing their structures, however, the impact is so slim that researchers deemed it more likely that they improve RNA-protein interactions [Karunatilaka and Rueda, 2014]. Following the structural rearrangement, the first transesterification reaction occurs leading to complex C containing splicing intermediates [Jurica et al., 2004]. Finally, the second transesterification reaction generates mature mRNA and lariat introns [Will and Lührmann, 2011].

Functions of Ψ in tRNA

Among non-coding RNAs, tRNAs are the most heavily modified RNA species with up to 25% of nucleotides being modified [Boccaletto et al., 2022]. Among those, Ψ sites are the most frequent RNA modification accounting for 4% of nucleotides in yeast tRNA [Davis and Allen, 1957]. While modification stoichiometries can vary between tRNA species, certain Ψ sites are considered as universally modified due to their high abundance and modification rate. This is the case for the universally conserved Ψ 55 which gave the T Ψ C loop its name. While its exact function is not understood, it

likely stabilizes the tRNA tertiary structure by enabling the formation of hydrogen bonds with the G18 in the opposing D loop [Kim et al., 1974].

Another highly abundant Ψ site is found at position 13 in the distal D stem where it base pairs with position 22 to stabilize this tRNA domain [Charette and Gray, 2000, Urban et al., 2009, Chawla et al., 2015]. Especially when paired with U or G, Ψ has more stable basepairing with the four canonical base pairs compared to an unmodified U [Hudson et al., 2013, Kierzek et al., 2014]. In line with this, Ψ 13 is present in 96% and 75% of tRNAs when position 22 is occupied by U or G, respectively, strongly indicating a stabilizing role at this position [Kaya and Ofengand, 2003].

A similar role in the stabilization of tRNA domains was attributed to pseudouridines in the anticodon arm which can contain multiple Ψ sites depending on the tRNA species. Here, Ψ 39 in the stem loop of tRNA^{Lys} could singlehandedly increase the melting temperature by 5°C [Durant and Davis, 1999]. This was attributed to increased base stacking but it was also likely enhanced by the formation of hydrogen bonds with water molecules [Arnez and Steitz, 1994] as well as keeping the ribose moiety in a C3'-endo conformation which extends onto neighboring nucleotides in the stem [Davis, 1995]. The combination of these properties of Ψ reinforces the more stable alpha-helical form in the anticodon loop [Lorenz et al., 2017]. Surprisingly, while Ψ 38 is present in at least 19 cytoplasmic tRNAs, only the lack of Ψ 38 in tRNA^{Gln}_{UUG} was responsible for a growth defect suggesting that certain tRNA species are more susceptible to a lack of RNA modification-dependent stabilization than others [Han et al., 2015]. Additionally, a green fluorescent protein (GFP) reporter assay revealed that Ψ 39 modified tRNA^{Trp}_{CCA} and tRNA^{Leu}_{CAA} can act as UAG nonsense suppressor tRNAs suggesting a role in decoding.

Summed up, many factors affect tRNA stability and folding rendering it oftentimes difficult to measure significant effects of individual RNA modifications. Regularly, deletion strains of RNA modifying enzymes do not generate phenotypes under normal growth conditions [Han et al., 2015]. Instead, multiple modified sites have to be removed as it has been demonstrated for the combined stabilizing effect of Ψ s catalyzed by Pus3 and Pus4 [Copela et al., 2006]. While the functions of some abundant tRNA modifications including few highly abundant pseudouridines have been unveiled, it has become clear that there is a surprising lack of knowledge especially regarding rare modifications which are often exclusive to certain tRNA species. The fact that different tissues or cell types express a different set of tRNA species or isodecoders adds an additional layer of complexity to this problem [Plotkin et al., 2004, Dittmar et al., 2006]. On top of this tRNA heterogeneity, [Brandmayr et al., 2012] revealed that different modifications can be over- or underrepresented in certain tissues, perhaps to accommodate translation of cell-type specific translatomers.

The effect of Ψ on RNA-protein interactions

While the effects of pseudouridine on RNA-RNA interactions have been discussed in various examples, some effects on RNA-protein interactions have been described. It was shown that pseudouridine can indirectly regulate the binding affinity of RBPs by reducing the flexibility of the RNA backbone in modified sequences. This was reported for toxic CUG repeats which play a central role in the

development of myotonic dystrophy where pseudouridylation reduced the binding of splicing proteins of the MBNL family [deLorimier et al., 2014, deLorimier et al., 2017]. Sequestration of these splicing factors into aggregates is a crucial step in the development of the disease.

Another example is the artificial pseudouridylation of polypyrimidine tracks of introns in pre-mRNAs which was shown to inhibit binding of the splicing factor U2AF65 [Chen et al., 2010]. Similarly, artificial pseudouridylation of U7 snRNA impairs efficient U7 snRNP formation which is necessary for the maturation of histone pre-mRNAs [Kolev and Steitz, 2006]. While these examples constitute changes in backbone rigidity, similar consequences as a result of stabilized RNA structures were reported. [Wu et al., 2016a] observed that two naturally occurring Ψ s in the branch site stem loop of U2 snRNA stabilized the binding of the yeast RNA helicase Prp5 which is required for efficient spliceosome assembly. While in these examples Ψ merely had an indirect effect through modulating RNA structure or rigidity, it can also directly modulate RBP binding.

Members of the PUF RNA-binding protein family (Pum) are involved in translational repression of mRNAs by binding their 3' UTR sequences at an 8-nt UGUANAUA core motif and play important roles for example in early embryogenesis of *Drosophila* [Murata and Wharton, 1995, Galgano et al., 2008]. Strikingly, both the presence of m6A or pseudouridine in modified RNA oligos reduced the binding affinity of human PUM2 in a cumulative manner with increasing number of modified sites [Vaidyanathan et al., 2017]. Interestingly, the hPUM2 consensus motif overlaps with the PUS7 UGUAR consensus motif suggesting that PUS7 dependent pseudouridines might affect hPUM2 binding. However, based on data from transcriptome-wide Ψ mapping, no candidate mRNAs could be identified that are both hPUM2 targets and pseudouridylated. Therefore, the biological relevance of this finding remains uncertain.

1.5 Human Ψ synthases with a role in disease

A growing interest in human Ψ synthases can be observed since multiple PUS enzymes have been linked to human disease including DKC1, PUS1, PUS3 and PUS7. The current knowledge about their clinical pictures and potential causes are discussed below.

Mutations in DKC1 cause Dyskeratosis congenita

Dyskeratosis congenita (DC) is a multigenic systemic disease that typically leads to nail dystrophy, leukoplakia and hyperpigmentation [AlSabbagh, 2020]. Molecularly, it is caused by a progressive shortening of the telomeres resulting in a loss of their self-renewal capability with more severe phenotypes being proportional to the shortening of telomere lengths [Alter et al., 2012]. The leading cause of death is bone marrow failure syndrome as a result of telomere shortening [Powell et al., 2014] which eventually leads to a decrease in the count of all blood cells. This can, in turn, cause further complications including anemia as well as bleeding and opportunistic infections [Angurana et al., 2014]. While it is a multigenic disease, most cases are caused by hereditary point mutations

in the DKC1 gene encoding the mammalian RNA-dependent Ψ synthase [AlSabbagh, 2020]. Since DKC1 is encoded on the X chromosome, X-linked DC is 13-fold more common in males [Kumar and Suthar, 2013]. Under normal circumstances, telomeres are renewed by reverse transcription of the telomerase RNA component (TERC RNA) by the telomerase enzyme complex consisting of hTERT and the accessory proteins DKC1, NOP10, NHOP2 and GAR1 [Cong et al., 2002]. Mutation of DKC1 in DC patients leads to a destabilization of telomerase RNA which is causative for DC pathophysiology in vivo [Zeng et al., 2012]. While DC is a rare disease with a prevalence of 1:1.000.000 in neonates [Cong et al., 2002], hundreds of patients have been described since the first patient description in 1906 [Zinsser, 1910].

Clinical features of PUS1 patients

Mutations in PUS1 have been observed in a total of 16 patients with 8 different homozygous variants causing myopathy, lactic acidosis, and sideroblastic anemia (MLASA) [Cao et al., 2016, Metodiev et al., 2015, Casas et al., 2004, Tesarova et al., 2018, Zeharia et al., 2005, Inbal et al., 1995, Fernandez-Vizarra et al., 2006, Oncul et al., 2021, Bykhovskaya et al., 2004]. The MLASA syndrome is a rare mitochondrial disorder with variable features typically consisting of failure to thrive, developmental delay and intellectual disability. Additionally, cognitive impairment, skeletal and dental abnormalities, delayed motor development and cardiomyopathy can arise among other symptoms. The most common type of MLASA syndrome is caused by mutations in the PUS1 gene resulting in hypomodification of mitochondrial tRNAs. Other variants of MLASA are caused by mutations in the YARS2 gene encoding a mitochondrial tyrosyl-transfer RNA synthetase [Riley et al., 2010] or in the ATP6 gene encoding a subunit of the mitochondrial ATP synthase [Burrage et al., 2014]. A common defect observed across all types of MLASA is a decrease in mitochondrial respiration indicative of defective mitochondrial protein synthesis. Interestingly, the defects caused by MLASA mostly affect the brain and muscles. It is intriguing to speculate that these tissues are impacted due to high expression of PUS1, YARS2 and ATP6 [Bykhovskaya et al., 2004], however, it cannot be ruled out that these tissues are merely more dependent on mitochondrial function than other tissues.

Clinical features of PUS3 patients

So far, 21 individuals with 17 different variants of PUS3 have been identified featuring a clinical picture dominated by global developmental delay, hypotonia, microcephaly, intellectual disability and motor delay often accompanied by speech delay [Gulkovskiy et al., 2015, Shaheen et al., 2016, Al-fares et al., 2017, Abdelrahman et al., 2018, Fang et al., 2019, de Paiva et al., 2019, Froukh et al., 2020, Nøstvik et al., 2021]. The occurrence of seizures is unique to mutations in PUS3 compared to defects in other PUS enzymes. The brain-centric clinical features of PUS3 mutation depict a clear picture of neurodevelopmental disease.

Clinical features of PUS7 patients

Patients carrying mutations in PUS7 have been the most recent addition to the spectrum of PUS dis-

eases. The first patients were described by our collaborators in 2018 and since then multiple studies identified new patients by performing whole genome or whole exon sequencing. By now, 16 different patients with 9 different variants of PUS7 have been described [de Brouwer et al., 2018, Darvish et al., 2019, Shaheen et al., 2019, Naseer et al., 2020, Han et al., 2022, Muda et al., 2023] featuring intellectual disability, microcephaly, developmental delay and speech delay often accompanied by short stature. Some patients additionally suffer from hyperactivity, visual problems, hearing problems and hypotonia. Aggressive or self-harming behavior depicts the hallmark of PUS7 mutation compared to other PUS diseases.

A striking similarity in the clinical features of PUS3 and PUS7 patients can be observed with patients of both diseases featuring microcephaly, intellectual disability and developmental delay. Both diseases mostly affect the brain, yet they feature specific hallmarks in their clinical phenotypes like aggression or seizures for PUS7 and PUS3, respectively. Further, patients of both syndromes suffer from sensory defects. Yet, in PUS7 patients this is more pronounced in the auditory system while PUS3 patients suffer frequently from visual problems. Mutation in PUS1 causes similar neurodevelopmental defects, however, at lower frequencies and at lower severity while leading to broader phenotypes with a stronger impact on muscle tissue including respiratory chain deficiencies and muscle hypotrophy (Table 1.1).

The mechanisms causing the brain-related phenotypes in PUS patients are not yet understood. It is intriguing to speculate whether this might be caused by the target-specificities of different PUS enzymes. While PUS1, PUS3 and PUS7 all target non-coding RNAs, they feature distinct specificities with PUS1 and PUS3 targeting both cytoplasmic and mitochondrial tRNAs while PUS7 is exclusively targeting cytoplasmic tRNAs. It is clear that at least some of the defects upon mutation in PUS1 are caused by mitochondrial dysfunction since the clinical picture of MLASA syndrome are similar upon PUS3, YARS2 and ATP6 mutation. Furthermore, the brain has been suggested to be especially susceptible to mitochondrial translation defects [Torres et al., 2014]. Mitochondrial dysfunction could be a common defect between PUS1 and PUS3 mutation. However, if mitochondrial dysfunction was conserved between all PUS diseases, it is unclear how loss of PUS7 could cause it. On the other hand, the underlying mechanism could be more complex than tRNA hypomodification. All three PUS enzymes were shown to target sites in mRNA. A GO term analysis of pseudouridylated sites in human mRNA revealed a striking enrichment of transcripts involved in translation or translation-related processes [Li et al., 2015]. Therefore, Ψ sites in mRNA might be generally involved in regulating gene expression of proteins involved in translation independent of the tRNA pseudouridylation role of the PUS enzyme in question.

Pseudouridine and PUS enzymes as biomarkers

RNA modifications have been suggested for the use as biomarkers to identify disease states very early as their degradation into free modified nucleosides floating in the blood stream and eventual urinary secretion could be quantified by mass-spectrometry in patients for diagnostic use [Xu et al., 1999].

Table 1.1: Clinical pictures of PUS patients. ID: Intellectual disability. *: aggression could be caused by psychosis in one patient. #: auditory hallucinations in one patient. ¹: Data obtained from [Nøstvik et al., 2021] with addition of data from [Borghesi et al., 2022].

PUS enzyme	ID	Microcephaly	Growth delay	Hyperactivity	Aggressive behavior
PUS1	10/16	5/16	7/16	1/16	1/16
PUS3	20/20 ¹	14/19 ¹	9/11	2/10	1/11*
PUS7	16/16	13/15	11/15	3/15	13/16
	Motor delay or impairment	Visual problems	Hearing problems	Speech delay	Failure to thrive
PUS1	13/16	4/16	1/16	0/16	6/16
PUS3	16/18 ¹	9/12	3/11 [#]	11/12 ¹	7/11
PUS7	12/16	2/15	6/15	16/16	10/13
	Short stature	Hypotonia	Facial abnormalities	Seizures	MLASA
PUS1	10/16	6/16	8/16	0/16	16/16
PUS3	11/18 ¹	11/14 ¹	18/19 ¹	14/19 ¹	0
PUS7	10/15	06/15	13/15	1/15	0
	Skeletal abnormalities	Muscle hypotrophy	C1/3/4 deficiency		
PUS1	1/16	5/15	5/12		
PUS3	0	0	0		
PUS7	0	0	0		

Since modified nucleosides are not substrates of salvage pathways, they are excreted in the urine at increased ratios facilitating their detection [Schram, 1998]. A growing amount of evidence is linking pseudouridine and the expression of PUS synthases to roles in cancer. For example, three independent studies identified PUS1 as a biomarker in breast cancer, hepatocellular carcinoma and renal cell carcinoma where it is overexpressed. In all cases, PUS1 expression levels are negatively correlated with patient survival as well as relapses and positively correlated with invasion capability [Fang et al., 2022, Lan et al., 2023, Li et al., 2023].

Similar observations have been made for PUS7 where its pseudouridine-dependent and pseudouridine-independent functions have been elucidated in more detail. PUS7 was found to be upregulated in colorectal cancer (CRC) where it is stabilized by directly interacting with HSP90 to prevent proteasomal degradation of PUS7 [Song et al., 2021]. Furthermore, PUS7 regulates expression of the transcriptional regulator LASP1 [Butt and Raman, 2018] in a pseudouridylation-independent manner, thereby enhancing the ability of CRC to metastasize. While its expression is negatively correlated with patient survival, the exact mechanism of action has not been understood. [Du et al., 2021] proposed that PUS7 is important for cell proliferation and the invasion ability of CRC by activating PI3K/AKT/mTOR signaling by regulating the phosphorylation levels of proteins in this pathway. Additionally, [Zhang et al., 2023] found that PUS7 promotes SIRT1 stability by directly interacting with each other [Dalal et al., 2019] and acting as an oncogene in multiple tumors [Luo et al., 2019] by stimulating the Wnt/ β -catenin pathway. Another recent study has also gained insights about the role of PUS7 in promoting glioblastoma growth. Similar to other cancer types, PUS7 was found to be overexpressed in glioblastoma stem cells (GSCs) compared to normal brain tissue. Here, [Cui et al., 2021] showed that PUS7 promotes cell growth by negatively regulating the expression of tumor

suppressor genes. They found that PUS7 modifies 13 sites at positions 13, 35 and 50 in eight tRNA species including tRNA^{Arg}_{CCG}. Surprisingly, polysome profiling revealed that the translation of Pus7 modified tRNA^{Arg}_{CCG} codons is increased upon PUS7 KO. This and other codons served by PUS7 dependent tRNAs were enriched in proteins including the tumor suppressor TYK2 [Moritsch et al., 2022] and promoted their translation upon PUS7 KO. However, how hypomodification of tRNAs promotes the translation of proteins enriched in the respective codons remains unknown. TYK2 regulates the interferon pathway and therefore induced the expression of interferon stimulated genes which are negatively correlated with tumorigenesis in GSCs [Zhu et al., 2020]. Therefore, inhibition of PUS7 could serve as a therapeutic treatment to arrest growth and proliferation of GSCs by upregulating the translation of tumor suppressor genes and interferon stimulated genes. As such, it is no surprise that pseudouridine levels as well as PUS1 and PUS7 expression levels have been proposed as biomarkers for cancers [Mohl et al., 2023].

Apart from PUS1 and PUS7, PUS10 was also predicted to be involved in multiple diseases. First of all, PUS10 expression was identified as a risk factor for Crohn's disease and celiac disease, however, the causative link is not understood [Festen et al., 2011]. Additionally, it was found to play a role in prostate cancer by regulating TRAIL-induced apoptosis [Jana et al., 2017]. In contrast to PUS1 and PUS7, PUS10 expression is reduced in multiple cancers where it would otherwise have a diminishing effect on cancer progression by promoting apoptosis. Similarly, [Ji et al., 2020] found that reduced expression of PUS10 enhanced the development of lung tumors as a result of reduced apoptosis, thereby promoting cancer immortality. Apart from its role in cancer, PUS10 was found to play a role in the aging process of hematopoietic stem cells. Here, PUS10 expression is a hallmark of aged HSC identity as a result of an aging-related decline in ubiquitination-dependent PUS10 degradation [Wang et al., 2020]. Finally, multiple studies have proposed Ψ levels as biomarkers for other diseases. For example, Ψ levels in the urine were proposed to predict alzheimers disease [Lee et al., 2007], in the plasma of patients it could predict chronic kidney disease [Sekula et al., 2017] as well as the development of heart failure [Razavi et al., 2020]. In contrast, low levels of Ψ were used to predict post-stroke depression in diabetes mellitus patients [Liang et al., 2019].

1.6 Other indications of Ψ in neuronal function.

A recent study by [Song et al., 2020b] has revealed neuronal functions for both RluA-1 and RluA-2 in *Drosophila* nociception. While RluA-1 has been identified to be specifically expressed in multi-dendritic (MD) neurons [Wang et al., 2011] which are relevant for nociception [Tracey et al., 2003], RluA-2 shows a ubiquitous expression pattern. However, loss of either of the enzymes increases thermal pain sensitivity in *Drosophila* larvae and leads to hyperbranching of nociceptor neurons accompanied by reduced branching lengths. While both enzymes share a nuclear localization and act in nociception, they do not act redundantly, and RluA-2 likely fulfills other additional functions in other cell types. [Song et al., 2020b] suggested that *Drosophila* RluA pus enzymes might regulate

neuronal morphogenesis by affecting mRNA granule transport or translation of transported mRNAs by affecting binding of RBPs.

1.7 Expression of cytoplasmic tRNA genes

1.7.1 tRNA transcription and maturation

In order to decode the 20 canonical amino acids plus a stop signal, at least a three letter code with four options per position is necessary. As a result, 64 possible mRNA codons exist with 61 codons encoding the 20 amino acids and the remaining three stop codons acting as stop signals. Therefore, the genetic code is degenerate, as most amino acids are encoded by more than one codon, with the exceptions of methionine (AUG) and tryptophane (UGG). To accommodate different codons corresponding to the same amino acid, tRNA isoacceptors have evolved. These isoacceptors are tRNA molecules that are charged with the same amino acid but contain different anticodons. Additionally, these tRNAs can differ in their tRNA body sequence giving rise to distinct tRNA isodecoders. Although only 64 codons are necessary, the human genome contains a seemingly excessive number of 429 tRNA genes to decode them [Chan and Lowe, 2016]. For example, in the human genome 35 genes exist solely for tRNA^{Ala}_{AGC} including all the isodecoders associated with this isoacceptor [Chan and Lowe, 2016]. This is in stark contrast to the compact mitochondrial genome, where only 22 tRNA genes exist, one for each amino acid except serine and leucine, which have two genes encoding distinct isoacceptors [Suzuki et al., 2020]. As a result of this lack of redundancy, posttranscriptional modifications and non-canonical base-pairing play important roles to allow one mitochondrial tRNA anticodon to decode multiple mRNA codons. Since the main body of this work focuses on the Pus7-dependent modification of cytoplasmic tRNAs, this section will focus on the steps involved in cytoplasmic tRNA expression which differs from mitochondrial tRNA expression. Moreover, certain steps in tRNA maturation are distinct between yeast and higher eukaryotes. In order to create a basis of understanding to discuss the effect of mutations in tRNA processing in human disease, this section will focus on the steps observed in higher eukaryotes.

tRNA genes are transcribed by RNA polymerase (Pol) III and are specified as type 2 Pol III genes due to the presence of conserved A and B boxes within the tRNA gene sequence [Galli et al., 1981]. These boxes encode the tRNA D and T loops and are necessary to recruit transcription factor (TF) IIIC (TFIIIC) [Lassar et al., 1983]. TFIIIC in turn recruits TFIIIB [Bieker et al., 1985, Setzer and Brown, 1985] consisting of the TATA box binding protein (TBP) [Huet and Sentenac, 1992], BRF1 [Colbert and Hahn, 1992] and BDP1 (Figure 7) [Kassavetis et al., 1995]. Next, TFIIIB recruits Pol III to initiate transcription [Kassavetis et al., 1990]. Transcription termination is triggered by the consensus termination signal consisting of four or more thymidine residues [Nielsen et al., 2013]. pre-tRNAs contain a 5' leader sequence and a 3' trailer sequence which are removed during tRNA maturation. Notably, while the length of the 5' leader of human pre-tRNAs is rather homogenous with a length of 6-10 nt, the 3' trailer length shows considerable variability with trailers of up to 40 nt

in length [Gogakos et al., 2017]. This is important in the next step of pre-tRNA maturation, where two separate mechanisms of pre-tRNA processing exist for different subsets of pre-tRNAs depending on the lengths of their 3' trailers.

In human, nascent pre-tRNAs with at least four uridines [Huang et al., 2005] are bound by the La protein which binds the UUU-OH 3' terminus with its binding pocket [Stefano, 1984, Teplova et al., 2006, Maraia and Lamichhane, 2011]. Consequently, La assists in pre-tRNA folding [Chakshumathi et al., 2003], protects the pre-tRNA against exosomal degradation and prevents premature nuclear export [Simons et al., 1996]. While La is bound to the pre-tRNA, introns in intron-containing pre-tRNAs are removed by the tRNA splicing machinery. This affects 28/429 tRNA genes in human including all 13 genes of the tRNA^{Tyr}_{GUA} and five genes each of the tRNA^{Ile}_{UAU}, tRNA^{Leu}_{CAA} and tRNA^{Arg}_{UCU} isodecoder families, respectively [Chan and Lowe, 2016].

The splicing process is performed by the TSEN complex [Trotta et al., 1997] which removes the intron resulting in 5' and 3' tRNA exon halves harboring a 2',3'-cyclic phosphate and a 5' OH terminus, respectively. These are subsequently ligated by the RTCB tRNA ligase complex [Popow et al., 2011, Dikfidan et al., 2014] in a concerted reaction with archease among other factors [Popow et al., 2014]. Simultaneously, RTCB linearizes the tRNA introns generating stable tricRNAs whose functions are still unknown [Lu et al., 2015, Schmidt et al., 2019]. The generation of tricRNAs is negatively regulated by CLP1 which associates with the TSEN complex [Paushkin et al., 2004]. CLP1 is an RNA kinase and can phosphorylate the 5' OH of the tRNA intron and the 3' tRNA exon, thereby blocking RTCB-mediated ligation of the exon halves [Popow et al., 2011, Hayne et al., 2020]. While CLP1 is not necessary for the tRNA splicing activity of the TSEN complex it might play a role in substrate recognition [Hayne et al., 2020] and stabilizes the TSEN complex [Karaca et al., 2014, Schaffer et al., 2014]. Following tRNA splicing, the La protein gets phosphorylated at serine 366 which is required for RNase P dependent maturation of the tRNA 5' end by endonucleolytic cleavage of the 5' leader [Intine et al., 2000, Xiao et al., 2002]. Subsequently, the 3' trailer is removed by endonucleolytic cleavage by ELAC2 (homologue of RNase Z) leading to dissociation of the La protein [Takaku et al., 2003].

In yeast, the La protein is not essential and a La-independent tRNA maturation pathway has been postulated. Here, pre-tRNAs possessing 3' oligo(U) termini too short for La binding are trimmed at the 3' trailer by the 3'-5' exonuclease Rex1 [Ozanick et al., 2009, Skowronek et al., 2014] followed by 5' maturation by RNase P. Hence, the 5'-3' order of tRNA end processing is reversed. The order in which intron splicing and end processing are orchestrated in the yeast pathway is not yet understood. Both pathways lead to a 1 nt overhang at the tRNA 3' end which is termed the discriminator base. Next, TRNT1 [Nagaike et al., 2001] adds the 3' CCA to allow charging by aminoacyl tRNA synthetases (aaRSs) [Hou, 2010]. Mature tRNAs are exported from the nucleus to the cytoplasm by exportin-T [Arts et al., 1998, LIPOWSKY et al., 1999] or exportin-5 [Bohnsack et al., 2004]. Before participation in translation, mature tRNAs are aminoacylated by aaRSs which recognize certain structural and sequence elements including RNA modifications which are referred to as identity determinants [Giegé and Eriani, 2023]. These tRNA modifications occur already early

on during the various maturation steps of the tRNA [Nishikura and De Robertis, 1981], probably already during La binding, as La-associated RNAs feature tRNA-like modifications [Hendrick et al., 1981].

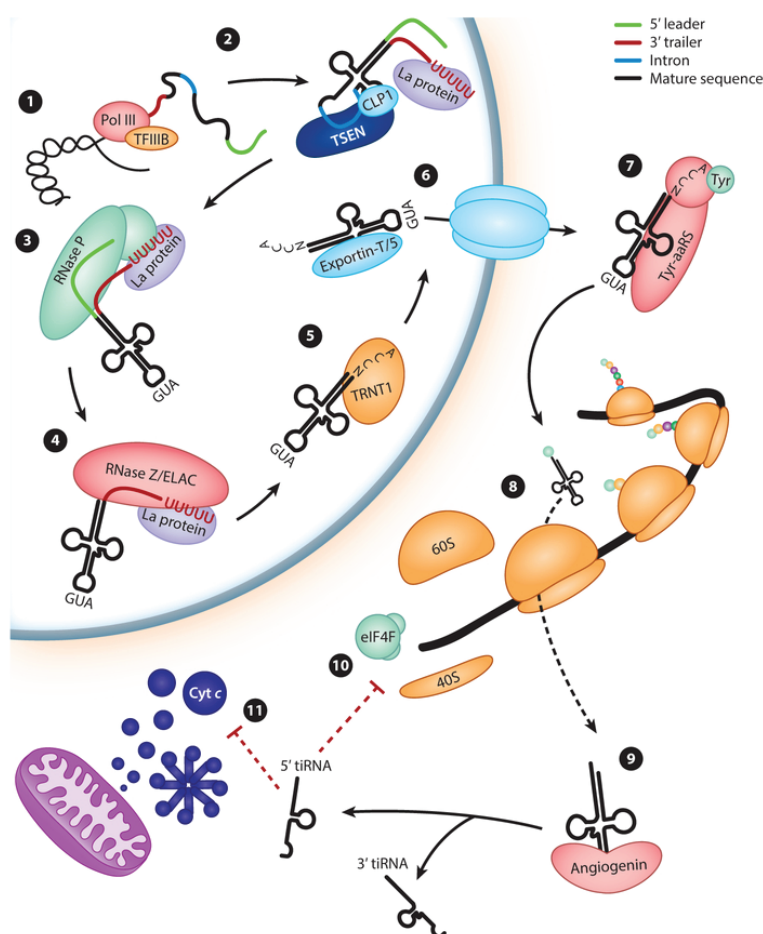


Figure 7: Processing and maturation of transfer RNA. (Step 1) RNA polymerase III (Pol III) is recruited to tRNA gene elements by the transcription factor TFIIB. The immature transcript contains 5' leader (green), intronic (blue), and 3' trailer (red) sequences. Mature sequences are shown in black. (Step 2) The La protein binds to the 3' oligouridylic acid [oligo(U)] sequence that protects against degradation by the nuclear exosome complex. TSEN and CLP1 form a complex to remove introns and ligate exonic sequences from intron-containing tRNA species. (Step 3) RNase P interacts with phosphorylated La protein to remove 5' leader sequences. (Step 4) ELAC isoforms remove 3' trailer sequences, leaving a single-nucleotide overhang termed the discriminator base. (Step 5) TRNT1 mediates the addition of CCA to the 3' terminus of immature species. (Step 6) tRNA species with proper addition of CCA as well as secondary and tertiary structure are bound by exportin-T or exportin-5. After translocation through the nuclear pore complex (light blue), the mature tRNAs are able to participate in aminoacylation. (Step 7) tRNA species are recognized by anticodon loop and acceptor stem sequences, and aminoacylation is added by cognate aminoacyl-tRNA synthetases (aaRSs). (Step 8) Aminoacylated tRNA species participate in translation through incorporation into the ribosomal A-site. (Step 9) In times of cellular stress, tRNA species may be cleaved by angiogenin into 5' and 3' tRNA halves (tiRNAs). (Step 10) The 5' tiRNA species inhibit translation initiation through competitive binding of the eIF4F complex. (Step 11) The 5' tiRNA species inhibit the formation of the apoptosome through competitive binding of cytochrome c (Cyt c). Figure and description from [Schaffer et al., 2019].

1.7.2 tRNA surveillance mechanisms

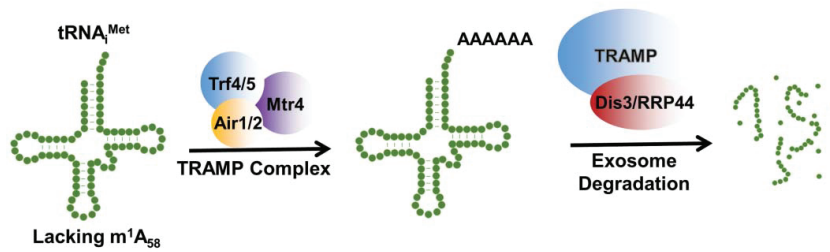
During tRNA expression, two surveillance pathways ensure the generation of correctly processed and folded tRNAs: The rapid tRNA decay (RTD) pathway and the nuclear surveillance pathway which

are both mainly studied in yeast (Figure 8).

The **RTD pathway** relies on the 5'-3' exonucleases Rat1 and Xrn1 which degrade mature tRNAs lacking structural integrity specifically in the acceptor and T stems. While many examples exist of the RTD targeting hypomodified tRNAs it is postulated that missing RNA modifications are only relevant if they are crucial for the stability of those structures [Whipple et al., 2011]. In such cases, the CCA-adding enzyme adds 2x CCA to hypomodified or unstable tRNAs to mark them for the rapid tRNA decay pathway. Thus, the RTD acts as a universally conserved proofreading mechanism for end-processed and spliced mature tRNAs [Wilusz et al., 2011]. For example, lack of TRM44 and TAN1 catalyzing Um44 and ac4C12, respectively, leads to degradation of tRNA^{Ser}_{CGA} and tRNA^{Ser}_{UGA} at higher temperatures [Kotelawala et al., 2008]. Also, yeast Trm8/Trm4 double mutants lacking m7G46 and m5C49 in tRNA^{Val}_{AAC} feature rapid tRNA degradation. A similar observation was made for tRNA^{Arg}_{CCG} upon loss of both Ψ55 catalyzed by Pus4 and m²₂G26 modified by Trm1 [Copela et al., 2006, Alexandrov et al., 2006].

The RTD is conserved in fission yeast, where loss of only Trm8 is sufficient to trigger degradation of tRNA^{Tyr}_{GUA}. While studies of the RTD are almost exclusive to lower eukaryotes it might be conserved in humans where Xrn1 and the human Rat1 orthologue Xrn2 can degrade tRNA_i^{Met} upon heatshock [Watanabe et al., 2013]. In addition to Rat1 and Xrn1, Met22 has been identified as an additional factor necessary for RTD activity. However, it was proposed that Met22 only indirectly affects RTD [Chernyakov et al., 2008] since loss of Met22 causes accumulation of adenosine 3',5'-bisphosphate which inhibits Xrn1 and Rat1 [Dichtl et al., 1997].

A. Nuclear Surveillance



B. Rapid tRNA Decay

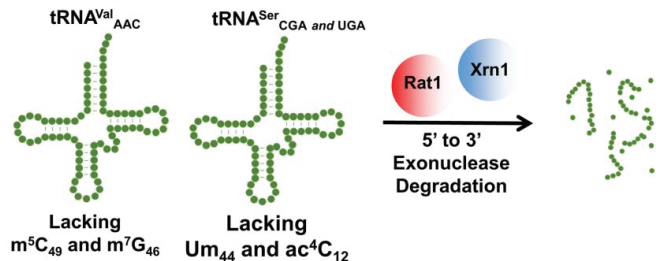


Figure 8: tRNA surveillance pathways. (A) tRNA_i^{Met} lacking m1A58 is polyadenylated by the TRAMP complex (Trf4/5, Air1/2). The helicase Mtr4 assists the TRAMP complex and targets TRAMP to the nuclear endonuclease complex consisting of several structural proteins and a 3' to 5' exonuclease. (B) The rapid tRNA decay pathway (RTD) degrades hypomodified tRNA^{Val} and tRNA^{Ser}. Figure and description from [Kessler et al., 2018].

However, a novel Met22-dependent surveillance mechanism for pre-tRNAs was recently proposed. Previously, Met22 was only implicated in the RTD targeting mature tRNAs with unstable acceptor stems resulting in exposure of the tRNA 5' end for exonucleolytic attack [Whipple et al., 2011]. Surprisingly, mutated tRNAs with destabilized anticodon stems also relied on Met22 for degradation, even though their 5' ends were not expected to be significantly destabilized, leading to an accumulation of end-processed but unspliced pre-tRNAs in Δ met22 strains. Specifically, these mutated pre-tRNAs harbored a destabilized conserved bulge-helix-bulge structure [Fruscoloni et al., 2001] formed by the anticodon stem-loop and the intron generating defective tRNA substrates for Met22-dependent RTD (MTD) [Payea et al., 2020]. Notably, tRNA end maturation precedes splicing in yeast. Therefore, the MTD pathway was proposed as an additional quality control step to check the integrity of the anticodon stem-loop and the exon-intron structure to ensure correct tRNA splicing after tRNA end processing. Eventually, this is followed by the proofreading of mature tRNAs by the RTD in yeast.

The **nuclear surveillance pathway** is not only involved in tRNA quality control [Huang et al., 2006] but also in rRNA processing and degradation [Thoms et al., 2015] as well as the regulation of histone mRNA levels [Reis and Campbell, 2007]. The central player of this pathway is the TRAMP complex consisting of a poly(A) polymerase Trf4 or Trf5, a Zn-knuckle protein Air1 or Air2 and the DExH-box helicase Mtr4 [LaCava et al., 2005, Hardwick and Luisi, 2013]. Together, the complex unwinds the substrate RNA and polyadenylates it for 3'-5' degradation via the nuclear exosome complex. During tRNA expression in yeast, La binding prevents degradation by the exosomes catalytic subunit Rrp6 [Huang et al., 2006] perhaps by masking the pre-tRNAs 3' end from polyadenylation. Consequently, pre-tRNAs lacking an oligo(U) signal which are therefore not bound by La get polyadenylated by the TRAMP complex and degraded by the nuclear exosome [LaCava et al., 2005]. In line with this, the TRAMP complex presumably degrades tRNAs very early during biogenesis since TRAMP-targeted tRNAs in yeast are not yet end-processed [Kadaba et al., 2006]. The exact mechanism of substrate recognition is not yet clear. Multiple studies have illustrated that the TRAMP complex targets destabilized tRNAs which might not be efficiently bound by La for protection. Strikingly, certain tRNAs seem to be more susceptible to destabilization upon loss of modifications. For instance, hypomodified tRNA_i^{Met}_{CAU} lacking m1A58 is readily degraded in Trm6 mutant yeast whereas hypomodified tRNA^{Leu}_{CAA} remains stable [Kadaba et al., 2004]. Surprisingly, a similar pathway exists even in bacteria where thermosensitive unstable tRNAs as a result of point mutations get polyadenylated by the poly(A) polymerase PAP and degraded by PNPase [Li et al., 2002] suggesting that this mechanism of RNA quality control is broadly conserved. Interestingly, the TRAMP complex is conserved in humans with MTR4, ZCCHC7 (Air2) and PAPD5 (Trf4) [Lubas et al., 2011, Sudo et al., 2016] and is involved in the regulation of telomerase RNA biogenesis [Nguyen et al., 2015].

1.8 The roles of tRNA fragmentation in gene expression

1.8.1 Classes of tRNA-derived small RNAs

tRNA-derived small RNAs (tsRNAs) were identified in the 1970s but initially considered as degradation products [Borek et al., 1977]. Nowadays, it is known that they fulfill a diverse set of biological functions including regulation of mRNA stability [Goodarzi et al., 2015], translation inhibition [Ivanov et al., 2011, Sobala and Hutvagner, 2013, Guzzi et al., 2018], ribosome biogenesis [Couvillion et al., 2012] and apoptosis [Saikia et al., 2014]. While tRNA fragmentation is a constitutive process in some cell types [Skorupa et al., 2012] and can occur naturally during development [Jöchel et al., 2008], most studies focus on induced tRNA cleavage in response to various stresses including amino acid deficiency, phosphate starvation, UV radiation, heat shock, hypoxia, oxidative damage, and viral infection [Fu et al., 2009, Yamasaki et al., 2009, Lee and Collins, 2005, Jöchel et al., 2008, Li et al., 2008, Thompson et al., 2008, Hsieh et al., 2009]. The catalytic cleavage is performed by several RNases including dicer, angiogenin (ANG) and other unknown enzymes. Based on their biogenesis and length, the resulting tsRNAs are grouped into two main types, the 15-32 nt long tRFs with several subclasses and 28-36 nt long tRNA-derived stress-induced RNAs (tiRNAs) [Kumar et al., 2015] (Figure 9): (1) Dicer produces tRF-5s by cutting within the D loop or inbetween D loop and the anticodon loop [Cole et al., 2009]. Depending on the cleavage site, this generates three subtypes of tRF-5s of different lengths: tRF-5a (14-16 nt), tRF-5b (22-24 nt) and tRF-5c (28-30 nt) [Kumar et al., 2014]. (2) tRF-3s are generated from the 3' end of tRNAs and therefore characteristically carry the CCA tail. They are dependent on cleavage by angiogenin or other unknown exonucleases at the T Ψ C loop. Depending on the cleavage site, two subtypes of tRF-3s exist: tRF-3a (18 nt) and tRF-3b (22 nt) subtypes [Kumar et al., 2014]. (3) tRF-1s are produced by RNase Z cleavage from the 3' UTR of the pre-tRNA and characteristically contain the oligo(U) 3' terminus [Karousi et al., 2019]. (4) tRF-2s contain only the anticodon loop, however, the responsible ribonuclease has not yet been identified [Goodarzi et al., 2015]. So far, they were found to derive from tRNA^{Glu/Asp/Gly/Tyr} and are involved in gene silencing of oncogenes in breast cancer. (5) internal tRFs (itRFs) originate by definition from the internal zone of tRNAs and never contain the 5' or 3' terminus. They comprise A-tRFs and V-tRFs which are generated by cuts in the anticodon loop and the variable loop while D-tRFs are generated by cuts in the D stem [Olvedy et al., 2016]. (6) Finally, tiRNAs are typically generated during stress conditions by cytoplasmic angiogenin in mammals [Fu et al., 2009] or Rny1 in yeast [Thompson and Parker, 2009] by cleaving the anticodon loop resulting in 28-36 nt long 5' tiRNAs or 3' tiRNAs [Li and Hu, 2012]. Notably, the stability of the generated tRNA halves can be asymmetric, meaning that in some cases either 5' or 3' fragments are detected, the other being rapidly degraded upon generation [Haiser et al., 2008, Garcia-Silva et al., 2010]. [Su et al., 2019] challenged this with experiments in human ANG knockout cells, where most stress-induced tRNA halves are generated not by ANG but by other unknown RNases. While not all tRNA cleaving enzymes have been identified, one candidate for this function is potentially human RNase L which

cleaves cytoplasmic tRNAs in the anticodon loop similar to angiogenin but closer to the 3' side of the loop [Donovan et al., 2017]. It was initially proposed that ANG-dependent tRNA cleavage occurs strictly in the presence of oxidative stress due to its constitutive inactivation by the cytoplasmic RNase inhibitor RNH1 [Yamasaki et al., 2009]. Furthermore, ANG transcription is transcriptionally upregulated during hypoxia [Lai et al., 2016] but also during other stress responses including the unfolded protein response [Pereira et al., 2010]. However, tRNA fragmentation was found to be a constitutive process in some cell types including motoneurons [Skorupa et al., 2012].

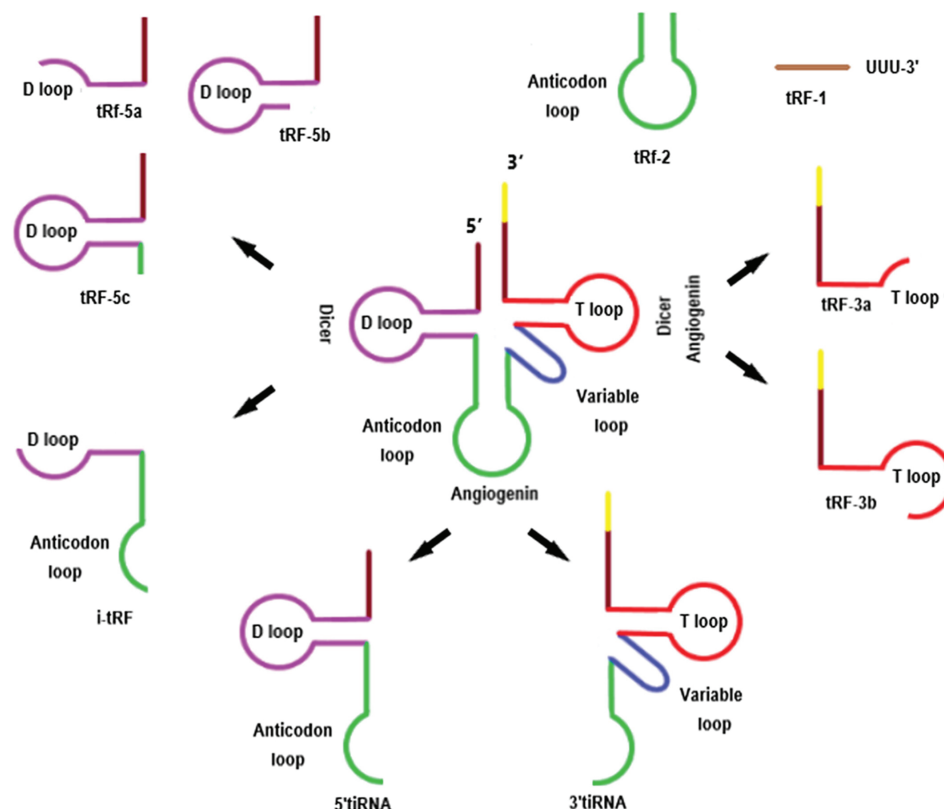


Figure 9: The biogenesis of tsRNAs. tsRNAs can be generally classified into the following two categories according to the cleavage sites in tRNAs and lengths: tiRNAs and tRFs. tiRNAs are classed by their source sequences from the 5'- or 3'-end of tRNA cleaved by ANG. tRFs are classified into three major types depending on the size and location of the source: tRF-5, tRF-3 and tRF-1. The current generation mechanisms of tRF-2s and i-tRF are still not completely clear. Figure and description from [Zong et al., 2021].

1.8.2 Effects of tRNA fragments on gene expression

In the last decades, growing evidence suggested a plethora of roles of tRNA fragments in regulating gene expression both on the transcriptional and post-transcriptional level. [Ivanov et al., 2011] identified 5' tiRNAs that inhibit translation initiation by displacing initiation factors by interacting with the mRNA binding protein YBX1. Since YBX1 usually binds and stabilizes mRNAs, this sequestration of YBX1 by tiRNAs additionally destabilizes mRNAs in breast cancer [Goodarzi et al., 2015]. A similar function in translation initiation was observed in a set of PUS7-modified 5' tRFs containing Ψ at position 8. They are enriched in mouse embryonic stem cells and necessary to inhibit

translation for the development to hematopoietic stem cells. Strikingly, [Guzzi et al., 2018] discovered that Ψ 8 is crucial for this repressive function by inhibiting the binding of YBX1 to these tRFs. Instead, Ψ -modified tRFs associate with PABPC1 which usually interacts with eIF4G to enhance eIF4F formation and stimulate translation. Therefore, PUS7-modified 5' tRFs repress cap-dependent translation initiation by sequestering PABPC1 [Guzzi et al., 2018].

While previous studies focused on the role of tRFs in translation initiation, [Gebetsberger et al., 2012] discovered stress-dependent 5' tRFs in archaea inhibiting translation elongation. A follow-up paper revealed that they interact with the small ribosomal subunit to displace the mRNA from the initiation complex. Surprisingly, archaeal tRFs can trigger this response both in eukaryotes as well as bacteria indicating a conserved mechanism of action [Gebetsberger et al., 2017]. A similar, yet stress-independent, function of tRFs was reported in human. [Sobala and Hutvagner, 2013] used a reporter system and showed that 5' tRFs derived from tRNA^{Gln} can inhibit translation of certain mRNAs by interacting with elongating polysomes.

While a plethora of mechanisms were identified for translation inhibition by 5' tiRNAs and tRFs, it came as a surprise when 3' tsRNAs were found to perform the opposite task of enhancing translation. For instance, [Fricker et al., 2019] identified tRNA^{Thr} 3' halves in trypanosomes which are upregulated during nutrient deprivation and associate with ribosomes and polysomes to promote protein synthesis. Furthermore, tRNA^{Leu}_{CAG} 3' tiRNA were discovered to promote translation of the ribosomal protein RPS28 in human and mice. This is facilitated by direct binding of 3' tiRNAs to the RPS28 mRNA both in the CDS and in the 3' UTR, thereby likely enhancing a post-initiation step like translation elongation [Kim et al., 2019]. Consequently, inhibiting the 3' tiRNAs by utilizing antisense oligos causes loss of RPS28 and ribosome biogenesis defects [Kim et al., 2017].

A growing number of studies has identified tRFs involved in the miRNA and piRNA pathways. First indications for this were the generation of 5' tRFs by dicer [Cole et al., 2009], a crucial endonuclease in miRNA biogenesis, as well as interaction of tRFs with argonaute proteins, the effector proteins in small RNA-dependent silencing pathways [Haussecker et al., 2010]. [Maute et al., 2013] provided the first hard evidence for tRFs with roles in the miRNA pathway by demonstrating that dicer-dependent tsRNAs target the 3' UTRs of mRNAs similar to miRNAs. Later, it was confirmed by [Kuscu et al., 2018] that 3' tRFs translationally repress target genes by recruiting GW182 in human cells.

First evidence for a role in the piRNA pathway was reported by [Zhang et al., 2016] who demonstrated that tRFs bind to PIWIL4 to facilitate H3K9 methylation for epigenetic silencing of protein-coding genes in human cells. Moreover, [Sharma et al., 2016] identified 5' tRFs which inhibit the expression of genes regulated by the long terminal repeat (LTR) promoters of the endogenous retroelement MERVL, however, the mechanism of action remained unknown. A study including a targeted search for tRNA-derived piRNAs by [Schorn et al., 2017] revealed a similar function for 3' tRFs in the following year. They discovered abundant 3' CCA containing tRFs in embryonic stem cells. Notably, these tRFs featured complementarity to LTR retrotransposons and endogenous retroviruses and transcriptionally silenced them by inhibiting their retrotransposition rather than epigenetically

marking them. Strikingly, the 3' CCA tail was necessary to convey this repressive function suggesting that the 5' tRFs lacking CCA tails identified in by [Sharma et al., 2016] utilize a different mechanism. Thus, tRFs were identified both in complexes of the miRNA and piRNA machinery as well as in previously unknown pathways of gene expression regulation.

1.8.3 Effects of tRNA modifications on fragmentation

Among all RNA species, tRNAs harbor the highest variety and frequency of RNA modifications [Boccaletto et al., 2022]. Consequently, it is not surprising that RNA modifications clustering in tRNA loops where tRNA cleaving enzymes cut have been found to affect tRNA fragmentation. In the last decade, many examples of tRNA modifications protecting against cleavage have been collected. The best studied case is depicted by m5C modification by DNMT2 which protects tRNA from cleavage both in *Drosophila* [Schaefer et al., 2010] and vertebrates [Blanco et al., 2014]. In *Drosophila*, lack of DNMT2-dependent m5C38 [Schaefer et al., 2010] but also of m5C48/49/50 [Blanco et al., 2014] leads to an increased production of tRNA fragments. Similarly, hypomodification of tRNAs results in increased fragmentation in mouse sperm. During high fat diet, DNMT2 expression is induced in a segment of the male reproductive tract where sperm maturation occurs and tRNA fragments are enriched [Sharma et al., 2016]. Importantly, tRFs in sperm contain paternal information and can convey paternal metabolic disorders resulting from high fat diet to the offspring in *wild type* mice [Chen et al., 2016]. Loss of DNMT2-dependent m5C38 leads to upregulated tRNA^{Gly} derived tiRNA levels which abolishes the transmission of high fat diet induced metabolic disorders to the offspring [Zhang et al., 2018b]. Therefore, tRNA fragmentation is regulated by RNA modification and plays a role in tRF mediated inheritance of diseases. Other protective functions have been reported for m1A and m3C. Demethylation by ALKBH3 renders targeted tRNAs more susceptible to fragmentation by angiogenin [Chen et al., 2019b]. Accordingly, loss of TRMT10a-dependent m1A9 in human cells triggers fragmentation of hypomethylated tRNA^{Gln} and tRNA_i^{Met} [Cosentino et al., 2018]. Furthermore, protective functions have been reported for modifications at the wobble position 34. For instance, loss of m5C34 catalyzed by NSUN2 significantly increased the levels of 5' tRFs derived from angiogenin dependent cleavage of tRNA^{Asp/Glu/Gly/His/Lys/Val} [Blanco et al., 2014]. Likewise, queuosine (Q) at position 34 protects tRNA^{His} and tRNA^{Asn} against fragmentation by angiogenin in human cells [Wang et al., 2018]. Consequently, loss of Q leads to an asymmetrical accumulation of 5' tiRNAs derived from tRNA^{His} and 3' tiRNAs from tRNA^{Asn}, respectively. Finally, lack of Nm at G34 catalyzed by Trm7-34 on tRNA^{Phe} increases fragmentation in *Drosophila* [Angelova et al., 2020]. Surprisingly, a Trm7-32, Trm7-34 double mutant lacking both Nm at C32 and G34 featured significantly less tRNA fragments suggesting that Nm at C32 might stabilize these tRFs after their generation. While tRNA fragments do not typically contain Nm modifications at their 3' ends, they do contain various Nm sites within their loop structures in close proximity to cleavage sites for tRF generation which could potentially become the 3' ends after partial trimming by exonucleases. Interestingly, tRFs derived from tRNA^{Glu}_{GUG} were found to be Nm modified [Cole et al., 2009]. It

is widely known that 2'-O-methylation at the 3' ends of small RNAs is a common mechanism of protection from exonucleolytic degradation [Yu et al., 2005, Kamminga et al., 2010, Ameres et al., 2010]. Therefore, Nm modifications in loops might stabilize tRFs after cleavage.

1.9 tRNA expression defects and human disease

Defects in almost every step of tRNA biogenesis including maturation, aminoacylation, modification, post-transcriptional stability and dysregulated fragmentation have been associated with human disease. Unfortunately, for most diseases the exact molecular mechanism is not yet understood. This is due to the fact that aberrations for example in tRNA sequence or folding can cause multiple downstream effects whose impacts on disease progression can not be gauged individually. Interestingly, diseases related to tRNA dysfunction mainly cause neurodegenerative and sporadically metabolic disorders with dysregulated proteostasis as a common occurrence (Figure 10). This section discusses the effects of aberrations of tRNA expression based on the tRNA biogenesis steps and the potential pathomechanisms.

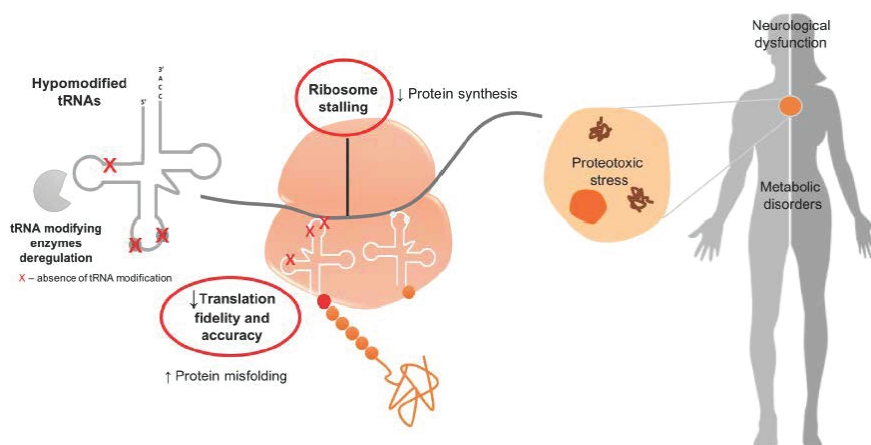


Figure 10: Mutations in tRNA metabolism cause neurological diseases. Mutations in tRNA sequences, tRNA-modifying enzymes or tRNA processing are linked to human diseases featuring disturbed proteostasis including neurological and metabolic disorders. Figure from [Pereira et al., 2018].

Mutations in tRNA genes preventing modification

Most mutations in tRNA genes are located in mitochondrial tRNA genes, presumably due to the fact that the mt. genome contains only one unique gene copy of each tRNA species resulting in a lack of redundancy. Interestingly, most mutations are linked to myopathies and neurodegenerative diseases [Ruiz-Pesini et al., 2007]. The two most frequent diseases associated with mutations in human mt. tRNAs are myopathy, encephalopathy, lactic acidosis, and stroke-like episodes (MELAS) and myoclonic epilepsy associated with raggedred fibers (MERRF). MELAS is caused by mutations in at least six different mt. tRNAs [Burgess and Storkebaum, 2023] including an A>G point mutation at the wobble position of mt. tRNA^{Leu} which prevents it from being modified to

5-taurinomethyluridine [Yasukawa et al., 2000]. This results in decreased decoding efficiency of UUG codons [Kirino et al., 2004] which are enriched in the complex 1 NADH dehydrogenase 6 (ND6) resulting in defects in mitochondrial respiration. Consistently, mutation of ND6 itself also causes MELAS [Ravn et al., 2001]. Similarly, a A>G point mutation at position 58 of mt. tRNA^{Lys} causes MERRF. Lack of A at position 58 prevents m1A formation resulting in decreased mt. tRNA^{Lys} levels as well as decreased mcm5s2U modification ratios at the wobble base. Similarly, this results in defects in translation of mitochondrial respiratory chain complex members [Richter et al., 2018]. Therefore, defects in mitochondrial respiration are likely the common mechanism in diseases caused by mutations in mitochondrial tRNA genes.

Defects in pre-tRNA splicing

Mutations in multiple tRNA splicing complex members (TSEN54, TSEN2, TSEN34, TSEN15) responsible for tRNA intron removal as well as the associated factor CLP1 have been linked to pontocerebellar hypoplasia (PH) resulting in microcephaly, intellectual disability and psychomotor delay [van Dijk et al., 2018]. Among those, CLP1 has received special attention. Studies with cells derived from CLP1 patients revealed that CLP1 mutation caused a destabilization of the TSEN complex resulting in an accumulation of pre-tRNAs and depletion of mature tRNAs. Dysregulations in the pool of mature tRNAs can lead to translational defects due to ribosome stalling which can be sufficient to trigger the ISR. Unfortunately, ribosome stalling or ISR activation have not yet been investigated in this background. However, activation of stress response pathways is supported by the fact that CLP1 mutant cells feature an increased sensitivity to oxidative stress resulting in p53-dependent motor neuron loss [Schaffer et al., 2014, Karaca et al., 2014, Sekulovski et al., 2021]. p53-dependent activation of apoptosis is typically triggered by prolonged ER stress suggesting a chronic activation of the UPR pathway [López et al., 2017]. Additionally, unphosphorylated 3' exon halves, the substrate of CLP1, are accumulating in CLP1 mutant cells. Interestingly, overexpression of these fragments was sufficient to trigger motor neuron loss in a mouse model suggesting that their accumulation is directly involved in the pathomechanism, albeit their mechanism of action is completely unknown [Hanada et al., 2013]. In the end, both chronic activation of stress responses and accumulation of tRNA splicing products could potentially be neurotoxic. Surprisingly, motorneurons seem to be exclusively affected by this, yet the reason for this susceptibility is still unclear.

Defects in tRNA aminoacyl synthetases

Mutations in aaRS genes are separated into monoallelic dominant or biallelic recessive mutations. Biallelic mutations have been identified both in cytoplasmic aaRSs and in all mt. aaRS genes featuring a wide variety of phenotypes including multi-organ phenotypes [van Meel et al., 2013], neurological defects [Taylor et al., 2014] and lung disease [Hadchouel et al., 2015]. However, most cases display CNS abnormalities, growth restriction, liver dysfunction and facial dysmorphisms [Fuchs et al., 2019]. A reduction in aminoacylation is a hallmark of these mutations but the downstream effects have only been investigated for few mutations. Oftentimes, they directly affect protein trans-

lation due to reduced availability of mature charged tRNAs. Mutations in mt. aaRSs most commonly cause combined oxidative phosphorylation deficiency (COXPD) resulting in defective mitochondrial translation and therefore damages to the CNS and neurological disease presumably due to its high energy demand [Sissler et al., 2017]. It is still not understood how biallelic mutations cause such a variety of phenotypes. Perhaps, this could be caused by tissue-specific tRNA demands.

Dominant monoallelic mutations are exclusive to cytoplasmic aaRS. Today, at least ten monoallelic mutations have been linked to peripheral neuropathy (PN), mostly in the form of Charcot-Marie-Tooth (CMT) disease [Turvey et al., 2022]. CMT is a degenerative disease affecting motor and sensory axons leading to loss of motor function, progressive weakness and sensory loss among other symptoms. The common pathogenic mechanism between all monoallelic aaRS mutations has not been understood. Some mutations affect aminoacylation activity [Edvardson et al., 2007, Wortmann et al., 2017, Kuo et al., 2019], sometimes due to reduced aaRS protein levels [Galatolo et al., 2020], which can directly affect translation. However, even hypermorphic alleles that increase aminoacylation efficiency cause PN suggesting a pathway independent of hypoaminoacylation [Weterman et al., 2018].

Consistently, accumulating evidence suggests that a lack of tRNA aminoacylation alone is likely not the disease-causing mechanism in aaRS diseases. Experiments in flies revealed that variants lacking aminoacylation capacity can cause less defects in motor performance than variants that retain catalytic activity [Storkebaum et al., 2009]. Similarly, overexpression of WT aaRS is not sufficient to rescue defects in a dominant negative glycyl-tRNA synthetase gene (GARS) background in mice [Motley et al., 2011]. These observations suggest a mechanism based on a gain-of-toxic-function in dominant CMT variants. Recently, experiments in GARS mutant mice provided new insights into a novel mechanism of aaRS diseases [Zuko et al., 2021, Spaulding et al., 2021]. While mutant GARS does not efficiently aminoacylate tRNA^{Gly}, it still possesses the ability to bind its substrate, yet does not efficiently release it leading to a sequestration of tRNA^{Gly} from the mature tRNA pool. As a result, ribosomes stall at Gly codons triggering a constitutive activation of the ISR through GCN2 activation. [Zuko et al., 2021] proposed that this results in neurotoxicity over an extended period and suggested GCN2 inhibitors as a therapeutic approach against PN. Notably, these observations could be unequivocally reproduced in human cells [Mendonsa et al., 2021]. Strikingly, experiments in flies highlighted that genetic inhibition of translation initiation by overexpressing d4E-BP, a target of ATF4 [Vasudevan et al., 2022, Kang et al., 2017], phenocopies CMT suggesting that prolonged translation impairment through the ISR might be a common mechanism in aaRS diseases [Niehues et al., 2015].

Defects in tRNA aminoacylation

Multiple mutations in tRNA genes have been linked to reduced efficiency of aminoacylation. In these cases, either the tRNA identity determinants or adjacent structures are affected by point mutations preventing recognition by the respective aaRS. For instance, the point mutation A9G in human mt. tRNA^{ASP} is associated with mitochondrial myopathy [Seneca et al., 2005]. Specifically, the mutation

disrupts a triplet interaction of positions 9:12:23 which are recognized by Asp aaRS and required for tRNA charging [Messmer et al., 2009]. Similarly, a G31A point mutation in mt. tRNA^{Ser}_{UCN} associated with polycystic ovary syndrome and insulin resistance disrupts the anticodon stem and inhibits aminoacylation [Ding et al., 2016]. While mechanistic studies for pathogenesis of these mutations are lacking, a similar mechanism as for aaRS mutations including ribosome stalling and ISR activation due to lack of mature tRNAs might be responsible.

Defects in tRNA stability

When mutations occur in structurally important regions of the tRNA body, a subsequent destabilization of the tRNA molecule can result in tRNA loss and disease. For instance, [Wang et al., 2016b] identified patients carrying a U55G mutation in mitochondrial tRNA^{Glu}. This prevented installation of the universally conserved Ψ 55 and resulted in inefficient basepairing of positions 18 and 55 causing conformational changes in the tRNA. Mutated tRNA^{Glu} featured severe destabilization indicated by a reduced melting point of 4°C resulting in a reduction of tRNA^{Glu} levels by 65% as well as increased angiogenin-dependent fragmentation. Furthermore, loss of tRNA^{Glu} impaired mitochondrial translation of proteins rich in Glu like ND1, ND6 and CO2 leading to reduced mitochondrial dysfunction of complexes I and IV, reduced ATP levels and increased ROS levels. Interestingly, the patients suffered from hearing loss and diabetes which are linked to ISR activation [Delépine et al., 2000], however, a potential activation was not quantified. tRNA stability can also be dependent on proper tRNA modification. For example, loss of NSUN2 responsible for depositing m5C at positions 37, 46, 47 and 48 in tRNA^{Gly} resulted in intellectual disability and myopathy in human patients [Martinez et al., 2012, Abbasi-Moheb et al., 2012, Khan et al., 2012, Komara et al., 2015]. A mouse model revealed that unmethylated tRNA^{Gly} was drastically destabilized resulting in a loss of 70% of this tRNA species. Consistently, Gly-rich proteins in the brain with roles in glutaminergic neurons were downregulated concomitant with defects in synaptic signaling [Blaze et al., 2021].

Dysregulation of tRNA fragmentation

Mutations in multiple tRNA modifying enzymes including DNMT2, NSUN2 and queuosine modifying enzymes have been reported to induce ANG-dependent tRNA fragmentation leading to neurodevelopmental disease and cancer as discussed above [Blanco et al., 2014, Schaefer et al., 2010, Wang et al., 2018]. Furthermore, variants in ANG have been found in multiple neurodegenerative diseases including ALS where ANG acts neuroprotective [Greenway et al., 2006, Wu et al., 2007]. While ANG performs multiple cellular functions, it is not yet completely clear whether these diseases are caused by a dysregulation of tRNA fragmentation. Most ANG mutations linked to neurodegenerative diseases harbor a loss of ribonucleolytic activity suggesting that a lack of cleavage of tRNAs or other ANG substrates is involved in the pathogenesis [Greenway et al., 2004]. Similarly, ANG variants that are predicted to be functionally impaired were identified in patients with parkinsons disease (PD) [Van Es et al., 2011, Rayaprolu et al., 2012] as well as in alzheimers disease [Gagliardi et al., 2019]. Strikingly, both in ALS and PD mouse models, injection of human angiogenin is sufficient

to prevent death of motoneurons and dopaminergic neurons, respectively, suggesting that a lack of ANG activity is directly responsible for the pathogenesis [Crivello et al., 2018, Steidinger et al., 2011].

As illustrated in the examples above, defects in almost every step of tRNA biogenesis can cause human disease. However, the exact mechanisms are often not understood as it is difficult to gauge the individual impact of multiple potentially cytotoxic downstream effects within a disease model. For example, loss of mature tRNAs can trigger (1) codon-specific translational defects, (2) ribosome stalling resulting in stress response pathways affecting global translation but also (3) reduced levels of species-specific tRNA fragments that could affect gene expression. In most cases, the exact pathomechanism has not been investigated in sufficient detail. However, impaired translation seems to be a common hallmark.

1.10 The integrated stress response in human disease

The integrated stress response (ISR) is a conserved signaling network to adapt to variable environments by acting as a central regulator of protein homeostasis. This is achieved by regulating global translation levels and inducing the expression of stress response genes and chaperones to reduce protein folding stress.

The central player of the ISR required to mediate these effects is eIF2 α which is phosphorylated by specialized kinases (PERK, GCN2, PKR, HRI) that are activated by various stress signals. This directly inhibits global translation levels by interfering with translation initiation (Figure 11A). During translation initiation, tRNA_i^{Met} is transferred to the 40S subunit where it forms a ternary complex (TC) with eIF2 and GTP. This results in the 43S complex, which binds to the capped 5' end of mRNAs to form the 48S complex which in turn scans for the transcription start site. Upon AUG detection, the GTP is hydrolyzed to GDP releasing eIF2-GDP and the 60S subunit joins to form the 80S initiation complex for protein synthesis. The released eIF2-GDP must be recycled to eIF2-GTP by the guanine nucleotide exchange factor (GEF) eIF2B to be able to reform the TC. Therefore, this reaction represents the rate-limiting step of translation initiation. Phosphorylated eIF2 α as a result of ISR activation is a strong competitive inhibitor of eIF2B resulting in drastic reductions in global cap-dependent protein synthesis [Harding et al., 2000, Spriggs et al., 2010].

Paradoxically, this translation inhibition is pivotal in ATF4 translation (Figure 11B). In humans, the *ATF4* gene region contains multiple regulatory upstream ORFs (uORFs). In unstressed cells at low levels of p-eIF2 α and normal levels of TC, translating ribosomes form at the regulatory upstream ORFs leading to termination slightly upstream of the ATF4 CDS. Since reinitiation following a uORF is inefficient, ATF4 is not translated [Kozak, 1983, Vattem and Wek, 2004].

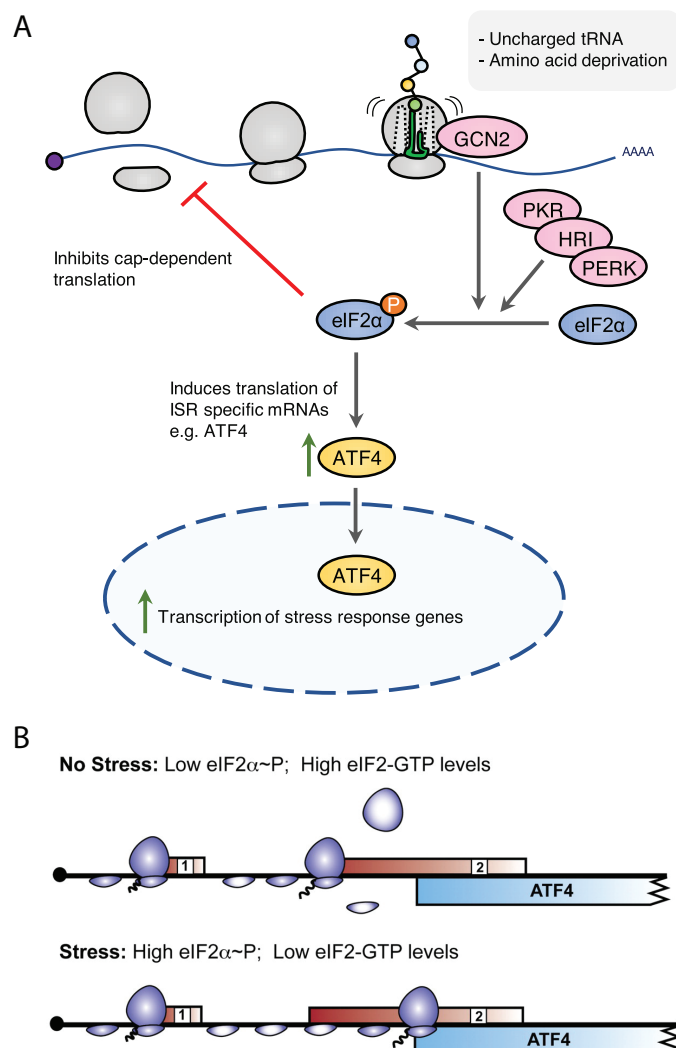


Figure 11: The integrated stress response. (A) The integrated stress response (ISR) converges on phosphorylation of eIF2 α , resulting in global inhibition of cap-dependent mRNA translation. GCN2 is the relevant ISR-kinase upon translational arrest. Cap-independent pathways allow for the selective translation of ISR-specific mRNAs including *ATF4*. ATF4 is a transcription factor and effector of ISR that controls expression of stress response genes. Figure and description from [Vind et al., 2020]. (B) In the delayed translation reinitiation model, two upstream open reading frames (uORF) (red boxes) in the 5' leader of the *ATF4* mRNA direct preferential translation. Figure and description adapted from [Baird and Wek, 2012].

During stress conditions, the first uORF is translated in the same manner and eIF2-GDP is released. The 40S subunit continues scanning for the next AUG, however, AUG recognition requires rebinding of a recycled TC [Cigan et al., 1988]. Since TC levels are reduced due to increased p-eIF2 α levels, translation reinitiation is delayed allowing about 50% of the 40S subunits to pass the regulatory uORFs and reinitiate translation at the ATF4 AUG instead. Thus, delaying translation initiation is a key mechanism to ensure translation of the transcription factor ATF4 which in turn elicits cytoprotective measures by regulating the expression of stress response genes and chaperones.

The stress factors to activate the ISR include translational stress resulting from unfolded proteins in the ER lumen mediated by the unfolded protein response (UPR). This can be triggered for instance by oxidative stress mediated by H₂O₂ treatment which can cause irreversible protein damage

including cysteine oxidation and accumulation of unfolded proteins [Schieber and Chandel, 2014]. These are detected in the endoplasmic reticulum (ER) by detector proteins binding to exposed hydrophobic domains to activate the UPR [Gething, 1999]. Consequently, signalling cascades including PKR-like ER kinase (PERK) are activated which leads to phosphorylation of eIF2 α [Halliday and Mallucci, 2015].

Apart from the PERK-UPR axis, both the ISR and the ribosome-associated protein quality control (RQC) pathway are activated by ribosome stalling. Interestingly, both pathways are competing for the same signal as deletion of one pathway promotes activation of the other, however, the exact signalling mechanism is not yet understood. While the RQC detects ribosome collisions through CG11414 (ZNF598 in vertebrates) at low translational stress levels without any preference, activation of the ISR requires high stalling levels and prefers vacant A sites in the ribosome indicative of slow translation [Yan and Zaher, 2021]. Therefore, the RQC corrects occasional ribosome collisions while the ISR is activated during acute translational stress to ensure protein homeostasis.

Furthermore, stalled ribosomes as a result of amino acid starvation were proposed as an additional mechanism to trigger the ISR via accessible ribosome P-stalks. The ribosomal P-stalk is a uL10/P1/P2 pentameric protein complex that is part of the ribosomal GTPase-associated center [Shimizu et al., 2002]. GCN2-mediated activation requires interactions with domain II of the uL10 subunit as well as the C-terminal tails of P1 and P2 to phosphorylate eIF2 α [Inglis et al., 2019]. During normal conditions, the ribosomal P-stalk interacts with elongation factors in translating ribosomes and is therefore not accessible to GCN2 [Baba et al., 2013]. During translational stress, however, the C-terminal tails of P1 and P2 might be accessible to interact with GCN2 to activate the ISR. Lastly, uncharged tRNAs indicative of starvation were identified as an activator of GCN2 [Inglis et al., 2019, Costa-Mattioli and Walter, 2020]. GCN2 possesses a HisRS domain preferentially binding to the acceptor stem of uncharged tRNAs [Ruff et al., 1991] which is sufficient for ISR activation [Wek et al., 1995].

The activation of the ISR has been observed in several models of neurological disease but conflicting observations have been made about whether it acts in a cytoprotective or cytotoxic manner. For instance, [Zuko et al., 2021] and [Spaulding et al., 2021] reported that the activation of the ISR through increased ribosome stalling is responsible for the development of peripheral neuropathy in a GARS mouse model. This can be prevented by rescuing the reduced tRNA^{Gly} levels, thereby stopping ribosome stalling, or by directly inactivating the ISR suggesting that it is directly involved in PN pathogenesis. Similarly, loss of the ribosomal rescue factor GTPBP2 is associated with PN, ID, microcephaly and movement disorders [Jaberi et al., 2016, Bertoli-Avella et al., 2018, Carter et al., 2019]. However, [Ishimura et al., 2016] and [Terrey et al., 2020] observed that activation of the ISR as a result of ribosome stalling in a background of tRNA^{Arg}_{UCU} loss acts neuroprotective.

By default, cellular stress responses like the ISR promote cell survival in stressful environments. To this end, the ISR induces expression of pro-survival genes in amino acid metabolism [Harding et al., 2000], oxidative stress resistance [Harding et al., 2003] and chaperones to reduce ER protein folding stress [Luo et al., 2003]. Additionally, ATF4 expression induces expression of the transcription factor

CHOP and both together induce expression of GADD34 which dephosphorylates eIF2 α to return to normal protein synthesis [Brush et al., 2003]. If proteostasis is not achieved over a prolonged period, however, stress responses harbor mechanisms to eventually trigger apoptosis of the cell. In case of the ISR, the intrinsically unstable CHOP and GADD34 mRNAs accumulate over extended stress exposure and reach protein levels [Rutkowski et al., 2006] sufficient to induce expression of apoptotic genes [Ron and Walter, 2007].

A similar mechanism exists for the UPR where chronic ER stress leads to a p53-dependent activation of apoptosis [López et al., 2017]. Specifically, p53 binds the mRNA of BiP, a chaperone sensing unfolded proteins in the ER, thereby inhibiting its translation and releasing the pro-apoptotic BIK which is sequestered by BiP during low stress levels. Therefore, regulation of mRNA translation poses a mechanistic switch between ensuring protein homeostasis and triggering apoptosis in cellular stress responses. As a result, the degree of ISR activation is presumably the deciding factor between a cytoprotective function and triggering apoptosis.

However, an increasing number of studies have attested a cytotoxic function of the ISR in several human diseases. For example, it is activated in an alzheimer's disease cell model where intracellular Tau aggregates induce oxidative stress and therefore the ISR in astrocytes. Interestingly, the cytotoxicity requires coculture with neurons suggesting a cell non-autonomous response [Batenburg et al., 2022]. Furthermore, mutations in the catalytic component Elp3 of the elongator complex responsible for U34 modification of multiple tRNA species have been linked to microcephaly in mice. Lack of U34 modification leads to ribosome pausing and subsequently codon-specific translation defects activating the UPR. Strikingly, activation of the PERK-eIF2 α branch of the UPR interferes with neurogenesis in mouse embryos. Interestingly, pharmacological activation of the UPR mimicks Elp3 loss and causes premature neurogenesis indicating that the UPR and perhaps by extension the ISR are directly involved in the pathomechanism [Laguesse et al., 2015]. A role of the ISR has also been implicated in diabetes where tight control of ISR activity is required. Downregulation of the ISR as a result of PERK mutation causes diabetes and growth retardation in human patients [Delépine et al., 2000]. Experiments in a mouse model uncovered that deletion of PERK causes loss of pancreatic islets accompanied by ER expansion and UPR activation in the pancreas. This results in beta cell loss, presumably due to accumulation of unfolded proteins [Gao et al., 2012]. On the other hand, constitutive upregulation of the ISR is also detrimental for pancreatic beta-cells. Patients with mutations in eIF2 γ [Moortgat et al., 2016, Stanik et al., 2018] or constitutive repressor of eIF2 α phosphorylation (CReP) suffer from diabetes and microcephaly [Abdulkarim et al., 2015]. Mechanistically, prolonged activation of the ISR probably causes cell death due to induction of the proapoptotic transcription factor CHOP. Thus, pancreatic beta cells require either a narrow level of p-eIF2 α or a dynamic regulation.

1.11 Project aim

Aim I: Deciphering the molecular origin of defects caused by mutation in Pus7 using high-throughput omics approaches.

We have previously established a fly model for *Pus7* mutation. We could reproduce neurological defects in *Pus7^{fs}* flies indicating a conserved neuronal role of Pus7 in flies and human. Since the expression patterns of Pus enzymes in *Drosophila* are unknown, we first aim to investigate the Pus7 expression pattern using transgenic lines to identify tissues of importance. These will be validated using the extensive genetic toolkit available in *Drosophila* to perform targeted depletion and targeted rescue experiments. Furthermore, we aim to identify the molecular changes caused by Pus7 mutation that are relevant for the disease. Therefore, we aim to use a multiomics approach to identify changes in transcription and translation to elucidate how Pus7 affects gene expression.

Aim II: Generation of further fly models for neurological diseases caused by mutation in PUS enzymes.

Drosophila serves as a favorable model organism to study neurodevelopmental diseases thanks to the presence of a complex brain. We have previously taken advantage of the genetic tractability of *Drosophila* to generate Pus7 mutant flies to establish a model for neurological disease using the CRISPR/Cas9 system. Mutations in PUS3 have been observed to cause a highly similar clinical picture with brain-specific defects. Furthermore, our collaborators have recently identified patients carrying mutations in PUSL1 featuring neurological defects. We aim to repeat our endeavours by establishing fly models for *PUS3* and *PUSL1* disease. This includes the generation of mutants using CRISPR/Cas9 followed by phenotypic characterization using standard assays as well as well-established behavioral assays to investigate potential neurological phenotypes. Additionally, we aim to investigate the subcellular localization using *Drosophila* cell culture.

Chapter 2: RESULTS

2.1 Expression patterns of Pus1, PusL1, Pus3 and Pus7

In order to gain insight into the functions of Pus enzymes in *Drosophila*, I analyzed their expression patterns using publicly available data from FlyAtlas (<https://motif.mvls.gla.ac.uk/FlyAtlas2>). Among the four investigated Pus enzymes, we observed that PusL1 featured a rather unspecific but high expression across most tissues except for its distinct depletion in the adult fat body (Figure 12). In contrast, Pus1, Pus3 and Pus7 showed a specific enrichment in ovaries suggesting functions in oogenesis. Interestingly, both Pus3 and Pus7 exhibited heightened expression in the larval central nervous system indicating potential neuronal functions. In general, the expression patterns of the analyzed Pus enzymes are rather ubiquitous and do not allow clear deductions about their functions. We therefore aimed to investigate the roles of these enzymes in more detail.

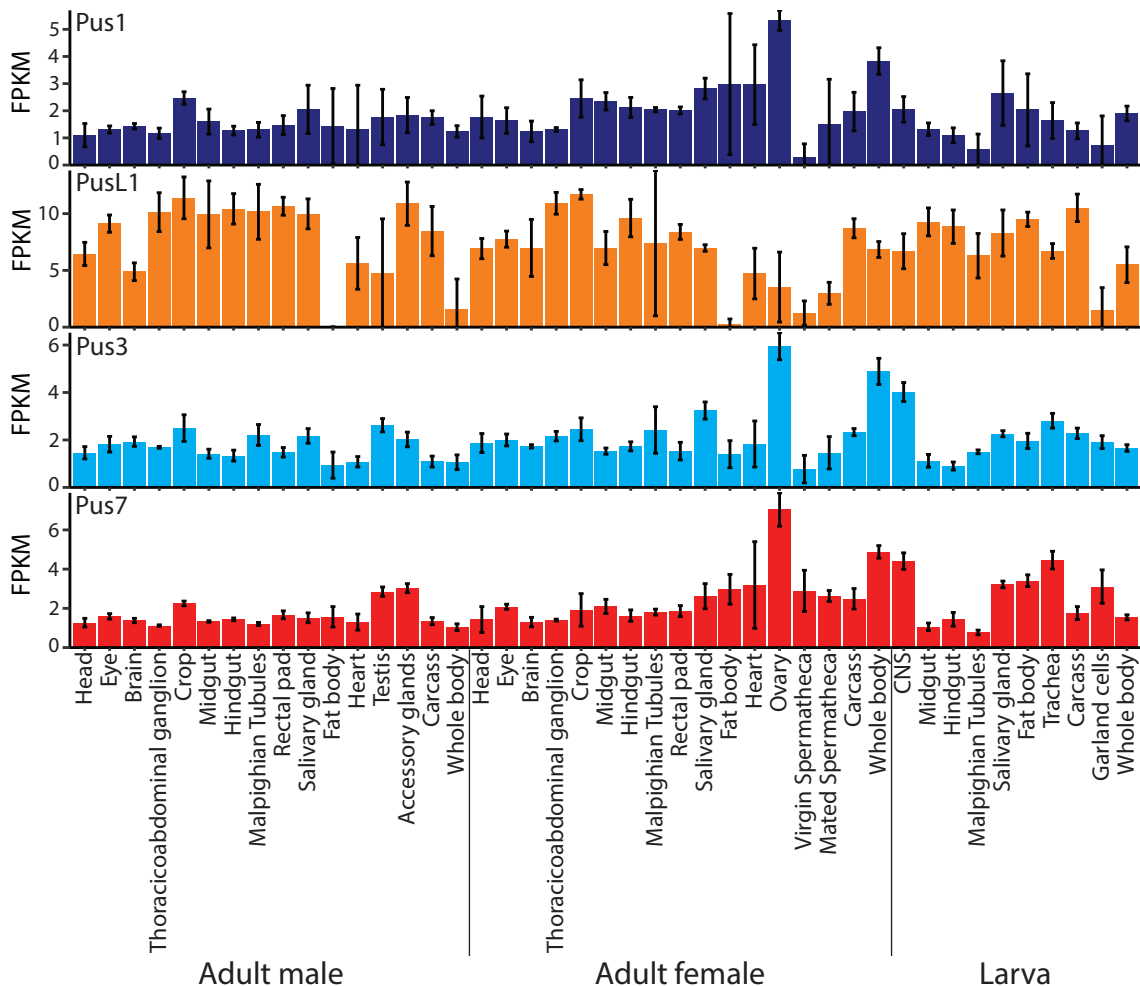


Figure 12: Expression patterns of Pus1, PusL1, Pus3 and Pus7. Expression profiles across various tissues in adult males, females and crawling L3 larva. FPKM (fragments per kilobase million) are plotted with standard deviation as error bars. Data obtained from FlyAtlas2.

2.2 Characterization of *Pus7* in *Drosophila*

2.2.1 Evaluation of the *Pus7* expression pattern

To investigate the function of *Pus7* in *Drosophila*, we aimed to investigate its expression pattern *in vivo*. Therefore, we ordered the generation of a transgenic fly line carrying an N-terminal EGFP tag (WellGenetics Inc.; Figure 13A). First, an EGFP-*Pus7*-3xP3-RFP cassette was integrated after the endogenous start codon of *Pus7*, effectively disrupting the *Pus7* ORF. This fly line is expected to not produce any mature *Pus7* protein and was termed *E3R-Pus7*. Following the integration, the 3xP3-RFP marker which is flanked by loxP sites was flipped out using Cre recombinase resulting in the *EGFP-Pus7* fly line which carries a 16 amino acid linker between the sequences encoding EGFP and *Pus7*.

To confirm the expression of EGFP-*Pus7*, protein lysates from these two fly lines were analyzed by western blot and mature EGFP-*Pus7* was only visible after excision of the 3xP3-RFP marker (Figure 13A). Next, I performed immunostainings against EGFP-*Pus7* in several tissues including embryos, brains of L3 larvae and whole mount ovaries. We could observe a ubiquitous expression of EGFP-*Pus7* in all tested tissues. This is in agreement with public databases for transcript expression (Figure 12). Furthermore, EGFP-*Pus7* localized to the nucleus which was previously observed in yeast (Figure 13B; [Schwartz et al., 2014]). Finally, to gain insights into the temporal expression pattern of *Pus7* during fly development, I quantified the expression of *Pus7* in different developmental stages from early embryo to adult flies using RT-qPCR. We identified peaks of *Pus7* expression in the early embryo before the maternal-to-zygotic transition as well as during 8-10 hours of larval development and in adult females, specifically in the ovaries (Figure 13C).

Since the *E3R-Pus7* line lacked *Pus7* expression, we considered using the abovementioned fly lines to further characterize *Pus7* function. I therefore validated the *Pus7* mRNA expression levels in comparison to the *Pus7* levels of *wild type* flies using RT-qPCR. While *E3R-Pus7* indeed showed reduced *Pus7* mRNA levels, presumably as a result of nonsense-mediated decay, the *Pus7* levels in *EGFP-Pus7* flies were increased by two-fold (Supplementary figure S.1). This was supposedly caused by the integration of the EGFP sequence affecting *Pus7* transcription. As a result, I used these fly lines exclusively for qualitative experiments regarding *Pus7* expression and proceeded to generate mutant fly lines with intact promoters for quantitative comparisons.

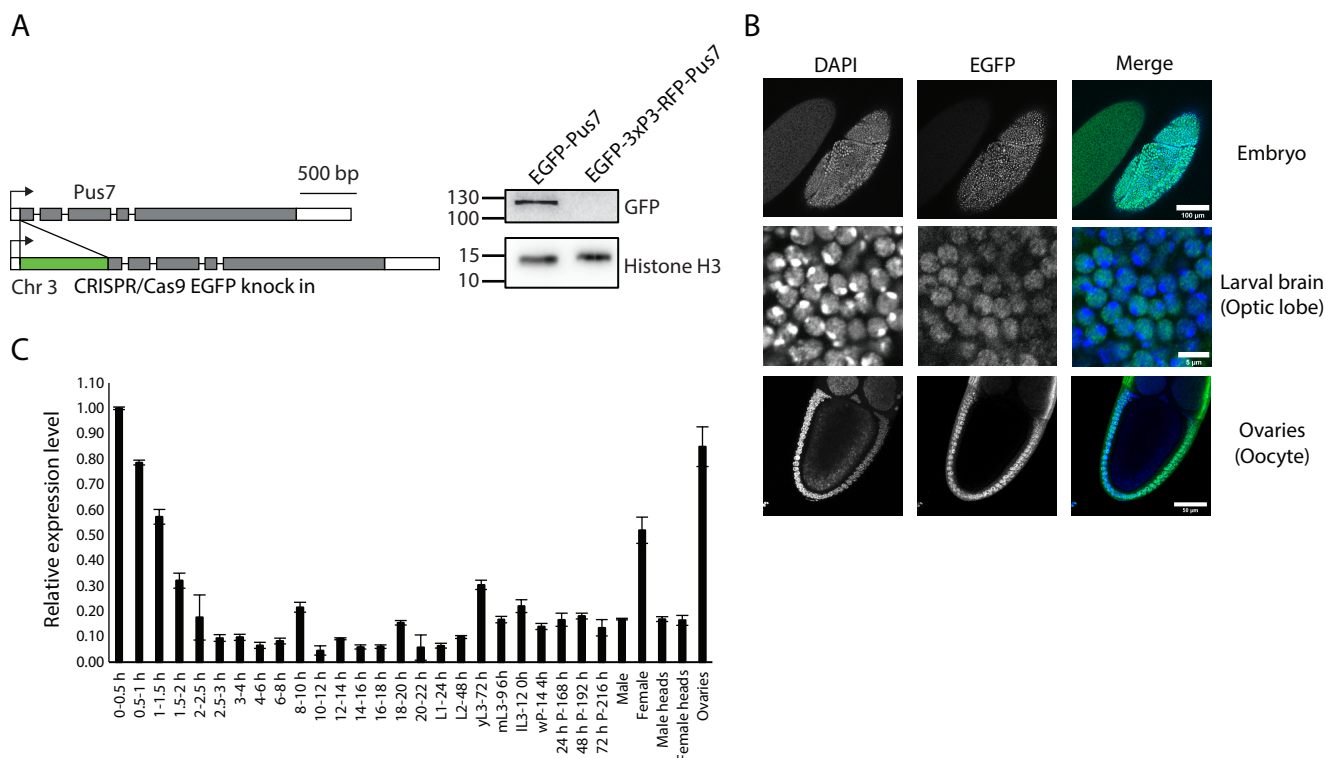


Figure 13: *Pus7* is ubiquitously expressed and localizes to the nucleus. (A) Schematic of the *Pus7* locus before and after the integration of *EGFP* at the N-terminus (left). Expression of *EGFP-Pus7* was confirmed by western blot (right). Protein sizes are indicated in kDa. (B) Immunostaining in embryos, the optic lobe and ovaries of *EGFP-Pus7* flies. (C) RT-qPCR to quantify *Pus7* mRNA expression in RNA samples of different developmental stages.

2.2.2 Phenotypic characterization of *Pus7* in *Drosophila*

Due to its complex brain structure, genetic tractability and powerful research tools, *Drosophila* has emerged as a premier model organism to investigate neurological diseases. We have previously used these advantages by generating a *Pus7* fly model to describe behavioral phenotypes in more detail in *Drosophila* which were first observed in *PUS7* patients. To this end, we previously generated fly lines mutant for *Pus7* using the CRISPR/Cas9 system as described in [de Brouwer et al., 2018] (Figure 14A). We aimed to remove the catalytic domain of *Pus7* by using gRNAs targeting exon 3 and exon 5 which encompass the catalytic Asp274. We successfully generated two *Pus7* mutant fly lines carrying indel mutations in exon 3 leading to a frameshift and a premature stop codon upstream of the catalytic Asp274. Both mutant fly lines are therefore expected to lack *Pus7* catalytic activity and the *Pus7* mRNAs are expected to be degraded by nonsense-mediated decay. To validate this, I quantified *Pus7* mRNA expression levels by RT-qPCR and observed a decrease of *Pus7* mRNA levels by approximately 95% in both mutant fly lines (Figure 14B).

In spite of having undergone six rounds of isogenization to remove off-target effects of CRISPR/Cas9 and being genetically very similar to the *Pus7^{fs}* 15-2 line, the *Pus7^{fs}* 15-1 line showed a more severe phenotype with distinct health problems suggesting the presence of remaining off-target effects. I therefore continued to characterize *Pus7^{fs}* line 15-2 which is subsequently termed *Pus7^{fs}* for *Pus7*

frameshift. I started to characterize the *Pus7^{fs}* flies by performing a classical lifespan assay. Interestingly, we observed a significant reduction in the lifespan of *Pus7^{fs}* males which could be partially rescued by overexpressing *Pus7* in the whole fly indicating defects in their general health (Figure 14C; Supplementary figure S.2).

We previously showed that *Pus7^{fs}* flies featured orientation defects and hyperactivity which are indicative of neurological defects [de Brouwer et al., 2018]. We further investigated markers for potential neurological defects and performed a bang sensitivity assay to check for seizures in response to mechanical stress. We could not observe any indications for seizures in *Pus7^{fs}* flies. Instead, we measured a significantly faster recovery, presumably as a result of the increased activity of *Pus7^{fs}* flies (Figure 14D). One of the hallmarks of *PUS7* mutation in human is increased aggression levels which we also observed in the *Drosophila Pus7* model [de Brouwer et al., 2018]. In flies, increased aggression manifested in an increase of time spent performing aggressive behaviors between *Pus7^{fs}* flies. I further validated this phenotype and found that it is most pronounced for behaviors classified as strong interactions of aggression like lunging and tussling [Chen et al., 2002] (Figure 14E & F). Strikingly, I could completely rescue this phenotype by overexpressing *Pus7* either in the whole fly or specifically in neurons substantiating the neuronal role of *Pus7* in this behavior (Figure 14E). Furthermore, this rescue capability required the catalytic activity of *Pus7* confirming the role of pseudouridine in this defect (Figure 14F).

Patients with mutations in *PUS3* and *PUS7* both showed mental and physical developmental delay. We aimed to verify whether developmental delay could be observed in the *Pus7* fly model by measuring the required time of a laid egg to develop to a hatching first instar larva. Remarkably, we observed a hatching delay of approximately two hours suggesting developmental delay in the embryogenesis of *Pus7^{fs}* flies (Figure 14G). Additionally, I observed a noticeable reduction in the number of offspring of *Pus7^{fs}* females. Therefore, I quantified the fertility of *Pus7^{fs}* flies by measuring the number of laid eggs and their hatching rate over a time course of 15 days. Notably, both the amount of laid eggs as well as their hatching rate was strongly reduced in *Pus7^{fs}* females and declined further during aging (Figure 14H). The egg-laying defect could be completely rescued by overexpressing *Pus7* in the whole fly. Since egg-laying behavior is also influenced by paternal contribution through seminal sex-peptides [Chapman et al., 2003], I further investigated the origin of the egg-laying defect by crossing *wild type* males to *Pus7^{fs}* females and vice versa. Mating *Pus7^{fs}* males to *wild type* females was not sufficient to cause an egg-laying defect (Figure 14I). The fact that this defect was exclusive to *Pus7^{fs}* females indicates a maternal role of *Pus7*. Further experiments are required to unravel the origin of the egg-laying phenotype. Possible causes include the progressive loss of germline stem cells which can be assessed by immunofluorescence stainings [Singh et al., 2013]. Furthermore, defects downstream of egg production can be revealed by quantifying the time required for ovulation as well as the transfer of the released oocyte through the oviduct and the uterus as demonstrated by [Knapp and Sun, 2017]. Ovulation requires the rupture of the posterior somatic follicle cells to release the oocytes into the oviduct [Knapp and Sun, 2017] while the subsequent motion of the egg requires octopaminergic neurons in the abdominal ganglion and intact oviduct musculature [Ferreira, 2022].

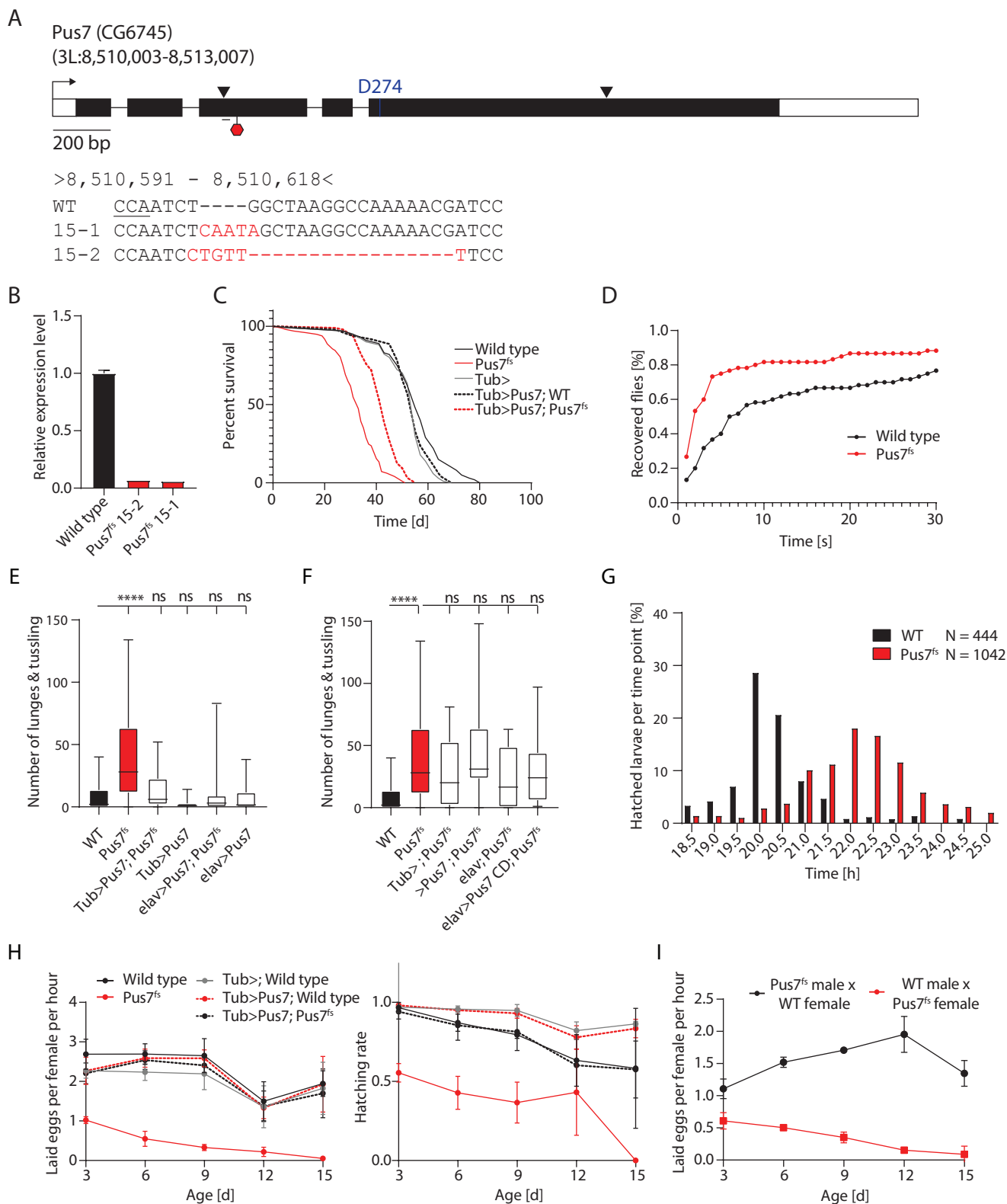


Figure 14: *Pus7^{fs}* mutant flies feature fertility defects, hyperactivity, increased aggression and developmental delay. (A) Schematic of the approach to generate *Pus7* mutants using CRISPR/Cas9. White boxes indicate UTRs. Black boxes represent exons. Lines indicate introns. Arrowheads indicate the gRNA target sites. The red hexagon shows the position of the premature stop codon in the *Pus7^{fs}* 15-2 mutant. The catalytic Asp274 is indicated in blue. The small line in the schematic indicates the zoomed location showcasing the indel mutation at the gRNA1 target site. The underlined sequence in the zoomout indicates the PAM sequence while indel mutations are shown in red. (B) *Pus7* mRNA levels as assayed by RT-qPCR. (C) Lifespan of *Pus7^{fs}* males is reduced on normal food. (D) Bang sensitivity assay to measure recovery time after mechanical stress. n = 30 males and 30 females per genotype. *Continued on next page.*

Figure 14 (previous page): (E & F) Aggression assays between 6-7 day old socially isolated male flies. Lunging and tussling were quantified for 20 minutes. Tussling events were scored twice. CD: catalytic dead. Statistic analysis was performed with a Kruskal-Wallis one-way ANOVA followed by a Dunn's post hoc test. (G) Time required for the development of laid eggs until hatching of the L1 instar larva. (H & I) Quantification of egg-laying rate or 1st instar larva hatching rate in 3-day intervals. Fresh food was provided daily. Average and standard deviation of four technical replicates are displayed.

Overexpression of *Pus7* in follicle cells, neurons or muscles, respectively, could pinpoint a function of *Pus7* in the respective cell type or tissue.

2.2.3 The role of *Pus7* in oogenesis

Both publicly available data as well as the analysis of the *Pus7* expression pattern in *Drosophila* revealed a distinct enrichment of *Pus7* in ovaries (Figure 12; Figure 13). Our observation of reduced fertility of *Pus7^{fs}* flies prompted us to further investigate a potential role of *Pus7* in oogenesis or embryogenesis. I started by extensively inspecting *Pus7^{fs}* embryos to find phenotypes hinting to potential defective processes during embryonic development. Interestingly, I observed the occurrence of three distinct phenotypes: (I) embryos with shorter and broader appendages, (II) shorter embryos with thin and severely shortened appendages reminiscent of ventralization phenotypes and (III) embryos with fused appendages (Figure 15A). The latter occurred only in singular cases and was therefore omitted from further quantifications. Quantifications of the embryo lengths revealed that ventralized embryos were approximately 13.5% shorter than normally shaped embryos (Figure 15B). Furthermore, I observed notable increases in the frequencies of these phenotypes with the broad appendages phenotype and the ventralized phenotypes occurring more than 2-times and 15-times as frequent in *Pus7^{fs}* embryos, respectively (Figure 15B; Table 2.1).

Ventralization of the *Drosophila* embryo requires correct localization and translation of certain mRNAs involved in dorso-ventral axis specification including *gurken* (*grk*) [Neuman-Silberberg and Schüpbach, 1993]. A screen for factors involved in the localisation and translational regulation of *gurken* mRNA revealed novel interactors including *Pus7* and *hephaestus* (*heph*), the fly homologue of the mammalian polypyrimidine tract binding protein 1 (PTBP1) [McDermott et al., 2012]. A follow-up study demonstrated that *heph* is involved in axis specification of *Drosophila* embryos by regulating *Grk* protein localization and the organization of the actin cytoskeleton. Strikingly, mutation of *heph* causes phenotypes closely resembling the ventralization phenotypes observed upon mutation of *Pus7*. Additionally, an enrichment of Ψ sites was discovered in the consensus motif of mammalian PTBP1 in unpublished work from our collaborators suggesting that PTBP1 and perhaps *Drosophila* *heph* might act as conserved Ψ reader proteins (Chuan He, personal communication).

Therefore, I performed genetic combination assays to test our hypothesis that *Pus7* might play a role in the same pathway of axis specification as *heph* [McDermott and Davis, 2013]. Since the *heph⁰³⁴²⁹* allele is homozygous lethal, I quantified the embryo phenotype frequency in the offspring of flies carrying one *heph⁰³⁴²⁹* allele in addition to one or two copies of the *Pus7^{fs}* allele. These females were crossed to *wild type* males so that only maternal effects on the phenotype frequency

could be observed. The frequency of ventralized embryos was not strongly altered in embryos of *Pus7^{fs}/heph⁰³⁴²⁹* females (Figure 15D). Similarly, no drastic changes were observed in *heph⁰³⁴²⁹*, *Pus7^{fs}/Pus7^{fs}* females. This suggests that the observed abnormalities in embryos of *Pus7^{fs}* females are caused by a mechanism independent of the *heph*-Grk axis.

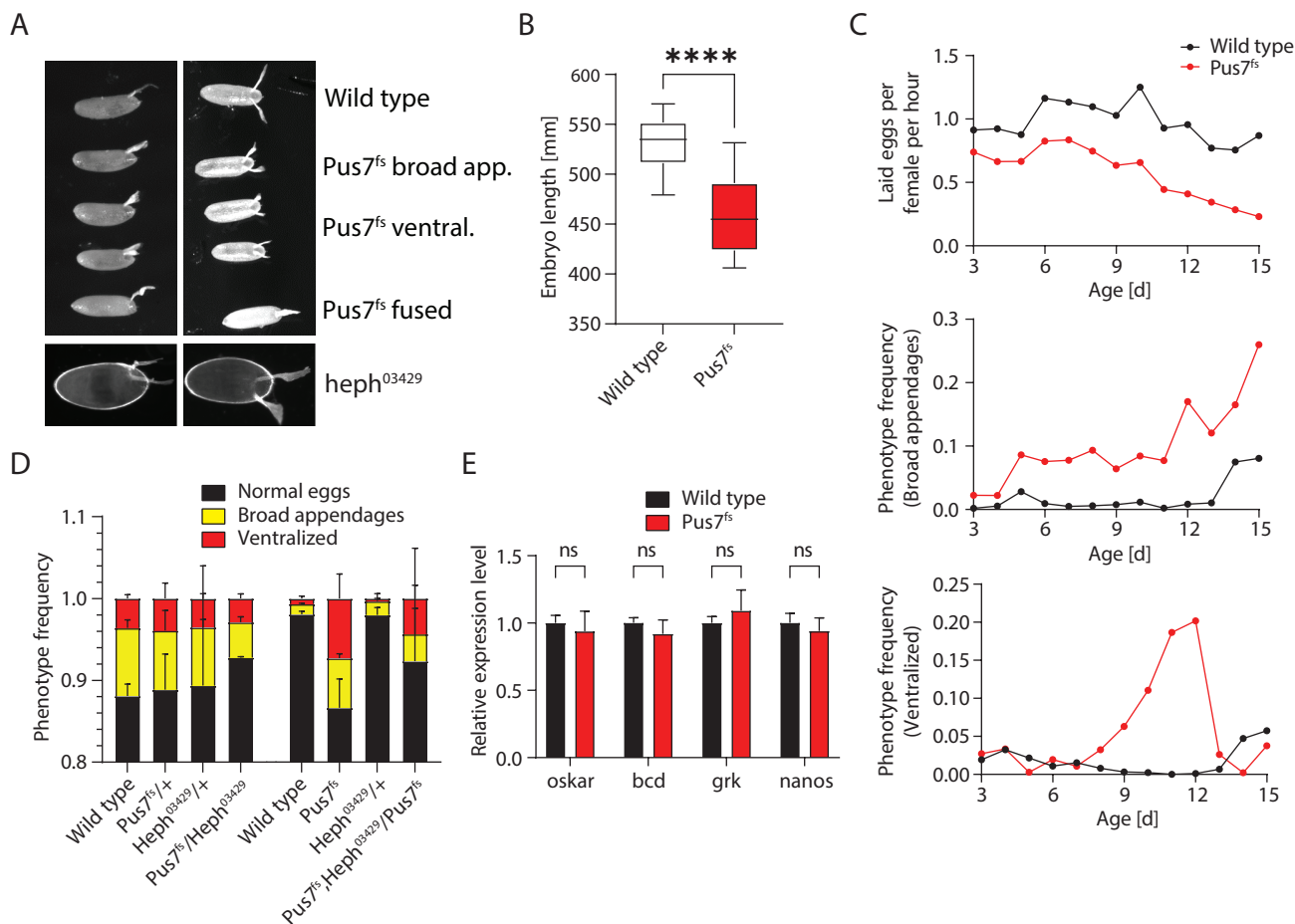


Figure 15: Lack of *Pus7* causes ventralization phenotypes in *Drosophila*. (A) Phenotypes observed in *Pus7^{fs}* embryos. Image adapted from [McDermott and Davis, 2013]. (B) Length of ventralized embryos laid by *wild type* females (n = 25) and *Pus7^{fs}* females (n = 14). A two-tailed unpaired t.test was used for statistic evaluation. (C) Distribution and frequency of ventralized phenotypes in embryos during aging of female mothers. (D) Genetic combination assays with *heph⁰³⁴²⁹* combined with one or two copies of *Pus7^{fs}*. Two technical replicates of ten females crossed to five *wild type* males were evaluated per genotype. (E) RT-qPCR evaluation of key mRNAs involved in oogenesis.

Table 2.1: Frequency of abnormal embryo phenotypes in *Pus7^{fs}* flies.

	Wildtype	<i>Pus7^{fs}</i>	Factor
Total	12754	7961	0.62
Normal	12578 (98.62%)	6967 (87.51%)	0.89
Broad appendages	135 (1.06%)	575 (2.78%)	2.62
Ventralized	41 (0.32%)	419 (5.26%)	16.44

2.2.4 *Pus7^{fs}* flies lack *Pus7* catalytic activity

Since the indel mutations in *Pus7^{fs}* caused a premature stop codon upstream of the catalytic domain of *Pus7*, we expected these flies to harbor no *Pus7* pseudouridylation activity (Figure 14). In order

to confirm this, we collaborated with the Schwartz lab to perform Ψ -seq to identify Ψ sites in a transcriptome wide manner in fly heads of 3-4 day old mated females. This method relies on chemical derivatization of Ψ by reaction with CMC which results in truncations in a subsequent reverse transcription step which can be mapped by NGS [Schwartz et al., 2014]. Among non-coding RNAs, we consistently found position 13 of six different tRNA species to be reduced in pseudouridylation which are known targets of Pus7 in yeast (Figure 16; Table 2.4) [Behm-Ansmant et al., 2003, de Brouwer et al., 2018]. Five of the nine tRNA targets were also identified as PUS7 targets in Epstein-Barr virus-transformed lymphoblastoid cells (EBV-LCLs) derived from *PUS7* patients indicating their conservation across species (Figure 16) [de Brouwer et al., 2018].

Multiple studies employing methods for transcriptome-wide mapping of pseudouridine identified sites in yeast, human and *Drosophila* mRNA [Schwartz et al., 2014, Carlile et al., 2014, Li et al., 2015, Song et al., 2023]. However, while Ψ -seq is well suited to map sites in abundant RNA species, its ability to detect sites in mRNA is quite limited [Safra et al., 2017b]. In Ψ -seq, the estimation of Ψ ratios strongly depends on sequencing depth and modification stoichiometry which are expected pitfalls in an attempt to map mRNA sites [Schwartz et al., 2014] where the average modification stoichiometries in PUS7-dependent Ψ sites can be as low as 10% in mammals [Dai et al., 2022]. Therefore, we aimed to identify Pus7-dependent mRNA sites in *Drosophila* by collaborating with the He lab who recently developed a highly sensitive transcriptome-wide mapping technique [Dai et al., 2022]. This technique is based on the reactivity of bisulfite (BS) with pseudouridine generating a Ψ -BS adduct leading to deletions during reverse transcription which can be readily mapped by NGS [Fleming et al., 2019]. An additional advantage of BID-seq is the higher accuracy of capturing the true modification stoichiometry. Fully modified sites feature deletion rates of 60-70%, whereas only 43% of reads at fully modified sites terminated at the Ψ site in Ψ -seq [Schwartz et al., 2014]. Thus, BID-seq harbors reduced chances of generating false negative sites. Additionally, BID-seq achieves a full conversion of Ψ to Ψ -BS adducts in a single reaction [Dai et al., 2022]. In contrast, Ψ -seq requires cleavage of non- Ψ -CMC residues after derivatization which bears an inherent risk of generating false positives [Zaringhalam and Papavasiliou, 2016]. Furthermore, the BS-dependent derivatization of Ψ turned out to be highly sensitive, enabling the detection of changes as low as 5% in modification ratio between two conditions, thereby enabling the detection of lowly modified sites [Khoddami et al., 2019, Dai et al., 2022].

Our attempt to map pseudouridine sites in polyA-enriched RNA of *Pus7^{fs}* ovaries using bisulfite-induced deletion sequencing (BID-seq) revealed five mRNAs and one lncRNA to be significantly less pseudouridylated in the *Pus7^{fs}* condition (Figure 16B; Table 2.3). Notably, only three of the six identified targets (CG8223, scu, PIG-K) contained the Pus7 UNUAR consensus sequence as well as 0% modification ratio in the *Pus7^{fs}* condition suggesting that these transcripts are solely targeted by Pus7. Coincidentally, the other three targets (CG9135, CG17691, lncRNA:CR40469) without a clear Pus7 motif showed residual Ψ ratios of 5-65% suggesting that they might also be targeted by other Pus enzymes (Table 2.3). Alternatively, the activity of other Pus enzymes targeting these sites might be reduced upon lack of Pus7.



Figure 16: Pus7 modifies cytoplasmic tRNAs, mRNAs and lncRNAs in *Drosophila*. tRNA targets of Pus7 as identified by Ψ -seq in heads of *Pus7*^{fs} flies and in samples from EBV-LCLs derived from *PUS7* patients, respectively. Data for human *PUS7* tRNA targets obtained from [de Brouwer et al., 2018]. (B) Schematic of the Pus7 targets as identified by BID-seq in 1x poly(A) enriched RNA. Arrowheads indicate the pseudouridine sites. White boxes indicate UTRs. Black boxes represent exons. Lines indicate introns or the RNA transcript of lncRNA:CR40469. (C) RT-qPCR to quantify the expression levels of Pus7 targets identified in BID-seq. Mann Whitney U test followed by Holm Sidak multiple comparisons test were used for statistic analysis.

Table 2.2: Putative *Pus7* substrates in *Drosophila*. P-values of chi-squared test (Chi-squ.) and t-test are indicated.

Coordinates	5-bp	$\Psi\%$ <i>Wild type</i>	$\Psi\%$ <i>Pus7^{fs}</i>	Chi-squ.	t-test	score
chr3L.trna31-ProCGG:13	TCTAG	32	1	5.51E-60	4.7E-07	0.676
chr2R.trna25-GluCTC:13	TCTAG	10	0	4.95E-199	5.8E-04	0.586
chr2L.trna12-AspGTC:13	TATAG	4	0	2.89E-86	5.9E-06	0.422
chr3R.trna24-GlyTCC:13	TGTAA	26	2	4.63E-61	3.3E-03	0.361
chr3L.trna3-GluCTC:13	TCTAG	10	1	2.21E-21	8.53E-03	0.352
chr2L.trna18-ProAGG:13	TCTAG	28	1	6.47E-24	1.6E-04	0.350
chr2R.trna26-GluTTC:13	TCTAG	25	0	6.73E-59	4.1E-03	0.344
chr2L.trna2-GlnCTG:13	TGTAA	30	1	8.48E-17	3.1E-03	0.197
chr3R.trna17-ProTGG:13	TCTAG	26	2	8.95E-19	5.8E-03	0.155
chr2R.trna17-HisGTG:13	TCTAG	2	0	8.91E-04	1.6E-03	0.038

Table 2.3: *Pus7* mRNA targets in ovaries.

Chromosome	Position	5-bp	Gene symbol	Annotation	$\Psi\%$ <i>Wild type</i>	$\Psi\%$ <i>Pus7^{fs}</i>
X	2008944	TGTAG	PIG-K	CDS	55	0
X	18092775	TCTAG	scu	3'UTR	29	0
3R	8753797	TCTAG	CG8223	stop codon	10.5	0
2R	1595021	GTTTT	CG17691	CDS	75	65
2L	6052747	GTTTA	CG9135	CDS	20.5	5
X	122617	ATTGA	lncRNA:CR40469	-	19.5	5

Interestingly, the Ψ site in CG8223 is located in the uridine of the UAG stop codon. It has been shown that pseudouridylation of stop codons in human mRNAs could cause stop codon readthrough [Dai et al., 2022]. Therefore, it is interesting to speculate that this site could perform a similar function in *Drosophila*. The Ψ site in scu is located in the 3' UTR which were shown to affect mRNA stability in human [Siegel et al., 2021]. We therefore investigated whether Ψ sites affected the expression levels of their transcripts. To this end, I performed RT-qPCR but found no significant differences in the expression levels of any of the *Pus7* target mRNAs (Figure 16C). We therefore conclude that few mRNAs are targeted by *Pus7* which are apparently not regulated in their expression levels by pseudouridine. Further experiments assessing the *in vivo* localization of *grk* mRNA and Grk protein are necessary to investigate a potential indirect role of *Pus7* in regulating its expression. Taken together, tRNAs seem to be more prominent targets at least in this *Pus7* fly model.

2.2.5 *Pus7* mutation leads to a reduction of tRNA^{Asp} levels

Ψ -seq in heads of *Pus7^{fs}* flies allowed us to identify the tRNA targets of *Pus7*. Furthermore, the NGS data acquired during Ψ -seq revealed changes in the expression levels of all detected tRNA species. Strikingly, we observed reduced levels of tRNA^{Asp} and to some extent of the two tRNA^{Pro} isoacceptors carrying the AGG and TGG anticodons (Figure 17).

One issue in the NGS dataset of Ψ -seq is that the high frequency of post-transcriptional modifications on tRNAs could cause errors and biases during the reverse transcription process which prompted us to confirm this observation with microscale thermophoresis (MST), a method that is not dependent on reverse transcription [Zheng et al., 2015, Kietrys et al., 2017, Potapov et al., 2018]. Essentially, MST enables us to quantify a specific tRNA species within a mixture of total tRNAs

by utilizing a fluorescently labeled probe that detects the tRNA of interest through base-pairing, as explained in [Jacob et al., 2019]. Through this method, we were able to verify that tRNA^{Asp} levels were noticeably diminished in *Pus7^{fs}* flies while tRNA^{Gly} remained unaffected (Supplementary figure S.3A&B). Moreover, when we overexpressed *Pus7* cDNA in the entire fly, the tRNA^{Asp} levels returned to the normal level seen in the *wild type*. These results were further confirmed through the use of northern blot analysis (Supplementary figure S.3C).

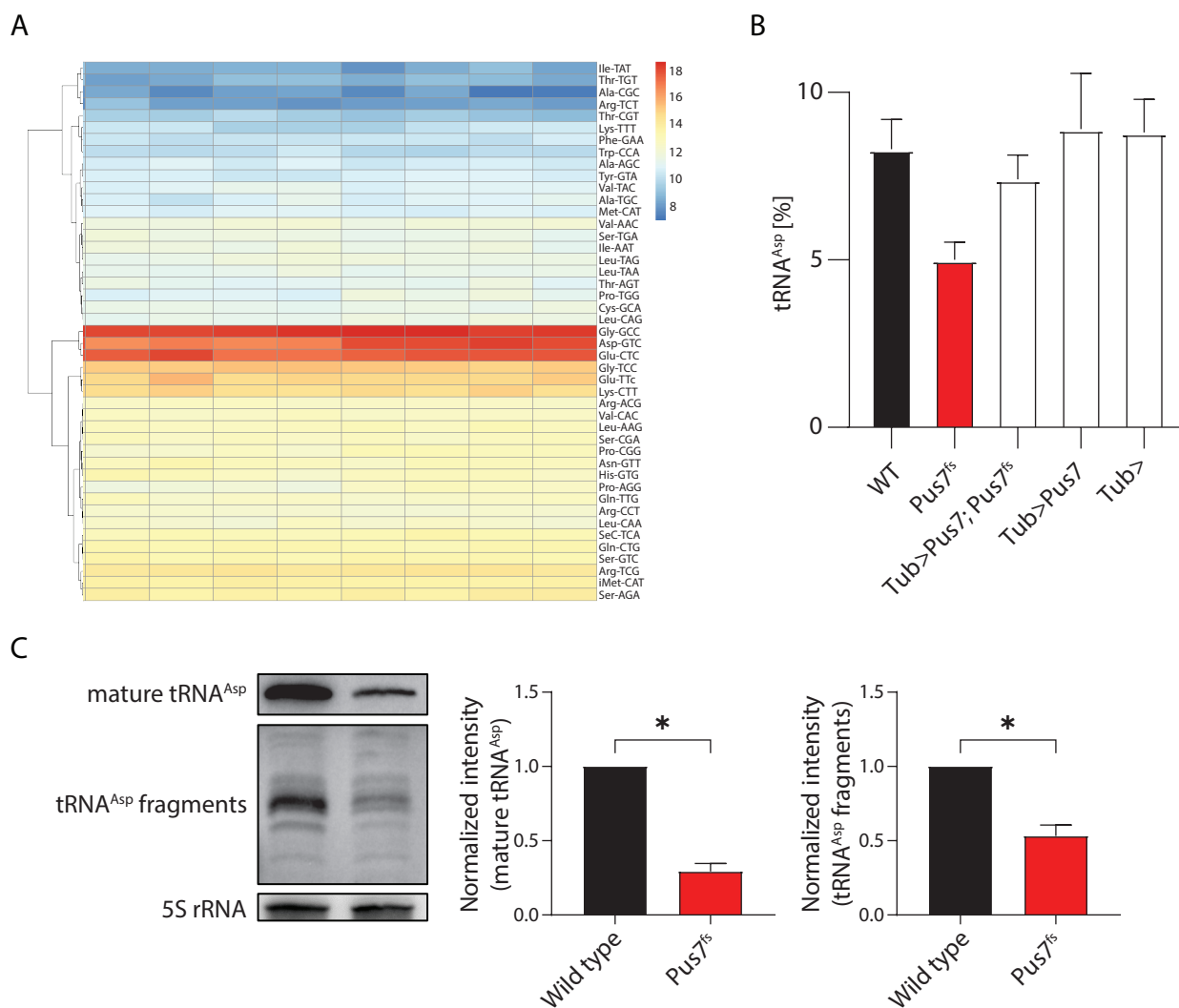


Figure 17: tRNA^{Asp} is downregulated in *Pus7^{fs}* mutants. (A) tRNA levels in heads of *Pus7^{fs}* flies according to Ψ -seq. (B) Absolute tRNA^{Asp} content in total tRNA according to MST. (C) Quantification of mature tRNA^{Asp} levels and tRNA^{Asp} fragment levels according to northern blot.

2.2.6 tRNA^{Asp} overexpression partially rescues the *Pus7^{fs}* phenotypes.

Next, we aimed to investigate whether the reduced levels of tRNA^{Asp} were involved in the mechanism causing the observed defects of *Pus7^{fs}* flies. Hence, I generated a plasmid carrying four copies of the first isodecoder of tRNA^{Asp} and used it to generate a transgenic fly line carrying up to eight copies of tRNA^{Asp} in the homozygous state (Figure 18A). I started by quantifying any possible ameliorations of the increased aggression levels in *Pus7^{fs}* flies. Strikingly, overexpression of tRNA^{Asp} completely

rescued the aggression levels back to *wild type* levels indicating a role of tRNA^{ASP} in this defect (Figure 18B). Next, I investigated whether tRNA^{ASP} overexpression could also boost the reduced egg-laying rate observed in *Pus7^{fs}* females. Interestingly, the egg-laying defect could be partially rescued by overexpressing the first isodecoder of tRNA^{ASP} (Figure 18C). Finally, I examined whether tRNA^{ASP} overexpression had any effect on the lifespan of *Pus7^{fs}* flies fed with 5% sucrose solution. Intriguingly, tRNA^{ASP} overexpression further decreased the lifespan indicating a negative effect of tRNA^{ASP} overexpression on fly health in these conditions (Figure 18E).

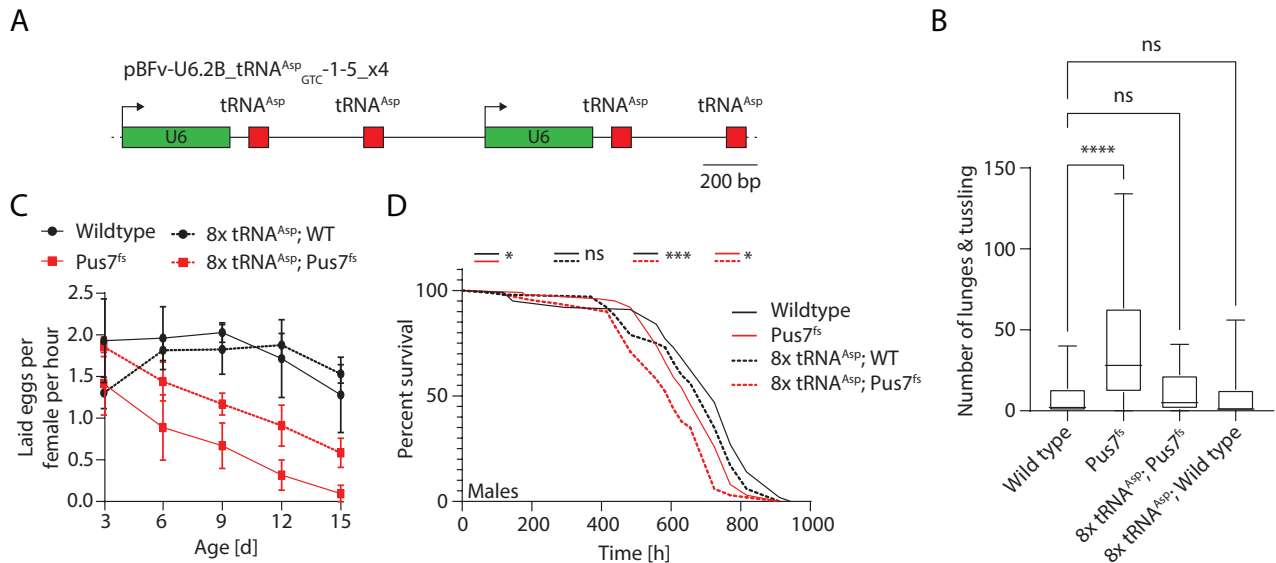


Figure 18: tRNA^{ASP} overexpression partially rescues the *Pus7^{fs}* phenotypes. (A) Schematic of the transgene carrying four copies of tRNA^{ASP}. Green boxes indicate U6 promoters. Red boxes indicate tRNA^{ASP} gene sequences. (B) tRNA^{ASP} overexpression rescues the strong aggression phenotype of *Pus7^{fs}*. (C) tRNA^{ASP} overexpression partially rescues the egg-laying defect of *Pus7^{fs}* flies. (D) tRNA^{ASP} overexpression does not rescue the lifespan defect of *Pus7^{fs}* flies on 5% sucrose solution. Statistic analysis was performed with a Kruskal-Wallis one-way ANOVA followed by a Dunn's post hoc test.

2.2.7 *Pus7* mutation leads to translational changes

After having employed multiple independent methods to confirm the downregulation of tRNA^{ASP} in *Pus7^{fs}* flies, we aimed to address the question whether this defect might cause any changes in the translatoome. Therefore, we performed ribosome profiling in collaboration with the Gatfield lab to assess global translational changes upon deletion of *Pus7* *in vivo* using heads of 3-4 day old mated females and identified 355 transcripts (203 downregulated, 152 upregulated) with significant changes in ribosome footprint count between *Pus7^{fs}* and *wild type*. An unbiased GO term analysis did not yield any specific common features of these dysregulated genes (data not shown). Therefore, we continued by investigating the effect of individual codons on translation by evaluating codon-dependent changes in ribosome occupancy. Strikingly, we observed an increase in ribosome occupancy specifically over aspartate codons in the *Pus7^{fs}* condition (Figure 19A). A similar but weaker effect was discovered for glutamate and proline codons (Figure 16A). While the reduced levels of tRNA^{Pro} could explain this observation for the proline codon, it is still unclear why glutamate codons seemed to be affected in

Pus7 mutant flies as tRNA^{Glu} levels are unchanged. Next, we evaluated ribosome footprints based on which codons were currently occupying the exit (E), peptidyl-transferase (P) and aminoacyl (A) site of the ribosome. Certain dicodons can drastically affect translation speed to facilitate protein folding which is reflected by changes in the ribosome occupancy over such codon pairs [Gamble et al., 2016]. This revealed that independent of the amino acid in the P site, ribosome occupancy is increased when an aspartate codon occupies the A site of the ribosome suggesting that translation is stalled until a mature tRNA^{Asp} enters the translating ribosome in the *Pus7^{fs}* condition (Figure 19B). Furthermore, we observed combinatoric effects of dicodons affecting translation speed. For example, dicodons of leucin and aspartate or methionine and aspartate in the P-site and A-site, respectively, featured the highest increase in ribosome occupancy while leucin-leucin dicodons showed a reduced ribosome occupancy (Figure 19B).

We next evaluated global changes in the translome based on the translation efficiency (TE) of all detected genes which is expressed as the amount of ribosome footprints that were detected per mRNA molecule by total RNA-seq. All detected genes were categorized by whether they are significantly changed in translation efficiency, transcription based on total RNA-seq or both as described in [Jansson et al., 2021] (Figure 19C). In general, changes in translation efficiency correlated well with changes in transcript levels suggesting that higher expressed transcripts contain a higher ribosome density (Figure 19D).

The dicodon analysis suggested strong effects of certain dicodons on ribosome occupancy. We therefore analyzed how the dicodon content of a gene affects its ribosome density as indicated by its translation efficiency. While the dicodons MD and LD lead to an increase in ribosome occupancy, they had no effect on the translation efficiency of the transcript (Figure 19E). This also applied to the LL dicodon which caused reduced ribosome occupancy but no changes in translation efficiency. This suggests that these dicodons might cause local changes in ribosome occupancies, however, they do not strongly affect the ribosome occupancy over the rest of the transcript.

We therefore aimed to check for ribosome stalling at aspartate codons upon lack of *Pus7* using an *in vitro* reporter system. I designed a dual reporter carrying both the coding sequences of GFP and mCherry under the control of two separate Actin5C promoters. In order to quantify the effects of stretches of different amino acids on translation, I modified this reporter to carry a stretch of aspartates upstream of the translation start site of GFP (Asp-GFP; Supplementary figure S.4A). In the case of ribosome stalling, this reporter was expected to show reduced GFP translation upon knockdown of *Pus7* as a result of impaired translation at the Asp codon stretch. As a negative control, I designed a plasmid containing a stretch of leucines fused to GFP (Leu-GFP). The final plasmids with aspartate and leucine stretches contained M(11xD)I or M(10xL)DI as additional codons upstream of the ATG of GFP, respectively. As a control, an unmodified plasmid with the CDS of GFP was used. Next, *Drosophila* S2R+ cells were treated with siRNA targeting *Pus7* and eventually transfected with one of the three plasmids. The *Pus7* knockdown efficiency was quantified by RT-qPCR and achieved 80-85% in the three technical replicates (Supplementary figure S.4B). Independent of siRNA treatment, we could observe a distinct reduction of GFP intensity both in Asp-GFP and

2.2 Characterization of *Pus7* in *Drosophila*

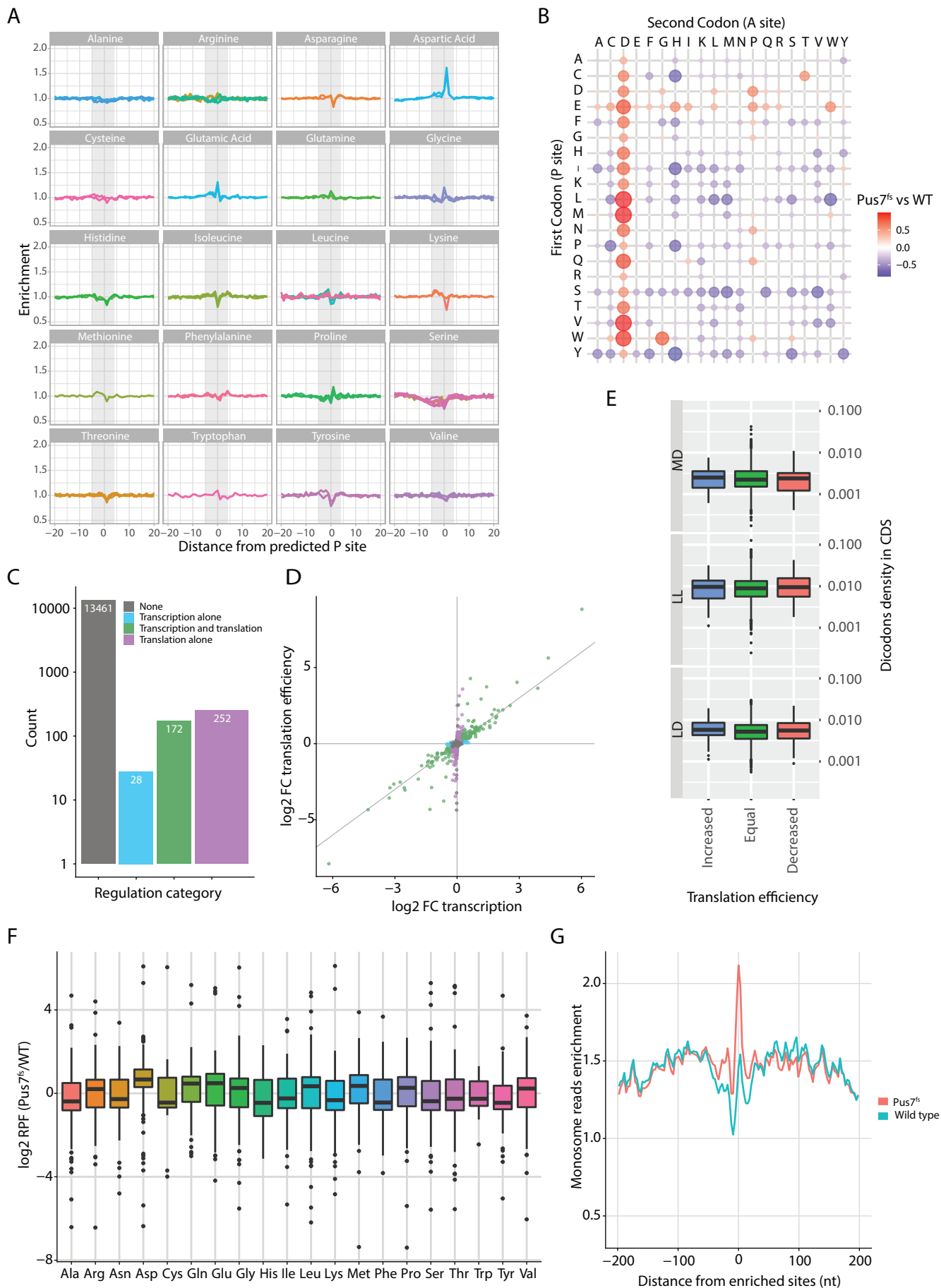


Figure 19 (previous page): Lack of *Pus7* causes increased ribosome occupancy over aspartate codons *in vivo*. Ribosome profiling was performed in heads of *Pus7^{fs}* and *wild type* flies. (A) Differential ribosome occupancies over all codons. (B) Effect of dicodons in the P and A site of the ribosome on the ribosome occupancy. (C) Categorizing genes with changes in translation, transcription or both based on translation efficiency and transcript levels. (D) Scatter plot of genes categorized in (C). (E) Effect of the density of LD, LL and MD dicodons on translation efficiency. (F) Enrichment of codons in pausing sites in the *Pus7^{fs}* or *wild type* condition. (G) Enrichment of ribosome reads between *Pus7^{fs}* or *wild type* around pausing sites.

Leu-GFP transfected cells suggesting that both Asp and Leu stretches negatively affect translation, although this effect was visibly more pronounced in the case of Asp stretches (Supplementary figure S.4C). Unfortunately, there was no visible difference upon knockdown of *Pus7* suggesting that either knockdown of *Pus7* is not sufficient to trigger the tRNA^{Asp} reduction, that the reduction in tRNA^{Asp} does not occur in S2R+ cells, or that translation in S2R+ cells is not affected upon loss of *Pus7* and concomitantly tRNA^{Asp} (Supplementary figure S.4D). Therefore, no clear conclusion could be drawn about whether a lack of *Pus7* could lead to ribosome stalling in S2R+ cells.

Finally, we returned to the *Pus7* fly model and attempted to address this question by identifying codons with ribosome pausing based on differential ribosome occupancies between *Pus7^{fs}* and *wild type* as described in [Stein et al., 2022]. This analysis revealed 1196 codons with increased and 1137 codons with reduced ribosome occupancy in *Pus7^{fs}* (Figure 19F). Remarkably, among all pausing sites, aspartate showed the highest ribosome occupancy in the *Pus7^{fs}* condition. Next, we investigated whether a potential reduction in translation speed could lead to collisions of ribosomes which would manifest in increased ribosome footprint counts upstream of the pausing sites. Interestingly, among the 1196 pausing sites with increased ribosome occupancy in *Pus7^{fs}* we could indeed observe a mild increase in ribosome footprint reads approximately 50 nt upstream of the pausing sites which could indicate disome formation (Figure 19G).

In the end, the riboseq dataset alone did not allow us to distinguish whether genes featuring a high translation efficiency showed a high ribosome occupancy as a result of high translation or due to ribosome stalling leading to reduced translation. To investigate potential effects of *Pus7* mutation on the proteome, we performed mass-spec with *Pus7^{fs}* heads of 3-4 day old mated females in collaboration with the protein analysis facility and identified 716 proteins with significant changes in their abundance (Supplementary table S.1). The intersection of the ribosome profiling and proteomics datasets included 674 of those significantly dysregulated genes (Figure 20A). Of those, 119 genes also featured significant changes in ribosome occupancy. In general, we observed a good correlation between ribosome occupancy and protein abundance indicating that higher RPF counts usually reflect increased translation. We could not identify any candidate genes which feature both significantly upregulated ribosome occupancies and significantly reduced protein levels indicative of impaired translation due to ribosome stalling. Hence, we investigated whether the aspartate codon density had any effect on the translation levels of significantly dysregulated proteins. We could not observe any enrichment or depletion of aspartate codons in proteins with dysregulated abundance (Figure 20B). These observations suggest that there is no direct association between protein abundance and Asp codon content.

2.2 Characterization of *Pus7* in *Drosophila*

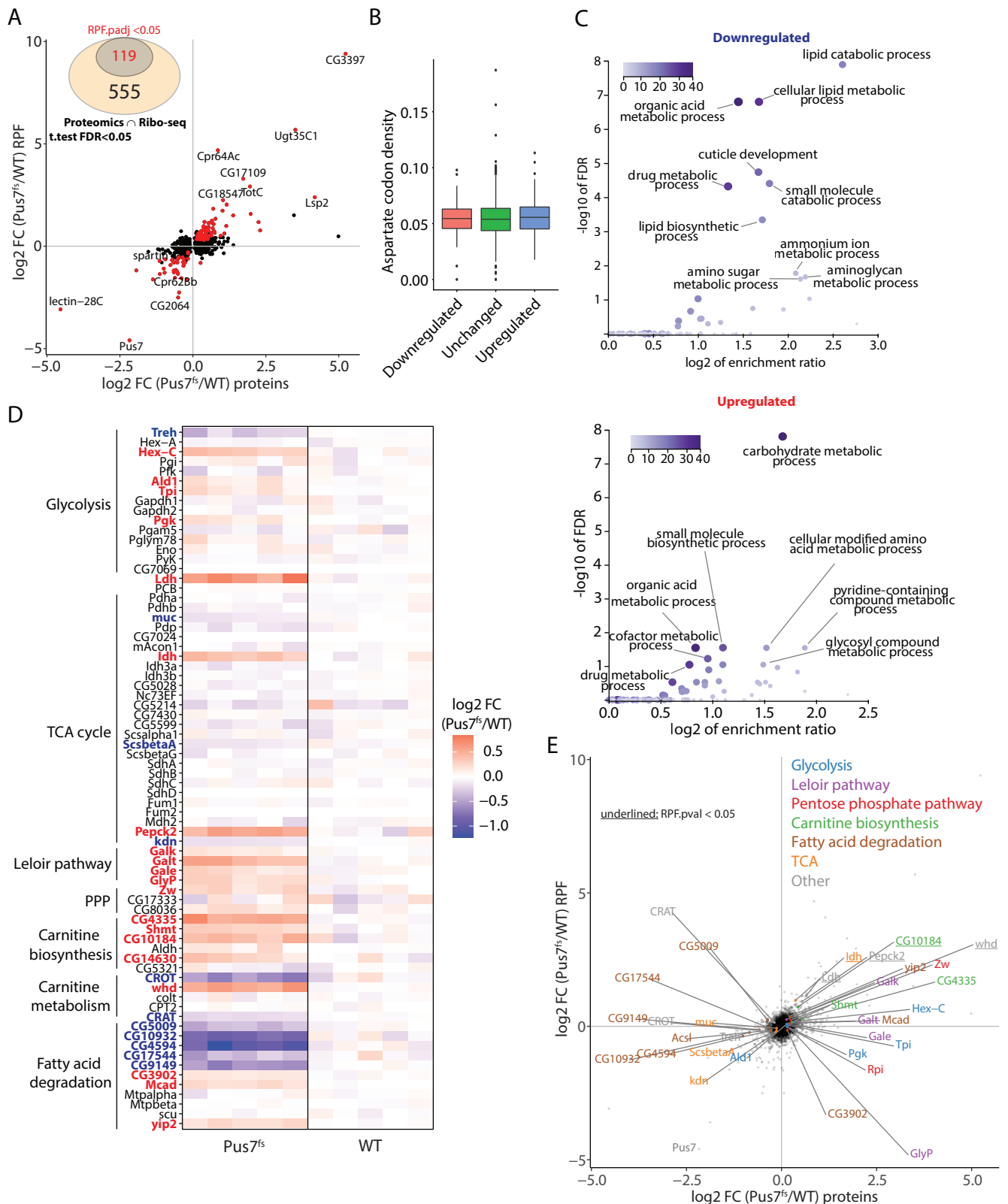


Figure 20: Metabolic enzymes are dysregulated in *Pus7*^{fs} flies. (A) Scatterplot of genes identified by ribosome profiling and mass-spectrometry which are dysregulated on the protein level. Genes with significant changes in ribosome occupancy are marked in red. (B) The aspartate density does not determine whether a protein is up or downregulated in *Pus7*^{fs} flies. (C) GO term analysis of up and downregulated proteins in *Pus7*^{fs}. (D) Heatmap depicts changes on the protein level in a manually curated list of proteins involved in metabolism in *Pus7*^{fs}. (E) Scatterplot of the intersection of the proteomics and ribosome profiling datasets. Genes of relevant cellular pathways are highlighted. Genes with significant changes in ribosome occupancy are underlined.

We therefore analyzed the changes in the translome in an unbiased manner by performing a GO term analysis and observed that upon mutation of *Pus7* multiple metabolic processes were affected (Figure 20C). While lipid metabolism was among the most downregulated pathways, carbohydrate metabolism including glycolytic genes was the most upregulated process. In total, multiple different metabolic pathways including glycolysis, pentose phosphate pathway (PPP), leloir pathway, tricarboxylic acid (TCA) cycle, carnitine biosynthesis and carnitine metabolism as well as fatty acid degradation were dysregulated on the protein level in *Pus7^{fs}* flies (Figure 20D). Of note, only five genes (*Ldh*, *Idh*, *Pepck2*, *CG10185*, *whd*) featured both significantly higher ribosome occupancy as well as protein levels indicating that most changes on the protein level were due to increased protein stability rather than due to increased translation (Figure 20E).

Finally, I attempted to further validate our ribosome profiling analysis using the proteomics dataset. I expected that genes featuring multiple ribosome pausing sites were more likely to be downregulated on the protein level as a result of slower translation. Hence, I analyzed whether there is a correlation between the amount of detected ribosome pausing sites in a gene and its protein level (Supplementary figure S.5). Surprisingly, all genes with pausing sites were upregulated on the protein level. Furthermore, among those candidates with more than five pausing sites we could observe a strong correlation between the protein level and the number of pausing sites in *Pus7^{fs}*. This suggests that the underlying ribosome occupancy which was used to define these sites in fact mostly represents their increased translation rate rather than impaired translation or ribosome stalling.

Since the changes in the proteome of *Pus7^{fs}* flies could not be explained by a lack of tRNA^{Asp}, we aimed to identify mechanisms that might indirectly cause the proteomic changes. Since many tRNA diseases feature activation of the ISR, I first investigated whether *crc*, the *Drosophila* homologue of ATF4 and main transcription factor of the ISR genes, is upregulated in its translation. The *ATF4* mRNA contains conserved uORFs that sequester translating ribosomes in unstressed cells, thereby negatively regulating translation of the ATF4 ORF [Xiao et al., 2022]. In stressed cells, delayed translation reinitiation due to a lack of eIF2-GTP causes scanning ribosomes to bypass the regulatory uORFs and reinitiate translation at the ATF4 ORF to facilitate its translation. According to our ribosome profiling data, translation at the *ATF4* locus is neither affected in the uORFs nor in its ORF in *Pus7^{fs}* flies suggesting that the ISR is not activated (Figure S.6A). To confirm this, I quantified the expression of downstream targets of the ISR. Both activation of the ISR and heatshock trigger the expression of the transcription factor dFoxo to regulate expression of stress response genes. To corroborate our previous observation that the ISR is not activated, I indirectly measured activation of the ISR by analyzing the protein levels of 356 genes regulated by dFoxo [Alic et al., 2011]. On average, dFoxo targets are not drastically dysregulated as only few candidate genes reach fold changes of $\pm 25\%$ and passed the significance threshold (Figure S.6B). Only *O-fut1* reached a fold change of approximately $>50\%$ on the protein level. *O-fut1* performs the fucosylation of Notch and is important for proper neuronal signaling [Stanley, 2007] and embryonic neurogenesis in *Drosophila* [Pandey et al., 2019] as well as neuronal development in vertebrates [Song et al., 2010, Yagi et al., 2012].

Finally, I quantified the expression of genes involved in the cytosolic and mitochondrial UPR

including the ER-associated protein degradation (ERAD) pathway. The UPR acts upstream of the ISR and is necessary to counteract protein folding stress in the ER. Importantly, chronic activation of the UPR causes age-related motor deficits in flies indicating that its dysregulation can lead to neurological defects [Sekiya et al., 2017]. Among a total of 70 unique genes annotated in these three gene groups in flybase, 37 genes were detected in our mass-spec dataset with only one protein (Spp, FBgn0031260) being significantly dysregulated (Supplementary table S.3). In summary, I could not identify any evidence for the activation of the UPR or ISR pathways in *Pus7^{fs}* flies.

Furthermore, I could not identify any dysregulated transcription factors which could explain the changes in the proteome observed in *Pus7^{fs}* flies (Supplementary figure S.6C). However, we can not rule out that only few cell types in the brain might be affected which might be masked by all other unaffected tissues in the omics datasets. Furthermore, the neurological defects might be caused by temporary activation of stress response pathways during earlier developmental timepoints, thereby not being visible in samples of adult heads.

2.2.8 *Pus7* mutation leads to changes in the metabolome

Our previous results revealed that multiple metabolic pathways were dysregulated on the protein level in *Pus7^{fs}* flies which raised the question whether these changes are also reflected on the metabolite level. Therefore, we performed mass-spectrometry in collaboration with the metabolomics unit at UNIL using heads of 3-4 day old mated females to quantify changes in approximately 200 metabolites upon loss of *Pus7* (Supplementary table S.2). Remarkably, this confirmed a glycolytic shift towards increased glycolysis and reduced mitochondrial function including TCA and beta oxidation on the metabolite level (Figure 21A). Especially glycolytic metabolites were upregulated by up to two-fold in *Pus7^{fs}* flies while multiple metabolites of the TCA cycle as well as fatty acids, foremost of medium length (C6-C12), were downregulated (Figure 21B).

To corroborate our observations in an unbiased manner, I performed a joint-pathway analysis. This approach considers the fold changes of both proteins and metabolites from the proteomics and metabolomics datasets, respectively, giving extra weight to pathways that are similarly affected in both datasets. The PPP, glycolysis, TCA cycle and fatty acid degradation were included among the most impacted pathways upon loss of *Pus7* confirming that the metabolome in *Pus7^{fs}* flies is significantly altered (Figure 21C). Furthermore, I observed many synthesis and degradation pathways of amino acids being dysregulated (Supplementary figure S.7A). Analyzing the levels of all detected amino acids revealed threonine, leucine and aspartate to be downregulated in *Pus7^{fs}* flies while serine, histidine, methionine, glycine and asparagine were upregulated (Figure 21D). This raised the question whether the reduced levels of aspartate were limiting the translation speeds at aspartate codons and thereby causative for the phenotypes observed in *Pus7^{fs}* flies.

Therefore, I investigated its involvement by performing rescue experiments with *Pus7^{fs}* flies supplemented with or without aspartate. First, I quantified lifespan on 5% sucrose solution with or without added aspartate but I could not ameliorate the lifespan reduction by aspartate supplemen-

tation (Supplementary figure S.7B). Next, I aimed to rescue the aggression phenotype. Thus, I quantified aggression in flies aged on food supplemented with or without additional aspartate after hatching from the pupa, however, I could also not observe any reduction in aggression levels upon aspartate supplementation (Supplementary figure S.7C). In order to exclude a developmental defect occurring before hatching of the fly, *Pus7^{fs}* flies were allowed to lay eggs on food supplemented with or without aspartate resulting in the offspring having access to additional aspartate during their whole development. Notably, this did not lead to an amelioration of aggression in the offspring suggesting that reduced aspartate levels alone are not causative for the aggression defect (Supplementary figure S.7C).

In addition to amino acids, we found several other dysregulated metabolites upon loss of Pus7 with potential links to defects observed in *Pus7^{fs}* flies. First, N-acetylneuraminate was upregulated which was reported to cause a spectrum of diseases in humans with a wide variety of severity with neurological phenotypes including seizures and developmental delay (Figure S.7D) [Aula et al., 2000, Kleta et al., 2003, Morse et al., 2005]. Second, citrulline, a member of the urea pathway, was upregulated. Its accumulation might be related to the reduction of aspartate which is necessary for argininosuccinate synthetase to produce argininosuccinate as part of the urea cycle. Disorders in urea cycle functionality can lead to neurological damage in humans [Rossignol et al., 2020]. Next, multiple metabolites of the kynurenate pathway including kynurenine and kynurenate were found to be downregulated in *Pus7^{fs}* flies. Dysregulations of the kynurenate pathway have been linked to neurological disorders as well as depression and schizophrenia [Schwarcz et al., 2012]. Also, oxoproline was significantly upregulated in *Pus7^{fs}* flies which was reported to cause neurological signs in human [Perlman and Volpe, 2018]. Further, epinephrine was downregulated in *Pus7^{fs}* flies which is strongly associated with ADHD as well as hyperactivity which is also observed in the Pus7 fly model [Pliszka et al., 1994, Hanna et al., 1996, Dover, 1998]. Additionally, cytidine 2',3'-cyclic phosphate (cP) was found to be upregulated in *Pus7^{fs}* flies. cP is generated by RNA cleavage processes including tRNA cleavage and cleavage of HAC1 mRNA, a necessary step in the activation of the unfolded protein response [Zhang and Kaufman, 2004, Shigematsu et al., 2018]. Finally, lack of Pus7 caused a significant increase in malonate levels which is a well-studied inhibitor of complex II of the mitochondrial respiratory chain [Greene and Greenamyre, 2002]. Summed up, we found widespread changes in the metabolome of *Pus7^{fs}* flies including energy-generating pathways like glycolysis, TCA cycle and beta-oxidation as well as dysregulated amino acid metabolism. Further, the levels of multiple metabolites with links to human disease were found to be affected. Therefore, more experiments are required to pinpoint which changes on the proteome or metabolome are involved in the mechanism of disease in the *Pus7* fly model.

2.2 Characterization of *Pus7* in *Drosophila*

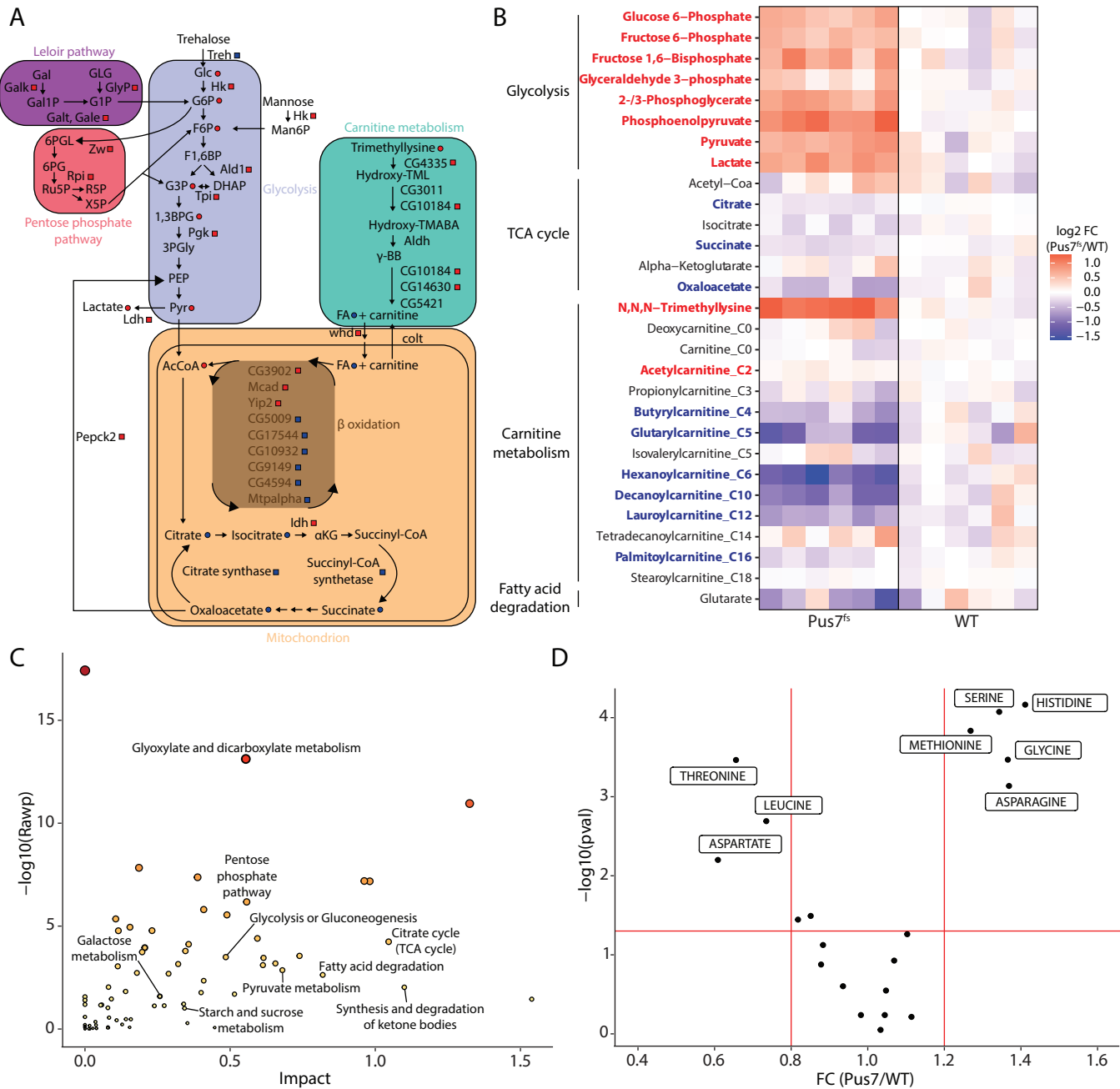


Figure 21: Lack of *Pus7* leads to a glycolytic shift in *Drosophila*. Changes in the metabolome of *Pus7^{fs}* flies were quantified by mass-spectrometry. (A) Schematic illustrating changes of metabolic pathways on the protein and metabolite level in *Pus7^{fs}* flies. (B) Heatmap depicting dysregulated metabolites involved in energy metabolism in *Pus7^{fs}*. (C) Joint-pathway analysis combining the proteomics and metabolomics datasets confirmed metabolic pathways to be dysregulated in *Pus7^{fs}* flies. (D) Dysregulated amino acids in *Pus7^{fs}* flies.

2.2.9 Mitochondrial function is reduced in *Pus7^{fs}* mutants

Mass-spectrometric analysis of the proteome and metabolome of *Pus7^{fs}* revealed multiple dysregulated processes in mitochondrial function including beta oxidation and the TCA cycle. Furthermore, the complex II inhibitor malonate was identified as an upregulated metabolite in *Pus7^{fs}*. These observations raised the question whether mitochondrial function is affected in flies lacking *Pus7* activity. We therefore investigated potential defects in mitochondrial function in collaboration with

the Bagni lab at UNIL by quantifying mitochondrial respiration in *Pus7^{fs}* flies using an oxygraph assay. Strikingly, we observed a significant reduction of complex I and complex II activity in head lysates of *Pus7^{fs}* flies (Figure 22A). Remarkably, this reduction could be rescued back to *wild type* levels by overexpression of tRNA^{Asp}. To identify potential causes of the reduction of mitochondrial respiration in *Pus7^{fs}* flies, I attempted to evaluate the protein levels of members of the mitochondrial respiratory chain. To this end, a comprehensive list comprising all core and supernumerary subunits of the mitochondrial complexes was generated and compared with the proteomics dataset (Figure 22B). Among all detected proteins only two members of the complex I core subunits were slightly but significantly downregulated (fold change <10%) indicating that the respiratory chain is mostly functional upon loss of *Pus7*.

It was shown that a dysregulation of the glycolysis:oxidative phosphorylation (OXPHOS) ratio is associated with increased aggression levels in bees and *Drosophila* [Li-Byarlay et al., 2014, Chandrasekaran et al., 2015]. Hence, we investigated whether the metabolic changes upon loss of *Pus7* are responsible for the increased aggression levels observed in *Pus7^{fs}* males. To this end, I aimed to manipulate the glycolysis:OXPHOS ratio by pharmacologically inhibiting either glycolysis in *Pus7^{fs}* or the mitochondrial complexes in *wild type* flies. Interestingly, supplementing the food of adult *Pus7^{fs}* males with the competitive glycolysis inhibitor 2-deoxyglucose (2-DG) was sufficient to completely rescue the aggression levels (Figure 22C). On the other hand, an artificial increase of the glycolysis:OXPHOS ratio by inhibiting individual members of the respiratory chain was not sufficient to trigger aggression in *wild type* flies (Figure 22D). This suggests that the upregulation of glycolysis is directly responsible for the increased aggression levels in the *Pus7* fly model. However, since 2-DG systemically affects glycolysis in the whole fly, further more targeted experiments utilizing genetic tools are required to establish the connection between *Pus7* functionality and glycolysis in the fly brain.

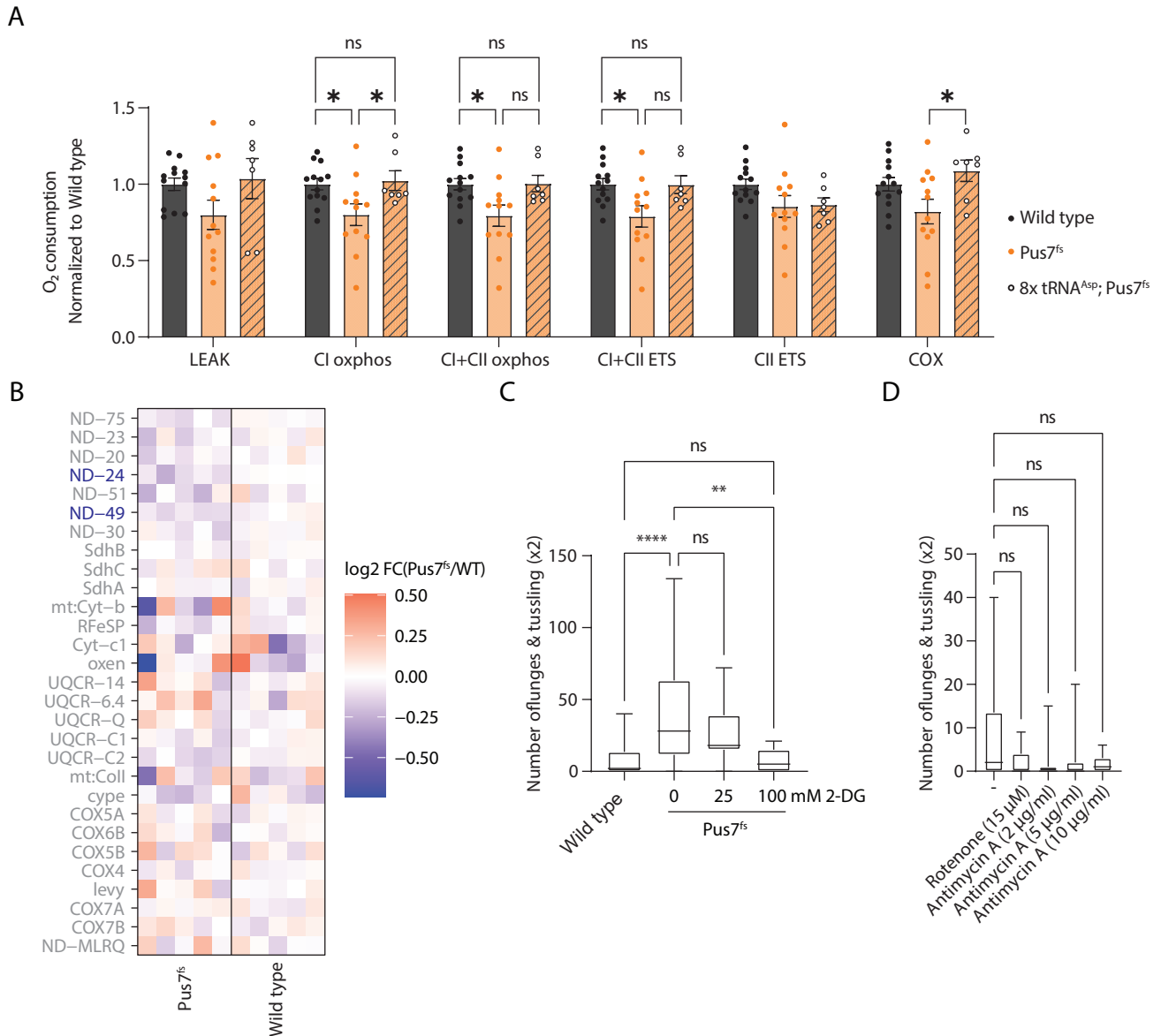


Figure 22: Upregulated glycolysis but not mitochondrial dysfunction causes aggression in *Pus7^{fs}* flies. (A) Oxygraph assay to measure O₂ consumption of individual mitochondrial complexes. (B) Heatmap depicting protein levels of all core subunits and supernumerary subunits detected by mass-spectrometry. (C) and (D) Aggression assay with (C) *Pus7^{fs}* flies aged on food supplemented with the glycolytic inhibitor 2-DG or (D) *wild type* flies aged on food supplemented with inhibitors of the mitochondrial respiratory chain.

2.3 PUSL1 mutation in humans causes developmental delay, microcephaly and intellectual disability

Recently, we have been approached by the group of Michal Minczuk who identified two patients carrying novel mutations in *PUSL1* featuring pathologies highly similar to those observed in patients carrying mutations in *PUS3* and *PUS7* (unpublished data):

The first patient is the first child of consanguineous parents and showed signs of hypotonia, psychomotor delay and progressive encephalopathy. The motor impairment persisted when he lost the ability to walk at six years of age which was followed up on by a brain MRI revealing cerebellar atrophy. A check-up at age 9 confirmed microcephaly, autistic signs with hyperkinesia and inappropriate laughing. Since PUSL1 is predicted to localize to the mitochondria, a muscle biopsy was performed revealing that the mitochondrial respiratory chain function was unaffected. Whole-exome sequencing showed a homozygous variant in *PUSL1* (p.R235Q). This arginine might be involved in the catalysis mechanism [Hoang et al., 2006].

Patient two is a 67 year old man who was initially treated for early dementia in a context of severe vascular leucopathy. According to relatives, he never managed to independently manage finances, could not read, and had language difficulties indicative of intellectual disability and neurodevelopmental delay prior to his cerebrovascular pathology. Furthermore, during the genetic consultation the patient was found to suffer from microcephaly.

Strikingly, both patients suffered from microcephaly and developmental delay which are hallmarks of PUS related pathologies. We therefore aimed to establish a *PusL1* fly model to further investigate its role in the brain.

2.3.1 *Drosophila* PusL1 is a mitochondrial protein

In order to characterize the function of *Drosophila* PusL1, we investigated its subcellular localization by performing immunostainings in *Drosophila* S2R+ cells. To this end, we expressed PusL1 fused to

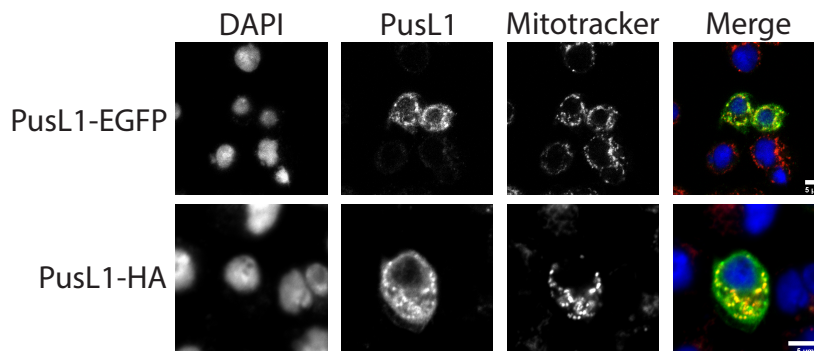


Figure 23: *Drosophila* PusL1 localizes to the mitochondria in S2R+ cells. Immunostaining of PusL1-EGFP from a plasmid containing the endogenous *PusL1* promoter and of overexpressed PusL1-HA in S2R+ cells, respectively. PusL1 localizes to the mitochondria as seen by the overlap with the mitotracker signal.

enhanced green fluorescent protein (EGFP) from a transgene containing the endogenous promoter of *PusL1* or overexpressed *PusL1*-HA from a transgene using the UAS/Gal4 system (Figure 23). In both cases, we observed a mitochondrial localization based on the overlap of the *PusL1* signal with mitotracker, a compound specifically labeling the mitochondria. This localization was conserved between *Drosophila* and human cells (Michal Minczuk, personal communication).

2.3.2 Generation of *PusL1* mutants in *Drosophila*

To investigate the role of *PusL1* in *Drosophila*, I started by generating mutants of *PusL1* using the CRISPR/Cas9 system using gRNAs targeting the 5' UTR 20 nt upstream of the ATG of exon 1 and the start of exon 3 containing the catalytic Asp61 (Figure 24). I successfully created three different mutant fly lines: KO17 carries an integration in the 5' UTR adding a 18 amino acid extension to the N-terminus of *PusL1*. Additionally, it contains a 3 nt deletion at the codon coding for the catalytic Asp61 effectively removing this amino acid without affecting the surrounding codons. As a result, *PusL1* KO17 is expected to generate a catalytically dead protein. Similarly, KO11 carries two deletions of 3 nt in the 5' UTR which are not expected to interfere with translation as well as a 6 nt deletion in exon 3 removing Thr60 and the catalytic Asp61 without affecting the surrounding codons. Analogous to KO17, an otherwise full-length *PusL1* lacking Thr60 and Asp61 is expected to be produced. In the case of KO10, both gRNAs generated cuts at their target sites leading to a 320 nt deletion including both the ATG of exon 1 and the catalytic Asp61.

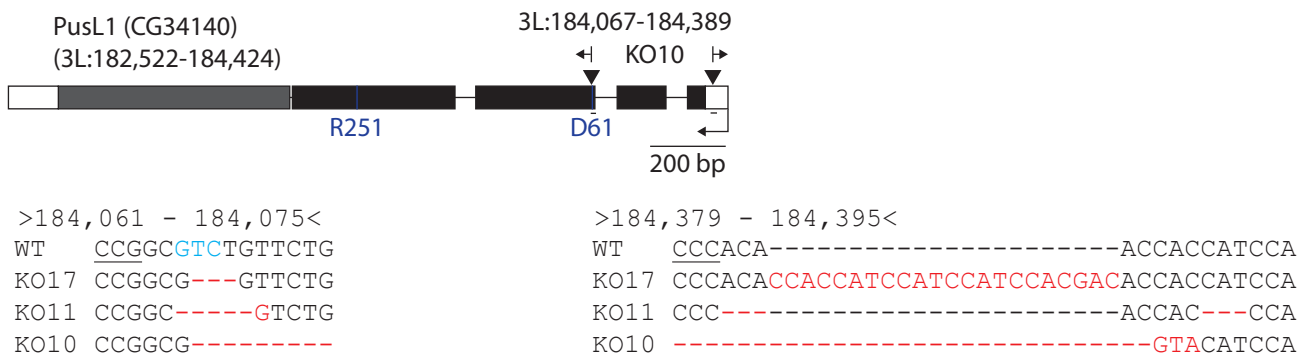


Figure 24: Generation of *Drosophila PusL1* mutants with CRISPR/Cas9. White boxes indicate UTRs. Black boxes represent exons. Lines indicate introns. The grey box illustrates the *Mkp* gene which is nested in the 3' UTR of the *PusL1* transcript on the + strand. Arrowheads indicate the gRNA target sites. The genomic locations of the deletion of KO10 are indicated by arrows. The catalytic Asp61 and Arg251 involved in the catalysis mechanism are indicated in blue. The small lines in the schematic indicate the zoomed locations showcasing the indel mutations at the gRNA target sites. The underlined sequences in the zoomout indicate PAM sequence while indel mutations are shown in red and the codon encoding the catalytic Asp61 is shown in blue.

2.3.3 Phenotypic characterization of *Drosophila PusL1*

Similar to observations made in PUS patients and the *Pus7* fly model, *PusL1* mutant flies were viable and showed no obvious defects. Since our localization studies indicated a potential role of *PusL1* in mitochondria, I aimed to investigate its role by performing environmental stress assays using our

PusL1 mutant fly lines. Therefore, a stress assay was performed in which flies were fed paraquat, a substance enhancing oxidative stress that can lead to mitochondrial dysfunction [Hosamani and Muralidhara, 2013]. Interestingly, flies completely devoid of *PusL1* (KO10) featured a significant increase in lifespan.

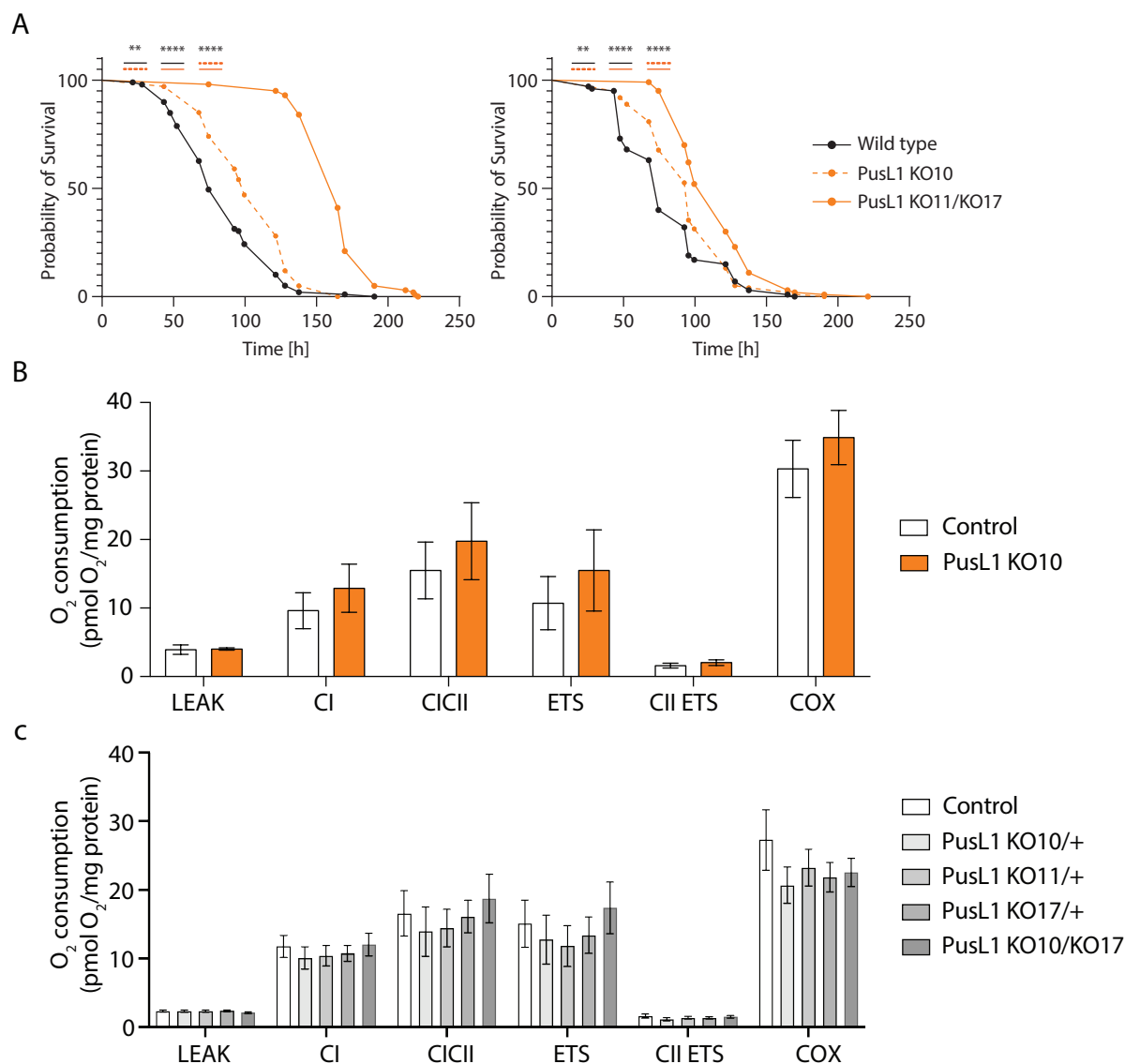


Figure 25: A potential role of *PusL1* in oxidative stress in mitochondria. (A) Lifespan of *PusL1* mutant flies during an oxidative stress assay. Flies were fed 5% sucrose solution supplemented with 5 mM paraquat. (B) Oxygraph assay displaying the O₂ consumption of protein lysates of fly heads.

Surprisingly, this was even more pronounced in transheterozygous flies expressing two catalytic dead *PusL1* variants (KO11/KO17) suggesting that retaining a catalytic dead protein is more harmful than a complete knockout (Figure 25A). Since this phenotype suggested a role of *PusL1* in mitochondrial function, we aimed to measure the effect of *PusL1* on mitochondrial respiration by performing oxygraph assays in collaboration with the Bagni lab at UNIL. However, we could not identify any effect of *PusL1* mutation on the O₂ consumption of mitochondria which is in line with the fact that mitochondrial function was unaffected in *PUSL1* patients (Figure 25B&C).

2.3.4 Lack of PusL1 affects activity in *Drosophila*

Since we could not show a direct role of PusL1 in mitochondrial function, I continued to further investigate its role in the brain by investigating markers of neurological defects in the *PusL1* mutants. To this end, I quantified the locomotion of *PusL1* mutant larvae in a crawling assay (Figure 26A). Interestingly, L3 larvae showed a slight but significant decrease in locomotion. In order to decipher whether the reduction in larval locomotion was caused by a muscular or a neuronal defect I analyzed the larval neuromuscular junction. I could not observe any changes in NMJ branching, length or the amount of synaptic boutons (Figure 26B). This observation indicated that the changes in larval crawling speed are instead caused by muscular defects, a reduction in crawling activity or the functionality of the synapses.

Next, I quantified locomotion by performing a negative geotaxis assay with adult flies. Surprisingly, in contrast to the reduction in larval locomotion, *PusL1* mutant flies featured a significant increase in climbing speed indicating separate functions of *PusL1* during development (Figure 26C). Of note, the adult climbing assay takes into account both climbing speed as well as the activity of the flies. 6-7d old flies were used which achieved a successful climb in 88% and 95% of the cases for *wild type* and *PusL1* mutants, respectively. Strikingly, repeating the assay with 11-12d old flies yielded a similar phenotype, however, the difference in success rate of older flies was vastly bigger with 56% and 79% for *wild type* and *PusL1 KO10* mutants, respectively, which was majorly caused by bouts of pausing during the climb of *wild type* flies. This suggests hyperactivity as a potential phenotype in *PusL1* mutant flies which was not observed in human *PUSL1* patients.

I further explored seizures as markers of potential neurological defects in adult *PusL1* mutants by performing a bang sensitivity assay which consists of vortexing the flies for several seconds and quantifying the time required to recover and climb 3 cm in a glass cylinder. While I could not observe any seizures, *PusL1* mutant flies still recovered significantly faster than their *wild type* counterpart, especially in the case of female flies, which again seemed to be caused by increased activity in *PusL1* mutant flies (Figure 26D). We therefore aimed to quantify activity with a free running assay in collaboration with the Bagni lab at UNIL. Surprisingly, heterozygous deletion mutants lacking one copy of *PusL1* showed a significant increase in activity, whereas transheterozygous catalytically dead mutants of *PusL1* did not show any changes in activity (Figure 26E). This experiment suggests that PusL1 affects fly activity independently of its catalytic function. Unfortunately, homozygous *PusL1 KO10* flies completely devoid of PusL1 were not included in this assay. Therefore, further experiments are required to directly compare activity in homozygous deletion mutants and transheterozygous catalytically dead mutants within the same assay.

2.4 Characterization of *Pus3* in *Drosophila*

2.4.1 *Drosophila* *Pus3* is a cytoplasmic protein

Human patients carrying mutations in *PUS3* feature a largely brain-specific phenotype including intellectual disability, microcephaly and developmental delay. In order to gain insights into the pathomechanism of diseases caused by mutations in PUS enzymes, we aimed to investigate the function of *Pus3* in *Drosophila*.

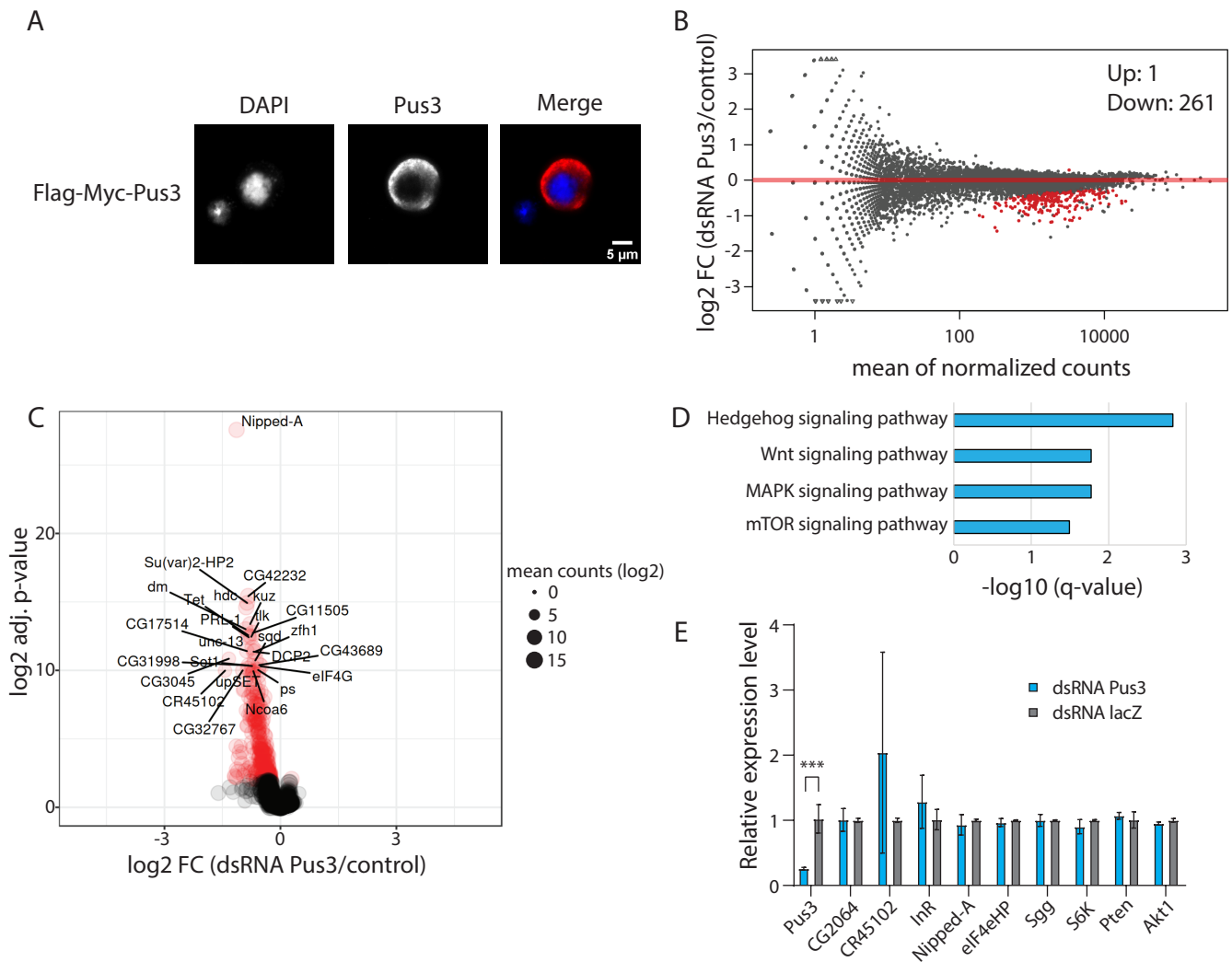


Figure 27: *Pus3* is cytoplasmic in *Drosophila* S2R+ cells. (A) Immunofluorescence of Flag-Myc-*Pus3* overexpressed in *Drosophila* S2R+ cells. (B) Scatterplot of differentially expressed genes upon knockdown of *Pus3* in S2R+ cells. (C) Volcano plot displaying the top dysregulated genes upon knockdown of *Pus3* in S2R+ cells. (D) GO term analysis of all downregulated genes upon siRNA *Pus3* treatment in S2R+ cells. (E) Validation of genes in the mTOR pathway indicated to be downregulated in RNA-seq using RT-qPCR.

In order to characterize *Pus3* in *Drosophila* I started by analyzing its subcellular localization in S2R+ cells by immunostaining. I observed a clear localization to the cytoplasm (Figure 27A). I started evaluating the functions of *Pus3* in a transcriptome-wide manner by knocking down *Pus3* by

siRNA treatment in S2R+ cells and performing RNA-seq to analyze changes in the transcriptome. Using stringent cutoffs (FDR < 0.01) we observed one single upregulated gene (*CG2064*) and 261 downregulated genes upon knockdown of *Pus3* (Figure 27B&C).

An unbiased evaluation of the downregulated genes using a GO term analysis revealed multiple signaling pathways being affected including the hedgehog, Wnt, MAPK and mTOR signaling pathways (Figure 27D). To corroborate these observations, I performed RT-qPCR on the same samples as for RNA-seq targeting multiple genes of the mTOR pathway, however, no significant changes in expression could be identified (Figure 27E).

2.4.2 Characterization of *Pus3* phenotypes in *Drosophila*

Since the analysis of *Pus3* in cells yielded no clear indications of its cellular functions, I aimed to investigate its roles *in vivo*. To this end, I used the CRISPR/Cas9 system to generate fly lines mutant for *Drosophila Pus3*. I designed gRNAs to target exon 1 and exon 4 of *Pus3* which contains the catalytic Asp154. We successfully generated a mutant with a 1033 nt deletion between the gRNA target sites (Figure 28A). This indel mutation is expected to cause a frameshift and a premature stop codon after 38 amino acids within exon 1. Therefore, no catalytically active *Pus3* should be expressed in this mutant. In order to confirm this, we performed Ψ -seq in collaboration with Schraga Schwartz, a method to identify Ψ sites in a transcriptome wide manner, using heads of 3-4 day old mated female flies. Among non-coding RNAs, we consistently found positions 38 and 39 of nine different tRNA species to be reduced in pseudouridylation which are known targets of *Pus3* in yeast (Figure 28B; [Lecoite et al., 1998]). While the modification ratios of these tRNA species were reduced, we did not observe any changes in their expression levels (data not shown).

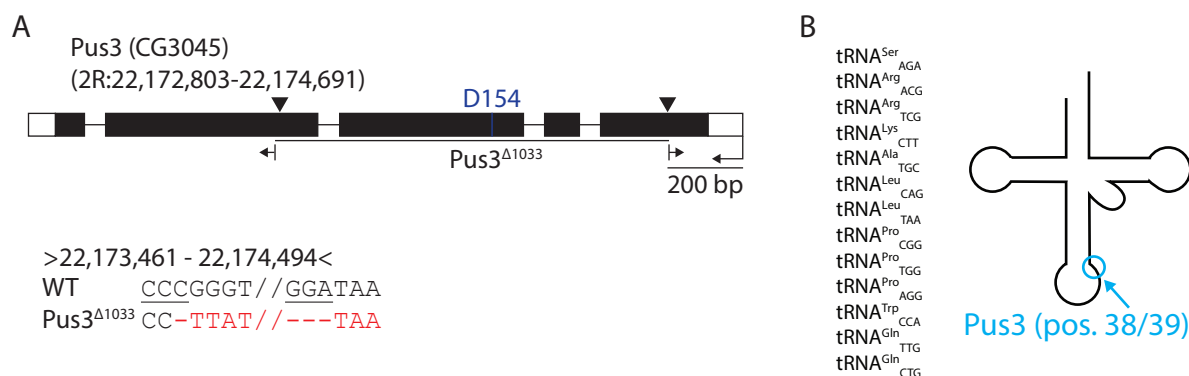


Figure 28: Generation of *Drosophila Pus3* mutants with CRISPR/Cas9. White boxes indicate UTRs. Black boxes represent exons. Lines indicate introns. Arrowheads indicate the gRNA target sites. The genomic locations of the deletion of *Pus3*^{Δ1033} are indicated by arrows. The catalytic Asp154 is indicated in blue. The small lines in the schematic indicate the zoomed locations showcasing the indel mutations at the gRNA target sites. The underlined sequences in the zoomout indicate PAM sequence while indel mutations are shown in red.

Table 2.4: Putative *Pus3* substrates in *Drosophila*. P-values of chi-squared test (Chi-squ.) and t-test are indicated.

Coordinates	5-bp	$\Psi\%$ <i>Wild type</i>	$\Psi\%$ Δ <i>Pus3</i>	Chi-squ.	t-test	score
chrX.trna13-SerAGA:39	AATCA	15	1	5.8E-122	3.3E-05	0.835
chr2R.trna1-ArgACG:39	GATCA	18	1	2.1E-56	2.8E-04	0.813
chrX.trna10-ArgTCG:39	GATCC	11	2	1.1E-24	1.4E-05	0.711
chr2R.trna100-LysCTT:39	AATCT	7	1	1.3E-97	7.3E-04	0.681
chr3R.trna1-ArgTCG:39	AATCC	15	2	4.5E-20	4.8E-06	0.679
chr3R.trna7-ArgTCG:39	GATCC	11	2	1.9E-24	1.5E-05	0.657
chr2R.trna29-AlaTGC:39	TGTGA	39	2	3.0E-32	6.3E-03	0.575
chr3L.trna42-LeuCAG:39	GGTCG	21	1	2.5E-56	8.7E-03	0.521
chr3L.trna31-ProCGG:37	GGTGC	7	1	5.9E-29	1.7E-03	0.452
chr3R.trna46-LeuTAA:40	GCTCT	19	1	1.5E-05	1.2E-02	0.343
chr2L.trna34-TrpCCA:38	GATCG	24	1	1.1E-11	3.7E-02	0.286
chr2L.trna2-GlnCTG:39	AATCC	4	0	9.1E-14	4.8E-03	0.284
chr3L.trna14-CysGCA:38	GATCG	9	1	8.3E-14	3.2E-02	0.283
chr2L.trna18-ProAGG:37	GGTGC	4	0	3.7E-08	1.5E-03	0.264
chrX.trna26-GlnTTG:39	AATCC	6	1	9.3E-08	1.4E-02	0.258
chr3L.trna38-GlnTTG:39	AATCC	6	1	7.0E-08	1.8E-02	0.210
chr3R.trna17-ProTGG:37	GGTGC	5	1	1.6E-05	4.0E-02	0.140

In order to characterize the function of *Drosophila Pus3 in vivo*, I performed classical survival assays using the mutants generated by CRISPR/Cas9. Of note, the experiments were performed with flies that underwent only one isogenization step to remove off-target effects of CRISPR/Cas9 activity. To avoid potential *Pus3* independent side-effects due to other unknown homozygous mutations, a fly line with a chromosome carrying a deletion including the *Pus3* gene was employed to generate heterozygous *Pus3^{def}* and transheterozygous *Pus3^{Δ1033} \ Pus3^{def}* flies.

To quantify the general health of flies upon *Pus3* deletion, a classical lifespan assay was performed. Surprisingly, I observed a sex-dependent increase of lifespan in males while the lifespan in females was decreased (Figure 29A). Since this effect was already visible upon lack of only one copy of *Pus3*, it can not be excluded that this was caused by the presence of the deficiency chromosome. To test the resistance of *Pus3* mutant flies to nutrient depletion, I performed a dry starvation assay where flies have no access to water or food. While there was no distinguishable difference in the lifespans of male flies, transheterozygous *Pus3* mutant females featured a significant increase in lifespan (Figure 29B). The changes in lifespan of *Pus3* mutant females depending on access to food indicated a metabolic phenotype. To investigate this further, I quantified the lifespan upon cultivation on 5% sucrose without access to amino acids. Strikingly, I observed a significant reduction in lifespan especially in females suggesting a negative impact of sugar intake on lifespan in the *Pus3* mutant background (Figure 29C). Next, I examined the resistance to oxidative stress by cultivating the flies on 5% sucrose supplemented with paraquat. While no changes in male lifespan could be observed, the presence of the *Pus3* deficiency chromosome was sufficient to significantly reduce female lifespan (Figure 29D). Since this effect was equally pronounced in heterozygous *Pus3* mutant females carrying

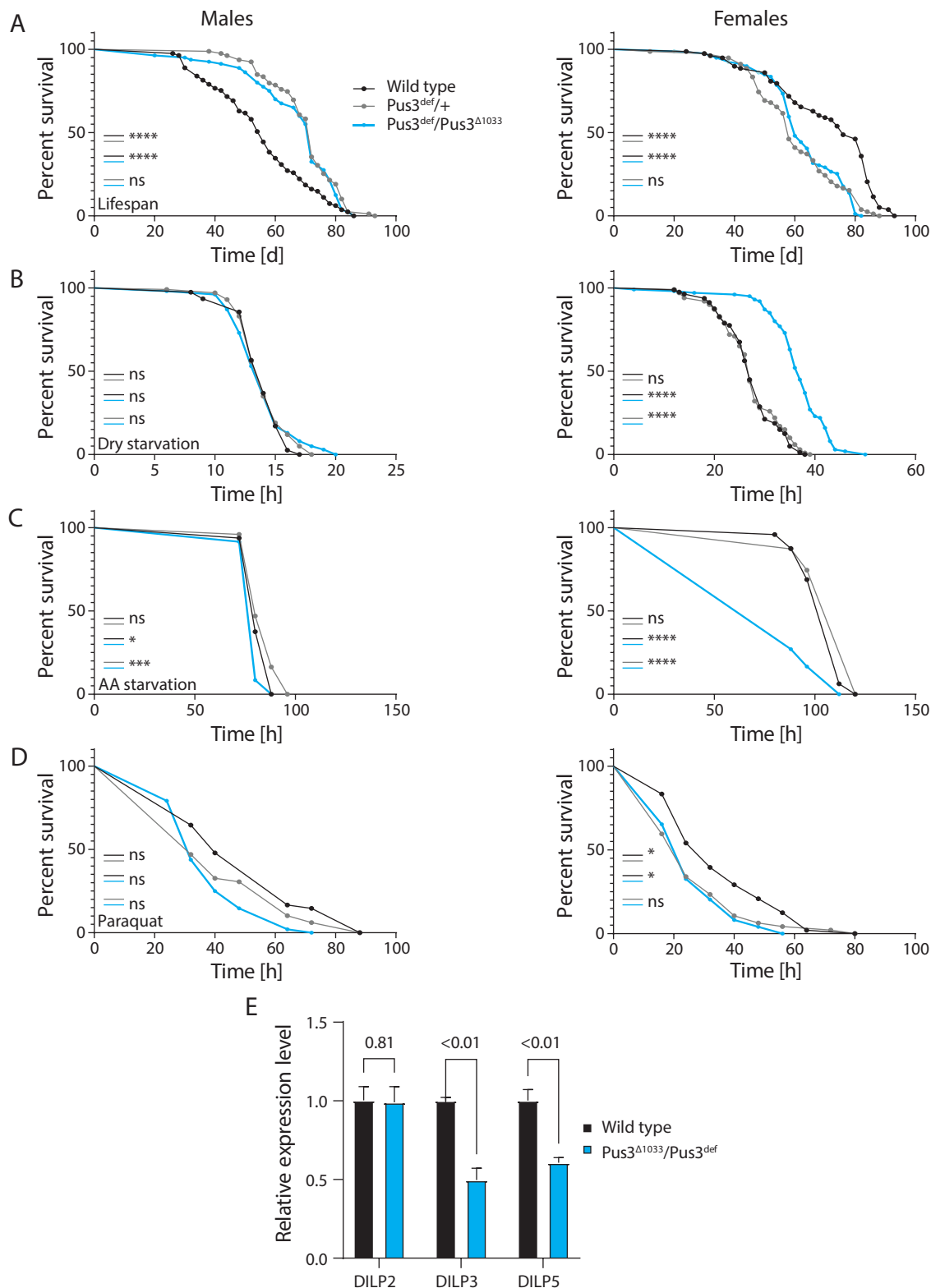


Figure 29: Lack of *Pus3* affects the lifespan upon metabolic stress in *Drosophila*. Lifespan assays on (A) normal food, (B) without food or water, (C) 5% sucrose solution, (D) 5% sucrose solution supplemented with 5 mM paraquat. All datasets were non-normal distributed. Mann Whitney U test followed by Holm Sidak multiple comparisons test were used for statistic analysis. (E) RT-qPCR targeting DILP genes.

the deficiency chromosome, it can not be linked directly to *Pus3* function. Altering the levels of *Drosophila* insulin-like peptides (DILPs) was shown to be involved in resistance to oxidative stress

2.4 Characterization of *Pus3* in *Drosophila*

and starvation as well as affecting lifespan [Broughton et al., 2005]. I therefore aimed to quantify DILP expression levels by RT-qPCR and identified a reduction in the levels of DILP3 and DILP5 by approximately 50% in *Pus3* mutant flies (Figure 29E). This observation further substantiates a potential metabolic function of *Pus3* in *Drosophila*.

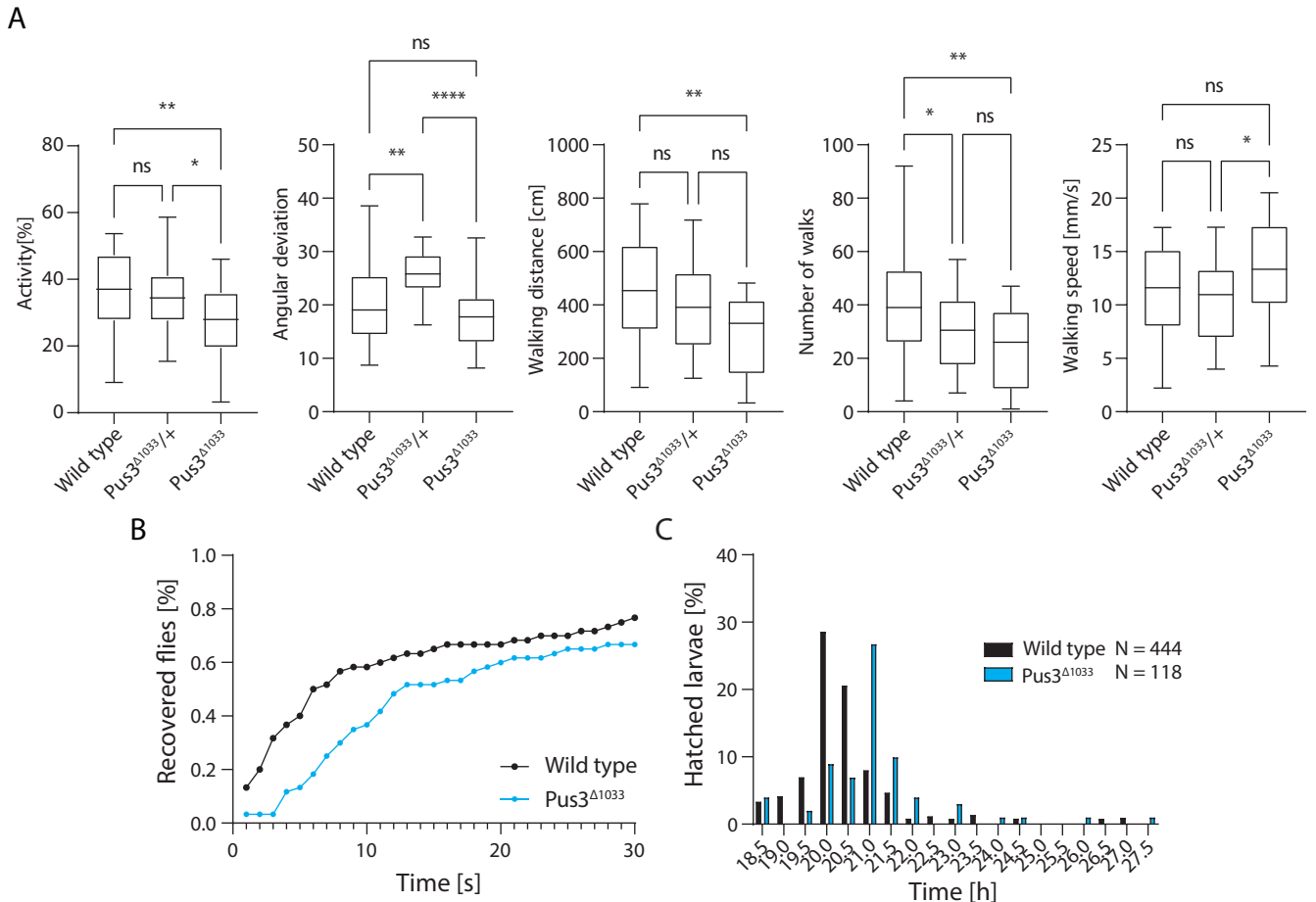


Figure 30: *Pus3* mutation causes reduced activity and developmental delay. (A) Quantification of activity, orientation and locomotion in a buridans paradigm assay. All datasets were checked for normal distribution. Statistics were performed using an ordinary one-way ANOVA followed by Tukey's post hoc test if datasets were normal distributed or by a Kruskal-Wallis one-way ANOVA followed by Dunn's post hoc test if at least one dataset was not normal distributed. (B) Bang sensitivity assay to quantify recovery time after mechanical stress. (C) Time required for the development of laid eggs until hatching of the L1 instar larva. Hatched larvae were counted every 30 min. Average of four or two technical replicates for *wild type* and *Pus3* mutants, respectively.

PUS3 patients showed phenotypes indicative of neurological defects. We therefore aimed to investigate possible neurological defects in *Drosophila Pus3* mutants. First, we performed a buridans paradigm assay to quantify changes in activity, orientation and locomotion. To this end, flies with clipped wings were placed into an arena with two visual landmarks and the movements of the flies between these landmarks were recorded with a camera. Interestingly, we observed a significant reduction in activity in *Pus3* mutant flies (Figure 30A). Additionally, orientation was quantified by measuring the angular deviation from a straight walking path between the two visual landmarks, however, *Pus3* mutant flies showed no significant changes. Lastly, the walking distance as well as the number of walks were significantly reduced in *Pus3* mutant flies while the walking speed was

unaffected indicating that these changes are a result of reduced activity rather than locomotion.

Next, since *PUS3* patients featured seizures among other defects, we aimed to examine whether this phenotype is conserved in *Pus3* mutant flies. To this end, we performed a bang sensitivity assay consisting of vortexing of the flies to induce epileptic seizures due to mechanical stress followed by quantifying the required time to recover and climb 3 cm in a glass cylinder. Interestingly, *Pus3* mutant flies recovered significantly slower than *wild type* controls indicating either a seizure phenotype or a slower recovery due to reduced activity (Figure 30B). Finally, *PUS3* patients featured developmental delay as one of the hallmarks of *Pus* mutation. We aimed to investigate a potential developmental delay phenotype in a hatching assay where the required time of development from the laid egg to the hatching of the first instar larva is measured. We therefore let flies lay eggs on applejuice agar plates and quantified the required time to hatch in 30 min intervals. While *wild type* flies hatched primarily around 20-20.5 hours, *Pus3* mutant larva featured a delay of 30-60 minutes (Figure 30C). Taken together, we could show that *Pus3* mutant flies feature reduced activity which is indicative of neurological defects as well as developmental delay which was also observed in human patients.

Chapter 3: DISCUSSION

3.1 Neuronal roles of Ψ synthases

3.1.1 Pus mutations as neurodevelopmental diseases

Pseudouridine is the most abundant RNA modification affecting almost every step of gene expression including splicing and translation. In the last decade, mutations in PUS enzymes featuring intellectual disability, microcephaly and developmental delay have been added to the spectrum of neurodevelopmental diseases. Using the *Drosophila* model, we aimed to unravel the molecular cause of PUS diseases by using the advantages of its genetic tractability. First of all, *Pus7* and to some extent *Pus3* mutant flies featured a developmental delay phenotype (Figure 14G). More importantly, we discovered that lack of *Pus7* causes several phenotypes indicative of neurological defects including orientation defects, increased activity [de Brouwer et al., 2018] and increased aggression levels (Figure 14E). Furthermore, both flies lacking *Pus7* or *PusL1* showed increased recovery speeds after mechanical stress in the absence of seizures suggesting hyperactivity (Figures 14D & 26D) while the opposite effect was observed for *Pus3* mutant flies (Figure 30B). Finally, rescue experiments in neurons of *Pus7^{fs}* flies confirmed that the aggression phenotype is caused by a brain defect due to a lack of *Pus7*-dependent pseudouridylation (Figure 14E&F). Therefore, the use of the fly model allowed us to pinpoint the behavioral abnormalities to defects in the central nervous system.

3.1.2 The central complex and mushroom body are potentially defective in flies carrying mutations in Pus enzymes

Studies with flies containing structural defects in the brain have uncovered the functional relationships between certain brain regions and behaviors. The behavioral changes observed during our phenotypic characterization of *Pus7^{fs}* flies point towards defects within two regions within the fly brain: the central complex (CX) and the mushroom body (MB) (Figure 31). The central complex consists of four neuropils: the fan-shaped body (FB), the ellipsoid body (EB), the protocerebral bridge (PB) and the paired noduli. The CX is considered the higher control center of locomotion as defects are linked to changes in walking activity, walking speed and orientation in *Drosophila* [Strauss and Heisenberg, 1993, Martin et al., 1999]. Specifically, the EB [Neuser et al., 2008], the PB [Triphan et al., 2010] and the FB are involved in orientation [Pan et al., 2009]. Simultaneously, the FB and EB are also required to regulate the walking speed [Hotta and Benzer, 1972]. Furthermore, especially the PB and potentially its interaction with the FB regulate normal walking activity [Strauss and Heisenberg, 1993, Leng and Strauss, 1996, Pielage et al., 2002]. Interestingly, the MB was also reported to be involved in locomotion as genetic inhibition of neurons within the mushroom body reduces the flies' walking activity [Martin et al., 1998]. Therefore, both the CX and the MB affect locomotion activity, yet in opposite directions.

Considering that the walking speed is unaffected in *Pus7^{fs}* and *Pus3* mutant flies, the FB and EB are likely intact. However, loss of *Pus7* causes hyperactivity and decreased orientation suggesting defects in the PB, the MB or both [de Brouwer et al., 2018]. Similarly, orientation and walking activity but not speed are affected in *Pus3* mutant flies, yet in the opposite directions (Figure 30). This suggests that in both fly models the structure or signalling between these areas of the CX and the MB are defective.

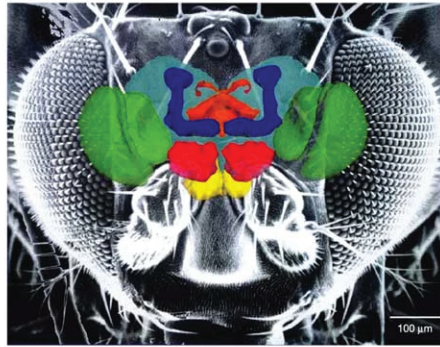


Figure 31: Regions of the fly brain. Green, optic lobes; yellow, subesophageal ganglion; red, antennal lobes; blue, mushroom bodies; orange, central complex. The various neuropil regions surrounding the mushroom bodies and central complex are shown in grey in the background. Figure and adapted description from [Heisenberg, 2003].

The MB is furthermore involved in regulating multiple fly behaviors including learning, sleep and aggression [Heisenberg et al., 1985, Joiner et al., 2006]. It performs a special role during aggression as a central integration center of the flies surroundings and internal state to decide whether to elicit an aggressive response [Zwarts et al., 2012]. To achieve this, it gauges several sensory cues including visual [Liu et al., 1999], olfactory [Stocker, 1994], gustatory [Vosshall and Stocker, 2007], tactile and pheromonal information [Kravitz and de la Paz Fernandez, 2015]. Furthermore, multiple neurotransmitters including octopamine [Baier et al., 2002], dopamine [Han et al., 1996] and serotonin [Johnson et al., 2009] affect aggression in *Drosophila*. Importantly, neurons expressing receptors for each of these neurotransmitters have been identified in the mushroom body [Han et al., 1998, Blenau and Thamm, 2011, Alekseyenko et al., 2013]. Additionally, a direct correlation has been reported between the size of the mushroom body lobes with the level of aggressive behavior [Zwarts et al., 2011]. Concomitantly, the genetic inhibition of the synaptic output of the mushroom body is sufficient to inhibit aggression highlighting its role as the final mediator of aggressive behavior [Baier et al., 2002].

Due to the role of the MB as a central integrator of aggression, it is not possible to pinpoint the neurological defects of *Pus7^{fs}* flies to a certain region within the MB. Defects in different areas of the brain may result in changes in aggression. These can include structural abnormalities in certain brain regions, changes in the signalling to or processing of sensory cues in the MB and dysregulations in the levels of neurotransmitters among others. Furthermore, recent studies have also implicated tachykininergic neurons in the regulation of aggression by regulating the activity of cholinergic neurons in the protocerebrum [Wohl et al., 2023]. Therefore, future experiments will elucidate in greater detail which brain regions or types of neurons are affected. To this end,

Gal4 driver lines were isogenized and combined with a *Pus7^{fs}* allele to perform targeted rescue or knockdown experiments. The cell types and tissues of interest include glia cells (repo & how), dopaminergic (ple), glutamatergic (VGlut), serotonergic (Trhn) and octopaminergic neurons (Tdc2) as well as different brain regions including the brain-adjacent fat body (Lsp2) and the mushroom body (R16A06). Using these genetic tools, the *Drosophila* fly model will allow us to further pinpoint the origin of the neurological defects upon loss of Pus enzymes.

3.2 The questionable role of mRNA Ψ sites

3.2.1 Challenges in reproducibility

Multiple studies have mapped Ψ sites in a transcriptome-wide manner in several organisms including yeast [Schwartz et al., 2014, Carlile et al., 2014, Lovejoy et al., 2014], mouse [Li et al., 2015, Dai et al., 2022], human [Carlile et al., 2014, Li et al., 2015, Martinez et al., 2022] and *Drosophila* [Song et al., 2023]. The number of identified mRNA Ψ sites varies drastically between datasets with as little as 300 sites in yeast and multiple thousands of sites in different regions of the mouse brain. For a long time, the impact of these Ψ sites has been questioned, however, recent studies proposed roles in the regulation of splicing and RBP binding to pre-mRNAs [Martinez et al., 2022] as well as transcript stabilization and facilitating read-through [Dai et al., 2022].

An ongoing problem of reproducibility between different Ψ mapping techniques has been revealed by an analysis of three studies employing HEK293 cells. [Safra et al., 2017b] compared the transcriptome-wide datasets of [Schwartz et al., 2014, Carlile et al., 2014, Li et al., 2015] using Ψ -seq, pseudo-seq and CeU-seq, respectively. All three methods take advantage of the specific reaction of CMC with Ψ to identify sites based on truncations upon RT. Ψ -seq and pseudo-seq are technically almost identical with the difference that in pseudo-seq cDNA strands are circularized before PCR amplification. Similarly, CeU-seq employs circularization but additionally increases sensitivity by introducing a step to conjugate biotin to CMC- Ψ derivatives to enrich Ψ -containing mRNAs by pulldown. Since sequencing depth and modification stoichiometry are limiting for the detection of Ψ sites in mRNA, this method allowed the detection of novel lowly expressed or lowly modified mRNA candidate sites. Notably, among the 91375 total Ψ sites detected in the three datasets, only 91 mRNA sites were shared among all three datasets [Safra et al., 2017b]. Possible explanations for this are the detection of false-positives and false-negatives due to insufficient sequencing depth or quality. Additionally, in spite of all studies using HEK293 cells, biological variability between the samples as well as slight distinctions in the cell lines might cause variations in the pseudouridylation landscape. Finally, stress-inducible Ψ sites due to slight differences in growth conditions might alter the Ψ profiles.

During this study, we realized that these challenges in reproducibility are not exclusive to mammalian cells. According to an increasing number of total Ψ sites with organism complexity, [Song et al., 2023] discovered about 1100 mRNA sites in female *Drosophila* fly heads using Ψ -seq. In our

attempt to identify novel Pus7-dependent mRNA Ψ sites, we collaborated with the He lab who established BID-seq which is expected to be more sensitive than CMC-based mapping approaches [Dai et al., 2022]. Despite using the same tissue as [Song et al., 2023], we were unable to identify any mRNA Ψ sites in heads of female flies. Reducing the stringency of the analysis revealed a small number of sites in mRNAs, snoRNAs and lncRNAs, however, none of them contained a Pus7 consensus motif (data not shown). Even when considering that two different methods were used, this does not explain the absence of sites in our dataset.

Also, this problem persists when comparing the Pus7 tRNA targets identified by our collaborators by Ψ -seq [de Brouwer et al., 2018] with those discovered by [Song et al., 2023]. In spite of using the same tissue, the same method and optimizing their protocol with the same in vitro transcribed spike-in RNA oligonucleotide as in [Schwartz et al., 2014], [Song et al., 2023] identified eight Ψ sites in tRNA, only one of which was located at position 13 and overlapped with our dataset (tRNA^{Glu}_{CTC}). Since position 13 in multiple tRNA species is conserved from yeast to human (see section 1.4.3) and tRNA Ψ sites are highly conserved, highly expressed and expected to feature little variability in modification stoichiometry, this raises concerns about the quality of the dataset of [Song et al., 2023]. Due to this discrepancy in detected tRNA sites between our group and [Song et al., 2023], we attempted to confirm the Pus7-dependent sites detected in our Ψ -seq dataset. To this end, we collaborated with the Glatt group (MCB, Krakow) who performed in vitro assays using synthetic *Drosophila* tRNAs and recombinant human PUS7. With this approach, we could confirm pseudouridylation of at least six of the nine Pus7-dependent tRNA sites detected in our Ψ -seq dataset further validating our results (data not shown).

3.2.2 Pus7 primarily targets tRNAs

Both data generated during this study as well as publicly available datasets support the notion that Pus7 primarily targets tRNA sites and modifies only few sites on coding RNA. First of all, only three out of the 91 mRNA Ψ sites common within the three datasets analyzed in [Safra et al., 2017b] were targeted by PUS7 in human cells. These high confidence sites were also used as candidates to identify PUS7-dependent mRNA Ψ sites in cells derived from PUS7 patients where nine sites were identified by our collaborators [de Brouwer et al., 2018].

Notably, the low number of PUS7-dependent mRNA Ψ sites in HEK293 cells might be due to tissue-specific expression patterns of PUS enzymes. This notion was brought forth by the transcriptome-wide mapping in different regions of the mouse brain, which harbored drastically different numbers of Ψ sites in different brain regions [Dai et al., 2022]. Therefore, Pus7-dependent sites on mRNA in the brain of *Drosophila* might be concealed due to the complex composition of the different brain areas and cell-types present within the fly head. However, we were able to identify five mRNA sites in ovaries of *Pus7^{fs}* flies which also feature a complex set of cell types (Figure 16).

[Dai et al., 2022] also highlighted that Pus7-dependent Ψ sites on mRNA feature the highest stoichiometries with up to 60% modification ratio in the case of UGUAG motifs. Therefore, the lack of

Pus7-dependent sites in heads using BID-seq is likely not a result of low modification stoichiometries. Strikingly, none of the approximately 1150 mRNA sites identified in [Song et al., 2023] in *Drosophila* heads contained a Pus7-specific UGUAA or UGUAG motif. Similarly, only 17 sites showed a motif specific for TRUB1 (GTTCRA) which modified almost 60% of the mammalian 91 Ψ sites on mRNA shared among the three datasets analyzed in [Safra et al., 2017b]. Thus, if this plethora of *Drosophila* mRNA Ψ sites is real, the Pus enzymes responsible for their modification still remain to be identified.

3.3 Potential role of Pus7 mRNA Ψ sites in embryogenesis

The enrichment of *Pus7* mRNA in ovaries and early embryos prompted us to investigate its potential roles during these developmental stages (Figure 12). Notably, we observed a maternally contributed fertility defect in *Pus7^{fs}* mothers suggesting a role of Pus7 in adult females. Additionally, eggs deposited by *Pus7^{fs}* females showed a reduced hatching rate (Figure 14H&I). Phenotypic analysis of these eggs revealed defects reminiscent of ventralization mutants.

Axis specification in *Drosophila* relies on the correct temporal and localized expression of proteins involved in axis specification required for embryonic development [Richter and Lasko, 2011]. To this end, mRNAs are bound by RBPs to form mRNA-protein complexes to ensure translational repression during the transport through the oocyte. Important players in axis specification of the future embryo are *grk*, *osk*, *bcd* and *nanos* mRNAs. For instance, localization of *grk* mRNA to the dorso-anterior corner of the oocyte in mid-oogenesis and local translation is required for the proper establishment of the dorso-ventral axis [Neuman-Silberberg and Schüpbach, 1993]. [McDermott and Davis, 2013] identified that the *Drosophila* RBP *heph* is required for correct localization of the Grk protein since mutation of *heph* leads to ventralized embryos (Figure 15A)

In order to test an involvement of Pus7 in the Grk pathway of dorso-ventral axis polarity, we performed genetic combination assays with a mutant *heph⁰³⁴²⁹* allele (Figure 15A). However, we could observe neither an increase nor amelioration of ventralized embryo frequencies suggesting that Pus7 acts through an independent pathway. Performing BID-seq with RNA from ovaries revealed five Pus7 mRNA targets in ovaries (Table 2.3). Analysis of their expression levels by RT-qPCR revealed no differences between *wild type* and *Pus7^{fs}* flies suggesting that Pus7-dependent Ψ does not regulate their transcript levels. However, Ψ sites in mRNA have been shown to inhibit RBP binding [Vaidyanathan et al., 2017]. It is interesting to speculate that Pus7-dependent Ψ sites in these mRNAs might affect their translational regulation or localization by disturbing RBP binding. Of note, only three of the five mRNA sites (CG8223, *scu*, PIG-K) are likely exclusively pseudouridylated by Pus7 due to the lack of modification in the *Pus7* mutant background. The other two sites on CG9135 and CG17691 feature a remaining modification ratio of 5% and 65%, respectively, and are thus perhaps redundantly modified by other Pus enzymes. The fact that overexpression of tRNA^{Asp} could only partially rescue the egg-laying defect in *Pus7^{fs}* females raises the possibility that tRNA-independent functions of Pus7, potentially through mRNA sites, might affect this phenotype.

Unfortunately, none of the identified mRNA targets have been characterized in *Drosophila* eggs so far. Therefore, further experiments upon mutation or knockdown of these candidate genes are necessary to identify their potential roles in oogenesis.

Importantly, both PIG-K and *scu* have been linked to human disease with brain-related phenotypes. Recently, multiple patients with mutations in PIG-K have been identified suffering from developmental delay, intellectual disability and facial dysmorphism [Nguyen et al., 2020]. PIG-K is part of a complex of the transamidase complex that transfers glycosylphosphatidylinositol (GPI) anchors onto nascent polypeptides in the ER to embed modified proteins into the monolayer of lipid membranes. Experiments in mutant yeast and human cells revealed the accumulation of GPI donors in the ER [Yu et al., 1997a, Chen et al., 1996]. While the pathomechanism of PIG-K mutation is not yet understood, it might involve accumulation of GPI anchors in the ER that could trigger the neurotoxic cascade of UPR and ISR pathways.

On the other hand, *scu* is part of the mitochondrial protein complex responsible for the processing of the 5' end of mt. tRNAs (RNase P). While *scu* is an essential protein, it forms a complex with *rswl* (TRMT10C) and *mldr* (PRORP), both of which have been linked to human disease upon mutation [Camelo et al., 2021, Hochberg et al., 2021]. Interestingly, patients with mutations in TRMT10C or PRORP bear a surprising resemblance to the phenotype of *PUS7* patients including developmental delay, cognition defects and mitochondrial dysfunction. While we could not confirm their pseudouridylation in fly heads, the similarities in patient phenotypes raises the possibility that lack of modification of these mRNA sites in the brain might contribute to the defects observed in *PUS7* patients. However, according to our proteomics dataset, the UPR and ISR pathways are not activated in the *Pus7* model suggesting that PIG-K is not involved (Supplementary table S.3 and figure S.6). To further investigate the pseudouridylation of *scu* mRNA in the fly brain, a low-throughput sanger sequencing-based BID-seq approach is being set up in the lab [Dai et al., 2022]. Perhaps, the presence of other tissues including eyes prevented the detection of brain-specific *Pus7*-dependent Ψ sites in fly heads. Hence, using RNA from dissected brains as input might allow us to confirm pseudouridylation of *scu* mRNA in brain tissue.

3.4 The *Pus7* phenotype is reminiscent of a tRNA disease

Using Ψ -seq, MST and northern blotting, we observed a significant decrease in tRNA^{ASP} levels of up to 60% (Figure 17). RNA modifications in the body of tRNAs can be important for their structural integrity. This has been demonstrated for modifications that affect interactions between the T Ψ C and the D loops. Loss of tRNA modifications in these regions can lead to a reduction in thermal stability causing reductions in tRNA levels and increased cleavage by Ang in human cells [Wang et al., 2016b]. It is important to note, though, that cleavage by Ang only affects a small pool of mature tRNAs and has never been observed to cause a reduction in mature tRNA levels in the absence of reduced tRNA stability. It is more likely that the reduction in mature tRNA levels as observed by [Wang et al.,

2016b] is caused by tRNA surveillance mechanisms (see section 1.7.2). The two identified tRNA surveillance mechanisms are the RTD which targets end-processed and spliced mature tRNAs with unstable acceptor or T stems and the nuclear surveillance pathway targeting pre-tRNAs that are not efficiently bound by La and therefore have accessible 3' ends for polyadenylation and degradation.

We hypothesized that loss of $\Psi 13$ in *Pus7^{fs}* flies might destabilize the D stem and thereby reduce the stability of tRNA^{Asp} leading to enzymatic degradation. To confirm this, fly lines have been prepared to genetically inhibit enzymes involved in the RTD or the TRAMP complex in a *Pus7^{fs}* background. An increase of tRNA levels upon knockdown of surveillance pathway complex members will indicate which one of the tRNA surveillance pathways is responsible for the loss of tRNA^{Asp} in *Pus7^{fs}* flies. Of note, the reduction of tRNA^{Asp} levels seems to be an integral part of the pathomechanism in the *Pus7* model since overexpression rescued the aggressive behavior, reduced the fertility defect, and rescued the mitochondrial dysfunction in flies (Figures 18B&C and 22A). It is important to note though that the tRNA^{Asp} molecules originating from the overexpression in the *Pus7^{fs}* background are expected to not be modified at position 13. Therefore, the observed rescues might be caused by a saturation of the respective surveillance pathway. As a result, a fraction of the overexpressed unmodified tRNA^{Asp} molecules might avoid degradation and participate in active translation to resolve the potential slow-down or stalling of translation at Asp codons.

3.5 Lack of Pus7 causes translational changes

Employing ribosome profiling, we could observe increased ribosome occupancies specifically over aspartate codons at translating ribosomes waiting for mature tRNA^{Asp} to enter into the ribosomal A site (Figure 19A&B). Similar observations regarding codon-specific translational defects have been made in other tRNA diseases. For instance, mitochondrial tRNA^{Lys} lacking tRNA modifications results in mitochondrial translation defects at the corresponding codons leading to mitochondrial respiration defects [Kirino et al., 2004]. Similarly, loss of mitochondrial tRNA^{Glu} causes defects in mitochondrial translation of Glu-rich respiration complex members ND1, ND6 and CO2 resulting in mitochondrial dysfunction [Wang et al., 2016b]. Furthermore, [Blaze et al., 2021] reported that reduction in cytoplasmic tRNA^{Gly} caused codon-specific translation defects in Gly-rich genes in glutaminergic neurons causing impaired synaptic signaling in mice. Interestingly, codon-specific translational changes related to loss of PUS7 have been previously investigated in human GSCs. [Cui et al., 2021] reported that tRNA^{Arg}_{CCG} lacking PUS7-dependent pseudouridylation results in increased translational efficiency of the respective CCG codon. Surprisingly, the global proteomic changes upon loss of PUS7 did not reflect this increase in translational speed. Instead, the tumor suppressor TYK2, an important regulator of the vertebrate-specific interferon pathway [Savan et al., 2009] and rich in CCG codons, was significantly upregulated. As a result, the observed proteomic changes upon loss of PUS7 are mainly caused indirectly by activation of interferon-stimulated genes rather than through direct codon-specific translational changes.

Inspired by this, we aimed to investigate potential proteomic changes employing mass-spectrometry and discovered notable changes in the proteome of *Pus7^{fs}* flies, especially in metabolic proteins. Similar to [Cui et al., 2021], we could not find a correlation between changes in the protein levels and their respective aspartate contents in spite of the drastic reduction in tRNA^{ASP} levels as well as the increased ribosome occupancy at Asp codons (Figures 20 & 19A&B). In line with this, the presumable sites of ribosome pausing that were identified based on high ribosome occupancies did not negatively correlate with protein levels suggesting that they rather reflect increased translation than ribosome stalling (Supplementary figure S.5). Importantly, a similar observation has been made in yeast, where loss of *pus3* or *pus7* causes codon-specific changes in ribosome occupancy that mostly reflect an increase in translational efficiency [Chou et al., 2017]. Interestingly, in this study, perturbation of several tRNA modifying enzymes including *pus7* consistently induced the ISR as measured by an increase in ATF4 translation.

Thus, we investigated other possible indirect effects on the proteome including the activation of stress response pathways. Activation of the ISR requires translation of the transcription factor ATF4 which can be triggered by various forms of stress including ribosome stalling. In our ribosome profiling dataset, we discovered minor increases in ribosome occupancy approximately 50 nt upstream of pausing sites indicating potential disome formation (Figure 19G). Furthermore, vacant A-sites as it is the case in stalled ribosomes at Asp codons specifically trigger the ISR [Yan and Zaher, 2021]. In spite of this, we could not identify any increase in the translation of ATF4 suggesting that the ISR is not activated (Supplementary figure S.6A). To confirm this, we quantified the protein levels of genes targeted by the transcription factor dFoxo which is itself a target of ATF4. Only very few genes regulated by dFoxo were slightly dysregulated indicating that, in general, downstream targets of the ISR are likely not activated (Supplementary figure S.6B). Next, activation of the UPR as a result of ER stress can function as an activating signal for the ISR. To test the involvement of the UPR pathway, we quantified the expression of relevant genes but could not measure consistent increases in the protein levels suggesting that the UPR is also not activated (Supplementary table S.3). Finally, we investigated the protein levels of all other predicted transcription factors in *Drosophila* to identify candidates that might explain the changes in the proteome of *Pus7^{fs}* flies. However, we could not identify dysregulated transcription factors that might explain our observations (Supplementary figure S.6C). To confirm this, we examined the transcription start sites of dysregulated genes but could not identify a significant enrichment of transcription factor binding sites that might regulate their expression (Supplementary figure S.6D).

Disome formation as a result of ribosome stalling does not only trigger the ISR but also the RQC pathway, however, RQC activation is more sensitive to ribosome stalling than ISR activation [Meydan and Guydosh, 2020, Yan and Zaher, 2021]. The central mediator of the RQC in *Drosophila* is CG11414 (ZNF598) which is upregulated by 15.7% on the protein level in *Pus7^{fs}* flies suggesting a potential activation (Supplementary table S.1). To investigate the involvement of the RQC pathway, we prepared fly lines expressing tagged CG11414 in combination with or without a *Pus7^{fs}* allele. Stabilization of CG11414 protein levels has been previously used as a readout for RQC activation in

Drosophila [Geng et al., 2022]. Using this reporter line, we will confirm a potential activation of the RQC pathway upon loss of Pus7 in future experiments.

Finally, we have not yet explored the possibility that tRF dysregulation might affect gene expression in *Pus7^{fs}* flies. tRFs can affect gene expression in various ways for instance by directly interacting with ribosomes or with complexes of the miRNA or piRNA machineries (see section 1.8.2). Using northern blotting, we observed a significant reduction of fragments derived from tRNA^{ASP} in *Pus7^{fs}* flies. However, instead of a linear decline of fragments and mature tRNA, we discovered an approximately 50% increase in fragments in *Pus7^{fs}* flies when normalizing to the amount of mature tRNA^{ASP} (Figure 17C). While the *Drosophila* enzyme responsible for tRNA cleavage has not been identified, increased fragmentation upon hypomodification has been previously observed in flies [Schaefer et al., 2010]. Therefore, we can not rule out that a lack of Ψ 13 in tRNAs might render them more susceptible to cleavage. Another explanation for the increase in fragmentation upon lack of Pus7 could be that the enzyme responsible for tRNA cleavage in *Drosophila* might be saturated with mature tRNA^{ASP} in spite of its reduced levels. Alternatively, this might be an artifact of northern blotting resulting from the increased impact of background subtraction on the quantification of fragments due to their very low expression levels. Therefore, non-fragmented small RNA-seq as performed in [Cui et al., 2021] might serve as an alternative approach to northern blotting to quantify tRNA-derived fragments with nucleotide precision.

3.6 Mitochondrial dysfunction, the glycolytic shift and aggression might be linked in *Pus7^{fs}* flies

Considering that the behavior defects observed in *Pus7^{fs}* flies might be caused by defects in the central complex or the mushroom body, we expected structural or signalling defects within these brain regions. In regard to the clinical picture of PUS patients, this would likely constitute a developmental defect. Surprisingly, we could rescue the aggressive behavior in adult flies by feeding them the glycolysis inhibitor 2-DG which should not affect any existing developmental defects in the brain (Figure 22C). Instead, this suggests that the increased glycolysis observed in *Pus7^{fs}* flies instead of neurodevelopmental defects are responsible for the induction of aggressive behavior (Figure 21A&B).

Additionally, mitochondrial function was reduced upon loss of Pus7 (Figure 22A). Strikingly, studies in bees revealed a link between mitochondrial dysfunction, aerobic glycolysis and increased aggression levels [Chandrasekaran et al., 2015]. Metabolic analysis of brains from bees that naturally show increased aggression levels including aged bees, soldier bees and bees that were exposed to alarm pheromones revealed an increase in aerobic glycolysis concomitant with a decrease in mitochondrial respiration. This is in agreement with results from another study which postulated that a reduction in mitochondrial activity directly causes aggression. Here, treatment of bees with complex I or complex V inhibitors readily increased their aggression levels [Li-Byarlay et al., 2014]. Furthermore, experiments in *Drosophila* provided evidence for a conservation of this relationship between

mitochondrial respiration and aggression. Specifically, genetic inhibition of complex I by 50% in neurons was sufficient to trigger strong aggressive behaviors in flies.

This concept was further reinforced by a recent study in flies. [Sorge et al., 2020] used a *Drosophila* eye tumor model where artificial Notch signaling caused a mild over-proliferation phenotype. A notable observation was that genetic inhibition of the electron transport chain (ETC) in this background is sufficient to enhance the over-proliferation phenotype. Further analysis revealed that knockdown of individual subunits of complexes I or IV triggered a transcriptional response through the PERK-ATF4 axis inducing a shift towards glycolysis.

Such a switch from OXPHOS metabolism to aerobic glycolysis was first identified in cancer cells by [Warburg, 1925]. It was postulated that this mechanism promotes cell growth by processing glucose to create building blocks for anabolism in the form of amino acids at the expense of energy generation through the TCA cycle [Vander Heiden et al., 2009]. [Sorge et al., 2020] proposed that a pH reduction as a result of ETC impairment might act as a cellular signal to induce aerobic glycolysis. Concomitantly, artificially increasing the intracellular pH by feeding flies L-carnosine which titrates hydrogen ions (H⁺) [Abe, 2000] was sufficient to rescue the eye-overgrowth phenotype upon knockdown of ETC subunits suggesting that glycolysis is restored to wild type levels. As a result, this study brought forth the notion that the induction of glycolysis through the ISR might be a downstream response to mitochondrial dysfunction.

Hence, we hypothesized that mitochondrial dysfunction might trigger aggression in *Pus7^{fs}* flies through a mechanism involving pH changes, the ISR and aerobic glycolysis. Admittedly, *Pus7^{fs}* flies merely suffer a mild mitochondrial dysfunction with a reduction of the O₂ consumption by approximately 20%, presumably caused by a slight reduction of the protein levels of two complex I subunits by ca. 10% (Figure 22A&B). However, complex I deficiency was reported to have the greatest effect on ETC activity as it represents the main entry point for most electrons into the respiratory chain [Telford et al., 2009]. Also, we could not yet identify any evidence for the activation of the ISR pathway (Figure 21B). Thus, further experiments are needed to test the hypothesized link between ETC impairment, pH, glycolysis and aggression in *Pus7^{fs}* flies. These include the quantification of the pH using, for instance, the pHerry reporter system [Rossano et al., 2017] or the Agilent Seahorse XFe96 Analyzer as well as measuring sugar levels in head protein extracts or the hemolymph using Glucose Assay Kits.

In the *Pus7^{fs}* background, overexpression of tRNA^{Asp} rescued both the mitochondrial respiration defect as well as the increased aggression levels (Figures 22A & 18B). Therefore, it is expected to revert the pH and sugar levels back to wild type levels. Furthermore, feeding of L-carnosine is expected to rescue the pH, the sugar levels as well as aggression but not mitochondrial dysfunction. Interestingly, carnosine levels are already upregulated (+50%) upon mutation of *Pus7* which might display a potential intracellular response to reduced pH levels (Supplementary figure S.7D). Finally, we already discovered that feeding of 2-DG to *Pus7^{fs}* flies rescues aggressive behavior but it should not affect mitochondrial dysfunction and intracellular pH levels. Importantly, systemic inhibition of glycolysis as performed in Figure 22C might have negative effects on fly activity and thereby reduce

the likelihood of performing energy-demanding behaviors like aggression. Thus, it is crucial to identify the relevant brain regions where loss of Pus7 causes these defects as discussed in section 3.1.2. Then, brain-region or cell-type-specific genetic inhibition of glycolysis could minimize unwanted side effects on fly behavior and confirm the link between local Pus7-dependent dysregulation of glycolysis and increased aggression levels. To this end, UAS lines to target the knockdown of several glycolytic genes including *Hex-A*, *Hex-C*, *Pfk*, *Tpi*, *Pgk*, *PyK* and *Ldh* were isogenized and combined with the *Pus7^{fs}* allele.

It is important to note that there are some discrepancies between the warburg effect and the defects observed in *Pus7^{fs}* flies. First of all, loss of Pus7 in head tissues caused a ubiquitous defect in mitochondrial function as well as a ubiquitous upregulation of glycolysis. Therefore, it is very puzzling that we can not observe a ubiquitous expression of ATF4 or any activation of the ISR in head tissues according to ribosome profiling (Figure S.6A). Perhaps, a yet to be identified mechanism prevents ATF4 translation in *Pus7^{fs}* flies. Alternatively, an ISR-independent mechanism might be responsible for induction of glycolysis. Furthermore, a study in *Drosophila* uncovered that the activation of the warburg effect requires the hypoxia-inducible transcription factor-1 α (Hif-1 α , *sima* in *Drosophila*) and c-Jun N-terminal kinase (JNK) which are activated and stabilized by ROS [Wang et al., 2016a]. However, expression of *sima* was not detected in our proteomics dataset neither in *wild type* nor in *Pus7^{fs}* flies, perhaps due to being expressed below the detection threshold. Also, none of the proteins involved in the JNK pathway or its targets were dysregulated or at least below the detection threshold (Supplementary table S.3). Thus, the prerequisites for activation of the warburg effect according to [Wang et al., 2016a] are not met upon loss of Pus7.

On the other hand, multiple observations support the occurrence of a warburg-like metabolism: For instance, regulating the levels of nicotinamide adenine dinucleotide (NAD⁺) is critical for proliferating cells as it is necessary for the synthesis of anabolic molecules. NAD⁺ is regenerated from NADH either through the ETC which is limited at high ATP levels [Luengo et al., 2021] or by conversion of pyruvate to lactate by lactate dehydrogenase (*Ldh*) [Hosios and Vander Heiden, 2018]. Therefore, cells with high ATP concentrations switch to aerobic fermentation of glucose to lactate to meet the demands of NAD⁺. In line with this, we observed increased levels of ATP (+97.8%), lactate (+71.5%) and *Ldh* (+57.2%) in *Pus7^{fs}* flies (Figure 21A). To import the required amounts of sugar into the cell for fermentation, glucose transporters are expected to be upregulated, yet Trehalase is significantly downregulated on the protein level (-17.5%) upon loss of Pus7 (Figure 21A). Instead, the mitochondrial enzyme phosphoenolpyruvate carboxykinase 2 (*Pepck2*), a direct target of ATF4 [Méndez-Lucas et al., 2014], is upregulated (+45.5%). This may promote the glycolytic shift by directly converting TCA intermediates into glycolytic substrates. In line with this, carnitine metabolism to transport lipids into the mitochondria is upregulated while TCA metabolites are downregulated in *Pus7^{fs}* flies (Figure 21A). These results suggests that the energy demand is met in spite of aerobic glycolysis being vastly less efficient for ATP generation and that Pus7-deficient cells switch to fermentation of pyruvate to generate NAD⁺ from both sugars and TCA intermediates. Therefore, we hypothesize that an ISR-independent mechanism triggers a warburg-like metabolic

state upon loss of Pus7 where glycolysis is fueled by lipids that are processed in the mitochondria.

3.7 Conclusion

Using the genetic tractability of the *Drosophila* model allowed us to pinpoint the origin of the behavioral defects caused by loss of Pus7 to neurological functions in the brain. While the cause for the neurological defects are not yet understood, we found indications that the aggressive behavior might be caused by increased glycolysis. It remains to be tested whether hyperglycemia is also involved in the orientation defect and hyperactivity. Based on the literature, we hypothesize that the defects originate in the central complex or the mushroom body and will test this by performing targeted rescue and knockdown experiments in these tissues. Our behavioral analysis indicates that the defects are specific to these areas in the brain suggesting that they are more susceptible to translational or metabolic changes than others.

The fact that tRNA^{Asp} overexpression rescues all of the tested defects, excluding the egg-laying defect, in the absence of functional Pus7 suggests that most of the phenotypes observed in *Pus7^{fs}* flies originate from defects in tRNA expression rather than a lack of modification of mRNA sites. This is in line with Ψ -seq and BID-seq revealing that the main target of Pus7 consists of tRNAs while only few mRNAs sites are modified in *Drosophila*, especially when considering the difference in transcript abundances between these two RNA species.

In agreement with this, defects in tRNA expression, maturation or stability have been reported to cause highly similar phenotypes in human patients. In the case of the *Pus7* fly model, the causal links between the reduction in tRNA^{Asp} levels and the translational dysregulation as well as the mitochondrial dysfunction are still unclear. However, we hypothesize that the lack of Pus7 activity results in neurological defects presumably as a result of cytoplasmic or mitochondrial translational defects which are a common hallmark of neurodevelopmental diseases.

MATERIALS AND METHODS

4.1 Materials

4.1.1 Cell lines

All *in cellulo* experiments were performed using *Drosophila* S2R+ cells.

4.1.2 Oligonucleotides

The gRNAs used for the generation of the *Pus7^{fs}* lines are described in [de Brouwer et al., 2018].

Table 4.1: List of gRNAs used for mutagenesis with CRISPR/Cas9.

Name	Sequence (5' to 3')
CG34140 gRNA1 fwd	cttcGCGATATGGATGGTGGTTGT
CG34140 gRNA1 Rev	aaacACAACCACCATCCATATCGC
CG34140 gRNA2 fwd	cttcGTAACTTTCAGAACAGACGC
CG34140 gRNA2 rev	aaacGCGTCTGTTCTGAAAGTTAC
CG3045 HR gRNA 2 fwd new	cttcGATCGACAAGGTTATCCAAC
CG3045 HR gRNA 2 rev new	aaacGTTGGATAACCTTGTCGATC
CG3045 gRNA II fwd	cttcGGCCAAAAAAGGAAAACCC
CG3045 gRNA II rev	aaacGGGTTTTTCCTTTTTTTGGCC

Table 4.2: List of primers used for PCR amplification and sequencing.

Name	Sequence (5' to 3')	Purpose
CG34140 T7 screen Fwd	CCGGGTACTTTGTTGTTGCC	Amplification and sequencing
CG34140 T7 screen Rev	TTCGGTTGAGCACACCAGTT	Amplification
CG3045 qPCR fwd new	CTTAAGCCGAGAGGCACTTG	Amplification and sequencing
3045 qPCR Rev	GCGGATTGACGGAATCTTGC	Amplification
Pus7 Intron1 Fwd	GTTAACC GGCGTTTTTCGTTGG	Amplification
Pus7 Intron3 Rev	CCCTGGGTAATCATTCTACTAACC	Amplification
6745KO screen DS Fwd	GAGTTCACTAACCCGGAGGC	Sequencing

Table 4.3: List of primers used for qPCR.

Name	Sequence (5' to 3')
CG3045 UTR qPCR fwd primer	GATGTGGAGTCTAATCCCTG
CG3045 UTR qPCR rev primer	GTATCCATGGCTTCTTCG
CG6745 CDSI/UTR qPCR rev primer	CCACCTCCTTTACCACCTCCA
CG6745 CDSI/UTR qPCR fwd primer	ACACATCGTCAGCATCGCAA
CG2064 qPCR Fwd	TCAAGAAGGAGCAACCCAAG
CG2064 qPCR Rev	TCAGTACGTCGAGCAGCAAG
Nipped-A qPCR Fwd	CAGGAGACGTTGTCCAGGAT
Nipped-A qPCR Rev	AGCCCCTTTAGAGCGTAAAA
Sgg qPCR Fwd	GTAATCACACCTTGCCCAACGG
Sgg qPCR Rev	TAGGCTGGGCTGTATTGAGAGC
eIF4EHP-Ex2 qPCR Fwd	ACTCCAATGCCGTTGTTAGAGGT
eIF4EHP-Ex2 qPCR Rev	CGGACTGCCACTGATATGACCA
Inr qPCR Fwd	ATCCCAGTCCGAAATGTGCAGA
Inr qPCR Rev	CGACCCTTTCTTGGCAGCAAAT
S6K qPCR Fwd	GAGCGATCCCAGCGAACT
S6K qPCR Rev	CACAATTCCGGTTCTAGGTCA

Continued on next page

Table 4.3 – continued from previous page

Name	Sequence (5' to 3')
eIF4EHP qPCR Fwd	CTGGCCGAGCTCTTATCAACC
eIF4EHP qPCR Rev	GGCTCTGAAGCAGAAATTGG
Akt1 qPCR Fwd	GCTCTGGGCTATCTGCATTC
Akt1 qPCR Rev	TACCGCAGAAGGTTTTTCGTT
Pten qPCR Fwd	TACGCTTCTCGGAGTCCAGT
Pten qPCR Rev	CCGGAAACTGGTATTGATGG
lncRNA_ CR45102 qPCR Fwd	GCAGATGGAGACGGAAAGAG
lncRNA_ CR45102 qPCR Rev	ATAAGTCCCCCGTGATGACA
DILP 2 Fwd Broughton	TCTGCAGTGAAAAGCTCAACGA
DILP 2 Rev Broughton	TCGGCACCGGGCATG
DILP 3 Fwd Broughton	AGAGAACTTTGGACCCCGTGAA
DILP 3 Rev Broughton	TGAACCGAACTATCACTCAACAGTCT
DILP 5 Fwd Broughton	GAGGCACCTTGGGCCTATTTC
DILP 5 Rev Broughton	CATGTGGTGAGATTCGGAGCTA
TRANSPOSON PRIMERS	TRANSPOSON PRIMERS
PIG-K qPCR Ex1 F1	GAGACTGGGCATTCCTGACT
PIG-K qPCR Ex1 R1	GATGTGCTGGTTGGCGTTAT
scu qPCR Ex2 F1	GTTTCGGTCTGCTGGATCTGA
scu qPCR Ex2 R1	GTGCCACGGTATTGATGTT
CG8223 qPCR Ex2-Ex3 F1	ACGCGAAGATTATGAGAAAGCA
CG8223 qPCR Ex3 R1	TCGCTCCTTCCCTTGTGAGT
CG17691 qPCR Ex1 F1	TGTGGGATTCGGTGGAGTTTT
CG17691-RF qPCR Ex2RF R1	AATAACGTACCCTGCGATTCC
CG17691-RE-RC qPCR Ex3 F1	TTGGACACGGAGCACTCTAC
CG17691-RE-RC qPCR Ex3-4 R1	GGGTACCACAACACGAAGTC
CG9135 qPCR Ex2 F1	TGCTTGCGGCAATAATCACA
CG9135 qPCR Ex3 R1	TCATTAAACGCGGCACCATT
Rpl15-qF	AGGATGCACTTATGGCAAGC
Rpl15-qR	GCGCAATCCAATACGAGTTC
gypsy_F	CCAGGTTCGGGCTGTTATAGG
gypsy_R	GAACCGGTGTACTCAAGAGC
297_F	AAAGGGCGCTCATACAAATG
297_R	TGTGCACATAAAATGGTTTCG
roo_F	CGTCTGCAATGTACTGGCTCT
roo_R	CGGCACTCCACTAACTTCTCC
I-element_F	TGAAATACGGCATACTGCCCCCA
I-element_R	GCTGATAGGGAGTCGGAGCAGATA
mdg1_F	CACATGTTCTCATTCCCAACC
mdg1_R	TTCGCTTTTTATATTTGCGCTAC
hobo-F	ACTCACACCCTACAATTTTGTGTG
hobo-R	GTGTTTAACGGTATAACCCACAAGTG
jockey_F	TGCAGTTGTTCCCTAACC
jockey_R	AGTTGGGCAAATGCTAGTGG
blood_F	TGCCACAGTACCTGATTTTCG
blood_R	GATTCGCCTTTTACGTTTTGC
412_F	CACCGGTTTGGTTCGAAAG
412_R	GGACATGCCTGGTATTTTTGG
P-element-F	TTAATATTAGCAGCGCGAAACGTC
P-element-R	GTTGATTAACCCTTAGCATGTCCG
diver_F	TTTTTGGAGCCGACCTTATG
diver_R	GGCGTGTAATATGCGTGTTG
Het-A_F	CGCGCGGAACCCATCTTCAGA
Het-A_R	CGCCGCAGTCGTTTTGGTGAGT
S-element_F	TGAAAAGCGTCATTCATTTCG
S-element_R	TGTTTCTAGCGCACTCAACG
17.31_F	AGCAAACGTCTGTTGGAAGG
17.31_R	CGACAGCAAAACAACACTGC
NoF_F	AGTTGGACCTGGAATTTGTGG
NoF_R	AATGCACACGGAAGAGGAAC

Continued on next page

Table 4.3 – continued from previous page

Name	Sequence (5' to 3')
Idefix_F	AACAAAATCGTGGCAGGAAG
Idefix_R	TCCATTTTTTCGCGTTTACTG
TAHRE_F	CTGTTGCACAAAGCCAAGAA
TAHRE_R	GTTGGTAATGTTTCGCGTCCT
burdock_F	CGGTAAAATCGCTTCATGGT
burdock_R	ACGTTGCATTTCCCTGTTTC

Table 4.4: List of primers used for generation of T7 PCR templates.

Name	Sequence (5' to 3')
CG3045 UTR KD fwd primer	TAATACGACTCACTATAGGGCCAAAGTAATTTTCACGTG
CG3045 UTR KD rev primer	TAATACGACTCACTATAGGGGAAGGCATTTGCTTGAATC
CG6745 KD fwd	TAATACGACTCACTATAGGCTGGATAAGGAGCAGCGAAC
CG6745 KD rev	TAATACGACTCACTATAGGCAGGCTTTGGTAAGCATGTGG

Table 4.5: List of oligonucleotides used for site directed mutagenesis.

Name	Sequence (5' to 3')
SDM CG6745 active site CDS fwd	CATCAAGGAGAAGCGGGCCA
SDM CG6745 active site CDS rev	TGGCCCGCTTCTCCTTGATG

Table 4.6: List of oligonucleotides used for northern blotting.

Name	Sequence (5' to 3')
tRNA31-Asp 5' probe AS 22nt	CTAACCACTATACTATCGAGGA
tRNA31-Asp 5' control S 22nt	TCCTCGATAGTATAGTGGTTAG
tRNA25Gly 5' probe AS 22nt	CTAACCATTAACACCACCGACGC
tRNA25Gly 5' ctrl S 22nt	GCGTCGGTGGTGTAAATGGTTAG

Table 4.7: Probes used for microscale thermophoresis.

Name	Sequence (5' to 3')
chr3R.trna25 ^{Gly} _{TCC}	GCGTCGGTGGTGTAAATGGTTAGCATAGTTGCCTTC CAAGCAGTTGACCCGGGTTTCGATTCCCGGCCGACGCA
chr2L.trna31 ^{Asp} _{GTC}	TCCTCGATAGTATAGTGGTTAGTATCCCCGCTGT CACGCGGAGACCGGGGTTCAATTCCCCGTCGGGGAG

d

Table 4.8: List of oligonucleotides used to generate plasmids.

Name	Sequence (5' to 3')	Plasmid
CG6745 5 Fwd NotI	ATGCgcgccgcTATGGGCAAGGATCGGGGCAG	pPFMW-Pus7
CG6745 3 Rev AscI	ATGCgcgccgcCACCGCCTCCTCGGCCCCCT	pPFMW-Pus7
CG3045 5 Fwd NotI	ATGCgcgccgcTATGAGTGCAACAAATGACAA	pPFMW-Pus3
CG3045 3 Rev AscI	ATGCgcgccgcCTCTGTTTCCGTTTCATTCT	pPFMW-Pus3
PusL1 pPWH Fwd	NotI ctccgcgccgcATGTATAGGTATTTGTTGAAC	pPWH-PusL1
PusL1 pPWH Rev	AscI TAGCGGCGCGCCACCCTTAATGTCCGTTTCTCGGTAGT	pPWH-PusL1
TAGC HindIII PusL1 Promoter	TAGC aagcttTCTAGTTACGTGGTGGGTGGAG	pPusL1-eGFP
PusL1 Rev -stop +EGFP overlap	ctcgccttctcaccatAATGTCCGTTTCTCGGTAGTGC	pPusL1-eGFP
GFP Fwd + PusL1 overlap	GCACTACCGAGAAACGGACATTaggtgagcaaggcgag	pPusL1-eGFP
GFP Rev +stop +NotI TAGC	cgcgccgcTTActgtacagctcgtccatgcc	pPusL1-eGFP
tRNA-Asp_Fragment1_F_U6_BglII	CCTGATGTTGATCATTATATAGGTATGTTTTCCTCAAT	pBFv-U6.2B_tRNA ^{Asp} _{GTC-1-5_x4}
tRNA-Asp_Fragment1_R_AatII	ACTTCGGGTCTTCAGATCTGTATAGATCAACAGCAAGTT	pBFv-U6.2B_tRNA ^{Asp} _{GTC-1-5_x4}
tRNA-Asp_Fragment2_F_AatII	ctcatcgtttactgaaaggaTAGAGACGTCGATGCGAGAGCATTMTTTCAC	pBFv-U6.2B_tRNA ^{Asp} _{GTC-1-5_x4}
tRNA-Asp_Fragment2_R_AgeI	GACGTCTCTAtcctttcagtaaacgatgagGTATAGATCAACAGCAAGTT	pBFv-U6.2B_tRNA ^{Asp} _{GTC-1-5_x4}
tRNA-Asp_Fragment3_F_AgeI	gctaattcacgtggaccacaTAGAACCGGTGATGCGAGAGCATTMTTTCAC	pBFv-U6.2B_tRNA ^{Asp} _{GTC-1-5_x4}
tRNA-Asp_Fragment3_R_NsiI	ACCGGTTCTAtgtgtccacgtgaattagcGTATAGATCAACAGCAAGTT	pBFv-U6.2B_tRNA ^{Asp} _{GTC-1-5_x4}
tRNA-Asp_Fragment4_F_NsiI	gagatcctaatcggcatgccTAGAATGCATGATGCGAGAGCATTMTTTCAC	pBFv-U6.2B_tRNA ^{Asp} _{GTC-1-5_x4}
tRNA-Asp_Fragment4_R_StuI	ATGCATTCTAggcatgccgattaggatctcGTATAGATCAACAGCAAGTT	pBFv-U6.2B_tRNA ^{Asp} _{GTC-1-5_x4}
tRNA-Asp_Fragment5_F_StuI	gattcgtgttctgcttgccaTAGAAGGCCTGATGCGAGAGCATTMTTTCAC	pBFv-U6.2B_tRNA ^{Asp} _{GTC-1-5_x4}
tRNA-Asp_Fragment5_R_MfeI_U6	AGGCCTTCTAtcgcaagcgaacacgaatcGTATAGATCAACAGCAAGTT	pBFv-U6.2B_tRNA ^{Asp} _{GTC-1-5_x4}
Asp-F	AACGGACTAGCCTTATTTTAACTTGCTATTTCTAGCTCTA	pAC5-Asp-GFP-stop-mCherr
Asp-R	ACGAGAATTCATGGACGACGACGACGACGACGACGACGACGATATCGACG	pAC5-Asp-GFP-stop-mCherr
Leu-F	CGTCGATATCGTCGTCGTCGTCGTCGTCGTCGTCGTCGTCATGAATTCCTCGT	pAC5-Leu-GFP-stop-mCherry
Leu-R	ACGAGAATTCATGTTATTATTATTATTATTATTATTATTATTATTAGATATCGACG	pAC5-Leu-GFP-stop-mCherry
	CGTCGATATCTAATAATAATAATAATAATAATAATAACATGAATTCCTCGT	

4.1.3 Plasmids

Table 4.9: List of plasmids used in this study.

Plasmid	Promoter	Transgene	Tag	Application	Source
pPFMW-Pus7	UAS	Pus7 CDS	N-term. Flag-Myc	Overexpression	Generated in this study
pPFMW-Pus3	UAS	Pus3 CDS	N-term. Flag-Myc	Overexpression	Generated in this study
pPWH-PusL1	UAS	PusL1 CDS	C-term. HA	Overexpression	Generated in this study
pPusL1-eGFP	PusL1	PusL1 CDS	C-term. eGFP	Expression at endogenous level	Generated in this study
pBFv-U6.2B_tRNA ^{Asp} _{GTC-1-5_x4}	U6.2	4x tRNA ^{Asp} _{GTC-1-5}		Overexpression	Generated in this study
pAC5-Asp-GFP-stop-mCherry	Actin5c	Asp-GFP & mCherry	-	Overexpression	Generated in this study
pAC5-Leu-GFP-stop-mCherry	Actin5c	Leu-GFP & mCherry	-	Overexpression	Generated in this study

Continued on next page

Table 4.9 – continued from previous page

Plasmid	Promoter	Transgene	Tag	Application	Source
pAC5-GFP-Stop-mCherry	Actin5c	GFP & mCherry	-	Overexpression	Lina Worpenberg
Act-Gal4	Actin5c	Gal4	-	Overexpression driver	-

4.1.4 Antibodies and beads

Table 4.10: List of antibodies used in this study.

Antibody	Dilution		Source	Application
	WB	IF		
rb α GFP	1:5000	1:5000	TP401	PusL1-eGFP in S2R+ (IF) EGFP-Pus7 in ovaries (IF) EGFP-Pus7 in embryos (IF) EGFP-Pus7 in larval brains (IF)
m α Myc	-	1:1000	2276, Cell Signaling	pPFM-Pus3 in S2R+ (IF) pPFM-Pus7 in S2R+ (IF)
m α HA	-	1:1000	sc7392, Santa Cruz	PusL1-HA in S2R+ (IF)
rb α Histone H3	1:2000	-	Ab1791, Abcam	loading control (WB)
m α Syt1	-	1:100	3H2 2D7, DSHB	NMJ analysis (IF)
m α Flag	1:2000	-	F1804, Sigma-Aldrich	Flag-Myc-Pus7 (WB)
α HRP TRITC	-	1:1000	323-025-021, Jackson ImmunoResearch	NMJ analysis (IF)
HRP α m	1:10000	-	Dianova	Flag-Myc-Pus7 (WB)
HRP α rb	1:10000	-	Dianova	EGFP-Pus7 & Histone H3 in flies (WB)
Alexa Fluor 488 α rb	-	1:400	Dianova	PusL1-eGFP in S2R+ (IF) PusL1-HA in S2R+ (IF)
Alexa Fluor 488 α m	-	1:400	Dianova	pPFM-Pus3 in S2R+ (IF) pPFM-Pus7 in S2R+ (IF)

4.1.5 Enzymes, reagents and commercially available kits

Table 4.11: Restriction enzymes used for cloning.

Name	Source
AscI	NEB
NotI-HF	NEB
HindIII	NEB
BbsI-HF	NEB
EcoRI-HF	NEB
EcoRV-HF	NEB

4.2 Methods

4.2.1 Drosophila cell culture

4.2.1.1 Cell culture maintenance

Drosophila S2R+ cells were grown in Schneider's medium (Gibco) supplemented with 10% FBS (Sigma) and 1% Penicillin-Streptomycin (Sigma).

4.2.1.2 Knockdown and transfection

RNA interference (RNAi) experiments were performed as described in [Rogers and Rogers, 2008]. dsRNA against bacterial β -galactosidase gene (*lacZ*) was used as a control for all RNAi experiments. S2R+ cells were seeded at the density of 10^6 cells/ml in serum-free medium and treated with 7.5 μ g

of dsRNA per 10^6 cells. After 6 h of cell starvation, serum supplemented medium was added to the cells. dsRNA treatment was repeated after 48 and 96 h and cells were collected 24 h after the last treatment. For transfection, 20 mio cells were plated out in 10 cm dishes and treated with Effectene (Qiagen) following the manufacturers protocol. 2 μ g of total plasmid were used for transfections per 20 mio cells. For plasmids with UAS promoters requiring Gal4 to drive expression, one quarter of the total plasmid amount consisted of the act-Gal4 plasmid. Cells were harvested after 72 h.

4.2.1.3 FACS sorting

1.6 ml of 10^6 mio cells per condition and replicate were depleted of Pus7 by siRNA treatment and transfected after the last siRNA treatment as described above. Three technical replicates were generated per condition. 72 hours after transfection the medium was removed and the cells resuspended in PBS supplemented with 5% FBS and 3 mM EDTA and used for Fluorescence-activated cell sorting (FACS). A total of 100.000 cells were analyzed from each batch and the mean intensity of GFP and mCherry positive cells was determined. Sorted cells were collected for RNA isolation to evaluate the *Pus7* knockdown efficiency by RT-qPCR.

4.2.2 Fly work

Flies were raised at 25°C at 50% humidity and a 12 h light/dark cycle.

4.2.2.1 *Drosophila melanogaster* stocks

Drosophila melanogaster Canton-S with mutant alleles for *Pus7* (CG6745) were described previously [de Brouwer et al., 2018]. Other fly stocks used are:

Table 4.12: Fly lines used in this study.

Stock name	Line description	Source
tub-GAL4	ubiquitous driver	[Lee and Luo, 2001]
elavC155-GAL4	neuronal driver	BL#458
heph ⁰³⁴²⁹	heph mutant	BL#11589
PusL1 KO10	PusL1 deletion mutant	generated in this study
PusL1 KO11	PusL1 catalytic dead mutant	generated in this study
PusL1 KO17	PusL1 catalytic dead mutant	generated in this study
Pus3 ^{Δ1033}	Pus3 deletion mutant	generated in this study
Pus3 ^{def}	Pus3 deficiency	BL#28486
EGFP-Pus7	endogenous knockin after excision	WellGenetics Inc.
EGFP-3xP3-RFP-Pus7	endogenous knockin before excision	WellGenetics Inc.
Pus7 ^{fs} 15-2	Pus7 frameshift mutant	generated in this study
Pus7 ^{fs} 15-1	Pus7 frameshift mutant	generated in this study
pPFM-Pus7; Wild type	Pus7 rescue line	generated in this study
pPFM-Pus7; Pus7 ^{fs}	Pus7 rescue line	generated in this study
pPFM-Pus7 catalytic dead; Wild type	catalytic dead Pus7 rescue line	generated in this study
pPFM-Pus7 catalytic dead; Pus7 ^{fs}	catalytic dead Pus7 rescue line	generated in this study
4x tRNA ^{ASP} ; Wild type	tRNA ^{ASP} rescue line	generated in this study
4x tRNA ^{ASP} ; Pus7 ^{fs}	tRNA ^{ASP} rescue line	generated in this study
TBX-0008	balancer line	DGRC, Indiana
TBX-0002	transformation line	DGRC, Indiana

Continued on next page

Table 4.12 – continued from previous page

Name	Sequence (5' to 3')	
Cas-0001	nos-Cas9 line	DGRC, Indiana

4.2.2.2 Generation of transgenic fly lines

gRNA constructs as well as the pPFM-Pus7 plasmid were injected into TBX-0002 embryos for phiC31 mediated integration at the attP40 site. Survivors with brown eyes indicative of successful integration were crossed to TBX-0008 for balancing. The Pus7 line with N-terminal endogenous EGFP tag was generated by WellGenetics (Taipei City, TW). First, an EGFP-loxP-3xP3-RFP-loxP cassette was integrated after the ATG of Pus7 using CRISPR/Cas9. Next, the 3xP3-RFP marker was flipped out using Cre recombinase leaving a 16 amino acid linker between EGFP and the Pus7 gene sequence. The U6.2B plasmid containing four copies of tRNA^{Asp}_{GTC}-1-5 was integrated at the attP40 site using the phiC31 system by BestGene Inc.

4.2.2.3 Generation of mutant fly lines using CRISPR/Cas9

Cas9 mutagenesis was achieved by crossing flies carrying the plasmid for gRNA expression to Cas-0001 flies expressing Cas9 under the control of the *nanos* promoter in the germline. Male flies carrying both transgenes and potential mutations were crossed to balancer lines respective to the chromosome targeted by the gRNAs for balancing. Heterozygous flies potentially carrying a mutation over a balancer chromosome were crossed again for balancing and screened for the presence of the mutation.

4.2.2.4 Isogenization

Stocks with isogenized chromosomes were generated by crossing females of mutant fly lines generated with the CRISPR/Cas9 system or transgenic lines repeatedly to wild type *Canton-S* males. This was repeated until at least five crosses with heterozygous females have occurred. The final recombination was performed by crossing heterozygous females to a male carrying an isogenized balancer chromosome. Finally, the balanced offspring was crossed with each other. The presence of the mutation or the transgene was confirmed by PCR at every cross in heterozygous females or in both parents of the final cross with balanced flies.

4.2.2.5 Survival assays

Lifespan assay

To evaluate the lifespan of *Pus3* mutants, flies were mated for 24 h after eclosion. Subsequently, males and females were separated and transferred to tubes with fresh food every two days under CO₂ anesthesia. Simultaneously, surviving flies were counted.

To evaluate lifespans of *Pus7^{fs}* flies, flies were mated for 48 h after eclosion. Subsequently, males and females were separated into batches of 20 flies under CO₂ anesthesia and transferred to tubes

with fresh food three times per week. Surviving flies were quantified during flipping. To quantify lifespan upon aspartate supplementation, 0-1 day old flies were mated in batches of 20 males and 20 females and flipped every 2 days to fresh food until the age of 5-6 days. Subsequently, flies were separated into batches of 10 males or females to fresh food. At 6-7 days of age, flies were flipped to empty tubes with Whatman paper discs (WHA1030024, Merck) and starved for 3 h. Finally, 200 μ l 5% sucrose solution with 0.54 mg/ml L-Aspartate (A9256, Sigma) and 0.01% Nipagin (3646.3, Roth) were added daily using a 20 g 1 $\frac{1}{2}$ " 0.9 x 40 mm Microlance needle (Becton Dickinson) with a 2 ml BD Plastipak Luer-Lok syringe (Becton Dickinson). Sucrose solution without aspartate was added to controls.

Oxidative stress assay and amino acid starvation assay

Flies were mated and aged until the age of 10 days. Afterwards, flies were transferred to tubes with a 3 mm filter paper (WHA1030024, Merck) at the bottom soaked with 200 μ l 5% sucrose and paraquat (75365-73-0, Sigma-Aldrich) diluted in water. 5 mM paraquat was used for the assay with *PusL1 KO* flies while a 10 mM solution was used for the assay with *Pus3 KO* flies. Surviving flies were counted every 8 hours. Untreated flies that were only fed with sucrose were considered as starved of amino acids and analyzed separately.

Dry starvation assay

Flies were mated and aged until the age of 9-10 days. Afterwards, flies were transferred to empty tubes and starved. Surviving flies were counted every hour.

Adult climbing assay

Locomotion defects were examined by analyzing 24 male flies of the respective genotype. The flies were transferred into a plexiglass cylinder by aspiration. The top was sealed off with a piece of cotton. After 20 min of habituation the climbing assay was performed. The flies were tapped to the bottom of the tube and the time required to climb past a 6 cm mark was measured. One fly was evaluated at a time. Flies that did not climb 6 cm within 30 seconds were omitted from the evaluation. Once all flies were measured, a second round of measurements was performed serving as second technical replicate. In every round of measurements, the flies were evenly split between mutant and control to prevent biases through effects of the circadian rhythm. The assay was performed with 6-7 day old and 11-12 day old *PusL1 KO10* flies. *Canton-S* flies were used as control.

Larval crawling assay

Crawling assays to quantify the locomotion of *PusL1 KO10* larvae were performed at 25°C on 15 cm dishes filled with 100 ml of 1% agarose in H₂O on a black background to improve contrast at 25°C. L3 larvae were washed in 1x PBS, transferred to the center of the agarose dish and allowed to recover for 2 min. Afterwards, the larvae were moved to the center of the dish using a brush and their movements were recorded for 2 minutes. Approximately 50 L3 larvae were evaluated per

genotype. Five larvae were recorded simultaneously. In between recordings, the agarose dish was cleaned gently with PBS or H₂O for reuse. To prevent potential effects of circadian rhythm on larval activity, the evaluated genotypes were alternated every run. The videos were cropped to 2 minutes and subsequently every fifth frame of the recordings was extracted using a bash script and ffmpeg. Individual frames were loaded into FIMtrack v2. The pixel per cm ratio was determined utilizing ImageJ and a ruler included in one of the video recordings. FIMtrack parameters were: grey threshold 160-220, min larvae area 40, max larvae area 300. The .csv file containing the larval tracking data was manually corrected for any occurring larval identity switches during the tracking process. The average velocity of 600 frames corresponding to 2 minutes of recording at five frames per second were used to calculate the average velocity of a single larva. The average velocities of all individual larvae were compared for statistical analysis.

4.2.2.6 Free running assay

5-7-day-old male flies raised in light/dark (LD)-entrained cultures were individually placed in 65 x 5 mm glass tubes containing 5% sucrose and 2% agar. Experiments were performed in an incubator with 60% humidity. Light was turned on at Zeitgeber Time 0 (ZT0) and off at ZT12. Fly activity was recorded for at least 3 consecutive days using the Drosophila Activity Monitoring (DAM) system (Trikinetics, Inc.). Activity records were collected in 1 min bins and analyzed using a custom-written R script (code available at: <https://github.com/adrianclo/dam3>).

4.2.2.7 Bang sensitivity assay

For *Pus3*^{Δ1033} and *Pus7*^{fs}, 5 day old flies were used for the experiment. For *PusL1* mutant flies, 6-7 day old flies were used. The flies were collected after hatching via cold anesthesia. Wild type *Canton-S* flies served as control. The protocol of [Ganetzky and Wu, 1982] served as basis for the experiment. Ten flies per genotype and sex were put into a glass cylinder and vortexed for 20 seconds. After vortexing, the recovery of the flies was recorded for 30 seconds and the number of recovered flies per second were quantified. A fly was counted as recovered when it passed a threshold line at 3 mm height by climbing. This experiment was repeated three times per genotype and sex in biological replicates.

4.2.2.8 Oxygraph assay

Mitochondrial respiration in *Drosophila* heads was assessed by high resolution respirometry using Oroboros O2k (OROBOROS, Innsbruck, Austria) at 25°C as previously in [Kanellopoulos et al., 2020]. Briefly, 15 fly heads from 3-4 day old females, mated were rapidly collected under a microscope, homogenized in MiR05 respiration buffer (20 mM HEPES, 110 mM sucrose, 10 mM KH₂PO₄, 20 mM taurine, 60 mM lactobionic acid, 3 mM MgCl₂, 0.5 mM EGTA, pH 7.1, 1 mg/ml fatty acid-free BSA) using a pestle. The lysate was loaded into an Oroboros O2k chamber with subsequent injections of the following substrates and specific inhibitors: 1) 2.5 mM pyruvate and 1 mM malate

(Leak), followed by 2.5 mM ADP to determine complex I-driven phosphorylating respiration (CI OXPHOS). 2) 5 mM succinate to determine the phosphorylating respiration driven by simultaneous activation of complex I and II (CI+CII OXPHOS). 3) Titrating concentrations of the mitochondrial uncoupler CCCP (Carbonyl cyanide 3-chlorophenylhydrazone) to reach the maximal, uncoupled respiration (CI+II electron transfer system, ETS). 4) 200 nM rotenone to fully inhibit complex I-driven respiration and measure complex II-driven uncoupled respiration (CII electron transfer system, CII ETS). 5) 0.5 μ M Antimycin A to block mitochondrial respiration at the level of complex III. Residual oxygen consumption (ROX) was always negligible. 6) 2 mM ascorbate, 0.5 mM TMPD (N,N,N',N'-Tetramethyl-p-phenylenediamine) to measure cytochrome c oxidase (CIV or COX)- driven respiration. 7) 300 μ M Sodium Azide to specifically block cytochrome c oxidase activity and measure residual background oxygen consumption caused by chemical interaction between ascorbate and TMPD. For the analysis ROX was subtracted from all the substrate-specific oxygen consumption rates (Leak, CI OXPHOS, CI-CII OXPHOS) while the maximal oxygen consumption rate of complex IV was corrected by subtracting the complex IV background. O₂ consumption rates were normalized over total protein content assessed by Pierce BCA Protein Assay Kit (ThermoFisher).

4.2.2.9 Aggression assay

Aggression assays were performed as described in [de Brouwer et al., 2018], however, only strong aggression events (lunges and tussling) were quantified. Since tussling involved two flies being aggressive, each event was scored twice. For the supplementation of food, standard fly food was melted using a microwave and cooled to below 50°C. Substances for supplementation were added under quick stirring to ensure homogenization. For the aging of individual flies, pupae were collected into tubes with 2 ml of manipulated food which was dispensed using an Eppendorf Multipette E3 with Combitips advanced 5 ml (0030089456, Eppendorf). To raise flies in supplemented food during their whole development, the parents were placed in larger tubes with 5 ml of supplemented food and resulting pupae were collected into small tubes with 2 ml of supplemented food. For aspartate supplementation, 12.5 mg/ml L-aspartate (A9256, Sigma) were dissolved in 0.1 M KOH solution by heating and stirring. Once dissolved, 4.26 ml were added per 100 ml of melted food for a 4.06 mM final concentration of additional Aspartate in the food. For 2-DG supplementation, powdered 2-deoxyglucose (D8375, Sigma) was added directly to melted standard food to achieve the necessary concentrations. For supplementation with mitochondrial inhibitors, a 2 mg/ml stock of Antimycin A (A8674, Sigma) in 100% EtOH was generated. Antimycin A was added 1:1000, 1:400 or 1:200 to melted fly food to achieve concentrations of 2 mg/ml, 5 mg/ml or 10 mg/ml, respectively. For rotenone (R8875, Sigma) supplementation, a 1 mM stock solution in 100% EtOH was generated by heating to 50°C under constant stirring. 1.05 ml were added per 70 ml of melted fly food.

4.2.2.10 Hatching assay

Flies were put into conical flasks 5 days before the collection and stored at 25°C to get used to the new environment. Flasks were closed with apple agar plates with a thin layer of yeast. Apple agar plates were changed every two hours during daytime to get the flies used to the frequent shaking. On the day of the collection, the plates were further changed in two-hour intervals until the number of laid eggs stabilized. Then, the number of laid eggs was quantified after 1 h and stored on room temperature for 18 h. Next, pre-hatched larvae were counted and removed from the plate. Finally, hatched larvae were counted and removed from the plate from 18.5 h until 29.5 h after laying in 30 min intervals. After 48 h past egg laying all remaining unhatched embryos were quantified.

4.2.2.11 Fertility assay

To quantify egg-laying and hatching rate, five male and ten female flies were housed in tubes with apple-juice agar plates and dry yeast (320010, Klipfel Hefe AG). Flies were 0-1 day old at the start of the assay. Two replicates with 3 males and five females or two replicates with 5 males and 10 females were quantified in parallel. For standard fertility assays, plates were exchanged daily but egg-laying and hatching was quantified only every third day for 15 days. For the quantification of embryo phenotypes quantification was performed daily. To determine the hatching rate, plates with eggs were stored at 25°C and the number of unhatched eggs was quantified after 48 h. Every day, the number of surviving females was determined to calculate the amount of laid eggs per female and per hour spent on the respective plate. To investigate potential combinatoric effects of *heph*⁰³⁴²⁹ and *Pus*^{7^{fs}, females of the indicated genotypes were crossed with *wild type* males. Two replicates of 5 females per tube were used per genotype.}

4.2.2.12 Measurement of embryo length

Embryos were collected using a brush and imaged using a Leica M205 FCA fluorescence stereo microscope. The length from the anterior to posterior pole was quantified using ImageJ. *Heph*-like embryos laid by *Pus*^{7^{fs} females were compared to normal embryos laid by *wild type* females.}

4.2.2.13 Dissection for NMJ

NMJ analysis of *PusL1 KO10* mutants was performed as described in [Worpenberg et al., 2021] using a Zeiss LSM 710 confocal microscope.

4.2.3 Molecular methods

4.2.3.1 Protein lysate preparation

Proteins were isolated by squishing flies or dissected tissues in squish buffer (50 mM Tris-HCl, 150 mM NaCl, 0.5% NP-40, 1 µg/ml leupeptin, pepstatin and aprotinin, 1 mM PMSF). Lipids were

removed by pipetting after sequential rounds of centrifugation at 21000 g for 10 min at 4°C. Protein concentration was determined using Bradford reagent (5000006, Biorad). Proteins were separated on 12% SDS-PAGE gels and transferred on a nitrocellulose membrane (10600002, Amersham). After blocking with 5% milk or BSA in PBS-Tw (0.05% Tween in PBS) for 1 h at RT, the membrane was incubated with primary antibodies in blocking solution over night at 4°C. The primary antibodies were rabbit anti-GFP (1:5000, TP401, Torrey Pines Biolabs), rabbit anti-Histone H3 (1:2000, Ab1791, Abcam). The membrane was washed three times in PBS-Tw for 15 min and incubated for 1 h at RT with respective secondary antibodies (111-035-003, Jackson ImmunoResearch) in blocking solution. Protein bands were detected using SuperSignal™ West Pico or Femto Chemiluminescent Substrate (Thermo Scientific). Blots were stripped of antibodies with mild stripping buffer (Abcam) prior to reblocking.

4.2.3.2 Western blotting

For western blot analysis, proteins were separated on 8-12% SDS-PAGE gel and transferred on a nitrocellulose membrane (neoLab). After blocking with 5% milk in PBST (0.1% Tween-20 in PBS) for 1 h at RT, the membrane was incubated with primary antibody (4.10) in blocking solution o. n. at 4°C. The membrane was washed three times in PBST for 15 min and incubated for 1 h at RT with secondary antibody (4.10) in blocking solution. Afterwards, the membrane was washed three additional times. Protein bands were detected using SuperSignal™ West Pico or Femto Chemiluminescent Substrate (Thermo Scientific).

4.2.3.3 Mass-spec analysis of the proteome

Sample preparation and protein digestion.

Five replicates of 20 heads per replicate and genotype of 3-4 day old mated females were prepared by flashfreezing whole flies in eppendorf tubes in liquid nitrogen and separating heads by repeatedly smashing the frozen tube on to a table. Heads separated from fly bodies were collected with a brush and immediately frozen in liquid nitrogen. *Drosophila* heads were crushed manually with a pestel in 1.5 ml tubes in 120 ul of miST lysis buffer (1% sodium deoxycholate, 100 mM Tris pH 8.6, 10 mM DTT). The suspension was heated at 95°C for 5 min, cooled down and sonicated with a tip sonicator for 20 s on ice, resulting in homogeneous suspensions. Consistency of protein extraction was controlled qualitatively by 1D-SDS-PAGE (data not shown). Samples were digested following a modified version of the iST method [Kulak et al., 2014] (named miST method). Based on tryptophane fluorescence quantification [Wisniewski and Gaugaz, 2015], 100 ug of proteins at 2 ug/ul in miST lysis buffer were transferred to new tubes. Samples were heated 5 min at 95°C, diluted 1:1 (v:v) with water containing 4 mM MgCl₂ and benzonase (Merck #70746, 100x dil of stock = 250 Units/ul), and incubated for 15 minutes at RT to digest nucleic acids. Reduced disulfides were alkylated by adding ¼ vol. of 160 mM chloroacetamide (32 mM final) and incubating for 45 min at RT in the dark. Samples were adjusted to 3 mM EDTA and digested with 1 ug Trypsin/LysC mix (Promega

#V5073) for 1 h at 37°C, followed by a second 1 h digestion with an additional 1 ug of proteases. To remove sodium deoxycholate, two sample volumes of isopropanol containing 1% TFA were added to the digests, and the samples were desalted on a strong cation exchange (SCX) plate (Oasis MCX; Waters Corp., Milford, MA) by centrifugation. After washing with isopropanol/1%TFA, peptides were eluted in 200 ul of 80% MeCN, 19% water, 1% (v/v) ammonia, and dried by centrifugal evaporation.

Peptide fractionation.

Basic reverse-phase (for library construction).

Aliquots of samples were pooled and separated into 6 fractions by off-line basic reversed-phase (bRP) using the Pierce High pH Reversed-Phase Peptide Fractionation Kit (Thermo Fisher Scientific). The fractions were collected in 7.5, 10, 12.5, 15, 17.5 and 50% acetonitrile in 0.1% triethylamine (pH 10). Dried bRP fractions were redissolved in 50 ul 2% acetonitrile with 0.5% TFA, and 5 ul were injected for LC-MS/MS analyses.

Liquid Chromatography-Mass Spectrometry analyses.

TIMS-TOF DIA (and library DDA).

LC-MS/MS analyses were carried out on a TIMS-TOF Pro (Bruker, Bremen, Germany) mass spectrometer interfaced through a nanospray ion source (“captive spray”) to an Ultimate 3000 RSLCnano HPLC system (Dionex). Peptides were separated on a reversed-phase custom packed 45 cm C18 column (75 μ m ID, 100Å, Reprosil Pur 1.9 μ m particles, Dr. Maisch, Germany) at a flow rate of 0.250 ul/min with a 2-27% acetonitrile gradient in 93 min followed by a ramp to 45% in 15 min and to 90% in 5 min (total method time: 140 min, all solvents contained 0.1% formic acid). Identical LC gradients were used for DDA and DIA measurements. For creation of the spectral library, data-dependent acquisitions (DDA) were carried out on the 6 bRP fractions sample pool using a standard TIMS PASEF method [Meier et al., 2018] with ion accumulation for 100 ms for each survey MS1 scan and the TIMS-coupled MS2 scans. Duty cycle was kept at 100%. Up to 10 precursors were targeted per TIMS scan. Precursor isolation was done with a 2 Th or 3 Th windows below or above m/z 800, respectively. The minimum threshold intensity for precursor selection was 2500. If the inclusion list allowed it, precursors were targeted more than one time to reach a minimum target total intensity of 20.000. Collision energy was ramped linearly based uniquely on the $1/k_0$ values from 20 (at $1/k_0=0.6$) to 59 eV (at $1/k_0=1.6$). Total duration of a scan cycle including one survey and 10 MS2 TIMS scans was 1.16 s. Precursors could be targeted again in subsequent cycles if their signal increased by a factor 4.0 or more. After selection in one cycle, precursors were excluded from further selection for 60 s. Mass resolution in all MS measurements was approximately 35.000. The data-independent acquisition (DIA) used mostly the same instrument parameters as the DDA method and was as reported previously [Meier et al., 2020]. Per cycle, the mass range 400-1200 m/z was covered by a total of 32 windows, each 25 Th wide and a $1/k_0$ range of 0.3. Collision energy and resolution settings were the same as in the DDA method. Two windows were acquired per TIMS

scan (100 ms) so that the total cycle time was 1.7 s.

Data processing.

Spectronaut (DIA).

Raw Bruker MS data were processed directly with Spectronaut 15.6 (Biognosys, Schlieren, Switzerland). A library was constructed from the DDA bRP fraction data by searching the reference *Drosophila melanogaster* proteome (www.uniprot.org) database of August 23rd, 2020 (22,039 sequences). For identification, peptides of 7-52 AA length were considered, cleaved with trypsin/P specificity and a maximum of 2 missed cleavages. Carbamidomethylation of cysteine (fixed), methionine oxidation and N-terminal protein acetylation (variable) were the modifications applied. Mass calibration was dynamic and based on a first database search. The Pulsar engine was used for peptide identification. Protein inference was performed with the IDPicker algorithm. Spectra, peptide and protein identifications were all filtered at 1% FDR against a decoy database. Specific filtering for library construction removed fragments corresponding to less than 3 AA and fragments outside the 300-1800 m/z range. Also, only fragments with a minimum base peak intensity of 5% were kept. Precursors with less than 3 fragments were also eliminated and only the best 6 fragments were kept per precursor. No filtering was done on the basis of charge state and a maximum of 2 missed cleavages was allowed. Shared (non proteotypic) peptides were kept. The library created contained 79,159 precursors mapping to 53,911 peptides, of which 27,089 were proteotypic. These corresponded to 6,459 protein groups (9,690 proteins). Of these, 941 were single hits (one peptide precursor). In total 465,866 fragments were used for quantitation. Peptide-centric analysis of DIA data was done with Spectronaut 15.6 using the library described above. Single hits proteins (defined as matched by one stripped sequence only) were kept in the Spectronaut analysis. Peptide quantitation was based on XIC area, for which a minimum of 1 and a maximum of 3 (the 3 best) precursors were considered for each peptide, from which the median value was selected. Quantities for protein groups were derived from inter-run peptide ratios based on MaxLFQ algorithm [Cox et al., 2014]. Global normalization of runs/samples was done based on the median of peptides.

Data analysis.

Perseus (DDA, DIA, TMT).

All subsequent analyses were done with the Perseus software package (version 1.6.15.0) [Tyanova et al., 2016]. Contaminant proteins were removed, and intensity values determined by Spectronaut were log₂-transformed. After assignment to groups, only proteins quantified in at least 4 samples in at least one group were kept (6,130 protein groups). After imputation of missing values (based on normal distribution using Perseus default parameters), t-tests were carried out among all conditions, with permutation-based FDR correction for multiple testing (q-value <0.05). 838 proteins passed the test with these conditions, including Pus7. The difference of means obtained from the tests were used for 1D enrichment analysis on associated GO/KEGG annotations as described [Cox and Mann, 2012]. The enrichment analysis was also FDR-filtered (Benjamini-Hochberg, q-val<0.02).

4.2.3.4 Mass-spec analysis of the metabolome

Metabolite extraction.

Six replicates of 50 Fly heads of 3-4 day old mated females were pre-extracted and homogenized by the addition of 150 μ L of MeOH:H₂O (4:1), in the Cryolys Precellys 24 sample Homogenizer (2 x 20 seconds at 10000 rpm, Bertin Technologies, Rockville, MD, US) with ceramic beads. The bead beater was air-cooled down at a flow rate of 110 L/min at 6 bar. Homogenized extracts were centrifuged for 15 minutes at 4000 g at 4°C (Hermle, Gosheim, Germany). The resulting supernatant was collected and injected into the LC-MS system.

Multiple pathway targeted analysis.

Extracted samples were analyzed by Hydrophilic Interaction Liquid Chromatography coupled to tandem mass spectrometry (HILIC - MS/MS) in both positive and negative ionization modes using a 6495 triple quadrupole system (QqQ) interfaced with 1290 UHPLC system (Agilent Technologies) [Gallart-Ayala et al., 2018, Medina et al., 2020] In positive mode, the chromatographic separation was carried out in an Acquity BEH Amide, 1.7 μ m, 100 mm \times 2.1 mm I.D. column (Waters, Massachusetts, US). Mobile phase was composed of A = 20 mM ammonium formate and 0.1% FA in water and B = 0.1% FA in ACN. The linear gradient elution from 95% B (0-1.5 min) down to 45% B was applied (1.5 min -17 min) and these conditions were held for 2 min. Then initial chromatographic condition were maintained as a post-run during 5 min for column re-equilibration. The flow rate was 400 μ L/min, column temperature 25°C and sample injection volume 2 μ L. ESI source conditions were set as follows: dry gas temperature 290°C, nebulizer 35 psi and flow 14 l/min, sheath gas temperature 350°C and flow 12 l/min, nozzle voltage 0 V, and capillary voltage 2000 V. Dynamic Multiple Reaction Monitoring (DMRM) was used as acquisition mode with a total cycle time of 600 ms. Optimized collision energies for each metabolite were applied.

In negative mode, a SeQuant ZIC-pHILIC (100 mm, 2.1 mm I.D. and 5 μ m particle size, Merck, Darmstadt, Germany) column was used. The mobile phase was composed of A = 20 mM ammonium Acetate and 20 mM NH₄OH in water at pH 9.7 and B = 100% ACN. The linear gradient elution from 90% (0-1.5 min) to 50% B (8-11 min) down to 45% B (12-15 min). Finally, the initial chromatographic conditions were established as a post-run during 9 min for column re-equilibration. The flow rate was 300 μ L/min, column temperature 30°C and sample injection volume 2 μ L. ESI source conditions were set as follows: dry gas temperature 290°C and flow 14 l/min, sheath gas temperature 350°C, nebulizer 45 psi, and flow 12 l/min, nozzle voltage 0 V, and capillary voltage -2000 V. Dynamic Multiple Reaction Monitoring (dMRM) was used as acquisition mode with a total cycle time of 600 ms. Optimized collision energies for each metabolite were applied.

Quality Control (QC).

Pooled QC samples (representative of the entire sample set) were analyzed periodically (every 6 samples) throughout the overall analytical run in order to assess the quality of the data, correct

the signal intensity drift (attenuation in most cases, that is inherent to LC-MS technique and MS detector due to sample interaction with the instrument over time) and remove the peaks with poor reproducibility ($CV > 30\%$) [Dunn et al., 2011, Broadhurst et al., 2018] In addition, a series of diluted quality controls (dQC) were prepared by dilution with methanol: 100% QC, 50%QC, 25%QC, 12.5%QC and 6.25%QC. Then metabolites were selected also considering the linear response on the diluted QC series.

Data (Pre) Processing.

Raw LC-MS/MS data was processed using the Agilent Quantitative analysis software (version B.07.00, MassHunter Agilent technologies). Relative quantification of metabolites was based on EIC (Extracted Ion Chromatogram) areas for the monitored MRM transitions. The obtained tables (containing peak areas of detected metabolites across all samples) were exported to “R” software <http://cran.r-project.org/> and signal intensity drift correction and noise filtering (if necessary using CV (QC features) $> 30\%$) was done within the MRM PROBS software [Tsugawa et al., 2014].

4.2.3.5 RNA isolation and RT-qPCR

Total RNA from S2R+ cells was isolated using Trizol reagent (Invitrogen). Genomic DNA was removed by treatment with DNase-I (NEB) at 37°C for 10 min. All steps were carried out at 4°C or on ice except drying and dissolving of the pellet. RNA was reverse transcribed into cDNA using M-MLV reverse transcriptase (Promega). RNA levels were quantified in technical triplicates with GoTaq qPCR master mix (A6002, Promega) using the oligonucleotides listed in table 4.3.

4.2.3.6 RNA-seq

NGS library prep was performed with Illumina’s TruSeq stranded mRNA LT Sample Prep Kit following Illumina’s standard protocol (Part # 15031047 Rev. E) using $\frac{1}{4}$ of the reagents. Libraries were prepared with a starting amount of 250 ng and amplified in 11 PCR cycles. Libraries were profiled in a High Sensitivity DNA on a 2100 Bioanalyzer (Agilent technologies) and quantified using the Qubit dsDNA HS Assay Kit, in a Qubit 2.0 Fluorometer (Life technologies). 15 samples were pooled together with 9 samples from another project in equimolar ratio and sequenced on 1 NextSeq 500 Highoutput Flowcell, PE for 2x42 cycles plus 7 cycles for the index read. Libraries were sequenced on Illumina HiSeq 2000. The read-length was 50 bp paired end. Library preparation and RNA-seq was performed by IMB genomics core facilities.

4.2.3.7 BID-seq

BID-seq using polyA RNA isolated from ovaries of ca. 20 2-3d old mated females was performed in triplicates as described in [Dai et al., 2022].

4.2.3.8 Microscale thermophoresis

Microscale thermophoresis experiments were performed as described in [Jacob et al., 2019]. The total RNA samples were generated from whole flies of mixed sex and age. Oligonucleotides used for tRNA detection are listed in table 4.7.

4.2.3.9 Northern blotting

Total RNA for northern blotting was isolated from flies as described above. Northern blotting was performed essentially as described in <http://cshprotocols.cshlp.org/content/2014/7/pdb.prot080838.full> with the following adaptations: Fresh 12% urea-polyacrylamide gels were generated using the ROTIPHORESE DNA sequencing system (A431.1, Roth) and polymerized for at least 30 min at RT. Gels were pre-run for at least 30 min in 0.5x tris-borate buffer without EDTA at 90 V. 12 μ g of total RNA were prepared in 2x RNA gel loading dye (R0641, Thermo Fisher). 10 fmol of a sense DNA oligo were loaded as a labeling control. RNA samples were denatured at 75°C for 3 min and kept on ice until loading. Electrophoresis was performed at 90 V until the loading dyes visibly separated and finished at 180 V until the bromophenol blue reached the bottom of the gel. Gels were stained in 1x TBE buffer with 1:10000 SYBR-Gold (S11494, Thermo Fisher) for 5 min while shaking at RT. Wet transfer to positively charged nylon membranes (11209299001, Roche) was performed in 0.5x TBE in Bio-Rad mini protean 3 chambers for 90 min at 200 mA. Membranes were dried on whatman paper for at least 5 min before UV crosslinking. Membranes were prehybridized for at least 60 min at 42°C in a screw cap flask in a heated oven in 10 ml hybridization buffer (5x SSC (S6639, Merck), 25 mM Na₂HPO₄ pH 7.2, 0.5% SDS, 1.25x Denhardt's solution (750018, Thermo Fisher). DNA probes were labeled with γ -³²P ATP (NEG502A250UC, Perkin Elmer) using T4 PNK according to the manufacturers protocol (Ek0031, Thermo Fisher). Excess ATP was removed using Microspin G-25 columns (GE27-5325-01, Sigma). Hybridization was performed over night at 42°C. Membranes were washed once with Buffer A (3x SSC, 5% SDS) and Buffer B (1x SSC, 1% SDS) for at least 15 min at 42°C, respectively. Finally, membranes were dried on whatman paper, enclosed in plastic wrap and exposed to a phosphor-imaging screen (Amersham Biosciences). Signal detection was performed using a Typhoon Trio+ Imager (Amersham Biosciences). For signal removal an 810-UNV Image Eraser (Amersham Biosciences) was used. Signals were quantified using ImageJ version 1.53i.

4.2.3.10 Mapping of Ψ sites with psi-seq

Total RNA from 20 heads of 3-4 day old mated females was used to perform psi-seq as described in [Schwartz et al., 2014]. *w¹¹¹⁸* served as *wild type* control. *Pus7^{def}/Pus7^{fs}* and *Pus3^{Δ1033}/Pus3^{def}* flies were used as *Pus7* and *Pus3* mutants, respectively.

4.2.3.11 Ribosome profiling

RNA samples for ribosome profiling were prepared as described in [Snieckute et al., 2022] with the adaptation that customized siTOOLS depletion pools for *Drosophila* rRNA were used. Libraries were generated from approximately 80 flashfrozen heads of 3-4 day old mated female flies in technical triplicates. The RUST analysis for E, P and A site occupancy was performed as described in [Arpat et al., 2020]. Putative ribosome pausing sites were identified as described in [Stein et al., 2022].

4.2.4 Immunostainings and confocal microscopy

Immunostaining of S2R+ cells.

For staining of *Drosophila* S2R+ cells, transfected cells were transferred to poly-lysine pretreated 8-well chambers (Ibidi) at the density of 2×10^5 cells/well. After cells have settled and attached to the surface for 60 min, cells were washed with 1x DPBS (Gibco), fixed with 4% formaldehyde for 10 min and permeabilized with PBST (0.5% Triton X-100 in PBS) for 15 min. Cells were incubated with mouse anti-Myc (1:2000; #9E10, Enzo) in PBST supplemented with 10% of Donkey serum at 4°C o. n. Cells were washed 3x for 15 min in PBST and then incubated with secondary antibody and 1x DAPI solution in PBST supplemented with 10% of Donkey serum for 2 h at 4°C. After three 15 min washes in PBST, cells were imaged with a Zeiss LSM 710 confocal microscope using a 63x oil immersion objective.

Immunostaining of embryos.

Embryos for immunofluorescence were dechorionated in 50% bleach for 2 min and fixed for 30 min in 2 ml 4% paraformaldehyde (PFA) in PBS mixed with 4 ml of heptane. Embryos were washed with methanol prior to devitellinization by shaking vigorously for 5 min in 1 ml of heptane and 2 ml methanol. Permeabilization was performed in methanol at -20°C for at least one night. Embryos were rehydrated by sequentially rotating once in 50% methanol in PBS with 0.1% Tween-20 (PBS-Tw), three times in PBS-Tw, three times in 50% PBS-Tw and three times in PBS-Tw for 5 min at RT. Unspecific binding sites were blocked by rotating six times in PBS-Tw with 10% normal donkey serum (ab7475, Abcam) for 10 min at RT. Embryos were incubated with primary antibody rabbit anti-GFP (1:5000, TP401, Torrey Pines Biolabs) in blocking solution over night at 4°C and subsequently washed six times in blocking solution. Incubation in secondary antibody Alexa Fluor 488 anti rabbit (1:400, 711-545-152, Dianova) in blocking solution was performed for 2 h at RT. Embryos were washed six times in PBS-Tw for 10 min at RT. Nuclei were stained by incubating in PBS with DAPI (1:1000, D9542, Sigma Aldrich) for 10 min at RT and embryos were mounted in Vectashield hardset (H-1500-10, Vector labs) for confocal microscopy using a Zeiss LSM 710 confocal microscope.

Immunostaining of larval brains.

Larval brains for immunofluorescence were dissected in ice-cold DPBS and were subsequently fixed in 4% PFA in PBS for 20 min at RT. Next, brains were washed twice for 5 min at RT in PBT (0.2%

PBS-Tw) and four times for 15 min in BBT (1% BSA, 0.1% Triton X-100 in PBS) at RT. Incubation with primary antibodies was performed overnight in BBT at 4°C. Next, brains were washed six times in BBT for 15 min at RT. Afterwards, the secondary antibody incubation was performed in BBT over night at 4°C. Finally, the larval brains were washed twice in BBT and four times in PBT. All incubation steps were performed with up-right tubes on an agitator. The stained brains were mounted onto a microscope slide in Vectashield hardset (H-1500-10, Vector labs) for confocal microscopy using a Zeiss LSM 880 confocal microscope with airyscan.

Immunostaining of ovaries.

Ovaries for immunofluorescence were dissected in ice-cold DPBS and subsequently fixed in 4% PFA in PBS for 20 min at RT. Next, ovaries were washed three times in PBST0.2 (0.2% Triton X-100 in PBS), once in PBST1 (1% Triton X-100 in PBS) for 10 min and once in PBST1 for 2 hours. Incubation with primary antibody was performed in PBTB (PBST0.2 with 10% donkey serum) at 4°C overnight. Afterwards, ovaries were washed twice for 30 min in PBTB and once for 1 hour in PBTB. Secondary antibody incubation was performed in PBTB for 2 hours at RT. Finally, ovaries were washed five times for at least 15 min in PBST0.2 and mounted onto a microscope slide in Vectashield hardset (H-1500-10, Vector labs) for confocal microscopy. Confocal images of ovaries were generated using a Zeiss LSM 710 confocal microscope. All incubations were performed on a spinning wheel.

4.2.5 Molecular Cloning

4.2.5.1 PCR

Amplification of DNA sequences to create templates for IVT (table 4.4), fly screening (table 4.2) and cloning (table 4.8) was performed by PCR in the Biometra TRIO 48 Thermocycler (analytikjena). Phusion High-Fidelity DNA Polymerase (NEB) or OneTaq DNA Polymerase (NEB) were used for these purposes. DNA templates were run on an agarose gel and desired bands were extracted.

4.2.5.2 Agarose gel electrophoresis and gel elution

Analysis of size and integrity of DNA and RNA fragments was performed by agarose gel electrophoresis. 1% or 2% agarose gels based on Tris, acetate and EDTA were poured for DNA and RNA, respectively. For detection of nucleic acids 0.05 µl/ml GelRed (41003, Biotum) were added to the gel mix. Fragments were separated by size at 80-130 V in 1x TBE buffer. For measurement of size the 100 bp DNA ladder (N3231, NEB) or 1 kb Plus DNA ladder (N3200, NEB) was used. Detection was performed by irradiation with blue light in a Safe Imager Transluminator (S37102, Invitrogen).

4.2.5.3 Digestion, ligation and transformation

Restriction of DNA fragments for ligation was performed for 2 h at 37°C using the respective restriction enzyme following the manufacturer's protocol. Digested DNA sequences were ran on an agarose gel and the desired fragments eluted for further cloning. All employed restriction enzymes are listed in table 4.11. Ligation reactions were performed using the T4-DNA-Ligase (M202, NEB) according to the manufacturer's protocol. A molar vector:insert ratio of 3:1 was used. Ligation reactions were incubated at 4°C o. n. Successful ligations were confirmed by PCR screening or digestion with restriction enzymes. For amplification of constructs, the vectors were transformed into competent DH5 α cells. Bacteria were thawed on ice for 3 min. 10 μ l ligation reaction were added to 50 μ l of bacteria, mixed and incubated on ice for 10 min. Heat shock was performed at 42°C for 1 min. 250 μ l pre-warmed LB medium were added and the cells and pre-cultured for 1 h at 37°C. Afterwards, the cells were plated on pre-warmed LB agar plates with ampicillin (75 mg/l) and incubated o. n. at 37°C.

4.2.5.4 DNA sequencing

DNA samples were sent for sequencing with economy run single tube sequencing (Microsynth) according to the companies specifications.

4.2.5.5 Cloning of expression vectors

Flag-Myc-Pus3, Flag-Myc-Pus7 and PusL1-HA overexpression

For overexpression of Pus3 or Pus7 from gateway vectors, the respective coding sequences were amplified from cDNA with primers containing restriction sites to allow cloning into the gateway-based vector with N-terminal 3xFLAG–6xMyc tag (pPFMW) via NotI and AscI restriction. For overexpression of C-terminally tagged PusL1, an analogue approach was performed using the pPHW backbone. The catalytic dead version of pPFM-Pus7 was generated by introducing a C>G point mutation at position 822 in the CDS of Pus7 changing the catalytic aspartate at position 274 to glutamate by site directed mutagenesis. For this, a forward and reverse primer overlapping the sequence encoding the catalytic aspartate were designed to introduce a point mutation (table 4.5). Next, a 5' fragment and a 3' fragment of the Pus7 coding sequence were generated by amplifying from the 5' end of Pus7 to the catalytic site or the catalytic site to the 3' end, respectively. A full-length mutated Pus7 coding sequence was generated by overlap PCR of the two fragments. Finally, the amplicon was inserted into the pPFMW backbone via restriction by NotI and AscI.

PusL1-EGFP expression

To generate a plasmid for the expression of the *PusL1* genomic sequence containing introns tagged by a C-terminal EGFP tag from the endogenous promoter the following cloning approach was used using primers indicated in table 4.8: The PusL1 sequence was amplified from genomic DNA. Also, an EGFP fragment was amplified from the pUAST-EGFP-attB vector (85621, Addgene). Next, both

fragments were combined by overlap PCR. The final PusL1-EGFP amplicon was introduced into the pUAST-EGFP-attB backbone via HindIII and NotI restriction.

tRNA^{Asp}_{GTC} overexpression

To generate plasmids for tRNA^{Asp} overexpression, five fragments containing tRNA^{Asp} and unique overhangs at the 5' and 3' ends were amplified from the endogenous tRNA^{Asp} isodecoder 1-5 sequence and inserted into BbsI digested pBFv-U6.2 plasmid using the NEBuilder® HiFi DNA Assembly Cloning Kit (E5520S, NEB). Clones containing only two of the fragments could be obtained. The 5' and 3' overhang of the first and last fragment, respectively, overlapped with the pBFv-U6.2 backbone and contained BbsI restriction sites which were used to integrate the two fragments of pBFv-U6.2_tRNA^{Asp}_{GTC}-1-5_x2 into pBFv-U6.2B_tRNA^{Asp}_{GTC}-1-5_x2 via restriction. Finally, the two fragments from pBFv-U6.2_tRNA^{Asp}_{GTC}-1-5_x2 were integrated into pBFv-U6.2B_tRNA^{Asp}_{GTC}-1-5_x2 via EcoRI and NotI restriction to gain the final plasmid pBFv-U6.2B_tRNA^{Asp}_{GTC}-1-5_x4.

Asp-GFP and Leu-GFP overexpression

To generate plasmids for the quantification of the impact of codon stretches in translation, the pAC5-GFP-Stop-mCherry plasmid was used. Oligonucleotide pairs were designed to encode for a stretch of ten codons of Asp_{GAC} or Leu_{TTA} upon annealing flanked by restriction enzyme sites for integration into pAC5-GFP-Stop-mCherry via EcoRI and EcoRV. 40 μM forward and reverse oligonucleotides were annealed by heating to 95°C and slowly cooling to RT in 1x Phusion HF buffer (NEB). Next, 2 μl of digested annealed oligonucleotide per 50 ng of plasmid were integrated into the column-purified heat-inactivated digested pAC5-GFP-Stop-mCherry backbone via ligation and transformation. Correct insertion was confirmed by sequencing.

4.2.5.6 Cloning of gRNA vectors

Constructs encoding the guide RNAs (gRNAs) to target Cas9-mediated cleavage were generated as described in [Kondo and Ueda, 2013] using the vectors pBFv-U6.2 and pBFv-U6.2B (table 4.9). gRNAs were designed using the Cas9 target finder of the National Institute of Genetics (<https://shigen.nig.ac.jp/fly/nigfly/cas9/cas9TargetFinder.jsp>) in order to delete sequences predicted to code for Pus domains by nucleotide NCBI blast [Coordinators, 2015]. Successful cloning of gRNA1 into U6.2 and gRNA2 into U6.2B was verified by PCR. Afterwards, both plasmids were digested using EcoRI and NotI and a fragment of U6.2 carrying the integrated gRNA was cloned into the backbone of U6.2B. This cloning step generated the final plasmid encoding both gRNAs. Successful integration was verified by PCR with the respective gRNA1 forward and gRNA2 reverse primer.

4.2.6 Computational work

4.2.6.1 GTerm analysis

Over-representation analysis of GO terms in differentially regulated proteins was performed using WebGestalt (accessed 15.12.2022). All unfiltered unique proteins detected by mass-spectrometry were used as reference. Used parameters were: Over-representation analysis, Gene ontology, Biological process no redundant.

4.2.6.2 Gene set enrichment analysis

Gene set enrichment analysis in differentially regulated proteins was performed using WebGestalt (accessed 27.07.2023) utilizing the fold changes of unique significantly dysregulated proteins detected by mass-spectrometry. Used parameters were: Gene set enrichment analysis, Network, Transcription factor target.

4.2.6.3 Joint pathway analysis

To perform a joint pathway analysis the online tool MetaboAnalyst 5.0 was employed. Only proteins with significant changes in expression levels were used for the analysis. Among the metabolites betaalanine and sarcosine as well as asymmetric and symmetric dimethylarginine were omitted from the analysis as they could not be distinguished via KEGG IDs. The used parameters were: All pathways as pathway database, hypergeometric test for enrichment analysis, degree centrality mode for topology measure and combine queries for integration method.

CONTRIBUTIONS

Nadja Dinges and Violeta Morin (Roignant group, IMB, Mainz)

Performed the injection for the generation of *Pus7^{fs}* mutant flies.

WellGenetics Inc. (Taiwan)

Designed and generated the *EGFP-3xP3-RFP-Pus7* and *EGFP-Pus7* transgenic fly lines.

Prof. Dr. Schraga Schwartz (Weizmann Institute of Science, Israel)

Performed Ψ -seq for *Pus3* and *Pus7* mutant flies.

Dominik Jacob and Prof. Dr. Mark Helm (Institute of Pharmacy and Biochemistry, JGU Mainz)

Performed microscale thermophoresis experiments for *Pus7* mutants and *Pus7* overexpression.

Angelica Liechi and René Dreos (Center for Integrative Genomics, UNIL)

Performed the preparation of samples and the analysis of riboseq data, aspartate density in dysregulated proteins as well as disome formation in *Pus7^{fs}* flies, respectively.

Dr. Vittoria Mariano and Maellie Midroit (Département des neurosciences fondamentales, UNIL)

Performed and analyzed the oxygraph assay to measure mitochondrial respiration in *Drosophila* lysates and provided the respective methods section.

Dr. Alexandros Kanellopoulos (Département des neurosciences fondamentales, UNIL)

Performed the free running assay to quantify the activity of *PusL1* mutant flies.

Nadine Körtel (Roignant group, IMB, Mainz)

Performed the buridan paradigm assays using equipment of the Strauss lab (JGU Mainz).

Dorothea Schall (Roignant group, IMB, Mainz)

Performed the larval hatching assay to quantify developmental delay of *Pus7* mutant flies as well as the bang sensitivity assay for *Pus7* and *Pus3* mutant flies.

Tina Lence and Giriram Kumar Mohana (Roignant group, IMB, Mainz)

Prepared RNA samples of different *Drosophila* developmental stages.

Dr. Hector Gallart Ayala and Dr. Julijana Ivanisevic (Metabolomics Unit, UNIL)

Performed the metabolomics extraction as well as mass spectrometric analysis and provided the respective methods section.

Manfredo Quadroni and Patrice Waridel (Protein Analysis Facility, UNIL)

Performed the protein extraction as well as mass spectrometric analysis and provided the respective methods section.

Michael Wiederkehr (Roignant group, CIG, UNIL)

Assisted in the isogenization of several transgenic fly lines.

Chiara Paolantoni (Roignant group, CIG, UNIL)

Provided training for the dissection and analysis of NMJs in *PusL1* mutant flies.

Dinis Barros (Center for Integrative Genomics, UNIL)

Provided R scripts for the evaluation of lifespan data.

Dr. Lisheng Zhang and Prof. Dr. Chuan He (Department of Chemistry, University of Chicago)

Processed samples for BID-seq and performed the data analysis.

The **Genomics core facilities (IMB, Mainz)** processed samples and performed the RNA-seq analysis of dysregulated genes in S2R+ cells upon knockdown of *Pus3*.

The chamber for aggression assays was fabricated by the **mechanical workshop of the Institute for Physics at JGU Mainz**.

Fluorescence-activated cell sorting (FACS) was performed by the **Flow Cytometry Facility of the University of Lausanne**.

References

- [Abbasi-Moheb et al., 2012] Abbasi-Moheb, L., Mertel, S., Gonsior, M., Nouri-Vahid, L., Kahrizi, K., Cirak, S., Wieczorek, D., Motazacker, M. M., Esmaeeli-Nieh, S., and Cremer, K. (2012). Mutations in *nsun2* cause autosomal-recessive intellectual disability. *The American Journal of Human Genetics*, 90(5):847–855.
- [Abdelrahman et al., 2018] Abdelrahman, H. A., Al-Shamsi, A. M., Ali, B. R., and Al-Gazali, L. (2018). A null variant in *pus* confirms its involvement in intellectual disability and further delineates the associated neurodevelopmental disease. *Clinical Genetics*, 94(6):586–587.
- [Abdulkarim et al., 2015] Abdulkarim, B., Nicolino, M., Igoillo-Esteve, M., Daures, M., Romero, S., Philippi, A., Senée, V., Lopes, M., Cunha, D. A., and Harding, H. P. (2015). A missense mutation in *ppp1r15b* causes a syndrome including diabetes, short stature, and microcephaly. *Diabetes*, 64(11):3951–3962.
- [Abe, 2000] Abe, H. (2000). Role of histidine-related compounds as intracellular proton buffering constituents in vertebrate muscle. *Biochemistry C/C Of Biokhimiia*, 65(7):757–765.
- [Abeyvirigunawardena and Chow, 2008] Abeyvirigunawardena, S. C. and Chow, C. S. (2008). pH-dependent structural changes of helix 69 from *escherichia coli* 23s ribosomal rna. *RNA*, 14(4):782–792.
- [Adachi and Yu, 2014] Adachi, H. and Yu, Y.-T. (2014). Insight into the mechanisms and functions of spliceosomal snrna pseudouridylation. *World Journal of Biological Chemistry*, 5(4):398.
- [Aguilo et al., 2016] Aguilo, F., Li, S., Balasubramanian, N., Sancho, A., Benko, S., Zhang, F., Vashisht, A., Rengasamy, M., Andino, B., and Chen, C.-h. (2016). Deposition of 5-methylcytosine on enhancer rnas enables the coactivator function of *pgc-1 α* . *Cell reports*, 14(3):479–492.
- [Alarcon et al., 2015] Alarcon, C., Goodarzi, H., Lee, H., Liu, X., Tavazoie, S., and Tavazoie, S. (2015). *Hnrnpa2b1* is a mediator of m6a-dependent nuclear rna processing events. *Cell*, 162(6):1299–1308.
- [Alekseyenko et al., 2013] Alekseyenko, O. V., Chan, Y.-B., Li, R., and Kravitz, E. A. (2013). Single dopaminergic neurons that modulate aggression in *drosophila*. *Proceedings of the National Academy of Sciences*, 110(15):6151–6156.
- [Alexandrov et al., 2006] Alexandrov, A., Chernyakov, I., Gu, W., Hiley, S. L., Hughes, T. R., Grayhack, E. J., and Phizicky, E. M. (2006). Rapid trna decay can result from lack of nonessential modifications. *Molecular cell*, 21(1):87–96.
- [Alfares et al., 2017] Alfares, A., Alfadhel, M., Wani, T., Alsahli, S., Alluhaydan, I., Mutairi, F. A., Alothaim, A., Albalwi, M., subaie, L. A., Alturki, S., Al-Twajjri, W., Alrifai, M., Al-Rumayya, A., Alameer, S., Faqeeh, E., Alasmari, A., Alsamman, A., Tashkandia, S., Alghamdi, A., Alhashem, A., Tabarki, B., AlShahwan, S., Hundallah, K., Wali, S., Al-Hebbi, H., Babiker, A., Mohamed, S., Eyaid,

- W., and Zada, A. A. P. (2017). A multicenter clinical exome study in unselected cohorts from a consanguineous population of saudi arabia demonstrated a high diagnostic yield. *Molecular Genetics and Metabolism*, 121(2):91–95.
- [Alic et al., 2011] Alic, N., Andrews, T. D., Giannakou, M. E., Papatheodorou, I., Slack, C., Hoddinott, M. P., Cochemé, H. M., Schuster, E. F., Thornton, J. M., and Partridge, L. (2011). Genome-wide dfoxo targets and topology of the transcriptomic response to stress and insulin signalling. *Molecular systems biology*, 7(1):502.
- [AlSabbagh, 2020] AlSabbagh, M. M. (2020). Dyskeratosis congenita: a literature review. *JDDG: Journal der Deutschen Dermatologischen Gesellschaft*, 18(9):943–967.
- [Alter et al., 2012] Alter, B. P., Rosenberg, P. S., Giri, N., Baerlocher, G. M., Lansdorp, P. M., and Savage, S. A. (2012). Telomere length is associated with disease severity and declines with age in dyskeratosis congenita. *Haematologica*, 97(3):353–359.
- [Ameres et al., 2010] Ameres, S. L., Horwich, M. D., Hung, J.-H., Xu, J., Ghildiyal, M., Weng, Z., and Zamore, P. D. (2010). Target rna-directed trimming and tailing of small silencing rnas. *Science*, 328(5985):1534–1539.
- [Amos and Korn, 1958] Amos, H. and Korn, M. (1958). 5-methyl cytosine in the rna of escherichia coli. *Biochimica et biophysica acta*, 29(2):444–445.
- [Angelova et al., 2020] Angelova, M. T., Dimitrova, D. G., Da Silva, B., Marchand, V., Jacquier, C., Achour, C., Brazane, M., Goyenvalle, C., Bourguignon-Igel, V., and Shehzada, S. (2020). trna 2'-o-methylation by a duo of trm7/ftsj1 proteins modulates small rna silencing in drosophila. *Nucleic Acids Research*, 48(4):2050–2072.
- [Angurana et al., 2014] Angurana, S. K., Angurana, R. S., and Thapa, B. R. (2014). Malrotation of gut and hiatus hernia in a child with familial dyskeratosis congenita. *JK Science*, 16(1):40.
- [Ansmant et al., 2000] Ansmant, I., Massenet, S., Grosjean, H., Motorin, Y., and Branlant, C. (2000). Identification of the saccharomyces cerevisiae rna: pseudouridine synthase responsible for formation of Ψ 2819 in 21s mitochondrial ribosomal rna. *Nucleic acids research*, 28(9):1941–1946.
- [Ansmant et al., 2001] Ansmant, I., Motorin, Y., Massenet, S., Grosjean, H., and Branlant, C. (2001). Identification and characterization of the trna: Ψ 31-synthase (pus6p) of saccharomyces cerevisiae. *Journal of Biological Chemistry*, 276(37):34934–34940.
- [Antonicka et al., 2016] Antonicka, H., Choquet, K., Lin, Z.-Y., Gingras, A.-C., Kleinman, C. L., and Shoubbridge, E. A. (2016). A pseudouridine synthase module is essential for mitochondrial protein synthesis and cell viability. *EMBO reports*, 18(1):28–38.
- [Arango et al., 2018] Arango, D., Sturgill, D., Alhusaini, N., Dillman, A. A., Sweet, T. J., Hanson, G., Hosogane, M., Sinclair, W. R., Nanan, K. K., and Mandler, M. D. (2018). Acetylation of cytidine in mrna promotes translation efficiency. *Cell*, 175(7):1872–1886. e24.

- [Arango et al., 2022] Arango, D., Sturgill, D., Yang, R., Kanai, T., Bauer, P., Roy, J., Wang, Z., Hosogane, M., Schiffers, S., and Oberdoerffer, S. (2022). Direct epitranscriptomic regulation of mammalian translation initiation through n4-acetylcytidine. *Molecular cell*, 82(15):2797–2814. e11.
- [Arluison et al., 1999] Arluison, V., Batelier, G., Riès-Kautt, M., and Grosjean, H. (1999). Rna: pseudouridine synthetase *pus1* from *saccharomyces cerevisiae*: Oligomerization property and stoichiometry of the complex with yeast *trnaph*. *Biochimie*, 81(7):751–756.
- [Arnez and Steitz, 1994] Arnez, J. G. and Steitz, T. A. (1994). Crystal structure of unmodified tRNAGln complexed with glutaminyl-tRNA synthetase and ATP suggests a possible role for pseudo-uridines in stabilization of RNA structure. *Biochemistry*, 33(24):7560–7567.
- [Arpat et al., 2020] Arpat, A. B., Liechti, A., De Matos, M., Dreos, R., Janich, P., and Gatfield, D. (2020). Transcriptome-wide sites of collided ribosomes reveal principles of translational pausing. *Genome research*, 30(7):985–999.
- [Arps et al., 1985] Arps, P. J., Marvel, C. C., Rubin, B. C., Tolan, D. A., Penhoet, E. E., and Winkler, M. E. (1985). Structural features of the *his* t operon of *escherichia coli* k-12. *Nucleic acids research*, 13(14):5297–5315.
- [Arts et al., 1998] Arts, G.-J., Kuersten, S., Romby, P., Ehresmann, B., and Mattaj, I. W. (1998). The role of exportin-t in selective nuclear export of mature *trnas*. *The EMBO journal*, 17(24):7430–7441.
- [Aula et al., 2000] Aula, N., Salomäki, P., Timonen, R., Verheijen, F., Mancini, G., Månsson, J.-E., Aula, P., and Peltonen, L. (2000). The spectrum of SLC17a5-gene mutations resulting in free sialic acid-storage diseases indicates some genotype-phenotype correlation. *The American Journal of Human Genetics*, 67(4):832–840.
- [Aza-Blanc et al., 2003] Aza-Blanc, P., Cooper, C. L., Wagner, K., Batalov, S., Deveraux, Q. L., and Cooke, M. P. (2003). Identification of modulators of trail-induced apoptosis via *rnai*-based phenotypic screening. *Molecular cell*, 12(3):627–637.
- [Baba et al., 2013] Baba, K., Tumuraya, K., Tanaka, I., Yao, M., and Uchiumi, T. (2013). Molecular dissection of the silkworm ribosomal stalk complex: the role of multiple copies of the stalk proteins. *Nucleic acids research*, 41(6):3635–3643.
- [Baier et al., 2002] Baier, A., Wittek, B., and Brembs, B. (2002). *Drosophila* as a new model organism for the neurobiology of aggression? *Journal of Experimental Biology*, 205(9):1233–1240.
- [Baird and Wek, 2012] Baird, T. D. and Wek, R. C. (2012). Eukaryotic initiation factor 2 phosphorylation and translational control in metabolism. *Advances in nutrition*, 3(3):307–321.
- [Bakin and Ofengand, 1993] Bakin, A. and Ofengand, J. (1993). Four newly located pseudouridylate residues in *escherichia coli* 23s ribosomal rna are all at the peptidyltransferase center: analysis by the application of a new sequencing technique. *Biochemistry*, 32(37):9754–9762.

- [Balakin et al., 1996] Balakin, A. G., Smith, L., and Fournier, M. J. (1996). The rna world of the nucleolus: two major families of small rnas defined by different box elements with related functions. *cell*, 86(5):823–834.
- [Basak and Query, 2014] Basak, A. and Query, C. C. (2014). A pseudouridine residue in the spliceosome core is part of the filamentous growth program in yeast. *Cell reports*, 8(4):966–973.
- [Baskin and Dekker, 1967] Baskin, F. and Dekker, C. A. (1967). A rapid and specific assay for sugar methylation in ribonucleic acid. *Journal of Biological Chemistry*, 242(22):5447–5449.
- [Batenburg et al., 2022] Batenburg, K. L., Kasri, N. N., Heine, V. M., and Scheper, W. (2022). Intra-neuronal tau aggregation induces the integrated stress response in astrocytes. *Journal of molecular cell biology*, 14(10):mjac071.
- [Batista et al., 2014] Batista, P. J., Molinie, B., Wang, J., Qu, K., Zhang, J., Li, L., Bouley, D. M., Lujan, E., Haddad, B., and Daneshvar, K. (2014). m6a rna modification controls cell fate transition in mammalian embryonic stem cells. *Cell stem cell*, 15(6):707–719.
- [Baudin-Baillieu et al., 2009] Baudin-Baillieu, A., Fabret, C., Liang, X.-h., Piekna-Przybylska, D., Fournier, M. J., and Rousset, J.-P. (2009). Nucleotide modifications in three functionally important regions of the *saccharomyces cerevisiae* ribosome affect translation accuracy. *Nucleic acids research*, 37(22):7665–7677.
- [Becker et al., 1997] Becker, H. F., Motorin, Y., Planta, R. J., and Grosjean, H. (1997). The yeast gene *ynl292w* encodes a pseudouridine synthase (*pus4*) catalyzing the formation of Ψ 55 in both mitochondrial and cytoplasmic trnas. *Nucleic acids research*, 25(22):4493–4499.
- [Behm-Ansmant et al., 2007] Behm-Ansmant, I., Branlant, C., and Motorin, Y. (2007). The *saccharomyces cerevisiae* *pus2* protein encoded by *yg1063w* orf is a mitochondrial trna: Ψ 27/28-synthase. *Rna*, 13(10):1641–1647.
- [Behm-Ansmant et al., 2004] Behm-Ansmant, I., Grosjean, H., Massenet, S., Motorin, Y., and Branlant, C. (2004). Pseudouridylation at position 32 of mitochondrial and cytoplasmic trnas requires two distinct enzymes in *saccharomyces cerevisiae*. *Journal of Biological Chemistry*, 279(51):52998–53006.
- [Behm-Ansmant et al., 2006] Behm-Ansmant, I., Massenet, S., Immel, F., Patton, J. R., Motorin, Y., and Branlant, C. (2006). A previously unidentified activity of yeast and mouse rna: pseudouridine synthases 1 (*pus1p*) on trnas. *Rna*, 12(8):1583–1593.
- [Behm-Ansmant et al., 2003] Behm-Ansmant, I., Urban, A., Ma, X., Yu, Y.-T., Motorin, Y., and Branlant, C. (2003). The *saccharomyces cerevisiae* *u2* snrna:pseudouridine-synthase *pus7p* is a novel multisite-multisubstrate rna:psi-synthase also acting on trnas. *RNA (New York, N. Y.)*, 9:1371–82.
- [Bertoli-Avella et al., 2018] Bertoli-Avella, A. M., Garcia-Aznar, J. M., Brandau, O., Al-Hakami, F., Yüksel, Z., Marais, A., Grüning, N.-M., Abbasi Moheb, L., Paknia, O., and Alshaikh, N. (2018). Biallelic inactivating variants in the *gtpbp2* gene cause a neurodevelopmental disorder with severe intellectual disability. *European Journal of Human Genetics*, 26(4):592–598.

- [Bieker et al., 1985] Bieker, J. J., Martin, P. L., and Roeder, R. G. (1985). Formation of a rate-limiting intermediate in 5s rna gene transcription. *Cell*, 40(1):119–127.
- [Björk et al., 2001] Björk, G. R., Jacobsson, K., Nilsson, K., Johansson, M. J. O., Byström, A. S., and Persson, O. P. (2001). A primordial trna modification required for the evolution of life? *The EMBO journal*, 20(1-2):231–239.
- [Björk et al., 1989] Björk, G. R., Wikström, P. M., and Byström, A. S. (1989). Prevention of translational frameshifting by the modified nucleoside 1-methylguanosine. *Science*, 244(4907):986–989.
- [Blanco et al., 2014] Blanco, S., Dietmann, S., Flores, J. V., Hussain, S., Kutter, C., Humphreys, P., Lukk, M., Lombard, P., Treps, L., and Popis, M. (2014). Aberrant methylation of trnas links cellular stress to neuro-developmental disorders. *The EMBO journal*, 33(18):2020–2039.
- [Blaze et al., 2021] Blaze, J., Navickas, A., Phillips, H. L., Heissel, S., Plaza-Jennings, A., Miglani, S., Asgharian, H., Foo, M., Katanski, C. D., and Watkins, C. P. (2021). Neuronal nsun2 deficiency produces trna epitranscriptomic alterations and proteomic shifts impacting synaptic signaling and behavior. *Nature communications*, 12(1):4913.
- [Blenau and Thamm, 2011] Blenau, W. and Thamm, M. (2011). Distribution of serotonin (5-HT) and its receptors in the insect brain with focus on the mushroom bodies. lessons from drosophila melanogaster and apis mellifera. *Arthropod Structure & Development*, 40(5):381–394.
- [Boccaletto et al., 2022] Boccaletto, P., Stefaniak, F., Ray, A., Cappannini, A., Mukherjee, S., Purta, E., Kurkowska, M., Shirvanizadeh, N., Destefanis, E., and Groza, P. (2022). Modomics: a database of rna modification pathways. 2021 update. *Nucleic acids research*, 50(D1):D231–D235.
- [Boehringer et al., 2004] Boehringer, D., Makarov, E. M., Sander, B., Makarova, O. V., Kastner, B., Lührmann, R., and Stark, H. (2004). Three-dimensional structure of a pre-catalytic human spliceosomal complex b. *Nature structural & molecular biology*, 11(5):463–468.
- [Bohnsack et al., 2004] Bohnsack, M. T., Czaplinski, K., and Görlich, D. (2004). Exportin 5 is a rangtp-dependent dsrna-binding protein that mediates nuclear export of pre-mirnas. *Rna*, 10(2):185–191.
- [Borchardt et al., 2020] Borchardt, E. K., Martinez, N. M., and Gilbert, W. V. (2020). Regulation and function of rna pseudouridylation in human cells. *Annual review of genetics*, 54:309–336.
- [Borek et al., 1977] Borek, E., Baliga, B. S., Gehrke, C. W., Kuo, C. W., Belman, S., Troll, W., and Waalkes, T. P. (1977). High turnover rate of transfer rna in tumor tissue. *Cancer research*, 37(9):3362–3366.
- [Borghesi et al., 2022] Borghesi, A., Plumari, M., Rossi, E., Viganò, C., Cerbo, R. M., Codazzi, A. C., Valente, E. M., and Gana, S. (2022). Pus3-related disorder: Report of a novel patient and delineation of the phenotypic spectrum. *American Journal of Medical Genetics Part A*, 188(2):635–641.
- [Brand et al., 1978] Brand, R. C., Klootwijk, J. A. C. O. B. U. S., Planta, R. J., and Maden, B. E. H. (1978). Biosynthesis of a hypermodified nucleotide in saccharomyces carlsbergensis 17s and hela-cell 18s ribosomal ribonucleic acid. *Biochemical Journal*, 169(1):71–77.

REFERENCES

- [Brandmayr et al., 2012] Brandmayr, C., Wagner, M., Brückl, T., Globisch, D., Pearson, D., Kneuttinger, A. C., Reiter, V., Hienzsch, A., Koch, S., and Thoma, I. (2012). Isotope-based analysis of modified trna nucleosides correlates modification density with translational efficiency. *Angewandte Chemie International Edition*, 51(44):11162–11165.
- [Breitman, 1970] Breitman, T. R. (1970). Pseudouridylate synthetase of escherichia coli: Correlation of its activity with utilization of pseudouridine for growth. *Journal of Bacteriology*, 103(1):263–264.
- [Brimacombe et al., 1993] Brimacombe, R., Mitchell, P., Osswald, M., Stade, K., and Bochkariov, D. (1993). Clustering of modified nucleotides at the functional center of bacterial ribosomal rna. *The FASEB journal*, 7(1):161–167.
- [Broadhurst et al., 2018] Broadhurst, D., Goodacre, R., Reinke, S. N., Kuligowski, J., Wilson, I. D., Lewis, M. R., and Dunn, W. B. (2018). Guidelines and considerations for the use of system suitability and quality control samples in mass spectrometry assays applied in untargeted clinical metabolomic studies. *Metabolomics*, 14(6).
- [Broughton et al., 2005] Broughton, S. J., Piper, M. D. W., Ikeya, T., Bass, T. M., Jacobson, J., Driege, Y., Martinez, P., Hafen, E., Withers, D. J., Leever, S. J., and Partridge, L. (2005). Longer lifespan, altered metabolism, and stress resistance in drosophila from ablation of cells making insulin-like ligands. *Proceedings of the National Academy of Sciences*, 102(8):3105–3110.
- [Brule et al., 1998] Brule, H., Holmes, W. M., Keith, G., Giege, R., and Florentz, C. (1998). Effect of a mutation in the anticodon of human mitochondrial tRNAPro on its post-transcriptional modification pattern. *Nucleic Acids Research*, 26(2):537–543.
- [Brunel and Romby, 2000] Brunel, C. and Romby, P. (2000). [1] probing rna structure and rna-ligand complexes with chemical probes.
- [Brush et al., 2003] Brush, M. H., Weiser, D. C., and Shenolikar, S. (2003). Growth arrest and dna damage-inducible protein gadd34 targets protein phosphatase 1 α to the endoplasmic reticulum and promotes dephosphorylation of the α subunit of eukaryotic translation initiation factor 2. *Molecular and cellular biology*, 23(4):1292–1303.
- [Burgess and Storkebaum, 2023] Burgess, R. W. and Storkebaum, E. (2023). trna dysregulation in neurodevelopmental and neurodegenerative diseases. *Annual Review of Cell and Developmental Biology*, 39.
- [Burrage et al., 2014] Burrage, L. C., Tang, S., Wang, J., Donti, T. R., Walkiewicz, M., Luchak, J. M., Chen, L.-C., Schmitt, E. S., Niu, Z., and Erana, R. (2014). Mitochondrial myopathy, lactic acidosis, and sideroblastic anemia (mlasa) plus associated with a novel de novo mutation (m. 8969g> a) in the mitochondrial encoded atp6 gene. *Molecular genetics and metabolism*, 113(3):207–212.
- [Butt and Raman, 2018] Butt, E. and Raman, D. (2018). New frontiers for the cytoskeletal protein lasp1. *Frontiers in oncology*, 8:391.

- [Bykhovskaya et al., 2004] Bykhovskaya, Y., Casas, K., Mengesha, E., Inbal, A., and Fischel-Ghodsian, N. (2004). Missense mutation in pseudouridine synthase 1 (PUS1) causes mitochondrial myopathy and sideroblastic anemia (MLASA). *The American Journal of Human Genetics*, 74(6):1303–1308.
- [Byrne and Wolfe, 2005] Byrne, K. P. and Wolfe, K. H. (2005). The yeast gene order browser: combining curated homology and syntenic context reveals gene fate in polyploid species. *Genome research*, 15(10):1456–1461.
- [Börner et al., 1996] Börner, G. V., Mörl, M., Janke, A., and Pääbo, S. (1996). Rna editing changes the identity of a mitochondrial trna in marsupials. *The EMBO Journal*, 15(21):5949–5957.
- [Caffarelli et al., 1996] Caffarelli, E., Fatica, A., Prislei, S., De Gregorio, E., Fragapane, P., and Bozzoni, I. (1996). Processing of the intron-encoded u16 and u18 snornas: the conserved c and d boxes control both the processing reaction and the stability of the mature snorna. *The EMBO Journal*, 15(5):1121–1131.
- [Camelo et al., 2021] Camelo, C. G., Silva, A. M. S., Rocha, A. J., Scaramuzzi, V., Moreno, C. d. A. M., Reed, U. C., and Zanoteli, E. (2021). Severe progressive brain involvement in a patient with trmt10c mutation. *Arquivos de Neuro-Psiquiatria*, 79(03):259–260.
- [Cantara et al., 2010] Cantara, W. A., Crain, P. F., Rozenski, J., McCloskey, J. A., Harris, K. A., Zhang, X., Vendeix, F. A. P., Fabris, D., and Agris, P. F. (2010). The rna modification database, rnamdb: 2011 update. *Nucleic acids research*, 39:D195–D201.
- [Cao et al., 2016] Cao, M., Donà, M., Valentino, L., Semplicini, C., Maresca, A., Cassina, M., Torracco, A., Galletta, E., Manfioli, V., and Sorarù, G. (2016). Clinical and molecular study in a long-surviving patient with mlasa syndrome due to novel pus1 mutations. *neurogenetics*, 17:65–70.
- [Carlile et al., 2019] Carlile, T. M., Martinez, N. M., Schaening, C., Su, A., Bell, T. A., Zinshteyn, B., and Gilbert, W. V. (2019). mrna structure determines modification by pseudouridine synthase 1. *Nature chemical biology*, 15(10):966–974.
- [Carlile et al., 2014] Carlile, T. M., Rojas-Duran, M. F., Zinshteyn, B., Shin, H., Bartoli, K. M., and Gilbert, W. V. (2014). Pseudouridine profiling reveals regulated mRNA pseudouridylation in yeast and human cells. *Nature*, 515(7525):143–146.
- [Carlson et al., 1999] Carlson, B. A., Kwon, S. Y., Chamorro, M., Oroszlan, S., Hatfield, D. L., and Lee, B. J. (1999). Transfer rna modification status influences retroviral ribosomal frameshifting. *Virology*, 255(1):2–8.
- [Carter et al., 2019] Carter, M. T., Venkateswaran, S., Shapira-Zaltsberg, G., Davila, J., Humphreys, P., Consortium, C. C., Kernohan, K. D., and Boycott, K. M. (2019). Clinical delineation of gtpbp2-associated neuro-ectodermal syndrome: Report of two new families and review of the literature. *Clinical Genetics*, 95(5):601–606.
- [Casas et al., 2004] Casas, K., Bykhovskaya, Y., Mengesha, E., Wang, D., Yang, H., Taylor, K., Inbal, A., and Fischel-Ghodsian, N. (2004). Gene responsible for mitochondrial myopathy and sideroblastic anemia (MSA) maps to chromosome 12q24.33. *American Journal of Medical Genetics Part A*, 127A(1):44–49.

- [Cate et al., 1999] Cate, J. H., Yusupov, M. M., Yusupova, G. Z., Earnest, T. N., and Noller, H. F. (1999). X-ray crystal structures of 70 s ribosome functional complexes. *Science*, 285(5436):2095–2104.
- [Cerneckis et al., 2022] Cerneckis, J., Cui, Q., He, C., Yi, C., and Shi, Y. (2022). Decoding pseudouridine: an emerging target for therapeutic development. *Trends in Pharmacological Sciences*.
- [Chakshusmathi et al., 2003] Chakshusmathi, G., Do Kim, S., Rubinson, D. A., and Wolin, S. L. (2003). A la protein requirement for efficient pre-trna folding. *The EMBO journal*, 22(24):6562–6572.
- [Chan and Lowe, 2016] Chan, P. P. and Lowe, T. M. (2016). Gtrnadb 2.0: an expanded database of transfer rna genes identified in complete and draft genomes. *Nucleic acids research*, 44(D1):D184–D189.
- [Chandrasekaran et al., 2015] Chandrasekaran, S., Rittschof, C. C., Djukovic, D., Gu, H., Raftery, D., Price, N. D., and Robinson, G. E. (2015). Aggression is associated with aerobic glycolysis in the honey bee brain. *Genes, Brain and Behavior*, 14(2):158–166.
- [Chapman et al., 2003] Chapman, T., Bangham, J., Vinti, G., Seifried, B., Lung, O., Wolfner, M. F., Smith, H. K., and Partridge, L. (2003). The sex peptide of drosophila melanogaster: female post-mating responses analyzed by using rna interference. *Proceedings of the National Academy of Sciences*, 100(17):9923–9928.
- [Charette and Gray, 2000] Charette, M. and Gray, M. W. (2000). Pseudouridine in rna: what, where, how, and why. *IUBMB life*, 49(5):341–352.
- [Chawla et al., 2015] Chawla, M., Oliva, R., Bujnicki, J. M., and Cavallo, L. (2015). An atlas of rna base pairs involving modified nucleobases with optimal geometries and accurate energies. *Nucleic acids research*, 43(14):6714–6729.
- [Chen et al., 2010] Chen, C., Zhao, X., Kierzek, R., and Yu, Y.-T. (2010). A flexible RNA backbone within the polypyrimidine tract is required for u2af65 binding and pre-mRNA splicing in vivo. *Molecular and Cellular Biology*, 30(17):4108–4119.
- [Chen et al., 2020] Chen, H., Gu, L., Orellana, E. A., Wang, Y., Guo, J., Liu, Q., Wang, L., Shen, Z., Wu, H., and Gregory, R. I. (2020). Mettl4 is an snrna m6am methyltransferase that regulates rna splicing. *Cell research*, 30(6):544–547.
- [Chen et al., 2019a] Chen, K., Wei, Z., Zhang, Q., Wu, X., Rong, R., Lu, Z., Su, J., de Magalhaes, J. P., Rigden, D. J., and Meng, J. (2019a). Whistle: a high-accuracy map of the human n 6-methyladenosine (m6a) epitranscriptome predicted using a machine learning approach. *Nucleic acids research*, 47(7):e41–e41.
- [Chen et al., 2016] Chen, Q., Yan, M., Cao, Z., Li, X., Zhang, Y., Shi, J., Feng, G.-h., Peng, H., Zhang, X., and Zhang, Y. (2016). Sperm tsrnas contribute to intergenerational inheritance of an acquired metabolic disorder. *Science*, 351(6271):397–400.
- [Chen et al., 1996] Chen, R., Udenfriend, S., Prince, G. M., Maxwell, S. E., Ramalingam, S., Gerber, L. D., Knez, J., and Medof, M. E. (1996). A defect in glycosylphosphatidylinositol (gpi) transamidase activity in mutant k cells is responsible for their inability to display gpi surface proteins. *Proceedings of the National Academy of Sciences*, 93(6):2280–2284.

- [Chen et al., 2002] Chen, S., Lee, A. Y., Bowens, N. M., Huber, R., and Kravitz, E. A. (2002). Fighting fruit flies: A model system for the study of aggression. *Proceedings of the National Academy of Sciences*, 99(8):5664–5668.
- [Chen et al., 2019b] Chen, Z., Qi, M., Shen, B., Luo, G., Wu, Y., Li, J., Lu, Z., Zheng, Z., Dai, Q., and Wang, H. (2019b). Transfer rna demethylase alkbh3 promotes cancer progression via induction of trna-derived small rnas. *Nucleic acids research*, 47(5):2533–2545.
- [Chernyakov et al., 2008] Chernyakov, I., Whipple, J. M., Kotelawala, L., Grayhack, E. J., and Phizicky, E. M. (2008). Degradation of several hypomodified mature trna species in *saccharomyces cerevisiae* is mediated by met22 and the 5′–3′ exonucleases rat1 and xrn1. *Genes & development*, 22(10):1369–1380.
- [Chou et al., 2017] Chou, H.-J., Donnard, E., Gustafsson, H. T., Garber, M., and Rando, O. J. (2017). Transcriptome-wide analysis of roles for trna modifications in translational regulation. *Molecular cell*, 68(5):978–992. e4.
- [Cigan et al., 1988] Cigan, A. M., Feng, L., and Donahue, T. F. (1988). trnaimet functions in directing the scanning ribosome to the start site of translation. *Science*, 242(4875):93–97.
- [Cohn, 1960] Cohn, W. E. (1960). Pseudouridine, a carbon-carbon linked ribonucleoside in ribonucleic acids: isolation, structure, and chemical characteristics. *Journal of Biological Chemistry*, 235(5):1488–1498.
- [Cohn and Volkin, 1951] Cohn, W. E. and Volkin, E. (1951). Nucleoside-5′-phosphates from ribonucleic acid. *Nature*, 167:483–484.
- [Colbert and Hahn, 1992] Colbert, T. and Hahn, S. (1992). A yeast tfiib-related factor involved in rna polymerase iii transcription. *Genes & Development*, 6(10):1940–1949.
- [Cole et al., 2009] Cole, C., Sobala, A., Lu, C., Thatcher, S. R., Bowman, A., Brown, J. W. S., Green, P. J., Barton, G. J., and Hutvagner, G. (2009). Filtering of deep sequencing data reveals the existence of abundant dicer-dependent small rnas derived from trnas. *Rna*, 15(12):2147–2160.
- [Cong et al., 2002] Cong, Y.-S., Wright, W. E., and Shay, J. W. (2002). Human telomerase and its regulation. *Microbiology and molecular biology reviews*, 66(3):407–425.
- [Conrad et al., 1998] Conrad, J., Sun, D., Englund, N., and Ofengand, J. (1998). The rluc gene of *escherichia coli* codes for a pseudouridine synthase that is solely responsible for synthesis of pseudouridine at positions 955, 2504, and 2580 in 23 s ribosomal rna. *Journal of Biological Chemistry*, 273(29):18562–18566.
- [Contreras-Sanz et al., 2012] Contreras-Sanz, A., Scott-Ward, T. S., Gill, H. S., Jacoby, J. C., Birch, R. E., Malone-Lee, J., Taylor, K. M. G., Peppiatt-Wildman, C. M., and Wildman, S. S. P. (2012). Simultaneous quantification of 12 different nucleotides and nucleosides released from renal epithelium and in human urine samples using ion-pair reversed-phase hplc. *Purinergic signalling*, 8:741–751.
- [Coordinators, 2015] Coordinators, N. R. (2015). Database resources of the National Center for Biotechnology Information. *Nucleic Acids Research*, 44(D1):D7–D19.

- [Copela et al., 2006] Copela, L. A., Chakshusmathi, G., Sherrer, R. L., and Wolin, S. L. (2006). The la protein functions redundantly with trna modification enzymes to ensure trna structural stability. *Rna*, 12(4):644–654.
- [Cortese et al., 1974] Cortese, R., Kammen, H. O., Spengler, S. J., and Ames, B. N. (1974). Biosynthesis of pseudouridine in transfer ribonucleic acid. *Journal of Biological Chemistry*, 249(4):1103–1108.
- [Cosentino et al., 2018] Cosentino, C., Toivonen, S., Diaz Villamil, E., Atta, M., Ravanat, J.-L., Demine, S., Schiavo, A. A., Pachera, N., Deglasse, J.-P., and Jonas, J.-C. (2018). Pancreatic β -cell trna hypomethylation and fragmentation link trmt10a deficiency with diabetes. *Nucleic acids research*, 46(19):10302–10318.
- [Costa-Mattioli and Walter, 2020] Costa-Mattioli, M. and Walter, P. (2020). The integrated stress response: From mechanism to disease. *Science*, 368(6489):eaat5314.
- [Couvillion et al., 2012] Couvillion, M. T., Bounova, G., Purdom, E., Speed, T. P., and Collins, K. (2012). A tetrahymena piwi bound to mature trna 3' fragments activates the exonuclease xrn2 for rna processing in the nucleus. *Molecular cell*, 48(4):509–520.
- [Cox et al., 2014] Cox, J., Hein, M. Y., Lubner, C. A., Paron, I., Nagaraj, N., and Mann, M. (2014). Accurate proteome-wide label-free quantification by delayed normalization and maximal peptide ratio extraction, termed maxlfq. *Molecular & cellular proteomics*, 13(9):2513–2526.
- [Cox and Mann, 2012] Cox, J. and Mann, M. (2012). 1d and 2d annotation enrichment: a statistical method integrating quantitative proteomics with complementary high-throughput data. *BMC bioinformatics*, 13:1–11.
- [Crain, 1998] Crain, P. F. (1998). Detection and structure analysis of modified nucleosides in rna by mass spectrometry. *Modification and Editing of RNA*, pages 47–57.
- [Crivello et al., 2018] Crivello, M., O’Riordan, S. L., Woods, I., Cannon, S., Halang, L., Coughlan, K. S., Hogg, M. C., Lewandowski, S. A., and Prehn, J. H. M. (2018). Pleiotropic activity of systemically delivered angiogenin in the sod1g93a mouse model. *Neuropharmacology*, 133:503–511.
- [Cui et al., 2021] Cui, Q., Yin, K., Zhang, X., Ye, P., Chen, X., Chao, J., Meng, H., Wei, J., Roeth, D., Li, L., Qin, Y., Sun, G., Zhang, M., Klein, J., Huynhle, M., Wang, C., Zhang, L., Badie, B., Kalkum, M., He, C., Yi, C., and Shi, Y. (2021). Targeting PUS7 suppresses tRNA pseudouridylation and glioblastoma tumorigenesis. *Nature Cancer*, 2(9):932–949.
- [Czudnochowski et al., 2013] Czudnochowski, N., Wang, A. L., Finer-Moore, J., and Stroud, R. M. (2013). In human pseudouridine synthase 1 (hPus1), a c-terminal helical insert blocks tRNA from binding in the same orientation as in the pus1 bacterial homologue TruA, consistent with their different target selectivities. *Journal of Molecular Biology*, 425(20):3875–3887.
- [Dai et al., 2022] Dai, Q., Zhang, L.-S., Sun, H.-L., Pajdzik, K., Yang, L., Ye, C., Ju, C.-W., Liu, S., Wang, Y., Zheng, Z., Zhang, L., Harada, B. T., Dou, X., Irkliyenko, I., Feng, X., Zhang, W., Pan, T., and He, C. (2022). Quantitative sequencing using BID-seq uncovers abundant pseudouridines in mammalian mRNA at base resolution. *Nature Biotechnology*, 41(3):344–354.

- [Dalal et al., 2019] Dalal, S., Deshmukh, P., Unni, S., Padavattan, S., and Padmanabhan, B. (2019). Biochemical insight into pseudouridine synthase 7 (*pus7*) as a novel interactor of sirtuin, *sirt1*. *Biochemical and Biophysical Research Communications*, 518(3):598–604.
- [Darvish et al., 2019] Darvish, H., Azcona, L. J., Alehabib, E., Jamali, F., Tafakhori, A., Ranji-Burachaloo, S., Jen, J. C., and Paisán-Ruiz, C. (2019). A novel *pus7* mutation causes intellectual disability with autistic and aggressive behaviors. *Neurology Genetics*, 5(5):e356.
- [Davis, 1995] Davis, D. R. (1995). Stabilization of rna stacking by pseudouridine. *Nucleic acids research*, 23(24):5020–5026.
- [Davis and Allen, 1957] Davis, F. F. and Allen, F. W. (1957). Ribonucleic acids from yeast which contain a fifth nucleotide. *J Biol Chem*, 227(2):907–15.
- [de Brouwer et al., 2018] de Brouwer, A. P., Jamra, R. A., Körtel, N., Soyris, C., Polla, D. L., Safra, M., Zisso, A., Powell, C. A., Rebelo-Guiomar, P., Dinges, N., Morin, V., Stock, M., Hussain, M., Shahzad, M., Riazuddin, S., Ahmed, Z. M., Pfundt, R., Schwarz, F., de Boer, L., Reis, A., Grozeva, D., Raymond, F. L., Riazuddin, S., Koolen, D. A., Minczuk, M., Roignant, J.-Y., van Bokhoven, H., and Schwartz, S. (2018). Variants in *pus7* cause intellectual disability with speech delay, microcephaly, short stature, and aggressive behavior. *The American Journal of Human Genetics*, 103(6):1045–1052.
- [de Paiva et al., 2019] de Paiva, A. R. B., Lynch, D. S., Melo, U. S., Lucato, L. T., Freua, F., de Assis, B. D. R., Barcelos, I., Listik, C., de Castro dos Santos, D., Macedo-Souza, L. I., Houlden, H., and Kok, F. (2019). *Pus3* mutations are associated with intellectual disability, leukoencephalopathy, and nephropathy. *Neurology Genetics*, 5(1):e306.
- [Decatur and Fournier, 2002] Decatur, W. A. and Fournier, M. J. (2002). rna modifications and ribosome function. *Trends in biochemical sciences*, 27(7):344–351.
- [Decatur and Schnare, 2008] Decatur, W. A. and Schnare, M. N. (2008). Different mechanisms for pseudouridine formation in yeast 5s and 5.8 s rrnas. *Molecular and cellular biology*, 28(10):3089–3100.
- [Del Campo Mark and James, 2001] Del Campo Mark, K. Y. and James, O. (2001). Identification and site of action of the remaining four putative pseudouridine synthases in *escherichia coli*. *Rna*, 7(11):1603–1615.
- [deLorimier et al., 2014] deLorimier, E., Coonrod, L. A., Copperman, J., Taber, A., Reister, E. E., Sharma, K., Todd, P. K., Guenza, M. G., and Berglund, J. A. (2014). Modifications to toxic *cug* rnas induce structural stability, rescue mis-splicing in a myotonic dystrophy cell model and reduce toxicity in a myotonic dystrophy zebrafish model. *Nucleic acids research*, 42(20):12768–12778.
- [deLorimier et al., 2017] deLorimier, E., Hinman, M. N., Copperman, J., Datta, K., Guenza, M., and Berglund, J. A. (2017). Pseudouridine modification inhibits muscleblind-like 1 (*mbnl1*) binding to *ccug* repeats and minimally structured rna through reduced rna flexibility. *Journal of Biological Chemistry*, 292(10):4350–4357.
- [Delépine et al., 2000] Delépine, M., Nicolino, M., Barrett, T., Golamaully, M., Mark Lathrop, G., and Julier, C. (2000). *Eif2ak3*, encoding translation initiation factor 2- α kinase 3, is mutated in patients with wolcott-rallison syndrome. *Nature genetics*, 25(4):406–409.

- [Deogharia et al., 2019] Deogharia, M., Mukhopadhyay, S., Joardar, A., and Gupta, R. (2019). The human ortholog of archaeal *pus10* produces pseudouridine 54 in select *trnas* where its recognition sequence contains a modified residue. *RNA*, 25(3):336–351.
- [Deryusheva and Gall, 2013] Deryusheva, S. and Gall, J. G. (2013). Novel small cajal-body-specific *rnas* identified in *drosophila*: probing guide rna function. *Rna*, 19(12):1802–1814.
- [Deryusheva and Gall, 2017] Deryusheva, S. and Gall, J. G. (2017). Dual nature of pseudouridylation in *u2 snrna*: *Pus1p*-dependent and *pus1p*-independent activities in yeasts and higher eukaryotes. *RNA*, 23(7):1060–1067.
- [Desaulniers et al., 2008] Desaulniers, J.-P., Chang, Y.-C., Aduri, R., Abeyisirigunawardena, S. C., SantaLucia Jr, J., and Chow, C. S. (2008). Pseudouridines in *rrna* helix 69 play a role in loop stacking interactions. *Organic & biomolecular chemistry*, 6(21):3892–3895.
- [Desrosiers et al., 1974] Desrosiers, R., Friderici, K., and Rottman, F. (1974). Identification of methylated nucleosides in messenger rna from novikoff hepatoma cells. *Proceedings of the National Academy of Sciences*, 71(10):3971–3975.
- [Dichtl et al., 1997] Dichtl, B., Stevens, A., and Tollervey, D. (1997). Lithium toxicity in yeast is due to the inhibition of rna processing enzymes. *The EMBO journal*, 16(23):7184–7195.
- [Dieci et al., 2009] Dieci, G., Preti, M., and Montanini, B. (2009). Eukaryotic *snornas*: a paradigm for gene expression flexibility. *Genomics*, 94(2):83–88.
- [Dikfidan et al., 2014] Dikfidan, A., Loll, B., Zeymer, C., Magler, I., Clausen, T., and Meinhart, A. (2014). Rna specificity and regulation of catalysis in the eukaryotic polynucleotide kinase *clp1*. *Molecular cell*, 54(6):975–986.
- [Ding et al., 2016] Ding, Y., Zhuo, G., Zhang, C., and Leng, J. (2016). Point mutation in mitochondrial *trna* gene is associated with polycystic ovary syndrome and insulin resistance. *Molecular medicine reports*, 13(4):3169–3172.
- [Dittmar et al., 2006] Dittmar, K. A., Goodenbour, J. M., and Pan, T. (2006). Tissue-specific differences in human transfer rna expression. *PLoS genetics*, 2(12):e221.
- [Dominissini et al., 2012] Dominissini, D., Moshitch-Moshkovitz, S., Schwartz, S., Salmon-Divon, M., Ungar, L., Osenberg, S., Cesarkas, K., Jacob-Hirsch, J., Amariglio, N., Kupiec, M., Sorek, R., and Rechavi, G. (2012). Topology of the human and mouse *m6a* RNA methylomes revealed by *m6a*-seq. *Nature*, 485(7397):201–206.
- [Dominissini et al., 2016] Dominissini, D., Nachtergaele, S., Moshitch-Moshkovitz, S., Peer, E., Kol, N., Ben-Haim, M. S., Dai, Q., Di Segni, A., Salmon-Divon, M., and Clark, W. C. (2016). The dynamic *n1*-methyladenosine methylome in eukaryotic messenger rna. *Nature*, 530(7591):441–446.
- [Donovan et al., 2017] Donovan, J., Rath, S., Kolet-Mandrikov, D., and Korennykh, A. (2017). Rapid *rnase1*-driven arrest of protein synthesis in the *dsrna* response without degradation of translation machinery. *Rna*, 23(11):1660–1671.

- [Dover, 1998] Dover, M. (1998). Urinary catecholamines and cortisol in attention deficit/hyperactivity disorder.
- [Du et al., 2021] Du, J., Gong, A., Zhao, X., and Wang, G. (2021). Pseudouridylate synthase 7 promotes cell proliferation and invasion in colon cancer through activating pi3k/akt/mtor signaling pathway. *Digestive Diseases and Sciences*, pages 1–11.
- [Dubin and Günalp, 1967] Dubin, D. T. and Günalp, A. (1967). Minor nucleotide composition of ribosomal precursor, and ribosomal, ribonucleic acid in escherichia coli. *Biochimica et Biophysica Acta (BBA) - Nucleic Acids and Protein Synthesis*, 134(1):106–123.
- [Dunn et al., 2011] Dunn, W. B., Broadhurst, D., Begley, P., Zelena, E., Francis-McIntyre, S., Anderson, N., Brown, M., Knowles, J. D., Halsall, A., Haselden, J. N., Nicholls, A. W., Wilson, I. D., Kell, D. B., and Goodacre, R. (2011). Procedures for large-scale metabolic profiling of serum and plasma using gas chromatography and liquid chromatography coupled to mass spectrometry. *Nature Protocols*, 6(7):1060–1083.
- [Durant and Davis, 1999] Durant, P. C. and Davis, D. R. (1999). Stabilization of the anticodon stem-loop of trn^{alys}, 3 by an a⁺-c base-pair and by pseudouridine. *Journal of molecular biology*, 285(1):115–131.
- [Dönmez et al., 2004] Dönmez, G., Hartmuth, K., and Lührmann, R. (2004). Modified nucleotides at the 5' end of human u2 snrna are required for spliceosomal e-complex formation. *Rna*, 10(12):1925–1933.
- [Edmonds et al., 1971] Edmonds, M., Vaughan Jr, M. H., and Nakazato, H. (1971). Polyadenylic acid sequences in the heterogeneous nuclear rna and rapidly-labeled polyribosomal rna of hela cells: possible evidence for a precursor relationship. *Proceedings of the National Academy of Sciences*, 68(6):1336–1340.
- [Edupuganti et al., 2017] Edupuganti, R. R., Geiger, S., Lindeboom, R. G. H., Shi, H., Hsu, P. J., Lu, Z., Wang, S.-Y., Baltissen, M. P. A., Jansen, P. W. T. C., and Rossa, M. (2017). N⁶-methyladenosine (m⁶a) recruits and repels proteins to regulate mrna homeostasis. *Nature structural & molecular biology*, 24(10):870–878.
- [Edvardson et al., 2007] Edvardson, S., Shaag, A., Kolesnikova, O., Gomori, J. M., Tarassov, I., Einbinder, T., Saada, A., and Elpeleg, O. (2007). Deleterious mutation in the mitochondrial arginyl-transfer rna synthetase gene is associated with pontocerebellar hypoplasia. *The American Journal of Human Genetics*, 81(4):857–862.
- [Ehresmann et al., 1987] Ehresmann, C., Baudin, F., Mougel, M., Romby, P., Ebel, J.-P., and Ehresmann, B. (1987). Probing the structure of rnas in solution. *Nucleic acids research*, 15(22):9109–9128.
- [Ejby et al., 2007] Ejby, M., Sørensen, M. A., and Pedersen, S. (2007). Pseudouridylation of helix 69 of 23s rna is necessary for an effective translation termination. *Proceedings of the National Academy of Sciences*, 104(49):19410–19415.
- [Emmrechts et al., 2005] Emmrechts, G., Herdewijn, P., and Rozenski, J. (2005). Pseudouridine detection improvement by derivatization with methyl vinyl sulfone and capillary hplc-mass spectrometry. *Journal of Chromatography B*, 825(2):233–238.

- [Enwerem et al., 2014] Enwerem, I. I., Velma, V., Broome, H. J., Kuna, M., Begum, R. A., and Hebert, M. D. (2014). Coilin association with box c/d scarna suggests a direct role for the cajal body marker protein in scarnp biogenesis. *Biology open*, 3(4):240–249.
- [Epstein et al., 1980] Epstein, P., Reddy, R., Henning, D., and Busch, H. (1980). The nucleotide sequence of nuclear u6 (4.7 s) rna. *Journal of Biological Chemistry*, 255(18):8901–8906.
- [Esteller, 2011] Esteller, M. (2011). Non-coding RNAs in human disease. *Nature Reviews Genetics*, 12(12):861–874.
- [Eyler et al., 2019] Eyler, D. E., Franco, M. K., Batool, Z., Wu, M. Z., Dubuke, M. L., Dobosz-Bartoszek, M., Jones, J. D., Polikanov, Y. S., Roy, B., and Koutmou, K. S. (2019). Pseudouridylation of mRNA coding sequences alters translation. *Proceedings of the National Academy of Sciences*, 116(46):23068–23074.
- [Fang et al., 2019] Fang, H., Zhang, L., Xiao, B., Long, H., and Yang, L. (2019). Compound heterozygous mutations in PUS3 gene identified in a chinese infant with severe epileptic encephalopathy and multiple malformations. *Neurological Sciences*, 41(2):465–467.
- [Fang et al., 2022] Fang, Z., Shen, H.-y., Xu, Q., Zhou, H.-l., Li, L., Yang, S.-Y., Zhu, Z., and Tang, J.-h. (2022). Pus1 is a novel biomarker for predicting poor outcomes and triple-negative status in breast cancer. *Frontiers in Oncology*, 12:1030571.
- [Fernandez-Vizarra et al., 2006] Fernandez-Vizarra, E., Berardinelli, A., Valente, L., Tiranti, V., and Zeviani, M. (2006). Nonsense mutation in pseudouridylylase synthase 1 (PUS1) in two brothers affected by myopathy, lactic acidosis and sideroblastic anaemia (MLASA). *Journal of Medical Genetics*, 44(3):173–180.
- [Fernández et al., 2013] Fernández, I. S., Ng, C. L., Kelley, A. C., Wu, G., Yu, Y.-T., and Ramakrishnan, V. (2013). Unusual base pairing during the decoding of a stop codon by the ribosome. *Nature*, 500(7460):107–110.
- [Ferreira, 2022] Ferreira, C. M. O. (2022). Neuronal control of suppression, initiation and completion of egg deposition in *drosophila melanogaster*.
- [Festen et al., 2011] Festen, E. A. M., Goyette, P., Green, T., Boucher, G., Beauchamp, C., Trynka, G., Dubois, P. C., Lagace, C., Stokkers, P. C. F., and Hommes, D. W. (2011). A meta-analysis of genome-wide association scans identifies il18rap, ptpn2, tagap, and pus10 as shared risk loci for crohn’s disease and celiac disease. *PLoS genetics*, 7(1):e1001283.
- [Fleissner and Borek, 1962] Fleissner, E. and Borek, E. (1962). A new enzyme of rna synthesis: Rna methylase. *Proceedings of the National Academy of Sciences*, 48(7):1199–1203.
- [Fleming et al., 2019] Fleming, A. M., Alenko, A., Kitt, J. P., Orendt, A. M., Flynn, P. F., Harris, J. M., and Burrows, C. J. (2019). Structural elucidation of bisulfite adducts to pseudouridine that result in deletion signatures during reverse transcription of rna. *Journal of the American Chemical Society*, 141(41):16450–16460.

- [Frank et al., 1994] Frank, D. N., Roiha, H., and Guthrie, C. H. R. I. S. T. I. N. E. (1994). Architecture of the u5 small nuclear rna. *Molecular and Cellular Biology*, 14(3):2180–2190.
- [Fricker et al., 2019] Fricker, R., Brogli, R., Luidalepp, H., Wyss, L., Fasnacht, M., Joss, O., Zywicki, M., Helm, M., Schneider, A., and Cristodero, M. (2019). A trna half modulates translation as stress response in trypanosoma brucei. *Nature communications*, 10(1):118.
- [Froukh et al., 2020] Froukh, T., Nafie, O., Hait, S. A. S. A., Laugwitz, L., Sommerfeld, J., Sturm, M., Baraghiti, A., Issa, T., Al-Nazer, A., Koch, P. A., Hanselmann, J., Kootz, B., Bauer, P., Al-Ameri, W., Jamra, R. A., Alfrook, A. J., Hamadallah, M., Sofan, L., Riess, A., Haack, T. B., Riess, O., and Buchert, R. (2020). Genetic basis of neurodevelopmental disorders in 103 jordanian families. *Clinical Genetics*, 97(4):621–627.
- [Fruscoloni et al., 2001] Fruscoloni, P., Baldi, M. I., and Tocchini-Valentini, G. P. (2001). Cleavage of non-trna substrates by eukaryal trna splicing endonucleases. *EMBO reports*, 2(3):217–221.
- [Fu et al., 2009] Fu, H., Feng, J., Liu, Q., Sun, F., Tie, Y., Zhu, J., Xing, R., Sun, Z., and Zheng, X. (2009). Stress induces trna cleavage by angiogenin in mammalian cells. *FEBS letters*, 583(2):437–442.
- [Fuchs et al., 2019] Fuchs, S. A., Schene, I. F., Kok, G., Jansen, J. M., Nikkels, P. G. J., van Gassen, K. L. I., Terheggen-Lagro, S. W. J., van der Crabben, S. N., Hoeks, S. E., and Niers, L. E. M. (2019). Aminoacyl-trna synthetase deficiencies in search of common themes. *Genetics in Medicine*, 21(2):319–330.
- [Furuichi et al., 1975] Furuichi, Y., Muthukrishnan, S., and Shatkin, A. J. (1975). 5'-terminal m-7g (5') ppp (5') gmp in vivo: identification in reovirus genome rna. *Proceedings of the National Academy of Sciences*, 72(2):742–745.
- [Gagliardi et al., 2019] Gagliardi, S., Davin, A., Bini, P., Sinfioriani, E., Poloni, T. E., Polito, L., Rivoiro, C., Binetti, G., Paterlini, A., and Benussi, L. (2019). A novel nonsense angiogenin mutation is associated with alzheimer disease. *Alzheimer Disease & Associated Disorders*, 33(2):163–165.
- [Galatolo et al., 2020] Galatolo, D., Kuo, M. E., Mullen, P., Meyer-Schuman, R., Doccini, S., Battini, R., Lieto, M., Tessa, A., Filla, A., and Francklyn, C. (2020). Bi-allelic mutations in hars1 severely impair histidyl-trna synthetase expression and enzymatic activity causing a novel multisystem ataxic syndrome. *Human mutation*, 41(7):1232–1237.
- [Galgano et al., 2008] Galgano, A., Forrer, M., Jaskiewicz, L., Kanitz, A., Zavolan, M., and Gerber, A. P. (2008). Comparative analysis of mrna targets for human puf-family proteins suggests extensive interaction with the mirna regulatory system. *PloS one*, 3(9):e3164.
- [Gallart-Ayala et al., 2018] Gallart-Ayala, H., Konz, I., Mehl, F., Teav, T., Oikonomidi, A., Peyratout, G., van der Velpen, V., Popp, J., and Ivanisevic, J. (2018). A global HILIC-MS approach to measure polar human cerebrospinal fluid metabolome: Exploring gender-associated variation in a cohort of elderly cognitively healthy subjects. *Analytica Chimica Acta*, 1037:327–337.
- [Galli et al., 1981] Galli, G., Hofstetter, H., and Birnstiel, M. L. (1981). Two conserved sequence blocks within eukaryotic trna genes are major promoter elements. *Nature*, 294(5842):626–631.

REFERENCES

- [Gamble et al., 2016] Gamble, C. E., Brule, C. E., Dean, K. M., Fields, S., and Grayhack, E. J. (2016). Adjacent codons act in concert to modulate translation efficiency in yeast. *Cell*, 166(3):679–690.
- [Ganetzky and Wu, 1982] Ganetzky, B. and Wu, C.-F. (1982). Indirect suppression involving behavioral mutants with altered nerve excitability in drosophila melanogaster. *Genetics*, 100(4):597–614.
- [Ganot et al., 1997] Ganot, P., Caizergues-Ferrer, M., and Kiss, T. (1997). The family of box aca small nucleolar rnas is defined by an evolutionarily conserved secondary structure and ubiquitous sequence elements essential for rna accumulation. *Genes & development*, 11(7):941–956.
- [Ganot et al., 1999] Ganot, P., Jady, B. E., Bortolin, M.-L., Darzacq, X., and Kiss, T. (1999). Nucleolar factors direct the 2'-o-ribose methylation and pseudouridylation of u6 spliceosomal rna. *Molecular and cellular biology*, 19(10):6906–6917.
- [Gao et al., 2012] Gao, Y., Sartori, D. J., Li, C., Yu, Q.-C., Kushner, J. A., Simon, M. C., and Diehl, J. A. (2012). Perk is required in the adult pancreas and is essential for maintenance of glucose homeostasis. *Molecular and cellular biology*.
- [Garcia-Silva et al., 2010] Garcia-Silva, M. R., Frugier, M., Tosar, J. P., Correa-Dominguez, A., Ronaltes-Alves, L., Parodi-Talice, A., Rovira, C., Robello, C., Goldenberg, S., and Cayota, A. (2010). A population of trna-derived small rnas is actively produced in trypanosoma cruzi and recruited to specific cytoplasmic granules. *Molecular and biochemical parasitology*, 171(2):64–73.
- [Gebetsberger et al., 2017] Gebetsberger, J., Wyss, L., Mleczko, A. M., Reuther, J., and Polacek, N. (2017). A trna-derived fragment competes with mrna for ribosome binding and regulates translation during stress. *RNA biology*, 14(10):1364–1373.
- [Gebetsberger et al., 2012] Gebetsberger, J., Zywicki, M., Künzi, A., and Polacek, N. (2012). trna-derived fragments target the ribosome and function as regulatory non-coding rna in haloferax volcanii. *Archaea*, 2012.
- [Geng et al., 2022] Geng, J., Li, Y., Wu, Z., Ohja, R., Li, S., and Lu, B. (2022). Znf598 responds to mitochondrial stress to abort stalled translation on mitochondrial outer membrane and maintain tissue homeostasis. *bioRxiv*, page 2022.02. 04.479092.
- [Gething, 1999] Gething, M.-J. (1999). Role and regulation of the er chaperone bip. In *Seminars in cell & developmental biology*, volume 10, pages 465–472. Elsevier.
- [Geula et al., 2015] Geula, S., Moshitch-Moshkovitz, S., Dominissini, D., Mansour, A. A., Kol, N., Salmon-Divon, M., Hershkovitz, V., Peer, E., Mor, N., and Manor, Y. S. (2015). m6a mrna methylation facilitates resolution of naïve pluripotency toward differentiation. *Science*, 347(6225):1002–1006.
- [Giegé and Eriani, 2023] Giegé, R. and Eriani, G. (2023). The trna identity landscape for aminoacylation and beyond. *Nucleic Acids Research*, 51(4):1528–1570.
- [Gilham and Ho, 1971] Gilham, P. T. and Ho, N. W. Y. (1971). Reaction of pseudouridine and inosine with n-cyclohexyl-n'-β-(4-methylmorpholinium) ethylcarbodiimide. *Biochemistry*, 10(20):3651–3657.

- [Gogakos et al., 2017] Gogakos, T., Brown, M., Garzia, A., Meyer, C., Hafner, M., and Tuschl, T. (2017). Characterizing expression and processing of precursor and mature human trnas by hydro-trnaseq and par-clip. *Cell reports*, 20(6):1463–1475.
- [Goh et al., 2020] Goh, Y. T., Koh, C. W. Q., Sim, D. Y., Roca, X., and Goh, W. S. S. (2020). Mettl4 catalyzes m6am methylation in u2 snrna to regulate pre-mrna splicing. *Nucleic Acids Research*, 48(16):9250–9261.
- [Goodarzi et al., 2015] Goodarzi, H., Liu, X., Nguyen, H. C. B., Zhang, S., Fish, L., and Tavazoie, S. F. (2015). Endogenous trna-derived fragments suppress breast cancer progression via ybx1 displacement. *Cell*, 161(4):790–802.
- [Greene and Greenamyre, 2002] Greene, J. G. and Greenamyre, J. T. (2002). Characterization of the excitotoxic potential of the reversible succinate dehydrogenase inhibitor malonate. *Journal of Neurochemistry*, 64(1):430–436.
- [Greenway et al., 2004] Greenway, M. J., Alexander, M. D., Ennis, S., Traynor, B. J., Corr, B., Frost, E., Green, A., and Hardiman, O. (2004). A novel candidate region for als on chromosome 14q11. 2. *Neurology*, 63(10):1936–1938.
- [Greenway et al., 2006] Greenway, M. J., Andersen, P. M., Russ, C., Ennis, S., Cashman, S., Donaghy, C., Patterson, V., Swingler, R., Kieran, D., and Prehn, J. (2006). Ang mutations segregate with familial and sporadic amyotrophic lateral sclerosis. *Nature genetics*, 38(4):411–413.
- [Grozhhik et al., 2019] Grozhik, A. V., Olarerin-George, A. O., Sindelar, M., Li, X., Gross, S. S., and Jaffrey, S. R. (2019). Antibody cross-reactivity accounts for widespread appearance of m1a in 5'utrs. *Nature communications*, 10(1):5126.
- [Großhans et al., 2001] Großhans, H., Lecointe, F., Grosjean, H., Hurt, E., and Simos, G. (2001). Pus1p-dependent trna pseudouridylation becomes essential when trna biogenesis is compromised in yeast. *Journal of Biological Chemistry*, 276(49):46333–46339.
- [Gu et al., 2005] Gu, A.-D., Zhou, H., Yu, C.-H., and Qu, L.-H. (2005). A novel experimental approach for systematic identification of box h/aca snornas from eukaryotes. *Nucleic acids research*, 33(22):e194–e194.
- [Gu et al., 2020] Gu, L., Wang, L., Chen, H., Hong, J., Shen, Z., Dhall, A., Lao, T., Liu, C., Wang, Z., and Xu, Y. (2020). Cg14906 (mettl4) mediates m6a methylation of u2 snrna in drosophila. *Cell discovery*, 6(1):44.
- [Gulkovskyi et al., 2015] Gulkovskyi, R. V., Chernushyn, S. Y., and Livshits, L. A. (2015). Novel gene pus3 c.a212g mutation in ukrainian family with intellectual disability. *Biopolymers and Cell*.
- [Gurha and Gupta, 2008] Gurha, P. and Gupta, R. (2008). Archaeal pus10 proteins can produce both pseudouridine 54 and 55 in trna. *Rna*, 14(12):2521–2527.
- [Gutgsell et al., 2005] Gutgsell, N. S., Deutscher, M. P., and Ofengand, J. (2005). The pseudouridine synthase rluD is required for normal ribosome assembly and function in escherichia coli. *Rna*, 11(7):1141–1152.

- [Guzzi et al., 2018] Guzzi, N., Cieřla, M., Ngoc, P. C. T., Lang, S., Arora, S., Dimitriou, M., Pimková, K., Sommarin, M. N., Munita, R., Lubas, M., Lim, Y., Okuyama, K., Soneji, S., Karlsson, G., Hansson, J., Jönsson, G., Lund, A. H., Sigvardsson, M., Hellström-Lindberg, E., Hsieh, A. C., and Bellodi, C. (2018). Pseudouridylation of tRNA-derived fragments steers translational control in stem cells. *Cell*, 173(5):1204–1216.e26.
- [Hadchouel et al., 2015] Hadchouel, A., Wieland, T., Griese, M., Baruffini, E., Lorenz-Depiereux, B., Enaud, L., Graf, E., Dubus, J. C., Halioui-Louhaichi, S., and Coulomb, A. (2015). Biallelic mutations of methionyl-trna synthetase cause a specific type of pulmonary alveolar proteinosis prevalent on réunion island. *The American Journal of Human Genetics*, 96(5):826–831.
- [Haiser et al., 2008] Haiser, H. J., Karginov, F. V., Hannon, G. J., and Elliot, M. A. (2008). Developmentally regulated cleavage of trnas in the bacterium streptomyces coelicolor. *Nucleic acids research*, 36(3):732–741.
- [Halliday and Mallucci, 2015] Halliday, M. and Mallucci, G. R. (2015). Modulating the unfolded protein response to prevent neurodegeneration and enhance memory. *Neuropathology and Applied Neurobiology*, 41(4):414–427.
- [Hamma and Ferré-D’Amaré, 2006] Hamma, T. and Ferré-D’Amaré, A. R. (2006). Pseudouridine synthases. *Chemistry & biology*, 13(11):1125–1135.
- [Han et al., 1998] Han, K.-A., Millar, N. S., and Davis, R. L. (1998). A novel octopamine receptor with preferential expression indrosophila mushroom bodies. *Journal of Neuroscience*, 18(10):3650–3658.
- [Han et al., 1996] Han, K.-A., Millar, N. S., Grotewiel, M. S., and Davis, R. L. (1996). Damb, a novel dopamine receptor expressed specifically in drosophila mushroom bodies. *Neuron*, 16(6):1127–1135.
- [Han et al., 2015] Han, L., Kon, Y., and Phizicky, E. M. (2015). Functional importance of Ψ 38 and Ψ 39 in distinct trnas, amplified for trnagln (uug) by unexpected temperature sensitivity of the s2u modification in yeast. *Rna*, 21(2):188–201.
- [Han et al., 2022] Han, S. T., Kim, A. C., Garcia, K., Schimmenti, L. A., Macnamara, E., Network, U. D., Gahl, W. A., Malicdan, M. C., and Tift, C. J. (2022). Pus7 deficiency in human patients causes profound neurodevelopmental phenotype by dysregulating protein translation. *Molecular Genetics and Metabolism*, 135(3):221–229.
- [Hanada et al., 2013] Hanada, T., Weitzer, S., Mair, B., Bernreuther, C., Wainger, B. J., Ichida, J., Hanada, R., Orthofer, M., Cronin, S. J., and Komnenovic, V. (2013). Clp1 links trna metabolism to progressive motor-neuron loss. *Nature*, 495(7442):474–480.
- [Hanna et al., 1996] Hanna, G. L., Ornitz, E. M., and Hariharan, M. (1996). Urinary catecholamine excretion and behavioral differences in ADHD and normal boys. *Journal of Child and Adolescent Psychopharmacology*, 6(1):63–73.
- [Harding et al., 2000] Harding, H. P., Novoa, I., Zhang, Y., Zeng, H., Wek, R., Schapira, M., and Ron, D. (2000). Regulated translation initiation controls stress-induced gene expression in mammalian cells. *Molecular cell*, 6(5):1099–1108.

- [Harding et al., 2003] Harding, H. P., Zhang, Y., Zeng, H., Novoa, I., Lu, P. D., Calfon, M., Sadri, N., Yun, C., Popko, B., and Paules, R. (2003). An integrated stress response regulates amino acid metabolism and resistance to oxidative stress. *Molecular cell*, 11(3):619–633.
- [Hardwick and Luisi, 2013] Hardwick, S. W. and Luisi, B. F. (2013). Rarely at rest: Rna helicases and their busy contributions to rna degradation, regulation and quality control. *RNA biology*, 10(1):56–70.
- [Hashimoto and Steitz, 1984] Hashimoto, C. and Steitz, J. A. (1984). U4 and u6 rnas coexist in a single small nuclear ribonucleoprotein particle. *Nucleic acids research*, 12(7):3283–3293.
- [Haussecker et al., 2010] Haussecker, D., Huang, Y., Lau, A., Parameswaran, P., Fire, A. Z., and Kay, M. A. (2010). Human trna-derived small rnas in the global regulation of rna silencing. *Rna*, 16(4):673–695.
- [Hayne et al., 2020] Hayne, C. K., Schmidt, C. A., Haque, M. I., Matera, A. G., and Stanley, R. E. (2020). Reconstitution of the human trna splicing endonuclease complex: insight into the regulation of pre-trna cleavage. *Nucleic acids research*, 48(14):7609–7622.
- [Heinrikson and Goldwasser, 1963] Heinrikson, R. L. and Goldwasser, E. (1963). The enzymatic synthesis of 5-ribosyluridylic acid. *ACRHH*, page 62.
- [Heisenberg, 2003] Heisenberg, M. (2003). Mushroom body memoir: from maps to models. *Nature Reviews Neuroscience*, 4(4):266–275.
- [Heisenberg et al., 1985] Heisenberg, M., Borst, A., Wagner, S., and Byers, D. (1985). Drosophila mushroom body mutants are deficient in olfactory learning. *Journal of neurogenetics*, 2(1):1–30.
- [Helm et al., 1998] Helm, M., Brule, H., Degoul, F., Capanec, C., Leroux, J.-P., Giege, R., and Florentz, C. (1998). The presence of modified nucleotides is required for cloverleaf folding of a human mitochondrial tRNA. *Nucleic Acids Research*, 26(7):1636–1643.
- [Hendrick et al., 1981] Hendrick, J. P., Wolin, S. L., Rinke, J. U. T. T. A., Lerner, M. R., and Steitz, J. A. (1981). Ro small cytoplasmic ribonucleoproteins are a subclass of la ribonucleoproteins: further characterization of the ro and la small ribonucleoproteins from uninfected mammalian cells. *Molecular and cellular biology*, 1(12):1138–1149.
- [Hens et al., 2011] Hens, K., Feuz, J.-D., Isakova, A., Iagovitina, A., Massouras, A., Bryois, J., Callaerts, P., Celniker, S. E., and Deplancke, B. (2011). Automated protein-dna interaction screening of drosophila regulatory elements. *Nature methods*, 8(12):1065–1070.
- [Hirabayashi et al., 2006] Hirabayashi, N., Sato, N. S., and Suzuki, T. (2006). Conserved loop sequence of helix 69 in escherichia coli 23 s rna is involved in a-site trna binding and translational fidelity. *Journal of Biological Chemistry*, 281(25):17203–17211.
- [Hoang et al., 2006] Hoang, C., Chen, J., Vizthum, C. A., Kandel, J. M., Hamilton, C. S., Mueller, E. G., and Ferré-D’Amaré, A. R. (2006). Crystal structure of pseudouridine synthase rlua: indirect sequence readout through protein-induced rna structure. *Molecular cell*, 24(4):535–545.

- [Hochberg et al., 2021] Hochberg, I., Demain, L. A. M., Richer, J., Thompson, K., Urquhart, J. E., Rea, A., Pagarkar, W., Rodríguez-Palmero, A., Schlüter, A., and Verdura, E. (2021). Bi-allelic variants in the mitochondrial rna p subunit prorp cause mitochondrial trna processing defects and pleiotropic multisystem presentations. *The American Journal of Human Genetics*, 108(11):2195–2204.
- [Hosamani and Muralidhara, 2013] Hosamani, R. and Muralidhara (2013). Acute exposure of drosophila melanogaster to paraquat causes oxidative stress and mitochondrial dysfunction. *Archives of insect biochemistry and physiology*, 83(1):25–40.
- [Hosios and Vander Heiden, 2018] Hosios, A. M. and Vander Heiden, M. G. (2018). The redox requirements of proliferating mammalian cells. *Journal of Biological Chemistry*, 293(20):7490–7498.
- [Hotta and Benzer, 1972] Hotta, Y. and Benzer, S. (1972). Mapping of behaviour in drosophila mosaics. *Drosophila mosaics*.
- [Hou, 2010] Hou, Y. (2010). Cca addition to trna: implications for trna quality control. *IUBMB life*, 62(4):251–260.
- [Hsieh et al., 2009] Hsieh, L.-C., Lin, S.-I., Shih, A. C.-C., Chen, J.-W., Lin, W.-Y., Tseng, C.-Y., Li, W.-H., and Chiou, T.-J. (2009). Uncovering small rna-mediated responses to phosphate deficiency in arabidopsis by deep sequencing. *Plant physiology*, 151(4):2120–2132.
- [Huang et al., 2018] Huang, H., Weng, H., Sun, W., Qin, X., Shi, H., Wu, H., Zhao, B. S., Mesquita, A., Liu, C., and Yuan, C. L. (2018). Recognition of rna n 6-methyladenosine by igf2bp proteins enhances mrna stability and translation. *Nature cell biology*, 20(3):285–295.
- [Huang et al., 1998] Huang, L., Ku, J., Pookanjanatavip, M., Gu, X., Wang, D., Greene, P. J., and Santi, D. V. (1998). Identification of two escherichia coli pseudouridine synthases that show multisite specificity for 23s rna. *Biochemistry*, 37(45):15951–15957.
- [Huang et al., 2006] Huang, Y., Bayfield, M. A., Intine, R. V., and Maraia, R. J. (2006). Separate rna-binding surfaces on the multifunctional la protein mediate distinguishable activities in trna maturation. *Nature structural & molecular biology*, 13(7):611–618.
- [Huang et al., 2005] Huang, Y., Intine, R. V., Mozlin, A., Hasson, S., and Maraia, R. J. (2005). Mutations in the rna polymerase iii subunit rpc11p that decrease rna 3' cleavage activity increase 3'-terminal oligo (u) length and la-dependent trna processing. *Molecular and Cellular Biology*, 25(2):621–636.
- [Hudson et al., 2013] Hudson, G. A., Bloomingdale, R. J., and Znosko, B. M. (2013). Thermodynamic contribution and nearest-neighbor parameters of pseudouridine-adenosine base pairs in oligoribonucleotides. *Rna*, 19(11):1474–1482.
- [Huet and Sentenac, 1992] Huet, J. and Sentenac, A. (1992). The tata-binding protein participates in tftiib assembly on trna genes. *Nucleic acids research*, 20(24):6451–6454.
- [Hussain et al., 2013] Hussain, S., Sajini, A. A., Blanco, S., Dietmann, S., Lombard, P., Sugimoto, Y., Paramor, M., Gleeson, J. G., Odom, D. T., and Ule, J. (2013). Nsun2-mediated cytosine-5 methylation of vault noncoding rna determines its processing into regulatory small rnas. *Cell reports*, 4(2):255–261.

- [Inbal et al., 1995] Inbal, A., Avissar, N., Shaklai, M., Kuritzky, A., Schejter, A., Ben-David, E., Shanske, S., and Garty, B.-Z. (1995). Myopathy, lactic acidosis, and sideroblastic anemia: A new syndrome. *American Journal of Medical Genetics*, 55(3):372–378.
- [Inglis et al., 2019] Inglis, A. J., Masson, G. R., Shao, S., Perisic, O., McLaughlin, S. H., Hegde, R. S., and Williams, R. L. (2019). Activation of *gcn2* by the ribosomal p-stalk. *Proceedings of the National Academy of Sciences*, 116(11):4946–4954.
- [Intine et al., 2000] Intine, R. V. A., Sakulich, A. L., Koduru, S. B., Huang, Y., Pierstorff, E., Goodier, J. L., Phan, L., and Maraia, R. J. (2000). Control of transfer rna maturation by phosphorylation of the human la antigen on serine 366. *Molecular cell*, 6(2):339–348.
- [Ishimura et al., 2016] Ishimura, R., Nagy, G., Dotu, I., Chuang, J. H., and Ackerman, S. L. (2016). Activation of *gcn2* kinase by ribosome stalling links translation elongation with translation initiation. *Elife*, 5:e14295.
- [Ito et al., 2014] Ito, S., Horikawa, S., Suzuki, T., Kawauchi, H., Tanaka, Y., Suzuki, T., and Suzuki, T. (2014). Human *nat10* is an atp-dependent rna acetyltransferase responsible for n4-acetylcytidine formation in 18 s ribosomal rna (rrna). *Journal of Biological Chemistry*, 289(52):35724–35730.
- [Ivanov et al., 2011] Ivanov, P., Emara, M. M., Villen, J., Gygi, S. P., and Anderson, P. (2011). Angiogenin-induced trna fragments inhibit translation initiation. *Molecular cell*, 43(4):613–623.
- [Iyer et al., 2013] Iyer, E. P. R., Iyer, S. C., Sullivan, L., Wang, D., Meduri, R., Graybeal, L. L., and Cox, D. N. (2013). Functional genomic analyses of two morphologically distinct classes of drosophila sensory neurons: post-mitotic roles of transcription factors in dendritic patterning. *PLoS one*, 8(8):e72434.
- [Jaberi et al., 2016] Jaberi, E., Rohani, M., Shahidi, G. A., Nafissi, S., Arefian, E., Soleimani, M., Rasooli, P., Ahmadi, H., Daftarian, N., and Carrami, E. M. (2016). Identification of mutation in *gtpbp2* in patients of a family with neurodegeneration accompanied by iron deposition in the brain. *Neurobiology of Aging*, 38:216. e11–216. e18.
- [Jackman and Alfonzo, 2013] Jackman, J. E. and Alfonzo, J. D. (2013). Transfer rna modifications: nature’s combinatorial chemistry playground. *Wiley Interdisciplinary Reviews: RNA*, 4(1):35–48.
- [Jacob et al., 2019] Jacob, D., Thüring, K., Galliot, A., Marchand, V., Galvanin, A., Ciftci, A., Scharmann, K., Stock, M., Roignant, J., and Leidel, S. A. (2019). Absolute quantification of noncoding rna by microscale thermophoresis. *Angewandte Chemie International Edition*, 58(28):9565–9569.
- [Jana et al., 2017] Jana, S., Hsieh, A. C., and Gupta, R. (2017). Reciprocal amplification of caspase-3 activity by nuclear export of a putative human rna-modifying protein, *pus10* during trail-induced apoptosis. *Cell Death & Disease*, 8(10):e3093–e3093.
- [Jansson et al., 2021] Jansson, M. D., Häfner, S. J., Altinel, K., Tehler, D., Krogh, N., Jakobsen, E., Andersen, J. V., Andersen, K. L., Schoof, E. M., Ménard, P., Nielsen, H., and Lund, A. H. (2021). Regulation of translation by site-specific ribosomal RNA methylation. *Nature Structural & Molecular Biology*, 28(11):889–899.

- [Ji et al., 2020] Ji, P., Ding, D., Qin, N., Wang, C., Zhu, M., Li, Y., Dai, J., Jin, G., Hu, Z., and Shen, H. (2020). Systematic analyses of genetic variants in chromatin interaction regions identified four novel lung cancer susceptibility loci. *Journal of Cancer*, 11(5):1075.
- [Ji et al., 2015] Ji, X., Dadon, D. B., Abraham, B. J., Lee, T. I., Jaenisch, R., Bradner, J. E., and Young, R. A. (2015). Chromatin proteomic profiling reveals novel proteins associated with histone-marked genomic regions. *Proceedings of the National Academy of Sciences*, 112(12):3841–3846.
- [Jia et al., 2011] Jia, G., Fu, Y. E., Zhao, X. U., Dai, Q., Zheng, G., Yang, Y., Yi, C., Lindahl, T., Pan, T., and Yang, Y.-G. (2011). N⁶-methyladenosine in nuclear rna is a major substrate of the obesity-associated fto. *Nature chemical biology*, 7(12):885–887.
- [Jia et al., 2022] Jia, Z., Meng, F., Chen, H., Zhu, G., Li, X., He, Y., Zhang, L., He, X., Zhan, H., and Chen, M. (2022). Human trub1 is a highly conserved pseudouridine synthase responsible for the formation of Ψ55 in mitochondrial trnaasn, trnagln, trnaglu and trnapro. *Nucleic Acids Research*, 50(16):9368–9381.
- [Jiang et al., 2015] Jiang, J., Kharel, D. N., and Chow, C. S. (2015). Modulation of conformational changes in helix 69 mutants by pseudouridine modifications. *Biophysical chemistry*, 200:48–55.
- [Johnson et al., 2009] Johnson, O., Becnel, J., and Nichols, C. (2009). Serotonin 5-HT₂ and 5-HT_{1a}-like receptors differentially modulate aggressive behaviors in drosophila melanogaster. *Neuroscience*, 158(4):1292–1300.
- [Johnston et al., 1980] Johnston, H. M., Barnes, W. M., Chumley, F. G., Bossi, L., and Roth, J. R. (1980). Model for regulation of the histidine operon of salmonella. *Proceedings of the National Academy of Sciences*, 77(1):508–512.
- [Joiner et al., 2006] Joiner, W. J., Crocker, A., White, B. H., and Sehgal, A. (2006). Sleep in drosophila is regulated by adult mushroom bodies. *Nature*, 441(7094):757–760.
- [Jorjani et al., 2016] Jorjani, H., Kehr, S., Jedlinski, D. J., Gumienny, R., Hertel, J., Stadler, P. F., Zavolan, M., and Gruber, A. R. (2016). An updated human snornaome. *Nucleic acids research*, 44(11):5068–5082.
- [Jullien, 1998] Jullien, D. (1998). *Clonage et caracterisation de nouvelles proteines at hook chez les mamiferes et la drosophile. Etude du gene de la paps synthetase de la drosophile: un nouveau marqueur des glandes salivaires*. PhD thesis, Toulouse 3.
- [Jurica et al., 2004] Jurica, M. S., Sousa, D., Moore, M. J., and Grigorieff, N. (2004). Three-dimensional structure of c complex spliceosomes by electron microscopy. *Nature structural & molecular biology*, 11(3):265–269.
- [Jády and Kiss, 2001] Jády, B. E. and Kiss, T. (2001). A small nucleolar guide rna functions both in 2'-o-ribose methylation and pseudouridylation of the u5 spliceosomal rna. *The EMBO journal*, 20(3):541–551.
- [Jöchl et al., 2008] Jöchl, C., Rederstorff, M., Hertel, J., Stadler, P. F., Hofacker, I. L., Schrettl, M., Haas, H., and Hüttenhofer, A. (2008). Small ncna transcriptome analysis from aspergillus fumigatus suggests a novel mechanism for regulation of protein synthesis. *Nucleic acids research*, 36(8):2677–2689.

- [Kadaba et al., 2004] Kadaba, S., Krueger, A., Trice, T., Krecic, A. M., Hinnebusch, A. G., and Anderson, J. (2004). Nuclear surveillance and degradation of hypomodified initiator trnamet in *s. cerevisiae*. *Genes & development*, 18(11):1227–1240.
- [Kadaba et al., 2006] Kadaba, S., Wang, X., and Anderson, J. T. (2006). Nuclear rna surveillance in *saccharomyces cerevisiae*: Trf4p-dependent polyadenylation of nascent hypomethylated trna and an aberrant form of 5s rrna. *Rna*, 12(3):508–521.
- [Kammen et al., 1988] Kammen, H. O., Marvel, C. C., Hardy, L., and Penhoet, E. E. (1988). Purification, structure, and properties of *escherichia coli* trna pseudouridine synthase i. *Journal of Biological Chemistry*, 263(5):2255–2263.
- [Kamma et al., 2010] Kamminga, L. M., Luteijn, M. J., Den Broeder, M. J., Redl, S., Kaaij, L. J. T., Roovers, E. F., Ladurner, P., Berezikov, E., and Ketting, R. F. (2010). Hen1 is required for oocyte development and pirna stability in zebrafish. *The EMBO journal*, 29(21):3688–3700.
- [Kanellopoulos et al., 2020] Kanellopoulos, A. K., Mariano, V., Spinazzi, M., Woo, Y. J., McLean, C., Pech, U., Li, K. W., Armstrong, J. D., Giangrande, A., Callaerts, P., Smit, A. B., Abrahams, B. S., Fiala, A., Achsel, T., and Bagni, C. (2020). Aralar sequesters GABA into hyperactive mitochondria, causing social behavior deficits. *Cell*, 180(6):1178–1197.e20.
- [Kang et al., 2017] Kang, M.-J., Vasudevan, D., Kang, K., Kim, K., Park, J.-E., Zhang, N., Zeng, X., Neubert, T. A., Marr, M. T., and Ryoo, H. D. (2017). 4e-bp is a target of the *gcn2-atf4* pathway during *drosophila* development and aging. *Journal of Cell Biology*, 216(1):115–129.
- [Karaca et al., 2014] Karaca, E., Weitzer, S., Pehlivan, D., Shiraishi, H., Gogakos, T., Hanada, T., Jhangiani, S. N., Wiszniewski, W., Withers, M., and Campbell, I. M. (2014). Human *clp1* mutations alter trna biogenesis, affecting both peripheral and central nervous system function. *Cell*, 157(3):636–650.
- [Karijolich and Yu, 2011] Karijolich, J. and Yu, Y.-T. (2011). Converting nonsense codons into sense codons by targeted pseudouridylation. *Nature*, 474(7351):395–398.
- [Karousi et al., 2019] Karousi, P., Katsaraki, K., Papageorgiou, S. G., Pappa, V., Scorilas, A., and Kontos, C. K. (2019). Identification of a novel trna-derived rna fragment exhibiting high prognostic potential in chronic lymphocytic leukemia. *Hematological oncology*, 37(4):498–504.
- [Karunatilaka and Rueda, 2014] Karunatilaka, K. S. and Rueda, D. (2014). Post-transcriptional modifications modulate conformational dynamics in human u2–u6 snrna complex. *RNA*, 20(1):16–23.
- [Kassavetis et al., 1990] Kassavetis, G. A., Braun, B. R., Nguyen, L. H., and Geiduschek, E. P. (1990). *S. cerevisiae* *tffiib* is the transcription initiation factor proper of rna polymerase iii, while *tffiia* and *tffiic* are assembly factors. *Cell*, 60(2):235–245.
- [Kassavetis et al., 1995] Kassavetis, G. A., Nguyen, S. T., Kobayashi, R., KuMAR, A. S. H. O. K., Geiduschek, E. P., and Pisano, M. (1995). Cloning, expression, and function of *tfc5*, the gene encoding the

REFERENCES

- b" component of the *saccharomyces cerevisiae* rna polymerase iii transcription factor tftiib. *Proceedings of the National Academy of Sciences*, 92(21):9786–9790.
- [Kaya and Ofengand, 2003] Kaya, Y. and Ofengand, J. (2003). A novel unanticipated type of pseudouridine synthase with homologs in bacteria, archaea, and eukarya. *Rna*, 9(6):711–721.
- [Keffer-Wilkes et al., 2016] Keffer-Wilkes, L. C., Veerareddygar, G. R., and Kothe, U. (2016). Rna modification enzyme trub is a trna chaperone. *Proceedings of the National Academy of Sciences*, 113(50):14306–14311.
- [Kellner et al., 2014] Kellner, S., Ochel, A., Thüring, K., Spenkuch, F., Neumann, J., Sharma, S., Entian, K.-D., Schneider, D., and Helm, M. (2014). Absolute and relative quantification of rna modifications via biosynthetic isotopomers. *Nucleic acids research*, 42(18):e142–e142.
- [Kessler et al., 2018] Kessler, A. C., Silveira d’Almeida, G., and Alfonzo, J. D. (2018). The role of intracellular compartmentalization on trna processing and modification. *RNA biology*, 15(4-5):554–566.
- [Khan et al., 2012] Khan, M. A., Rafiq, M. A., Noor, A., Hussain, S., Flores, J. V., Rupp, V., Vincent, A. K., Malli, R., Ali, G., and Khan, F. S. (2012). Mutation in *nsun2*, which encodes an rna methyltransferase, causes autosomal-recessive intellectual disability. *The American Journal of Human Genetics*, 90(5):856–863.
- [Khoddami et al., 2019] Khoddami, V., Yerra, A., Mosbrugger, T. L., Fleming, A. M., Burrows, C. J., and Cairns, B. R. (2019). Transcriptome-wide profiling of multiple rna modifications simultaneously at single-base resolution. *Proceedings of the National Academy of Sciences*, 116(14):6784–6789.
- [Kierzek et al., 2014] Kierzek, E., Malgowska, M., Lisowiec, J., Turner, D. H., Gdaniec, Z., and Kierzek, R. (2014). The contribution of pseudouridine to stabilities and structure of rnas. *Nucleic acids research*, 42(5):3492–3501.
- [Kietrys et al., 2017] Kietrys, A. M., Velema, W. A., and Kool, E. T. (2017). Fingerprints of modified rna bases from deep sequencing profiles. *Journal of the American Chemical Society*, 139(47):17074–17081. PMID: 29111692.
- [Kim et al., 2017] Kim, H. K., Fuchs, G., Wang, S., Wei, W., Zhang, Y., Park, H., Roy-Chaudhuri, B., Li, P., Xu, J., and Chu, K. (2017). A transfer-rna-derived small rna regulates ribosome biogenesis. *Nature*, 552(7683):57–62.
- [Kim et al., 2019] Kim, H. K., Xu, J., Chu, K., Park, H., Jang, H., Li, P., Valdmanis, P. N., Zhang, Q. C., and Kay, M. A. (2019). A trna-derived small rna regulates ribosomal protein s28 protein levels after translation initiation in humans and mice. *Cell reports*, 29(12):3816–3824. e4.
- [Kim et al., 1974] Kim, S. H., Suddath, F. L., Quigley, G. J., McPherson, A., Sussman, J. L., Wang, A. H. J., Seeman, N. C., and Rich, A. (1974). Three-dimensional tertiary structure of yeast phenylalanine transfer rna. *Science*, 185(4149):435–440.

- [Kirino et al., 2004] Kirino, Y., Yasukawa, T., Ohta, S., Akira, S., Ishihara, K., Watanabe, K., and Suzuki, T. (2004). Codon-specific translational defect caused by a wobble modification deficiency in mutant trna from a human mitochondrial disease. *Proceedings of the National Academy of Sciences*, 101(42):15070–15075.
- [Kiss et al., 2004] Kiss, A. M., Jády, B. E., Bertrand, E., and Kiss, T. (2004). Human box h/aca pseudouridylation guide rna machinery. *Molecular and cellular biology*, 24(13):5797–5807.
- [Kiss-Laszlo et al., 1998] Kiss-Laszlo, Z., Henry, Y., and Kiss, T. (1998). Sequence and structural elements of methylation guide snornas essential for site-specific ribose methylation of pre-rrna. *The EMBO journal*, 17(3):797–807.
- [Kiss-László et al., 1996] Kiss-László, Z., Henry, Y., Bachellerie, J.-P., Caizergues-Ferrer, M., and Kiss, T. (1996). Site-specific ribose methylation of preribosomal rna: a novel function for small nucleolar rnas. *Cell*, 85(7):1077–1088.
- [Kleta et al., 2003] Kleta, R., Aughton, D. J., Rivkin, M. J., Huizing, M., Strovel, E., Anikster, Y., Orvisky, E., Natowicz, M., Krasnewich, D., and Gahl, W. A. (2003). Biochemical and molecular analyses of infantile free sialic acid storage disease in north american children. *American Journal of Medical Genetics*, 120A(1):28–33.
- [Knapp and Sun, 2017] Knapp, E. and Sun, J. (2017). Steroid signaling in mature follicles is important for drosophila ovulation. *Proceedings of the National Academy of Sciences*, 114(4):699–704.
- [Kolev and Steitz, 2006] Kolev, N. G. and Steitz, J. A. (2006). In vivo assembly of functional u7 snrnp requires rna backbone flexibility within the sm-binding site. *Nature structural & molecular biology*, 13(4):347–353.
- [Komara et al., 2015] Komara, M., Al-Shamsi, A. M., Ben-Salem, S., Ali, B. R., and Al-Gazali, L. (2015). A novel single-nucleotide deletion (c. 1020delA) in nsun2 causes intellectual disability in an emirati child. *Journal of Molecular Neuroscience*, 57:393–399.
- [Kondo and Ueda, 2013] Kondo, S. and Ueda, R. (2013). Highly improved gene targeting by germline-specific cas9 expression in drosophila. *Genetics*, 195(3):715–721.
- [Kondo et al., 2015] Kondo, Y., Oubridge, C., van Roon, A.-M. M., and Nagai, K. (2015). Crystal structure of human u1 snrnp, a small nuclear ribonucleoprotein particle, reveals the mechanism of 5' splice site recognition. *elife*, 4:e04986.
- [Koonin, 1996] Koonin, E. V. (1996). Pseudouridine synthases: four families of enzymes containing a putative uridine-binding motif also conserved in dutpases and dctp deaminases. *Nucleic acids research*, 24(12):2411–2415.
- [Koonin et al., 2003] Koonin, E. V., Galperin, M. Y., Koonin, E. V., and Galperin, M. Y. (2003). Genomics: From phage to human. *Sequence—Evolution—Function: Computational Approaches in Comparative Genomics*, pages 3–24.

- [Kotelawala et al., 2008] Kotelawala, L., Grayhack, E. J., and Phizicky, E. M. (2008). Identification of yeast trna um44 2'-o-methyltransferase (trm44) and demonstration of a trm44 role in sustaining levels of specific trnasec species. *Rna*, 14(1):158–169.
- [Kowalak et al., 1993] Kowalak, J. A., Pomerantz, S. C., Crain, P. F., and McCloskey, J. A. (1993). A novel method for the determination of posttranscriptional modification in rna by mass spectrometry. *Nucleic Acids Research*, 21(19):4577–4585.
- [Kozak, 1983] Kozak, M. (1983). Comparison of initiation of protein synthesis in procaryotes, eucaryotes, and organelles. *Microbiological reviews*, 47(1):1–45.
- [Kravitz and de la Paz Fernandez, 2015] Kravitz, E. A. and de la Paz Fernandez, M. (2015). Aggression in drosophila. *Behavioral Neuroscience*, 129(5):549–563.
- [Krol et al., 1981] Krol, A., Gallinaro, H., Lazar, E., Jacob, M., and Branlant, C. (1981). The nuclear 5s rnas from chicken, rat and man. us rnas are encoded by multiple genes. *Nucleic Acids Research*, 9(4):769–787.
- [Kulak et al., 2014] Kulak, N. A., Pichler, G., Paron, I., Nagaraj, N., and Mann, M. (2014). Minimal, encapsulated proteomic-sample processing applied to copy-number estimation in eukaryotic cells. *Nature methods*, 11(3):319–324.
- [Kumar et al., 2014] Kumar, P., Anaya, J., Mudunuri, S. B., and Dutta, A. (2014). Meta-analysis of trna derived rna fragments reveals that they are evolutionarily conserved and associate with ago proteins to recognize specific rna targets. *BMC biology*, 12(1):1–14.
- [Kumar et al., 2015] Kumar, P., Mudunuri, S. B., Anaya, J., and Dutta, A. (2015). trfdb: a database for transfer rna fragments. *Nucleic acids research*, 43(D1):D141–D145.
- [Kumar and Suthar, 2013] Kumar, S. and Suthar, R. (2013). Dyskeratosis congenita. *JK Science*, 15(2):56.
- [Kunzmann et al., 1998] Kunzmann, A., Brennicke, A., and Marchfelder, A. (1998). 5' end maturation and rna editing have to precede trna 3' processing in plant mitochondria. *Proceedings of the National Academy of Sciences*, 95(1):108–113.
- [Kuo et al., 2019] Kuo, M. E., Theil, A. F., Kievit, A., Malicdan, M. C., Introne, W. J., Christian, T., Verheijen, F. W., Smith, D. E. C., Mendes, M. I., and Hussaarts-Odijk, L. (2019). Cysteinyln-trna synthetase mutations cause a multi-system, recessive disease that includes microcephaly, developmental delay, and brittle hair and nails. *The American Journal of Human Genetics*, 104(3):520–529.
- [Kurimoto et al., 2020] Kurimoto, R., Chiba, T., Ito, Y., Matsushima, T., Yano, Y., Miyata, K., Yashiro, Y., Suzuki, T., Tomita, K., and Asahara, H. (2020). The trna pseudouridine synthase trub1 regulates the maturation of let-7 mirna. *The EMBO Journal*, 39(20):e104708.
- [Kuscu et al., 2018] Kuscu, C., Kumar, P., Kiran, M., Su, Z., Malik, A., and Dutta, A. (2018). trna fragments (trfs) guide ago to regulate gene expression post-transcriptionally in a dicer-independent manner. *Rna*, 24(8):1093–1105.

- [LaCava et al., 2005] LaCava, J., Houseley, J., Saveanu, C., Petfalski, E., Thompson, E., Jacquier, A., and Tollervey, D. (2005). Rna degradation by the exosome is promoted by a nuclear polyadenylation complex. *Cell*, 121(5):713–724.
- [Laguesse et al., 2015] Laguesse, S., Creppe, C., Nedialkova, D. D., Prevot, P.-P., Borgs, L., Huysseune, S., Franco, B., Duysens, G., Krusy, N., and Lee, G. (2015). A dynamic unfolded protein response contributes to the control of cortical neurogenesis. *Developmental cell*, 35(5):553–567.
- [Lai et al., 2016] Lai, K., Luo, C., Zhang, X., Ye, P., Zhang, Y., He, J., and Yao, K. (2016). Regulation of angiogenin expression and epithelial-mesenchymal transition by hif-1 α signaling in hypoxic retinal pigment epithelial cells. *Biochimica et Biophysica Acta (BBA)-Molecular Basis of Disease*, 1862(9):1594–1607.
- [Lan et al., 2023] Lan, C., Huang, X., Liao, X., Zhou, X., Peng, K., Wei, Y., Han, C., Peng, T., Wang, J., and Zhu, G. (2023). Pus1 may be a potential prognostic biomarker and therapeutic target for hepatocellular carcinoma. *Pharmacogenomics and Personalized Medicine*, pages 337–355.
- [Lassar et al., 1983] Lassar, A. B., Martin, P. L., and Roeder, R. G. (1983). Transcription of class iii genes: formation of preinitiation complexes. *Science*, 222(4625):740–748.
- [Lecointe et al., 2002] Lecointe, F., Namy, O., Hatin, I., Simos, G., Rousset, J.-P., and Grosjean, H. (2002). Lack of pseudouridine 38/39 in the anticodon arm of yeast cytoplasmic trna decreases in vivo recoding efficiency. *Journal of Biological Chemistry*, 277(34):30445–30453.
- [Lecointe et al., 1998] Lecointe, F., Simos, G., Sauer, A., Hurt, E. C., Motorin, Y., and Grosjean, H. (1998). Characterization of yeast protein deg1 as pseudouridine synthase (pus3) catalyzing the formation of Ψ 38 and Ψ 39 in trna anticodon loop*. *Journal of Biological Chemistry*, 273(3):1316–1323.
- [Lee et al., 2007] Lee, S. H., Kim, I., and Chung, B. C. (2007). Increased urinary level of oxidized nucleosides in patients with mild-to-moderate alzheimer’s disease. *Clinical biochemistry*, 40(13-14):936–938.
- [Lee and Collins, 2005] Lee, S. R. and Collins, K. (2005). Starvation-induced cleavage of the trna anticodon loop in tetrahymena thermophila. *Journal of Biological Chemistry*, 280(52):42744–42749.
- [Lee and Luo, 2001] Lee, T. and Luo, L. (2001). Mosaic analysis with a repressible cell marker (MARCM) for drosophila neural development. *Trends in Neurosciences*, 24(5):251–254.
- [Lence et al., 2016] Lence, T., Akhtar, J., Bayer, M., Schmid, K., Spindler, L., Ho, C. H., Kreim, N., Andrade-Navarro, M. A., Poeck, B., Helm, M., and Roignant, J.-Y. (2016). m6a modulates neuronal functions and sex determination in drosophila. *Nature*, 540(7632):242–247.
- [Leng and Strauss, 1996] Leng, S. and Strauss, R. (1996). A new walking impaired drosophila mutant has a structural defect in the protocerebral bridge of the central complex. In *24th Göttingen Neurobiology Conference: Brain and Evolution*, page 134. Thieme.
- [Levin and Hartman, 1963] Levin, A. P. and Hartman, P. E. (1963). Action of a histidine analogue, 1, 2, 4-triazole-3-alanine, in salmonella typhimurium. *Journal of Bacteriology*, 86(4):820–828.

- [Li et al., 2023] Li, L., Zhu, C., Xu, S., Xu, Q., Xu, D., Gan, S., Cui, X., and Tang, C. (2023). PUS1 is a novel biomarker for evaluating malignancy of human renal cell carcinoma. *Ageing*.
- [Li et al., 2018] Li, M., Zhao, X., Wang, W., Shi, H., Pan, Q., Lu, Z., Perez, S. P., Suganthan, R., He, C., and Bjørås, M. (2018). Ythdf2-mediated m⁶a mrna clearance modulates neural development in mice. *Genome biology*, 19:1–16.
- [Li et al., 2017a] Li, Q., Li, X., Tang, H., Jiang, B., Dou, Y., Gorospe, M., and Wang, W. (2017a). Nsun2-mediated m⁵c methylation and mettl3/mettl14-mediated m⁶a methylation cooperatively enhance p21 translation. *Journal of cellular biochemistry*, 118(9):2587–2598.
- [Li and Hu, 2012] Li, S. and Hu, G. (2012). Emerging role of angiogenin in stress response and cell survival under adverse conditions. *Journal of cellular physiology*, 227(7):2822–2826.
- [Li et al., 2016a] Li, X., Ma, S., and Yi, C. (2016a). Pseudouridine: the fifth RNA nucleotide with renewed interests. *Current Opinion in Chemical Biology*, 33:108–116.
- [Li et al., 2016b] Li, X., Xiong, X., Wang, K., Wang, L., Shu, X., Ma, S., and Yi, C. (2016b). Transcriptome-wide mapping reveals reversible and dynamic n¹-methyladenosine methylome. *Nature chemical biology*, 12(5):311–316.
- [Li et al., 2017b] Li, X., Xiong, X., Zhang, M., Wang, K., Chen, Y., Zhou, J., Mao, Y., Lv, J., Yi, D., and Chen, X.-W. (2017b). Base-resolution mapping reveals distinct m¹a methylome in nuclear-and mitochondrial-encoded transcripts. *Molecular cell*, 68(5):993–1005. e9.
- [Li et al., 2015] Li, X., Zhu, P., Ma, S., Song, J., Bai, J., Sun, F., and Yi, C. (2015). Chemical pulldown reveals dynamic pseudouridylation of the mammalian transcriptome. *Nature Chemical Biology*, 11(8):592–597.
- [Li et al., 2008] Li, Y., Luo, J., Zhou, H., Liao, J.-Y., Ma, L.-M., Chen, Y.-Q., and Qu, L.-H. (2008). Stress-induced trna-derived rnas: a novel class of small rnas in the primitive eukaryote giardia lamblia. *Nucleic acids research*, 36(19):6048–6055.
- [Li et al., 2002] Li, Z., Reimers, S., Pandit, S., and Deutscher, M. P. (2002). Rna quality control: degradation of defective transfer rna. *The EMBO journal*, 21(5):1132–1138.
- [Li-Byarlay et al., 2014] Li-Byarlay, H., Rittschof, C. C., Massey, J. H., Pittendrigh, B. R., and Robinson, G. E. (2014). Socially responsive effects of brain oxidative metabolism on aggression. *Proceedings of the National Academy of Sciences*, 111(34):12533–12537.
- [Liang and Li, 2011] Liang, B. and Li, H. (2011). Structures of ribonucleoprotein particle modification enzymes. *Quarterly reviews of biophysics*, 44(1):95–122.
- [Liang et al., 2009] Liang, X.-h., Liu, Q., and Fournier, M. J. (2009). Loss of rrna modifications in the decoding center of the ribosome impairs translation and strongly delays pre-rrna processing. *Rna*, 15(9):1716–1728.

- [Liang et al., 2019] Liang, Z.-H., Jia, Y.-B., Li, Z.-R., Li, M., Wang, M.-L., Yun, Y.-L., Yu, L.-J., Shi, L., and Zhu, R.-X. (2019). Urinary biomarkers for diagnosing poststroke depression in patients with type 2 diabetes mellitus. *Diabetes, Metabolic Syndrome and Obesity: Targets and Therapy*, pages 1379–1386.
- [Linder et al., 2015] Linder, B., Grozhik, A. V., Olarerin-George, A. O., Meydan, C., Mason, C. E., and Jaffrey, S. R. (2015). Single-nucleotide-resolution mapping of m6a and m6am throughout the transcriptome. *Nature methods*, 12(8):767–772.
- [LIPOWSKY et al., 1999] LIPOWSKY, G. E. R. D., BISCHOFF, F. R. A. L. F., IZAURRALDE, E. L. I. S. A., KUTAY, U. L. R. I. K. E., SCHAEFER, S. T. E. F. A. N., GROSS, H. J., BEIER, H. I. L. D. B. U. R. G., and GOERLICH, D. I. R. K. (1999). Coordination of trna nuclear export with processing of trna. *Rna*, 5(4):539–549.
- [Liu et al., 1999] Liu, L., Wolf, R., Ernst, R., and Heisenberg, M. (1999). Context generalization in drosophila visual learning requires the mushroom bodies. *Nature*, 400(6746):753–756.
- [Liu et al., 2015] Liu, N., Dai, Q., Zheng, G., He, C., Parisien, M., and Pan, T. (2015). N 6-methyladenosine-dependent rna structural switches regulate rna–protein interactions. *Nature*, 518(7540):560–564.
- [Liu et al., 2013] Liu, N., Parisien, M., Dai, Q., Zheng, G., He, C., and Pan, T. (2013). Probing n6-methyladenosine rna modification status at single nucleotide resolution in mrna and long noncoding rna. *Rna*, 19(12):1848–1856.
- [Long et al., 2016] Long, T., Li, J., Li, H., Zhou, M., Zhou, X.-L., Liu, R.-J., and Wang, E.-D. (2016). Sequence-specific and shape-selective rna recognition by the human rna 5-methylcytosine methyltransferase nsun6. *Journal of Biological Chemistry*, 291(46):24293–24303.
- [Lorenz et al., 2017] Lorenz, C., Lünse, C. E., and Mörl, M. (2017). trna modifications: impact on structure and thermal adaptation. *Biomolecules*, 7(2):35.
- [Lovejoy et al., 2014] Lovejoy, A. F., Riordan, D. P., and Brown, P. O. (2014). Transcriptome-wide mapping of pseudouridines: Pseudouridine synthases modify specific mRNAs in *s. cerevisiae*. *PLoS ONE*, 9(10):e110799.
- [Lu et al., 2015] Lu, Z., Filonov, G. S., Noto, J. J., Schmidt, C. A., Hatkevich, T. L., Wen, Y., Jaffrey, S. R., and Matera, A. G. (2015). Metazoan trna introns generate stable circular rnas in vivo. *Rna*, 21(9):1554–1565.
- [Lubas et al., 2011] Lubas, M., Christensen, M. S., Kristiansen, M. S., Domanski, M., Falkenby, L. G., Lykke-Andersen, S., Andersen, J. S., Dziembowski, A., and Jensen, T. H. (2011). Interaction profiling identifies the human nuclear exosome targeting complex. *Molecular cell*, 43(4):624–637.
- [Luengo et al., 2021] Luengo, A., Li, Z., Gui, D. Y., Sullivan, L. B., Zagorulya, M., Do, B. T., Ferreira, R., Naamati, A., Ali, A., and Lewis, C. A. (2021). Increased demand for nad⁺ relative to atp drives aerobic glycolysis. *Molecular cell*, 81(4):691–707. e6.

- [Luo et al., 2003] Luo, S., Baumeister, P., Yang, S., Abcouwer, S. F., and Lee, A. S. (2003). Induction of grp78/bip by translational block: activation of the grp78 promoter by atf4 through an upstream atf/cre site independent of the endoplasmic reticulum stress elements. *Journal of Biological Chemistry*, 278(39):37375–37385.
- [Luo et al., 2019] Luo, Y., Chen, J.-J., Lv, Q., Qin, J., Huang, Y.-Z., Yu, M.-H., and Zhong, M. (2019). Long non-coding rna neat1 promotes colorectal cancer progression by competitively binding mir-34a with sirt1 and enhancing the wnt/ β -catenin signaling pathway. *Cancer letters*, 440:11–22.
- [López et al., 2017] López, I., Tournillon, A.-S., Prado Martins, R., Karakostis, K., Malbert-Colas, L., Nylander, K., and Fåhræus, R. (2017). p53-mediated suppression of bip triggers bik-induced apoptosis during prolonged endoplasmic reticulum stress. *Cell Death & Differentiation*, 24(10):1717–1729.
- [Ma et al., 2018] Ma, C., Chang, M., Lv, H., Zhang, Z.-W., Zhang, W., He, X., Wu, G., Zhao, S., Zhang, Y., and Wang, D. (2018). Rna m6a methylation participates in regulation of postnatal development of the mouse cerebellum. *Genome biology*, 19:1–18.
- [Ma et al., 2019] Ma, H., Wang, X., Cai, J., Dai, Q., Natchiar, S. K., Lv, R., Chen, K., Lu, Z., Chen, H., and Shi, Y. G. (2019). N 6-methyladenosine methyltransferase zcchc4 mediates ribosomal rna methylation. *Nature chemical biology*, 15(1):88–94.
- [Ma et al., 2005] Ma, X., Yang, C., Alexandrov, A., Grayhack, E. J., Behm-Ansmant, I., and Yu, Y. (2005). Pseudouridylation of yeast u2 snrna is catalyzed by either an rna-guided or rna-independent mechanism. *The EMBO journal*, 24(13):2403–2413.
- [Ma et al., 2003] Ma, X., Zhao, X., and Yu, Y.-T. (2003). Pseudouridylation (Ψ) of u2 snrna in *s. cerevisiae* is catalyzed by an rna-independent mechanism. *The EMBO journal*, 22(8):1889–1897.
- [Maden, 2001] Maden, B. E. H. (2001). Mapping 2-o'-methyl groups in ribosomal rna. *Methods*, 25(3):374–382.
- [Maden et al., 1995] Maden, B. E. H., Corbett, M. E., Heeney, P. A., Pugh, K., and Ajuh, P. M. (1995). Classical and novel approaches to the detection and localization of the numerous modified nucleotides in eukaryotic ribosomal rna. *Biochimie*, 77(1-2):22–29.
- [Madison, 1968] Madison, J. T. (1968). Primary structure of rna. *Annual review of biochemistry*, 37(1):131–148.
- [Maraia and Lamichhane, 2011] Maraia, R. J. and Lamichhane, T. N. (2011). 3' processing of eukaryotic precursor trnas. *Wiley Interdisciplinary Reviews: RNA*, 2(3):362–375.
- [Marchfelder et al., 1996] Marchfelder, A., Brennicke, A., and Binder, S. (1996). Rna editing is required for efficient excision of trnaphe from precursors in plant mitochondria. *Journal of Biological Chemistry*, 271(4):1898–1903.
- [Marechal-Drouard et al., 1996] Marechal-Drouard, L., Cosset, A., Remacle, C., Ramamonjisoa, D., and Dietrich, A. (1996). A single editing event is a prerequisite for efficient processing of potato mitochondrial phenylalanine trna. *Molecular and cellular biology*, 16(7):3504–3510.

- [Marnef et al., 2014] Marnef, A., Richard, P., Pinzon, N., and Kiss, T. (2014). Targeting vertebrate intron-encoded box c/d 2'-o-methylation guide rnas into the cajal body. *Nucleic acids research*, 42(10):6616–6629.
- [Martin et al., 1998] Martin, J.-R., Ernst, R., and Heisenberg, M. (1998). Mushroom bodies suppress locomotor activity in drosophila melanogaster. *Learning & Memory*, 5(1):179–191.
- [Martin et al., 1999] Martin, J.-R., Raabe, T., and Heisenberg, M. (1999). Central complex substructures are required for the maintenance of locomotor activity in drosophila melanogaster. *Journal of Comparative Physiology A*, 185:277–288.
- [Martinez et al., 2012] Martinez, F. J., Lee, J. H., Lee, J. E., Blanco, S., Nickerson, E., Gabriel, S., Frye, M., Al-Gazali, L., and Gleeson, J. G. (2012). Whole exome sequencing identifies a splicing mutation in nsun2 as a cause of a dubowitz-like syndrome. *Journal of medical genetics*, 49(6):380–385.
- [Martinez et al., 2022] Martinez, N. M., Su, A., Burns, M. C., Nussbacher, J. K., Schaening, C., Sathe, S., Yeo, G. W., and Gilbert, W. V. (2022). Pseudouridine synthases modify human pre-mRNA co-transcriptionally and affect pre-mRNA processing. *Molecular Cell*, 82(3):645–659.e9.
- [Marz et al., 2011] Marz, M., Gruber, A. R., Höner zu Siederdisen, C., Amman, F., Badelt, S., Bartschat, S., Bernhart, S. H., Beyer, W., Kehr, S., and Lorenz, R. (2011). Animal snornas and scarnas with exceptional structures. *RNA biology*, 8(6):938–946.
- [Massenet et al., 1999] Massenet, S., Motorin, Y., Lafontaine, D. L. J., Hurt, E. C., Grosjean, H., and Branlant, C. (1999). Pseudouridine mapping in the saccharomyces cerevisiae spliceosomal u small nuclear rnas (snrnas) reveals that pseudouridine synthase pus1p exhibits a dual substrate specificity for u2 snrna and trna. *Molecular and cellular biology*, 19(3):2142–2154.
- [Massenet et al., 1998] Massenet, S., Mouglin, A., and Branlant, C. (1998). Posttranscriptional modifications in the u small nuclear rnas. *Modification and Editing of RNA*, pages 201–227.
- [Mathur et al., 2021] Mathur, L., Jung, S., Jang, C., and Lee, G. (2021). Quantitative analysis of m6a rna modification by lc-ms. *STAR protocols*, 2(3):100724.
- [Maute et al., 2013] Maute, R. L., Schneider, C., Sumazin, P., Holmes, A., Califano, A., Basso, K., and Dalla-Favera, R. (2013). trna-derived microrna modulates proliferation and the dna damage response and is down-regulated in b cell lymphoma. *Proceedings of the National Academy of Sciences*, 110(4):1404–1409.
- [McCown et al., 2020] McCown, P. J., Ruzkowska, A., Kunkler, C. N., Breger, K., Hulewicz, J. P., Wang, M. C., Springer, N. A., and Brown, J. A. (2020). Naturally occurring modified ribonucleosides. *Wiley Interdisciplinary Reviews: RNA*, 11(5):e1595.
- [McDermott and Davis, 2013] McDermott, S. M. and Davis, I. (2013). Drosophila hephaestus/polypyrimidine tract binding protein is required for dorso-ventral patterning and regulation of signalling between the germline and soma. *PLoS ONE*, 8(7):e69978.
- [McDermott et al., 2012] McDermott, S. M., Meignin, C., Rappsilber, J., and Davis, I. (2012). Drosophila syncrip binds the gurken mrna localisation signal and regulates localised transcripts during axis specification. *Biology Open*, 1(5):488–497.

- [Medina et al., 2020] Medina, J., van der Velpen, V., Teav, T., Guitton, Y., Gallart-Ayala, H., and Ivanisevic, J. (2020). Single-step extraction coupled with targeted HILIC-MS/MS approach for comprehensive analysis of human plasma lipidome and polar metabolome. *Metabolites*, 10(12):495.
- [Meier et al., 2020] Meier, F., Brunner, A.-D., Frank, M., Ha, A., Bludau, I., Voytik, E., Kaspar-Schoenefeld, S., Lubeck, M., Raether, O., and Bache, N. (2020). diapasef: parallel accumulation–serial fragmentation combined with data-independent acquisition. *Nature methods*, 17(12):1229–1236.
- [Meier et al., 2018] Meier, F., Brunner, A.-D., Koch, S., Koch, H., Lubeck, M., Krause, M., Goedecke, N., Decker, J., Kosinski, T., and Park, M. A. (2018). Online parallel accumulation–serial fragmentation (pasef) with a novel trapped ion mobility mass spectrometer. *Molecular & Cellular Proteomics*, 17(12):2534–2545.
- [Mendel et al., 2018] Mendel, M., Chen, K.-M., Homolka, D., Gos, P., Pandey, R. R., McCarthy, A. A., and Pillai, R. S. (2018). Methylation of structured rna by the m6a writer mettl16 is essential for mouse embryonic development. *Molecular cell*, 71(6):986–1000. e11.
- [Mendonsa et al., 2021] Mendonsa, S., von Kuegelgen, N., Bujanic, L., and Chekulaeva, M. (2021). Charcot–marie–tooth mutation in glycyl-trna synthetase stalls ribosomes in a pre-accommodation state and activates integrated stress response. *Nucleic Acids Research*, 49(17):10007–10017.
- [Meroueh et al., 2000] Meroueh, M., Grohar, P. J., Qiu, J., SantaLucia Jr, J., Scaringe, S. A., and Chow, C. S. (2000). Unique structural and stabilizing roles for the individual pseudouridine residues in the 1920 region of escherichia coli 23s rrna. *Nucleic acids research*, 28(10):2075–2083.
- [Messmer et al., 2009] Messmer, M., Gaudry, A., Sissler, M., and Florentz, C. (2009). Pathology-related mutation a7526g (a9g) helps in the understanding of the 3d structural core of human mitochondrial trnaasp. *RNA*, 15(8):1462–1468.
- [Metodiev et al., 2015] Metodiev, M. D., Assouline, Z., Landrieu, P., Chretien, D., Bader-Meunier, B., Guitton, C., Munnich, A., and Rötig, A. (2015). Unusual clinical expression and long survival of a pseudouridylate synthase (pus1) mutation into adulthood. *European Journal of Human Genetics*, 23(6):880–882.
- [Meydan and Guydosh, 2020] Meydan, S. and Guydosh, N. R. (2020). Disome and trisome profiling reveal genome-wide targets of ribosome quality control. *Molecular cell*, 79(4):588–602. e6.
- [Meyer et al., 2015] Meyer, K. D., Patil, D. P., Zhou, J., Zinoviev, A., Skabkin, M. A., Elemento, O., Pestova, T. V., Qian, S.-B., and Jaffrey, S. R. (2015). 5' utr m6a promotes cap-independent translation. *Cell*, 163(4):999–1010.
- [Meyer et al., 2012] Meyer, K. D., Saletore, Y., Zumbo, P., Elemento, O., Mason, C. E., and Jaffrey, S. R. (2012). Comprehensive analysis of mrna methylation reveals enrichment in 3' utrs and near stop codons. *Cell*, 149(7):1635–1646.
- [Moazed and Noller, 1989] Moazed, D. and Noller, H. F. (1989). Interaction of trna with 23s rrna in the ribosomal a, p, and e sites. *Cell*, 57(4):585–597.

- [Moazed et al., 1986] Moazed, D., Stern, S., and Noller, H. F. (1986). Rapid chemical probing of conformation in 16 s ribosomal rna and 30 s ribosomal subunits using primer extension. *Journal of molecular biology*, 187(3):399–416.
- [Mohl et al., 2023] Mohl, D. A., Lagies, S., Zodel, K., Zumkeller, M., Peighambari, A., Ganner, A., Platner, D. A., Neumann-Haefelin, E., Adlesic, M., and Frew, I. J. (2023). Integrated metabolomic and transcriptomic analysis of modified nucleosides for biomarker discovery in clear cell renal cell carcinoma. *Cells*, 12(8):1102.
- [Moortgat et al., 2016] Moortgat, S., Désir, J., Benoit, V., Boulanger, S., Pendeville, H., Nassogne, M., Lederer, D., and Maystadt, I. (2016). Two novel eif2s3 mutations associated with syndromic intellectual disability with severe microcephaly, growth retardation, and epilepsy. *American journal of medical genetics Part A*, 170(11):2927–2933.
- [Morais et al., 2021] Morais, P., Adachi, H., and Yu, Y.-T. (2021). Spliceosomal snrna epitranscriptomics. *Frontiers in Genetics*, 12:652129.
- [Moritsch et al., 2022] Moritsch, S., Mödl, B., Scharf, I., Janker, L., Zwolanek, D., Timelthaler, G., Casanova, E., Sibia, M., Mohr, T., and Kenner, L. (2022). Tyk2 is a tumor suppressor in colorectal cancer. *Oncoimmunology*, 11(1):2127271.
- [Morse et al., 2005] Morse, R. P., Kleta, R., Alroy, J., and Gahl, W. A. (2005). Novel form of intermediate salla disease: Clinical and neuroimaging features. *Journal of Child Neurology*, 20(10):814–816.
- [Motley et al., 2011] Motley, W. W., Seburn, K. L., Nawaz, M. H., Miers, K. E., Cheng, J., Antonellis, A., Green, E. D., Talbot, K., Yang, X.-L., and Fischbeck, K. H. (2011). Charcot-marie-tooth–linked mutant gars is toxic to peripheral neurons independent of wild-type gars levels. *PLoS genetics*, 7(12):e1002399.
- [Motorin et al., 1998] Motorin, Y., Keith, G., Simon, C., Foiret, D., Simos, G., Hurt, E., and Grosjean, H. (1998). The yeast trna: pseudouridine synthase pus1p displays a multisite substrate specificity. *Rna*, 4(7):856–869.
- [Motorin et al., 2007] Motorin, Y., Muller, S., Behm-Ansmant, I., and Branlant, C. (2007). Identification of modified residues in rnas by reverse transcription-based methods. *Methods in enzymology*, 425:21–53.
- [Muda et al., 2023] Muda, A., Malerba, L., Giordano, L., Fazzi, E., and Accorsi, P. (2023). A pus7 gene pathogenic variant causing self-injurious behavior, sleep disturbances, and developmental delay: A case report. *American Journal of Medical Genetics Part A*.
- [Mukhopadhyay et al., 2021] Mukhopadhyay, S., Deogharia, M., and Gupta, R. (2021). Mammalian nuclear trub1, mitochondrial trub2, and cytoplasmic pus10 produce conserved pseudouridine 55 in different sets of trna. *RNA*, 27(1):66–79.
- [Muramatsu et al., 1988] Muramatsu, T., Nishikawa, K., Nemoto, F., Kuchino, Y., Nishimura, S., Miyazawa, T., and Yokoyama, S. (1988). Codon and amino-acid specificities of a transfer rna are both converted by a single post-transcriptional modification. *Nature*, 336(6195):179–181.

- [Murata and Wharton, 1995] Murata, Y. and Wharton, R. P. (1995). Binding of pumilio to maternal hunchback mRNA is required for posterior patterning in drosophila embryos. *Cell*, 80(5):747–756.
- [Méndez-Lucas et al., 2014] Méndez-Lucas, A., Hyroššová, P., Novellademunt, L., Viñals, F., and Perales, J. C. (2014). Mitochondrial phosphoenolpyruvate carboxykinase (pepck-m) is a pro-survival, endoplasmic reticulum (er) stress response gene involved in tumor cell adaptation to nutrient availability. *Journal of Biological Chemistry*, 289(32):22090–22102.
- [Nachtergaele and He, 2017] Nachtergaele, S. and He, C. (2017). The emerging biology of rna post-transcriptional modifications. *RNA biology*, 14(2):156–163.
- [Nagaike et al., 2001] Nagaike, T., Suzuki, T., Tomari, Y., Takemoto-Hori, C., Negayama, F., Watanabe, K., and Ueda, T. (2001). Identification and characterization of mammalian mitochondrial trna nucleotidyl-transferases. *Journal of Biological Chemistry*, 276(43):40041–40049.
- [Nanda et al., 1974] Nanda, R. K., Tewari, R., Govil, G., and Smith, I. C. P. (1974). The conformation of β -pseudouridine about the glycosidic bond as studied by 1h homonuclear overhauser measurements and molecular orbital calculations. *Canadian Journal of Chemistry*, 52(3):371–375.
- [Naseer et al., 2020] Naseer, M. I., Abdulkareem, A. A., Jan, M. M., Chaudhary, A. G., Alharazy, S., and AlQahtani, M. H. (2020). Next generation sequencing reveals novel homozygous frameshift in PUS7 and splice acceptor variants in AASS gene leading to intellectual disability, developmental delay, dysmorphic feature and microcephaly. *Saudi Journal of Biological Sciences*, 27(11):3125–3131.
- [Natchiar et al., 2017] Natchiar, S. K., Myasnikov, A. G., Kratzat, H., Hazemann, I., and Klaholz, B. P. (2017). Visualization of chemical modifications in the human 80s ribosome structure. *Nature*, 551(7681):472–477.
- [Neuman-Silberberg and Schüpbach, 1993] Neuman-Silberberg, F. S. and Schüpbach, T. (1993). The drosophila dorsoventral patterning gene gurken produces a dorsally localized rna and encodes a $\text{tgf}\alpha$ -like protein. *Cell*, 75(1):165–174.
- [Neuser et al., 2008] Neuser, K., Triphan, T., Mronz, M., Poeck, B., and Strauss, R. (2008). Analysis of a spatial orientation memory in drosophila. *Nature*, 453(7199):1244–1247.
- [Newby and Greenbaum, 2001] Newby, M. I. and Greenbaum, N. L. (2001). A conserved pseudouridine modification in eukaryotic u2 snrna induces a change in branch-site architecture. *Rna*, 7(6):833–845.
- [Newby and Greenbaum, 2002] Newby, M. I. and Greenbaum, N. L. (2002). Sculpting of the spliceosomal branch site recognition motif by a conserved pseudouridine. *Nature Structural Biology*, 9(12):958–965.
- [Newman and Norman, 1992] Newman, A. J. and Norman, C. (1992). U5 snrna interacts with exon sequences at 5' and 3' splice sites. *Cell*, 68(4):743–754.
- [Nguyen et al., 2015] Nguyen, D., St-Sauveur, V. G., Bergeron, D., Dupuis-Sandoval, F., Scott, M. S., and Bachand, F. (2015). A polyadenylation-dependent 3' end maturation pathway is required for the synthesis of the human telomerase rna. *Cell reports*, 13(10):2244–2257.

- [Nguyen et al., 2020] Nguyen, T. T. M., Murakami, Y., Mobilio, S., Niceta, M., Zampino, G., Philippe, C., Moutton, S., Zaki, M. S., James, K. N., Musaev, D., Mu, W., Baranano, K., Nance, J. R., Rosenfeld, J. A., Braverman, N., Ciolfi, A., Millan, F., Person, R. E., Bruel, A.-L., Thauvin-Robinet, C., Ververi, A., DeVile, C., Male, A., Efthymiou, S., Maroofian, R., Houlden, H., Maqbool, S., Rahman, F., Baratang, N. V., Rousseau, J., St-Denis, A., Elrick, M. J., Anselm, I., Rodan, L. H., Tartaglia, M., Gleeson, J., Kinoshita, T., and Campeau, P. M. (2020). Bi-allelic variants in the GPI transamidase subunit PIGK cause a neurodevelopmental syndrome with hypotonia, cerebellar atrophy, and epilepsy. *The American Journal of Human Genetics*, 106(4):484–495.
- [Nie et al., 2022] Nie, F., Tang, Q., Liu, Y., Qin, H., Liu, S., Wu, M., Feng, P., and Chen, W. (2022). Rname: A comprehensive database of rna modification enzymes. *Computational and Structural Biotechnology Journal*, 20:6244–6249.
- [Niehues et al., 2015] Niehues, S., Bussmann, J., Steffes, G., Erdmann, I., Köhrer, C., Sun, L., Wagner, M., Schäfer, K., Wang, G., and Koerdt, S. N. (2015). Impaired protein translation in drosophila models for charcot–marie–tooth neuropathy caused by mutant trna synthetases. *Nature communications*, 6(1):7520.
- [Nielsen et al., 2013] Nielsen, S., Yuzenkova, Y., and Zenkin, N. (2013). Mechanism of eukaryotic rna polymerase iii transcription termination. *Science*, 340(6140):1577–1580.
- [Nishikura and De Robertis, 1981] Nishikura, K. and De Robertis, E. M. (1981). Rna processing in microinjected xenopus oocytes: sequential addition of base modifications in a spliced transfer rna. *Journal of molecular biology*, 145(2):405–420.
- [Nøstvik et al., 2021] Nøstvik, M., Kateta, S. M., Schönewolf-Greulich, B., Afenjar, A., Barth, M., Boschann, F., Doummar, D., Haack, T. B., Keren, B., Livshits, L. A., Mei, D., Park, J., Pisano, T., Prouteau, C., Umair, M., Waqas, A., Ziegler, A., Guerrini, R., Møller, R. S., and Tümer, Z. (2021). Clinical and molecular delineation of pus3-associated neurodevelopmental disorders. *Clinical Genetics*, 100(5):628–633.
- [Nurse et al., 1995] Nurse, K. E. L. V. I. N., Wrzesinski, J., Bakin, A. N. D. R. E. Y., Lane, B. G., and Ofengand, J. A. M. E. S. (1995). Purification, cloning, and properties of the trna psi 55 synthase from escherichia coli. *Rna*, 1(1):102.
- [O’Connor and Dahlberg, 1995] O’Connor, M. and Dahlberg, A. E. (1995). The involvement of two distinct regions of 23 s ribosomal rna in trna selection. *Journal of molecular biology*, 254(5):838–847.
- [Olvedy et al., 2016] Olvedy, M., Scaravilli, M., Hoogstrate, Y., Visakorpi, T., Jenster, G., and Martens, E. S. (2016). A comprehensive repertoire of trna-derived fragments in prostate cancer. *Oncotarget*, 7(17):24766.
- [Oncul et al., 2021] Oncul, U., Unal-Ince, E., Kuloglu, Z., Teber-Tiras, S., Kaygusuz, G., and Eminoglu, F. T. (2021). A novel pus1 mutation in 2 siblings with mlas syndrome: a review of the literature. *Journal of Pediatric Hematology/Oncology*, 43(4):e592–e595.

- [Ozanick et al., 2009] Ozanick, S. G., Wang, X., Costanzo, M., Brost, R. L., Boone, C., and Anderson, J. T. (2009). Rex1p deficiency leads to accumulation of precursor initiator trnmet and polyadenylation of substrate rnas in *saccharomyces cerevisiae*. *Nucleic acids research*, 37(1):298–308.
- [Pan et al., 2009] Pan, Y., Zhou, Y., Guo, C., Gong, H., Gong, Z., and Liu, L. (2009). Differential roles of the fan-shaped body and the ellipsoid body in *drosophila* visual pattern memory. *Learning & Memory*, 16(5):289–295.
- [Pandey et al., 2019] Pandey, A., Harvey, B. M., Lopez, M. F., Ito, A., Haltiwanger, R. S., and Jafar-Nejad, H. (2019). Glycosylation of specific notch egf repeats by o-fut1 and fringe regulates notch signaling in *drosophila*. *Cell reports*, 29(7):2054–2066. e6.
- [Patton et al., 2005] Patton, J. R., Bykhovskaya, Y., Mengesha, E., Bertolotto, C., and Fischel-Ghodsian, N. (2005). Mitochondrial myopathy and sideroblastic anemia (mlasa): missense mutation in the pseudouridine synthase 1 (pus1) gene is associated with the loss of trna pseudouridylation. *Journal of Biological Chemistry*, 280(20):19823–19828.
- [Paushkin et al., 2004] Paushkin, S. V., Patel, M., Furia, B. S., Peltz, S. W., and Trotta, C. R. (2004). Identification of a human endonuclease complex reveals a link between trna splicing and pre-mrna 3' end formation. *Cell*, 117(3):311–321.
- [Payea et al., 2020] Payea, M. J., Hauke, A. C., De Zoysa, T., and Phizicky, E. M. (2020). Mutations in the anticodon stem of trna cause accumulation and met22-dependent decay of pre-trna in yeast. *RNA*, 26(1):29–43.
- [Pendleton et al., 2017] Pendleton, K. E., Chen, B., Liu, K., Hunter, O. V., Xie, Y., Tu, B. P., and Conrad, N. K. (2017). The u6 snrna m6a methyltransferase mettl16 regulates sam synthetase intron retention. *Cell*, 169(5):824–835. e14.
- [Pereira et al., 2010] Pereira, E. R., Liao, N., Neale, G. A., and Hendershot, L. M. (2010). Transcriptional and post-transcriptional regulation of proangiogenic factors by the unfolded protein response. *PloS one*, 5(9):e12521.
- [Pereira et al., 2018] Pereira, M., Francisco, S., Varanda, A. S., Santos, M., Santos, M. A. S., and Soares, A. R. (2018). Impact of trna modifications and trna-modifying enzymes on proteostasis and human disease. *International journal of molecular sciences*, 19(12):3738.
- [Perlman and Volpe, 2018] Perlman, J. M. and Volpe, J. J. (2018). Organic acids. In *Volpe's Neurology of the Newborn*, pages 793–820.e4. Elsevier.
- [Perry and Kelley, 1974] Perry, R. P. and Kelley, D. E. (1974). Existence of methylated messenger rna in mouse l cells. *Cell*, 1(1):37–42.
- [Persson et al., 1992] Persson, B. C., Gustafsson, C., Berg, D. E., and Björk, G. R. (1992). The gene for a trna modifying enzyme, m5u54-methyltransferase, is essential for viability in *escherichia coli*. *Proceedings of the National Academy of Sciences*, 89(9):3995–3998.

- [Pielage et al., 2002] Pielage, J., Steffes, G., Lau, D. C., Parente, B. A., Crews, S. T., Strauss, R., and Klämbt, C. (2002). Novel behavioral and developmental defects associated with drosophila single-minded. *Developmental Biology*, 249(2):283–299.
- [Pinto et al., 2020] Pinto, R., Vågbø, C. B., Jakobsson, M. E., Kim, Y., Baltissen, M. P., O’Donohue, M.-F., Guzmán, U. H., Małecki, J. M., Wu, J., and Kirpekar, F. (2020). The human methyltransferase zcchc4 catalyses n 6-methyladenosine modification of 28s ribosomal rna. *Nucleic acids research*, 48(2):830–846.
- [Pliszka et al., 1994] Pliszka, S. R., Maas, J. W., Javors, M. A., Rogeness, G. A., and Baker, J. (1994). Urinary catecholamines in attention-deficit hyperactivity disorder with and without comorbid anxiety. *Journal of the American Academy of Child and Adolescent Psychiatry*, 33(8):1165–1173.
- [Plotkin et al., 2004] Plotkin, J. B., Robins, H., and Levine, A. J. (2004). Tissue-specific codon usage and the expression of human genes. *Proceedings of the National Academy of Sciences*, 101(34):12588–12591.
- [Polikanov et al., 2015] Polikanov, Y. S., Melnikov, S. V., Söll, D., and Steitz, T. A. (2015). Structural insights into the role of rna modifications in protein synthesis and ribosome assembly. *Nature structural & molecular biology*, 22(4):342–344.
- [Popow et al., 2011] Popow, J., Englert, M., Weitzer, S., Schleiffer, A., Mierzwa, B., Mechtler, K., Trowitzsch, S., Will, C. L., Lührmann, R., and Söll, D. (2011). Hspc117 is the essential subunit of a human trna splicing ligase complex. *Science*, 331(6018):760–764.
- [Popow et al., 2014] Popow, J., Jurkin, J., Schleiffer, A., and Martinez, J. (2014). Analysis of orthologous groups reveals archease and ddx1 as trna splicing factors. *Nature*, 511(7507):104–107.
- [Potapov et al., 2018] Potapov, V., Fu, X., Dai, N., Corrêa, I. R. J., Tanner, N. A., and Ong, J. L. (2018). Base modifications affecting rna polymerase and reverse transcriptase fidelity. *Nucleic acids research*, 46:5753–5763.
- [Powell et al., 2014] Powell, J. B., Dokal, I., Carr, R., Taibjee, S., Cave, B., and Moss, C. (2014). X-linked dyskeratosis congenita presenting in adulthood with photodamaged skin and epiphora. *Clinical and Experimental Dermatology*, 39(3):310–314.
- [Purchal et al., 2022] Purchal, M. K., Eyler, D. E., Tardu, M., Franco, M. K., Korn, M. M., Khan, T., McNassor, R., Giles, R., Lev, K., and Sharma, H. (2022). Pseudouridine synthase 7 is an opportunistic enzyme that binds and modifies substrates with diverse sequences and structures. *Proceedings of the National Academy of Sciences*, 119(4):e2109708119.
- [Puri et al., 2014] Puri, P., Wetzell, C., Saffert, P., Gaston, K. W., Russell, S. P., Cordero Varela, J. A., van der Vlies, P., Zhang, G., Limbach, P. A., and Ignatova, Z. (2014). Systematic identification of trnaome and its dynamics in *lactococcus lactis*. *Molecular microbiology*, 93(5):944–956.
- [Query et al., 1997] Query, C. C., McCaw, P. S., and Sharp, P. A. (1997). A minimal spliceosomal complex recognizes the branch site and polypyrimidine tract. *Molecular and cellular biology*, 17(5):2944–2953.
- [Ragunathan and Guthrie, 1998] Ragunathan, P. L. and Guthrie, C. (1998). Rna unwinding in u4/u6 snrnps requires atp hydrolysis and the deih-box splicing factor brr2. *Current biology*, 8(15):847–855.

- [Ravn et al., 2001] Ravn, K., Wibrand, F., Hansen, F. J., Horn, N., Rosenberg, T., and Schwartz, M. (2001). An mtdna mutation, 14453g→ a, in the nadh dehydrogenase subunit 6 associated with severe melas syndrome. *European Journal of Human Genetics*, 9(10):805–809.
- [Rayaprolu et al., 2012] Rayaprolu, S., Soto-Ortolaza, A., Rademakers, R., Uitti, R. J., Wszolek, Z. K., and Ross, O. A. (2012). Angiotensin variation and parkinson’s disease. *Annals of neurology*, 71(5):725.
- [Raychaudhuri et al., 1998] Raychaudhuri, S., Conrad, J., Hall, B. G., and Ofengand, J. (1998). A pseudouridine synthase required for the formation of two universally conserved pseudouridines in ribosomal rna is essential for normal growth of escherichia coli. *Rna*, 4(11):1407–1417.
- [Raychaudhuri et al., 1999] Raychaudhuri, S., Niu, L., Conrad, J., Lane, B. G., and Ofengand, J. (1999). Functional effect of deletion and mutation of the escherichia coli ribosomal rna and trna pseudouridine synthase rlua. *Journal of Biological Chemistry*, 274(27):18880–18886.
- [Razavi et al., 2020] Razavi, A. C., Bazzano, L. A., He, J., Li, S., Fernandez, C., Whelton, S. P., Krousel-Wood, M., Nierenberg, J. L., Shi, M., and Li, C. (2020). Pseudouridine and n-formylmethionine associate with left ventricular mass index: metabolome-wide association analysis of cardiac remodeling. *Journal of molecular and cellular cardiology*, 140:22–29.
- [Reddy et al., 1988] Reddy, R., Busch, H., and Birnstiel, M. L. (1988). Structure and function of major and minor small nuclear ribonucleoprotein particles. *Small Nuclear RNAs: RNA Sequences, Structure and Modifications*, pages 1–38.
- [Reis and Campbell, 2007] Reis, C. C. and Campbell, J. L. (2007). Contribution of trf4/5 and the nuclear exosome to genome stability through regulation of histone mrna levels in saccharomyces cerevisiae. *Genetics*, 175(3):993–1010.
- [Richard et al., 2003] Richard, P., Darzacq, X., Bertrand, E., Jády, B. E., Verheggen, C., and Kiss, T. (2003). A common sequence motif determines the cajal body-specific localization of box h/aca scarnas. *The EMBO journal*, 22(16):4283–4293.
- [Richter and Lasko, 2011] Richter, J. D. and Lasko, P. (2011). Translational control in oocyte development. *Cold Spring Harbor perspectives in biology*, 3(9):a002758.
- [Richter et al., 2018] Richter, U., Evans, M. E., Clark, W. C., Marttinen, P., Shoubbridge, E. A., Suomalainen, A., Wredenberg, A., Wedell, A., Pan, T., and Battersby, B. J. (2018). Rna modification landscape of the human mitochondrial trna regulates protein synthesis. *Nature communications*, 9(1):3966.
- [Riley et al., 2010] Riley, L. G., Cooper, S., Hickey, P., Rudinger-Thirion, J., McKenzie, M., Compton, A., Lim, S. C., Thorburn, D., Ryan, M. T., Giegé, R., Bahlo, M., and Christodoulou, J. (2010). Mutation of the mitochondrial tyrosyl-tRNA synthetase gene, YARS2, causes myopathy, lactic acidosis, and sideroblastic anemia—MLASA syndrome. *The American Journal of Human Genetics*, 87(1):52–59.
- [Rintala-Dempsey and Kothe, 2017] Rintala-Dempsey, A. and Kothe, U. (2017). Eukaryotic stand-alone pseudouridine synthases - rna modifying enzymes and emerging regulators of gene expression? *RNA Biology*, 14(9):1185–1196.

- [Roca and Krainer, 2009] Roca, X. and Krainer, A. R. (2009). Recognition of atypical 5' splice sites by shifted base-pairing to u1 snrna. *Nature structural & molecular biology*, 16(2):176–182.
- [Rogers and Rogers, 2008] Rogers, S. L. and Rogers, G. C. (2008). Culture of drosophila s2 cells and their use for RNAi-mediated loss-of-function studies and immunofluorescence microscopy. *Nature Protocols*, 3(4):606–611.
- [Ron and Walter, 2007] Ron, D. and Walter, P. (2007). Signal integration in the endoplasmic reticulum unfolded protein response. *Nature reviews Molecular cell biology*, 8(7):519–529.
- [Rossano et al., 2017] Rossano, A. J., Kato, A., Minard, K. I., Romero, M. F., and Macleod, G. T. (2017). Na⁺/h⁺ exchange via the drosophila vesicular glutamate transporter mediates activity-induced acid efflux from presynaptic terminals. *The Journal of physiology*, 595(3):805–824.
- [Rossignol et al., 2020] Rossignol, F., Mew, N. A., Meltzer, M. R., and Gropman, A. L. (2020). Urea cycle disorders. In *Rosenbergs Molecular and Genetic Basis of Neurological and Psychiatric Disease*, pages 827–848. Elsevier.
- [Roth et al., 1966] Roth, J. R., Antón, D. N., and Hartman, P. E. (1966). Histidine regulatory mutants in salmonella typhimurium: I. isolation and general properties. *Journal of Molecular Biology*, 22(2):305–323.
- [Roundtree et al., 2017] Roundtree, I. A., Luo, G.-Z., Zhang, Z., Wang, X., Zhou, T., Cui, Y., Sha, J., Huang, X., Guerrero, L., and Xie, P. (2017). Ythdc1 mediates nuclear export of n6-methyladenosine methylated mrnas. *elife*, 6:e31311.
- [Ruff et al., 1991] Ruff, M., Krishnaswamy, S., Boeglin, M., Poterszman, A., Mitschler, A., Podjarny, A., Rees, B., Thierry, J. C., and Moras, D. (1991). Class ii aminoacyl transfer rna synthetases: crystal structure of yeast aspartyl-trna synthetase complexed with trnaasp. *Science*, 252(5013):1682–1689.
- [Ruiz-Pesini et al., 2007] Ruiz-Pesini, E., Lott, M. T., Procaccio, V., Poole, J. C., Brandon, M. C., Mishmar, D., Yi, C., Kreuziger, J., Baldi, P., and Wallace, D. C. (2007). An enhanced mitomap with a global mtDNA mutational phylogeny. *Nucleic acids research*, 35:D823–D828.
- [Ruskin et al., 1988] Ruskin, B., Zamore, P. D., and Green, M. R. (1988). A factor, u2af, is required for u2 snrnp binding and splicing complex assembly. *Cell*, 52(2):207–219.
- [Rutkowski et al., 2006] Rutkowski, D. T., Arnold, S. M., Miller, C. N., Wu, J., Li, J., Gunnison, K. M., Mori, K., Sadighi Akha, A. A., Raden, D., and Kaufman, R. J. (2006). Adaptation to ER stress is mediated by differential stabilities of pro-survival and pro-apoptotic mrnas and proteins. *PLoS biology*, 4(11):e374.
- [Safra et al., 2017a] Safra, M., Nir, R., Farouq, D., Slutskin, I. V., and Schwartz, S. (2017a). Trub1 is the predominant pseudouridine synthase acting on mammalian mRNA via a predictable and conserved code. *Genome research*, 27(3):393–406.
- [Safra et al., 2017b] Safra, M., Sas-Chen, A., Nir, R., Winkler, R., Nachshon, A., Bar-Yaacov, D., Erlacher, M., Rossmanith, W., Stern-Ginossar, N., and Schwartz, S. (2017b). The m1A landscape on cytosolic and mitochondrial mRNA at single-base resolution. *Nature*, 551(7679):251–255.

- [Saikia et al., 2014] Saikia, M., Jobava, R., Parisien, M., Putnam, A., Krokowski, D., Gao, X.-H., Guan, B.-J., Yuan, Y., Jankowsky, E., and Feng, Z. (2014). Angiogenin-cleaved trna halves interact with cytochrome c, protecting cells from apoptosis during osmotic stress. *Molecular and cellular biology*, 34(13):2450–2463.
- [Saletore et al., 2012] Saletore, Y., Meyer, K., Korlach, J., Vilfan, I. D., Jaffrey, S., and Mason, C. E. (2012). The birth of the epitranscriptome: deciphering the function of rna modifications. *Genome biology*, 13:1–12.
- [Sas-Chen et al., 2020] Sas-Chen, A., Thomas, J. M., Matzov, D., Taoka, M., Nance, K. D., Nir, R., Bryson, K. M., Shachar, R., Liman, G. L. S., and Burkhart, B. W. (2020). Dynamic rna acetylation revealed by quantitative cross-evolutionary mapping. *Nature*, 583(7817):638–643.
- [Savan et al., 2009] Savan, R., Ravichandran, S., Collins, J. R., Sakai, M., and Young, H. A. (2009). Structural conservation of interferon gamma among vertebrates. *Cytokine & growth factor reviews*, 20(2):115–124.
- [Schaefer et al., 2010] Schaefer, M., Pollex, T., Hanna, K., Tuorto, F., Meusburger, M., Helm, M., and Lyko, F. (2010). Rna methylation by dnmt2 protects transfer rnas against stress-induced cleavage. *Genes & development*, 24(15):1590–1595.
- [Schaffer et al., 2014] Schaffer, A. E., Eggens, V. R. C., Caglayan, A. O., Reuter, M. S., Scott, E., Coufal, N. G., Silhavy, J. L., Xue, Y., Kayserili, H., and Yasuno, K. (2014). Clp1 founder mutation links trna splicing and maturation to cerebellar development and neurodegeneration. *Cell*, 157(3):651–663.
- [Schaffer et al., 2019] Schaffer, A. E., Pinkard, O., and Collier, J. M. (2019). trna metabolism and neurodevelopmental disorders. *Annual review of genomics and human genetics*, 20:359–387.
- [Schattner et al., 2006] Schattner, P., Barberan-Soler, S., and Lowe, T. M. (2006). A computational screen for mammalian pseudouridylation guide h/aca rnas. *Rna*, 12(1):15–25.
- [Schattner et al., 2004] Schattner, P., Decatur, W. A., Davis, C. A., Ares Jr, M., Fournier, M. J., and Lowe, T. M. (2004). Genome-wide searching for pseudouridylation guide snornas: analysis of the *saccharomyces cerevisiae* genome. *Nucleic acids research*, 32(14):4281–4296.
- [Schieber and Chandel, 2014] Schieber, M. and Chandel, N. S. (2014). Ros function in redox signaling and oxidative stress. *Current biology*, 24(10):R453–R462.
- [Schmidt et al., 2019] Schmidt, C. A., Giusto, J. D., Bao, A., Hopper, A. K., and Matera, A. G. (2019). Molecular determinants of metazoan tricrna biogenesis. *Nucleic acids research*, 47(12):6452–6465.
- [Schorn et al., 2017] Schorn, A. J., Gutbrod, M. J., LeBlanc, C., and Martienssen, R. (2017). Ltr-retrotransposon control by trna-derived small rnas. *Cell*, 170(1):61–71. e11.
- [Schram, 1998] Schram, K. H. (1998). Urinary nucleosides. *Mass spectrometry reviews*, 17(3):131–251.
- [Schwarcz et al., 2012] Schwarcz, R., Bruno, J. P., Muchowski, P. J., and Wu, H.-Q. (2012). Kynurenines in the mammalian brain: when physiology meets pathology. *Nature Reviews Neuroscience*, 13(7):465–477.

- [Schwartz et al., 2014] Schwartz, S., Bernstein, D. A., Mumbach, M. R., Jovanovic, M., Herbst, R. H., León-Ricardo, B. X., Engreitz, J. M., Guttman, M., Satija, R., Lander, E. S., Fink, G., and Regev, A. (2014). Transcriptome-wide mapping reveals widespread dynamic-regulated pseudouridylation of ncRNA and mRNA. *Cell*, 159(1):148–162.
- [Sekiya et al., 2017] Sekiya, M., Maruko-Otake, A., Hearn, S., Sakakibara, Y., Fujisaki, N., Suzuki, E., Ando, K., and Iijima, K. M. (2017). Edem function in erad protects against chronic er proteinopathy and age-related physiological decline in drosophila. *Developmental cell*, 41(6):652–664. e5.
- [Sekula et al., 2017] Sekula, P., Dettmer, K., Vogl, F. C., Gronwald, W., Ellmann, L., Mohny, R. P., Eckardt, K.-U., Suhre, K., Kastenmüller, G., and Oefner, P. J. (2017). From discovery to translation: characterization of c-mannosyltryptophan and pseudouridine as markers of kidney function. *Scientific Reports*, 7(1):17400.
- [Sekulovski et al., 2021] Sekulovski, S., Devant, P., Panizza, S., Gogakos, T., Pitiriciu, A., Heitmeier, K., Ramsay, E. P., Barth, M., Schmidt, C., and Tuschl, T. (2021). Assembly defects of human trna splicing endonuclease contribute to impaired pre-trna processing in pontocerebellar hypoplasia. *Nature communications*, 12(1):5610.
- [Selmi et al., 2021] Selmi, T., Hussain, S., Dietmann, S., Heiß, M., Borland, K., Flad, S., Carter, J.-M., Dennison, R., Huang, Y.-L., and Kellner, S. (2021). Sequence-and structure-specific cytosine-5 mrna methylation by nsun6. *Nucleic acids research*, 49(2):1006–1022.
- [Seneca et al., 2005] Seneca, S., Goemans, N., Coster, R. V., Givron, P., Reybrouck, T., Sciote, R., Meulemans, A., Smet, J., and Van Hove, J. L. K. (2005). A mitochondrial trna aspartate mutation causing isolated mitochondrial myopathy. *American Journal of Medical Genetics Part A*, 137(2):170–175.
- [Setzer and Brown, 1985] Setzer, D. R. and Brown, D. D. (1985). Formation and stability of the 5 s rna transcription complex. *Journal of Biological Chemistry*, 260(4):2483–2492.
- [Shaheen et al., 2016] Shaheen, R., Han, L., Fageih, E., Ewida, N., Alobeid, E., Phizicky, E. M., and Alkuraya, F. S. (2016). A homozygous truncating mutation in PUS3 expands the role of tRNA modification in normal cognition. *Human Genetics*, 135(7):707–713.
- [Shaheen et al., 2019] Shaheen, R., Tasak, M., Maddirevula, S., Abdel-Salam, G. M. H., Sayed, I. S. M., Alazami, A. M., Al-Sheddi, T., Alobeid, E., Phizicky, E. M., and Alkuraya, F. S. (2019). PUS7 mutations impair pseudouridylation in humans and cause intellectual disability and microcephaly. *Human Genetics*, 138(3):231–239.
- [Sharma et al., 2016] Sharma, U., Conine, C. C., Shea, J. M., Boskovic, A., Derr, A. G., Bing, X. Y., Belleannee, C., Kucukural, A., Serra, R. W., and Sun, F. (2016). Biogenesis and function of trna fragments during sperm maturation and fertilization in mammals. *Science*, 351(6271):391–396.
- [Shatkin, 1976] Shatkin, A. J. (1976). Capping of eucaryotic mRNAs. *Cell*, 9(4):645–653.
- [Shi et al., 2017] Shi, H., Wang, X., Lu, Z., Zhao, B. S., Ma, H., Hsu, P. J., Liu, C., and He, C. (2017). Ythdf3 facilitates translation and decay of m6-methyladenosine-modified rna. *Cell research*, 27(3):315–328.

- [Shi et al., 2019] Shi, H., Wei, J., and He, C. (2019). Where, when, and how: context-dependent functions of rna methylation writers, readers, and erasers. *Molecular cell*, 74(4):640–650.
- [Shigematsu et al., 2018] Shigematsu, M., Kawamura, T., and Kirino, Y. (2018). Generation of 2',3'-cyclic phosphate-containing RNAs as a hidden layer of the transcriptome. *Frontiers in Genetics*, 9.
- [Shimizu et al., 2002] Shimizu, T., Nakagaki, M., Nishi, Y., Kobayashi, Y., Hachimori, A., and Uchiumi, T. (2002). Interaction among silkworm ribosomal proteins p1, p2 and p0 required for functional protein binding to the gtpase-associated domain of 28s rna. *Nucleic acids research*, 30(12):2620–2627.
- [Sibert and Patton, 2012] Sibert, B. S. and Patton, J. R. (2012). Pseudouridine synthase 1: a site-specific synthase without strict sequence recognition requirements. *Nucleic acids research*, 40(5):2107–2118.
- [Siegel et al., 2021] Siegel, D. A., Tonqueze, O. L., Biton, A., Zaitlen, N., and Erle, D. J. (2021). Massively parallel analysis of human 3' UTRs reveals that AU-rich element length and registration predict mRNA destabilization. *G3 Genes|Genomes|Genetics*, 12(1).
- [Simons et al., 1996] Simons, F. H. M., Broers, F. J. M., van Venrooij, W. J., and Pruijn, G. J. M. (1996). Characterization of cis-acting signals for nuclear import and retention of the la (ss-b) autoantigen. *Experimental cell research*, 224(2):224–236.
- [Singer et al., 1972] Singer, C. E., Smith, G. R., Cortese, R., and Ames, B. N. (1972). Mutant trnahis ineffective in repression and lacking two pseudouridine modifications. *Nature New Biology*, 238(81):72–74.
- [Singh et al., 2013] Singh, S. R., Liu, Y., Kango-Singh, M., and Nevo, E. (2013). Genetic, immunofluorescence labeling, and in situ hybridization techniques in identification of stem cells in male and female germline niches. *Stem Cell Niche: Methods and Protocols*, pages 9–23.
- [Sissler et al., 2017] Sissler, M., González-Serrano, L. E., and Westhof, E. (2017). Recent advances in mitochondrial aminoacyl-trna synthetases and disease. *Trends in molecular medicine*, 23(8):693–708.
- [Skorupa et al., 2012] Skorupa, A., King, M. A., Aparicio, I. M., Dussmann, H., Coughlan, K., Breen, B., Kieran, D., Concannon, C. G., Marin, P., and Prehn, J. H. M. (2012). Motoneurons secrete angiogenin to induce rna cleavage in astroglia. *Journal of Neuroscience*, 32(15):5024–5038.
- [Skowronek et al., 2014] Skowronek, E., Grzechnik, P., Späth, B., Marchfelder, A., and Kufel, J. (2014). trna 3' processing in yeast involves trnase z, rex1, and rrp6. *Rna*, 20(1):115–130.
- [Sloan et al., 2017] Sloan, K. E., Warda, A. S., Sharma, S., Entian, K.-D., Lafontaine, D. L. J., and Bohnsack, M. T. (2017). Tuning the ribosome: the influence of rna modification on eukaryotic ribosome biogenesis and function. *RNA biology*, 14(9):1138–1152.
- [Snieckute et al., 2022] Snieckute, G., Genzor, A. V., Vind, A. C., Ryder, L., Stoneley, M., Chamois, S., Dreos, R., Nordgaard, C., Sass, F., and Blasius, M. (2022). Ribosome stalling is a signal for metabolic regulation by the ribotoxic stress response. *Cell Metabolism*, 34(12):2036–2046. e8.

- [Sobala and Hutvagner, 2013] Sobala, A. and Hutvagner, G. (2013). Small rnas derived from the 5' end of trna can inhibit protein translation in human cells. *RNA biology*, 10(4):553–563.
- [Song et al., 2020a] Song, B., Tang, Y., Wei, Z., Liu, G., Su, J., Meng, J., and Chen, K. (2020a). Piano: a web server for pseudouridine-site (Ψ) identification and functional annotation. *Frontiers in genetics*, 11:88.
- [Song et al., 2021] Song, D., Guo, M., Xu, S., Song, X., Bai, B., Li, Z., Chen, J., An, Y., Nie, Y., Wu, K., Wang, S., and Zhao, Q. (2021). HSP90-dependent PUS7 overexpression facilitates the metastasis of colorectal cancer cells by regulating LASP1 abundance. *Journal of Experimental & Clinical Cancer Research*, 40(1).
- [Song et al., 2019] Song, J., Zhuang, Y., Zhu, C., Meng, H., Lu, B., Xie, B., Peng, J., Li, M., and Yi, C. (2019). Differential roles of human PUS10 in miRNA processing and tRNA pseudouridylation. *Nature Chemical Biology*, 16(2):160–169.
- [Song et al., 2023] Song, W., Podicheti, R., Rusch, D. B., and Tracey Jr, W. D. (2023). Transcriptome-wide analysis of pseudouridylation in drosophila melanogaster. *G3*, 13(3):jkac333.
- [Song et al., 2020b] Song, W., Ressler, S., and Tracey, W. D. (2020b). Loss of pseudouridine synthases in the rluA family causes hypersensitive nociception in drosophila. *G3 Genes Genomes Genetics*, 10(12):4425–4438.
- [Song et al., 2010] Song, Y., Willer, J. R., Scherer, P. C., Panzer, J. A., Kugath, A., Skordalakes, E., Gregg, R. G., Willer, G. B., and Balice-Gordon, R. J. (2010). Neural and synaptic defects in slytherin, a zebrafish model for human congenital disorders of glycosylation. *PLoS One*, 5(10):e13743.
- [Sorge et al., 2020] Sorge, S., Theelke, J., Yildirim, K., Hertenstein, H., McMullen, E., Müller, S., Altbürger, C., Schirmeier, S., and Lohmann, I. (2020). Atf4-induced warburg metabolism drives over-proliferation in drosophila. *Cell Reports*, 31(7):107659.
- [Spaulding et al., 2021] Spaulding, E. L., Hines, T. J., Bais, P., Tadenev, A. L. D., Schneider, R., Jewett, D., Pattavina, B., Pratt, S. L., Morelli, K. H., and Stum, M. G. (2021). The integrated stress response contributes to trna synthetase-associated peripheral neuropathy. *Science*, 373(6559):1156–1161.
- [Spriggs et al., 2010] Spriggs, K. A., Bushell, M., and Willis, A. E. (2010). Translational regulation of gene expression during conditions of cell stress. *Molecular cell*, 40(2):228–237.
- [Squires et al., 2012] Squires, J. E., Patel, H. R., Nousch, M., Sibbritt, T., Humphreys, D. T., Parker, B. J., Suter, C. M., and Preiss, T. (2012). Widespread occurrence of 5-methylcytosine in human coding and non-coding rna. *Nucleic acids research*, 40(11):5023–5033.
- [Stadler et al., 2013] Stadler, C., Rexhepaj, E., Singan, V. R., Murphy, R. F., Pepperkok, R., Uhlén, M., Simpson, J. C., and Lundberg, E. (2013). Immunofluorescence and fluorescent-protein tagging show high correlation for protein localization in mammalian cells. *Nature methods*, 10(4):315–323.

REFERENCES

- [Stanik et al., 2018] Stanik, J., Skopkova, M., Stanikova, D., Brennerova, K., Barak, L., Ticha, L., Hornova, J., Klimes, I., and Gasperikova, D. (2018). Neonatal hypoglycemia, early-onset diabetes and hypopituitarism due to the mutation in *eif2s3* gene causing mehm syndrome. *Physiol Res*, 67(2):331–337.
- [Stanley and Vassilenko, 1978] Stanley, J. and Vassilenko, S. (1978). A different approach to rna sequencing. *Nature*, 274(5666):87–89.
- [Stanley, 2007] Stanley, P. (2007). Regulation of notch signaling by glycosylation. *Current opinion in structural biology*, 17(5):530–535.
- [Stefano, 1984] Stefano, J. E. (1984). Purified lupus antigen la recognizes an oligouridylylate stretch common to the 3' termini of rna polymerase iii transcripts. *Cell*, 36(1):145–154.
- [Steidinger et al., 2011] Steidinger, T. U., Standaert, D. G., and Yacoubian, T. A. (2011). A neuroprotective role for angiogenin in models of parkinson's disease. *Journal of neurochemistry*, 116(3):334–341.
- [Stein et al., 2022] Stein, K. C., Morales-Polanco, F., van der Lienden, J., Rainbolt, T. K., and Frydman, J. (2022). Ageing exacerbates ribosome pausing to disrupt cotranslational proteostasis. *Nature*, 601(7894):637–642.
- [Stocker, 1994] Stocker, R. F. (1994). The organization of the chemosensory system in *drosophila melanogaster*: a review. *Cell and tissue research*, 275:3–26.
- [Storkebaum et al., 2009] Storkebaum, E., Leitão-Gonçalves, R., Godenschwege, T., Nangle, L., Mejia, M., Bosmans, I., Ooms, T., Jacobs, A., Van Dijk, P., and Yang, X.-L. (2009). Dominant mutations in the tyrosyl-trna synthetase gene recapitulate in *drosophila* features of human charcot–marie–tooth neuropathy. *Proceedings of the National Academy of Sciences*, 106(28):11782–11787.
- [Strauss and Heisenberg, 1993] Strauss, R. and Heisenberg, M. (1993). A higher control center of locomotor behavior in the *drosophila* brain. *Journal of Neuroscience*, 13(5):1852–1861.
- [Su et al., 2019] Su, Z., Kuscu, C., Malik, A., Shibata, E., and Dutta, A. (2019). Angiogenin generates specific stress-induced trna halves and is not involved in trf-3-mediated gene silencing. *Journal of Biological Chemistry*, 294(45):16930–16941.
- [Sudo et al., 2016] Sudo, H., Nozaki, A., Uno, H., Ishida, Y., and Nagahama, M. (2016). Interaction properties of human tramp-like proteins and their role in pre-rrna 5' ends turnover. *FEBS letters*, 590(17):2963–2972.
- [Sumita et al., 2005] Sumita, M., Desaulniers, J.-P., Chang, Y.-C., Chui, H. M.-P., LAWRENCE, C. L. O. S., and Chow, C. S. (2005). Effects of nucleotide substitution and modification on the stability and structure of helix 69 from 28s rna. *Rna*, 11(9):1420–1429.
- [Suzuki and Hochster, 1966] Suzuki, T. and Hochster, R. M. (1966). On the biosynthesis of pseudouridine and of pseudouridylic acid in *agrobacterium tumefaciens*. *Canadian Journal of Biochemistry*, 44(2):259–272.

- [Suzuki et al., 2020] Suzuki, T., Yashiro, Y., Kikuchi, I., Ishigami, Y., Saito, H., Matsuzawa, I., Okada, S., Mito, M., Iwasaki, S., and Ma, D. (2020). Complete chemical structures of human mitochondrial trnas. *Nature communications*, 11(1):4269.
- [Szkukalek et al., 1995] Szkukalek, A., Myslinski, E., Mougin, A., Luhrmann, R., and Branlant, C. (1995). Phylogenetic conservation of modified nucleotides in the terminal loop 1 of the spliceosomal u5 snrna. *Biochimie*, 77(1-2):16–21.
- [Szweykowska-Kulinska et al., 1994] Szweykowska-Kulinska, Z., Senger, B., Keith, G., Fasiolo, F., and Grosjean, H. (1994). Intron-dependent formation of pseudouridines in the anticodon of *saccharomyces cerevisiae* minor trna (ile). *The EMBO journal*, 13(19):4636–4644.
- [Takaku et al., 2003] Takaku, H., Minagawa, A., Takagi, M., and Nashimoto, M. (2003). A candidate prostate cancer susceptibility gene encodes trna 3' processing endoribonuclease. *Nucleic acids research*, 31(9):2272–2278.
- [Tang et al., 2015] Tang, H., Fan, X., Xing, J., Liu, Z., Jiang, B., Dou, Y., Gorospe, M., and Wang, W. (2015). Nsun2 delays replicative senescence by repressing p27 (kip1) translation and elevating cdk1 translation. *Aging (Albany NY)*, 7(12):1143.
- [Taoka et al., 2018] Taoka, M., Nobe, Y., Yamaki, Y., Sato, K., Ishikawa, H., Izumikawa, K., Yamauchi, Y., Hirota, K., Nakayama, H., and Takahashi, N. (2018). Landscape of the complete rna chemical modifications in the human 80s ribosome. *Nucleic acids research*, 46(18):9289–9298.
- [Tardu et al., 2019] Tardu, M., Jones, J. D., Kennedy, R. T., Lin, Q., and Koutmou, K. S. (2019). Identification and quantification of modified nucleosides in *saccharomyces cerevisiae* mrnas. *ACS chemical biology*, 14(7):1403–1409.
- [Taylor et al., 2014] Taylor, R. W., Pyle, A., Griffin, H., Blakely, E. L., Duff, J., He, L., Smertenko, T., Alston, C. L., Neeve, V. C., and Best, A. (2014). Use of whole-exome sequencing to determine the genetic basis of multiple mitochondrial respiratory chain complex deficiencies. *Jama*, 312(1):68–77.
- [Telford et al., 2009] Telford, J. E., Kilbride, S. M., and Davey, G. P. (2009). Complex i is rate-limiting for oxygen consumption in the nerve terminal. *Journal of Biological Chemistry*, 284(14):9109–9114.
- [Teplova et al., 2006] Teplova, M., Yuan, Y.-R., Phan, A. T., Malinina, L., Ilin, S., Teplov, A., and Patel, D. J. (2006). Structural basis for recognition and sequestration of uuuoh 3' termini of nascent rna polymerase iii transcripts by la, a rheumatic disease autoantigen. *Molecular cell*, 21(1):75–85.
- [Terrey et al., 2020] Terrey, M., Adamson, S. I., Gibson, A. L., Deng, T., Ishimura, R., Chuang, J. H., and Ackerman, S. L. (2020). Gtpbp1 resolves paused ribosomes to maintain neuronal homeostasis. *Elife*, 9:e62731.
- [Tesarova et al., 2018] Tesarova, M., Vondrackova, A., Stufkova, H., Veprekova, L., Stranecky, V., Berankova, K., Hansikova, H., Magner, M., Galoova, N., Honzik, T., Vodickova, E., Stary, J., and Zeman, J. (2018). Sideroblastic anemia associated with multisystem mitochondrial disorders. *Pediatric Blood & Cancer*, 66(4):e27591.

REFERENCES

- [Thompson et al., 2008] Thompson, D. M., Lu, C., Green, P. J., and Parker, R. (2008). trna cleavage is a conserved response to oxidative stress in eukaryotes. *Rna*, 14(10):2095–2103.
- [Thompson and Parker, 2009] Thompson, D. M. and Parker, R. (2009). The rnase rny1p cleaves trnas and promotes cell death during oxidative stress in *saccharomyces cerevisiae*. *Journal of Cell Biology*, 185(1):43–50.
- [Thoms et al., 2015] Thoms, M., Thomson, E., Baßler, J., Gnädig, M., Griesel, S., and Hurt, E. (2015). The exosome is recruited to rna substrates through specific adaptor proteins. *Cell*, 162(5):1029–1038.
- [Torres et al., 2014] Torres, A. G., Batlle, E., and de Poupplana, L. R. (2014). Role of tRNA modifications in human diseases. *Trends in Molecular Medicine*, 20(6):306–314.
- [Tracey et al., 2003] Tracey, W. D., Wilson, R. I., Laurent, G., and Benzer, S. (2003). painless, a drosophila gene essential for nociception. *Cell*, 113(2):261–273.
- [Trakhanov et al., 1987] Trakhanov, S. D., Yusupov, M. M., Agalarov, S. C., Garber, M. B., Ryazantsev, S. N., Tischenko, S. V., and Shirokov, V. A. (1987). Crystallization of 70 s ribosomes and 30 s ribosomal subunits from *thermus thermophilus*. *Febs Letters*, 220(2):319–322.
- [Triphan et al., 2010] Triphan, T., Poeck, B., Neuser, K., and Strauss, R. (2010). Visual targeting of motor actions in climbing drosophila. *Current biology*, 20(7):663–668.
- [Trotta et al., 1997] Trotta, C. R., Miao, F., Arn, E. A., Stevens, S. W., Ho, C. K., Rauhut, R., and Abelson, J. N. (1997). The yeast trna splicing endonuclease: a tetrameric enzyme with two active site subunits homologous to the archaeal trna endonucleases. *Cell*, 89(6):849–858.
- [Tsugawa et al., 2014] Tsugawa, H., Kanazawa, M., Ogiwara, A., and Arita, M. (2014). MRMPROBS suite for metabolomics using large-scale MRM assays. *Bioinformatics*, 30(16):2379–2380.
- [Turvey et al., 2022] Turvey, A. K., Horvath, G. A., and Cavalcanti, A. R. O. (2022). Aminoacyl-trna synthetases in human health and disease. *Frontiers in Physiology*, page 2220.
- [Tyanova et al., 2016] Tyanova, S., Temu, T., Sinitcyn, P., Carlson, A., Hein, M. Y., Geiger, T., Mann, M., and Cox, J. (2016). The perseus computational platform for comprehensive analysis of (prote) omics data. *Nature methods*, 13(9):731–740.
- [Urban et al., 2009] Urban, A., Behm-Ansmant, I., Branlant, C., and Motorin, Y. (2009). Rna sequence and two-dimensional structure features required for efficient substrate modification by the *saccharomyces cerevisiae* rna: Ψ -synthase *pus7p*. *Journal of Biological Chemistry*, 284(9):5845–5858.
- [Vaidyanathan et al., 2017] Vaidyanathan, P. P., AlSadhan, I., Merriman, D. K., Al-Hashimi, H. M., and Herschlag, D. (2017). Pseudouridine and n6-methyladenosine modifications weaken puf protein/rna interactions. *RNA*, 23(5):611–618.
- [van der Feltz et al., 2018] van der Feltz, C., DeHaven, A. C., and Hoskins, A. A. (2018). Stress-induced pseudouridylation alters the structural equilibrium of yeast u2 snRNA stem II. *Journal of Molecular Biology*, 430(4):524–536.

- [van der Werf et al., 2021] van der Werf, J., Chin, C. V., and Fleming, N. I. (2021). Snorna in cancer progression, metastasis and immunotherapy response. *Biology*, 10(8):809.
- [van Dijk et al., 2018] van Dijk, T., Baas, F., Barth, P. G., and Poll-The, B. T. (2018). What’s new in pontocerebellar hypoplasia? an update on genes and subtypes. *Orphanet Journal of Rare Diseases*, 13:1–16.
- [Van Es et al., 2011] Van Es, M. A., Schelhaas, H. J., Van Vught, P. W. J., Ticozzi, N., Andersen, P. M., Groen, E. J. N., Schulte, C., Blauw, H. M., Koppers, M., and Diekstra, F. P. (2011). Angiogenin variants in parkinson disease and amyotrophic lateral sclerosis. *Annals of neurology*, 70(6):964–973.
- [van Meel et al., 2013] van Meel, E., Wegner, D. J., Cliften, P., Willing, M. C., White, F. V., Kornfeld, S., and Cole, F. (2013). Rare recessive loss-of-function methionyl-trna synthetase mutations presenting as a multi-organ phenotype. *BMC medical genetics*, 14(1):1–10.
- [van Nues and Watkins, 2017] van Nues, R. W. and Watkins, N. J. (2017). Unusual c’/d’ motifs enable box c/d snorncps to modify multiple sites in the same rrna target region. *Nucleic acids research*, 45(4):2016–2028.
- [Vander Heiden et al., 2009] Vander Heiden, M. G., Cantley, L. C., and Thompson, C. B. (2009). Understanding the warburg effect: the metabolic requirements of cell proliferation. *science*, 324(5930):1029–1033.
- [Vasudevan et al., 2022] Vasudevan, D., Katow, H., Huang, H.-W., Tang, G., and Ryoo, H. D. (2022). A protein-trap allele reveals roles for drosophila atf4 in photoreceptor degeneration, oogenesis and wing development. *Disease Models & Mechanisms*, 15(3):dmm049119.
- [Vattem and Wek, 2004] Vattem, K. M. and Wek, R. C. (2004). Reinitiation involving upstream orfs regulates atf4 mrna translation in mammalian cells. *Proceedings of the National Academy of Sciences*, 101(31):11269–11274.
- [Veerareddygari et al., 2016] Veerareddygari, G. R., Singh, S. K., and Mueller, E. G. (2016). The pseudouridine synthases proceed through a glycol intermediate. *Journal of the American Chemical Society*, 138(25):7852–7855.
- [Vind et al., 2020] Vind, A. C., Genzor, A. V., and Bekker-Jensen, S. (2020). Ribosomal stress-surveillance: three pathways is a magic number. *Nucleic acids research*, 48(19):10648–10661.
- [Vosshall and Stocker, 2007] Vosshall, L. B. and Stocker, R. F. (2007). Molecular architecture of smell and taste in drosophila. *Annu. Rev. Neurosci.*, 30:505–533.
- [Wagner and Ofengand, 1970] Wagner, L. P. and Ofengand, J. (1970). Chemical evidence for the presence of inosinic acid in the anticodon of an arginine trna of escherichia coli. *Biochimica et Biophysica Acta (BBA)-Nucleic Acids and Protein Synthesis*, 204(2):620–623.
- [Wang et al., 2011] Wang, C.-C., Lo, J.-C., Chien, C.-T., and Huang, M.-L. (2011). Spatially controlled expression of the drosophila pseudouridine synthase RluA-1. *The International Journal of Developmental Biology*, 55(2):223–227.

- [Wang et al., 2016a] Wang, C.-W., Purkayastha, A., Jones, K. T., Thaker, S. K., and Banerjee, U. (2016a). In vivo genetic dissection of tumor growth and the warburg effect. *Elife*, 5:e18126.
- [Wang et al., 2016b] Wang, M., Liu, H., Zheng, J., Chen, B., Zhou, M., Fan, W., Wang, H., Liang, X., Zhou, X., and Eriani, G. (2016b). A deafness-and diabetes-associated trna mutation causes deficient pseudouridylation at position 55 in trnaglu and mitochondrial dysfunction. *Journal of Biological Chemistry*, 291(40):21029–21041.
- [Wang et al., 2018] Wang, X., Matuszek, Z., Huang, Y., Parisien, M., Dai, Q., Clark, W., Schwartz, M. H., and Pan, T. (2018). Queuosine modification protects cognate trnas against ribonuclease cleavage. *Rna*, 24(10):1305–1313.
- [Wang et al., 2015] Wang, X., Zhao, B. S., Roundtree, I. A., Lu, Z., Han, D., Ma, H., Weng, X., Chen, K., Shi, H., and He, C. (2015). N6-methyladenosine modulates messenger RNA translation efficiency. *Cell*, 161(6):1388–1399.
- [Wang et al., 2013] Wang, X.-R., Luo, H., Li, H.-L., Cao, L., Wang, X.-F., Yan, W., Wang, Y.-Y., Zhang, J.-X., Jiang, T., and Kang, C.-S. (2013). Overexpressed let-7a inhibits glioma cell malignancy by directly targeting k-ras, independently of pten. *Neuro-oncology*, 15(11):1491–1501.
- [Wang et al., 2014] Wang, Y., Li, Y., Toth, J. I., Petroski, M. D., Zhang, Z., and Zhao, J. C. (2014). N6-methyladenosine modification destabilizes developmental regulators in embryonic stem cells. *Nature cell biology*, 16(2):191–198.
- [Wang et al., 2020] Wang, Y., Zhang, Z., He, H., Song, J., Cui, Y., Chen, Y., Zhuang, Y., Zhang, X., Li, M., and Zhang, X. (2020). Aging-induced pseudouridine synthase 10 impairs hematopoietic stem cells. *Haematologica*.
- [Wang et al., 2022] Wang, Z.-W., Pan, J.-J., Hu, J.-F., Zhang, J.-Q., Huang, L., Huang, Y., Liao, C.-Y., Yang, C., Chen, Z.-W., and Wang, Y.-D. (2022). Srsf3-mediated regulation of n6-methyladenosine modification-related lncrna anril splicing promotes resistance of pancreatic cancer to gemcitabine. *Cell reports*, 39(6).
- [Warburg, 1925] Warburg, O. (1925). The metabolism of carcinoma cells. *The Journal of Cancer Research*, 9(1):148–163.
- [Warda et al., 2017] Warda, A. S., Kretschmer, J., Hackert, P., Lenz, C., Urlaub, H., Höbartner, C., Sloan, K. E., and Bohnsack, M. T. (2017). Human mettl16 is a n6-methyladenosine (m6a) methyltransferase that targets pre-mrnas and various non-coding rnas. *EMBO reports*, 18(11):2004–2014.
- [Watanabe et al., 2013] Watanabe, K., Miyagawa, R., Tomikawa, C., Mizuno, R., Takahashi, A., Hori, H., and Ijiri, K. (2013). Degradation of initiator trna met by xrn1/2 via its accumulation in the nucleus of heat-treated hela cells. *Nucleic acids research*, 41(8):4671–4685.
- [Watanabe and Gray, 2000] Watanabe, Y.-i. and Gray, M. W. (2000). Evolutionary appearance of genes encoding proteins associated with box h/aca snornas: cbf5p in euglena gracilis, an early diverging eukaryote, and candidate gar1p and nop10p homologs in archaeobacteria. *Nucleic acids research*, 28(12):2342–2352.

- [Wei et al., 1975] Wei, C.-M., Gershowitz, A., and Moss, B. (1975). Methylated nucleotides block 5' terminus of hela cell messenger rna. *Cell*, 4(4):379–386.
- [Wei et al., 2018] Wei, Z., Panneerdoss, S., Timilsina, S., Zhu, J., Mohammad, T. A., Lu, Z.-L., De Magalhães, J. P., Chen, Y., Rong, R., and Huang, Y. (2018). Topological characterization of human and mouse m5c epitranscriptome revealed by bisulfite sequencing. *International Journal of Genomics*, 2018.
- [Wek et al., 1995] Wek, S. A., Zhu, S., and Wek, R. C. (1995). The histidyl-trna synthetase-related sequence in the eif-2 alpha protein kinase gcn2 interacts with trna and is required for activation in response to starvation for different amino acids. *Molecular and cellular biology*.
- [Weterman et al., 2018] Weterman, M. A. J., Kuo, M., Kenter, S. B., Gordillo, S., Karjosukarso, D. W., Takase, R., Bronk, M., Oprescu, S., van Ruissen, F., and Witteveen, R. J. W. (2018). Hypermorphic and hypomorphic aars alleles in patients with cmt2n expand clinical and molecular heterogeneities. *Human Molecular Genetics*, 27(23):4036–4050.
- [Wetzel and Limbach, 2016] Wetzel, C. and Limbach, P. A. (2016). Mass spectrometry of modified rnas: recent developments. *Analyst*, 141(1):16–23.
- [Whipple et al., 2011] Whipple, J. M., Lane, E. A., Chernyakov, I., D'Silva, S., and Phizicky, E. M. (2011). The yeast rapid trna decay pathway primarily monitors the structural integrity of the acceptor and t-stems of mature trna. *Genes & development*, 25(11):1173–1184.
- [Will and Lührmann, 2011] Will, C. L. and Lührmann, R. (2011). Spliceosome structure and function. *Cold Spring Harbor perspectives in biology*, 3(7):a003707.
- [Wilusz et al., 2011] Wilusz, J. E., Whipple, J. M., Phizicky, E. M., and Sharp, P. A. (2011). trnas marked with ccacca are targeted for degradation. *Science*, 334(6057):817–821.
- [Wisniewski and Gaugaz, 2015] Wisniewski, J. R. and Gaugaz, F. Z. (2015). Fast and sensitive total protein and peptide assays for proteomic analysis. *Analytical chemistry*, 87(8):4110–4116.
- [Wohl et al., 2023] Wohl, M. P., Liu, J., and Asahina, K. (2023). Drosophila tachykininergic neurons modulate the activity of two groups of receptor-expressing neurons to regulate aggressive tone. *Journal of Neuroscience*, 43(19):3394–3420.
- [Wolffe and Matzke, 1999] Wolffe, A. P. and Matzke, M. A. (1999). Epigenetics: regulation through repression. *science*, 286(5439):481–486.
- [Worpenberg et al., 2021] Worpenberg, L., Paolantoni, C., Longhi, S., Mulorz, M. M., Lence, T., Wessels, H.-H., Dassi, E., Aiello, G., Sutandy, F. X. R., Scheibe, M., Edupuganti, R. R., Busch, A., Möckel, M. M., Vermeulen, M., Butter, F., König, J., Notarangelo, M., Ohler, U., Dieterich, C., Quattrone, A., Soldano, A., and Roignant, J.-Y. (2021). Ythdf is a n6-methyladenosine reader that modulates fmr1 target mRNA selection and restricts axonal growth in drosophila. *The EMBO Journal*, 40(4).

REFERENCES

- [Wortmann et al., 2017] Wortmann, S. B., Timal, S., Venselaar, H., Wintjes, L. T., Kopajtich, R., Feichtinger, R. G., Onnekink, C., Mühlmeister, M., Brandt, U., and Smeitink, J. A. (2017). Biallelic variants in *wars2* encoding mitochondrial tryptophanyl-trna synthase in six individuals with mitochondrial encephalopathy. *Human Mutation*, 38(12):1786–1795.
- [Wrzesinski et al., 1995a] Wrzesinski, J., Bakin, A., Nurse, K., Lane, B. G., and Ofengand, J. (1995a). Purification, cloning, and properties of the 16s rna pseudouridine 516 synthase from *escherichia coli*. *Biochemistry*, 34(27):8904–8913.
- [Wrzesinski et al., 1995b] Wrzesinski, J., Nurse, K., Bakin, A., Lane, B. G., and Ofengand, J. (1995b). A dual-specificity pseudouridine synthase: an *escherichia coli* synthase purified and cloned on the basis of its specificity for psi 746 in 23s rna is also specific for psi 32 in trna (phe). *Rna*, 1(4):437–448.
- [Wu et al., 2007] Wu, D., Yu, W., Kishikawa, H., Folkert, R. D., Iafrate, A. J., Shen, Y., Xin, W., Sims, K., and Hu, G. (2007). Angiogenin loss-of-function mutations in amyotrophic lateral sclerosis. *Annals of Neurology: Official Journal of the American Neurological Association and the Child Neurology Society*, 62(6):609–617.
- [Wu et al., 2016a] Wu, G., Adachi, H., Ge, J., Stephenson, D., Query, C. C., and Yu, Y. (2016a). Pseudouridines in u2 snrna stimulate the atpase activity of prp5 during spliceosome assembly. *The EMBO Journal*, 35(6):654–667.
- [Wu et al., 2016b] Wu, G., Radwan, M. K., Xiao, M., Adachi, H., Fan, J., and Yu, Y.-T. (2016b). The tor signaling pathway regulates starvation-induced pseudouridylation of yeast u2 snrna. *Rna*, 22(8):1146–1152.
- [Wu et al., 2011] Wu, G., Xiao, M., Yang, C., and Yu, Y. (2011). U2 snrna is inducibly pseudouridylated at novel sites by *pus7p* and *snr81 rnp*. *The EMBO journal*, 30(1):79–89.
- [Wu et al., 1999] Wu, S., Romfo, C. M., Nilsen, T. W., and Green, M. R. (1999). Functional recognition of the 3' splice site ag by the splicing factor *u2af35*. *Nature*, 402(6763):832–835.
- [Xiao et al., 2002] Xiao, S., Scott, F., Fierke, C. A., and Engelke, D. R. (2002). Eukaryotic ribonuclease p: a plurality of ribonucleoprotein enzymes. *Annual review of biochemistry*, 71(1):165–189.
- [Xiao et al., 2016] Xiao, W., Adhikari, S., Dahal, U., Chen, Y.-S., Hao, Y.-J., Sun, B.-F., Sun, H.-Y., Li, A., Ping, X.-L., and Lai, W.-Y. (2016). Nuclear m6a reader *ythdc1* regulates mrna splicing. *Molecular cell*, 61(4):507–519.
- [Xiao et al., 2022] Xiao, W., Sun, Y., Xu, J., Zhang, N., and Dong, L. (2022). uorf-mediated translational regulation of *atf4* serves as an evolutionarily conserved mechanism contributing to non-small-cell lung cancer (nsc) and stress response. *Journal of Molecular Evolution*, 90(5):375–388.
- [Xing et al., 2015] Xing, J., Yi, J., Cai, X., Tang, H., Liu, Z., Zhang, X., Martindale, J. L., Yang, X., Jiang, B., and Gorospe, M. (2015). *Nsun2* promotes cell growth via elevating cyclin-dependent kinase 1 translation. *Molecular and cellular biology*, 35(23):4043–4052.

- [Xu et al., 1999] Xu, G., Di Stefano, C., Liebich, H. M., Zhang, Y., and Lu, P. (1999). Reversed-phase high-performance liquid chromatographic investigation of urinary normal and modified nucleosides of cancer patients. *Journal of Chromatography B: Biomedical Sciences and Applications*, 732(2):307–313.
- [Yagi et al., 2012] Yagi, H., Saito, T., Yanagisawa, M., Robert, K. Y., and Kato, K. (2012). Lewis x-carrying n-glycans regulate the proliferation of mouse embryonic neural stem cells via the notch signaling pathway. *Journal of Biological Chemistry*, 287(29):24356–24364.
- [Yamasaki et al., 2009] Yamasaki, S., Ivanov, P., Hu, G.-f., and Anderson, P. (2009). Angiogenin cleaves trna and promotes stress-induced translational repression. *Journal of Cell Biology*, 185(1):35–42.
- [Yan and Zaher, 2021] Yan, L. L. and Zaher, H. S. (2021). Ribosome quality control antagonizes the activation of the integrated stress response on colliding ribosomes. *Molecular cell*, 81(3):614–628. e4.
- [Yang et al., 2005] Yang, C., McPheeters, D. S., and Yu, Y.-T. (2005). Ψ 35 in the branch site recognition region of u2 small nuclear rna is important for pre-mrna splicing in *saccharomyces cerevisiae*. *Journal of Biological Chemistry*, 280(8):6655–6662.
- [Yang et al., 2017] Yang, X., Yang, Y., Sun, B.-F., Chen, Y.-S., Xu, J.-W., Lai, W.-Y., Li, A., Wang, X., Bhattarai, D. P., and Xiao, W. (2017). 5-methylcytosine promotes mrna export-nsun2 as the methyltransferase and alyref as an m5c reader. *Cell research*, 27(5):606–625.
- [Yang et al., 2019] Yang, Y., Wang, L., Han, X., Yang, W.-L., Zhang, M., Ma, H.-L., Sun, B.-F., Li, A., Xia, J., and Chen, J. (2019). Rna 5-methylcytosine facilitates the maternal-to-zygotic transition by preventing maternal mrna decay. *Molecular cell*, 75(6):1188–1202. e11.
- [Yasukawa et al., 2000] Yasukawa, T., Suzuki, T., Suzuki, T., Ueda, T., Ohta, S., and Watanabe, K. (2000). Modification defect at anticodon wobble nucleotide of mitochondrial trnasleu (uur) with pathogenic mutations of mitochondrial myopathy, encephalopathy, lactic acidosis, and stroke-like episodes. *Journal of Biological Chemistry*, 275(6):4251–4257.
- [Yoon, 2017] Yoon, M.-S. (2017). The role of mammalian target of rapamycin (mTOR) in insulin signaling. *Nutrients*, 9(11):1176.
- [Young et al., 2005] Young, J. I., Hong, E. P., Castle, J. C., Crespo-Barreto, J., Bowman, A. B., Rose, M. F., Kang, D., Richman, R., Johnson, J. M., and Berget, S. (2005). Regulation of rna splicing by the methylation-dependent transcriptional repressor methyl-cpg binding protein 2. *Proceedings of the national academy of sciences*, 102(49):17551–17558.
- [Yu et al., 2005] Yu, B., Yang, Z., Li, J., Minakhina, S., Yang, M., Padgett, R. W., Steward, R., and Chen, X. (2005). Methylation as a crucial step in plant microRNA biogenesis. *Science*, 307(5711):932–935.
- [Yu et al., 1997a] Yu, J., Nagarajan, S., Knez, J. J., Udenfriend, S., Chen, R., and Medof, M. E. (1997a). The affected gene underlying the class k glycosylphosphatidylinositol (GPI) surface protein defect codes for the GPI transamidase. *Proceedings of the National Academy of Sciences*, 94(23):12580–12585.

REFERENCES

- [Yu et al., 2021] Yu, X., Xie, Y., Zhang, S., Song, X., Xiao, B., and Yan, Z. (2021). tRNA-derived fragments: Mechanisms underlying their regulation of gene expression and potential applications as therapeutic targets in cancers and virus infections. *Theranostics*, 11(1):461.
- [Yu et al., 1997b] Yu, Y. T., Shu, M. D., and Steitz, J. A. (1997b). A new method for detecting sites of 2'-O-methylation in RNA molecules. *Rna*, 3(3):324.
- [Yu et al., 1998] Yu, Y.-T., Shu, M.-D., and Steitz, J. A. (1998). Modifications of U2 snRNA are required for snRNP assembly and pre-mRNA splicing. *The EMBO journal*, 17(19):5783–5795.
- [Yusupov et al., 2001] Yusupov, M. M., Yusupova, G. Z., Baucom, A., Lieberman, K., Earnest, T. N., Cate, J. H. D., and Noller, H. F. (2001). Crystal structure of the ribosome at 5.5 Å resolution. *science*, 292(5518):883–896.
- [Zaganelli et al., 2017] Zaganelli, S., Rebelo-Guiomar, P., Maundrell, K., Rozanska, A., Pierredon, S., Powell, C. A., Jourdain, A. A., Hulo, N., Lightowers, R. N., and Chrzanowska-Lightowers, Z. M. (2017). The pseudouridine synthase rpusd4 is an essential component of mitochondrial RNA granules. *Journal of Biological Chemistry*, 292(11):4519–4532.
- [Zaringhalam and Papavasiliou, 2016] Zaringhalam, M. and Papavasiliou, F. N. (2016). Pseudouridylation meets next-generation sequencing. *Methods*, 107:63–72.
- [Zeharia et al., 2005] Zeharia, A., Fischel-Ghodsian, N., Casas, K., Bykhovskaya, Y., Tamari, H., Lev, D., Mimouni, M., and Lerman-Sagie, T. (2005). Mitochondrial myopathy, sideroblastic anemia, and lactic acidosis: An autosomal recessive syndrome in Persian Jews caused by a mutation in the PUS1 gene. *Journal of Child Neurology*, 20(5):449–452.
- [Zeng et al., 2012] Zeng, X.-L., Thumati, N. R., Fleisig, H. B., Hukezalie, K. R., Savage, S. A., Giri, N., Alter, B. P., and Wong, J. M. Y. (2012). The accumulation and not the specific activity of telomerase ribonucleoprotein determines telomere maintenance deficiency in X-linked dyskeratosis congenita. *Human molecular genetics*, 21(4):721–729.
- [Zerby and Patton, 1997] Zerby, D. B. and Patton, J. R. (1997). Modification of human U4 RNA requires U6 RNA and multiple pseudouridine synthases. *Nucleic acids research*, 25(23):4808–4815.
- [Zhang and Kaufman, 2004] Zhang, K. and Kaufman, R. J. (2004). Signaling the unfolded protein response from the endoplasmic reticulum. *Journal of Biological Chemistry*, 279(25):25935–25938.
- [Zhang et al., 2023] Zhang, Q., Fei, S., Zhao, Y., Liu, S., Wu, X., Lu, L., and Chen, W. (2023). PUS7 promotes the proliferation of colorectal cancer cells by directly stabilizing SIRT1 to activate the Wnt/ β -catenin pathway. *Molecular Carcinogenesis*, 62(2):160–173.
- [Zhang et al., 2016] Zhang, X., He, X., Liu, C., Liu, J., Hu, Q., Pan, T., Duan, X., Liu, B., Zhang, Y., and Chen, J. (2016). IL-4 inhibits the biogenesis of an epigenetically suppressive piwi-interacting RNA to upregulate CD1A molecules on monocytes/dendritic cells. *The Journal of Immunology*, 196(4):1591–1603.
- [Zhang et al., 2018a] Zhang, X., Yan, C., Zhan, X., Li, L., Lei, J., and Shi, Y. (2018a). Structure of the human activated spliceosome in three conformational states. *Cell research*, 28(3):307–322.

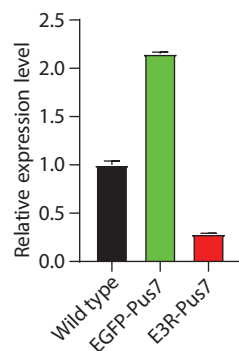
- [Zhang et al., 2018b] Zhang, Y., Zhang, X., Shi, J., Tuorto, F., Li, X., Liu, Y., Liebers, R., Zhang, L., Qu, Y., and Qian, J. (2018b). Dnmt2 mediates intergenerational transmission of paternally acquired metabolic disorders through sperm small non-coding rnas. *Nature cell biology*, 20(5):535–540.
- [Zhao et al., 2002] Zhao, X., Li, Z.-H., Terns, R. M., Terns, M. P., and Yu, Y.-T. (2002). An h/aca guide rna directs u2 pseudouridylation at two different sites in the branchpoint recognition region in xenopus oocytes. *Rna*, 8(12):1515–1525.
- [Zhao et al., 2007] Zhao, X., Patton, J. R., Ghosh, S. K., Fischel-Ghodsian, N., Shen, L., and Spanjaard, R. A. (2007). Pusp3p-and pusp1p-dependent pseudouridylation of steroid receptor rna activator controls a functional switch that regulates nuclear receptor signaling. *Molecular Endocrinology*, 21(3):686–699.
- [Zhao et al., 2014] Zhao, X., Yang, Y., Sun, B.-F., Shi, Y., Yang, X., Xiao, W., Hao, Y.-J., Ping, X.-L., Chen, Y.-S., and Wang, W.-J. (2014). Fto-dependent demethylation of n6-methyladenosine regulates mrna splicing and is required for adipogenesis. *Cell research*, 24(12):1403–1419.
- [Zhao and YI-TAO, 2004] Zhao, X. and YI-TAO, Y. U. (2004). Pseudouridines in and near the branch site recognition region of u2 snrna are required for snrnp biogenesis and pre-mrna splicing in xenopus oocytes. *Rna*, 10(4):681–690.
- [Zhao and Yu, 2004] Zhao, X. and Yu, Y.-T. (2004). Detection and quantitation of rna base modifications. *Rna*, 10(6):996–1002.
- [Zhao et al., 2018] Zhao, Y., Dunker, W., Yu, Y.-T., and Karijolich, J. (2018). The role of noncoding rna pseudouridylation in nuclear gene expression events. *Frontiers in bioengineering and biotechnology*, 6:8.
- [Zheng et al., 2013] Zheng, G., Dahl, J. A., Niu, Y., Fedorcsak, P., Huang, C.-M., Li, C. J., Vågbø, C. B., Shi, Y., Wang, W.-L., and Song, S.-H. (2013). Alkbh5 is a mammalian rna demethylase that impacts rna metabolism and mouse fertility. *Molecular cell*, 49(1):18–29.
- [Zheng et al., 2015] Zheng, G., Qin, Y., Clark, W. C., Dai, Q., Yi, C., He, C., Lambowitz, A. M., and Pan, T. (2015). Efficient and quantitative high-throughput trna sequencing. *Nature methods*, 12:835–837.
- [Zhu et al., 2020] Zhu, Z., Mesci, P., Bernatchez, J. A., Gimple, R. C., Wang, X., Schafer, S. T., Wettersten, H. I., Beck, S., Clark, A. E., and Wu, Q. (2020). Zika virus targets glioblastoma stem cells through a sox2-integrin $\alpha\beta 5$ axis. *Cell stem cell*, 26(2):187–204. e10.
- [Zinsser, 1910] Zinsser, F. (1910). Atrophia cutis reticularis cum pigmentatione dystrophia unguium et leukoplakia oris. *Ikonogr Dermat Kioto*, 5:219–223.
- [Zong et al., 2021] Zong, T., Yang, Y., Zhao, H., Li, L., Liu, M., Fu, X., Tang, G., Zhou, H., Aung, L. H. H., and Li, P. (2021). tsrnas: Novel small molecules from cell function and regulatory mechanism to therapeutic targets. *Cell proliferation*, 54(3):e12977.
- [Zuko et al., 2021] Zuko, A., Mallik, M., Thompson, R., Spaulding, E. L., Wienand, A. R., Been, M., Tadenev, A. L. D., van Bakel, N., Sijlmans, C., and Santos, L. A. (2021). trna overexpression rescues peripheral neuropathy caused by mutations in trna synthetase. *Science*, 373(6559):1161–1166.

REFERENCES

[Zwarts et al., 2011] Zwarts, L., Magwire, M. M., Carbone, M. A., Versteven, M., Herteleer, L., Anholt, R. R. H., Callaerts, P., and Mackay, T. F. C. (2011). Complex genetic architecture of drosophila aggressive behavior. *Proceedings of the National Academy of Sciences*, 108(41):17070–17075.

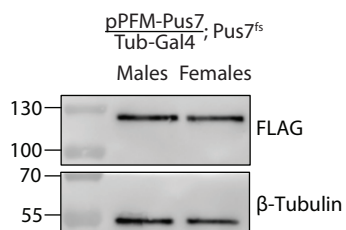
[Zwarts et al., 2012] Zwarts, L., Versteven, M., and Callaerts, P. (2012). Genetics and neurobiology of aggression in drosophila. *Fly*, 6(1):35–48.

SUPPLEMENTARIES

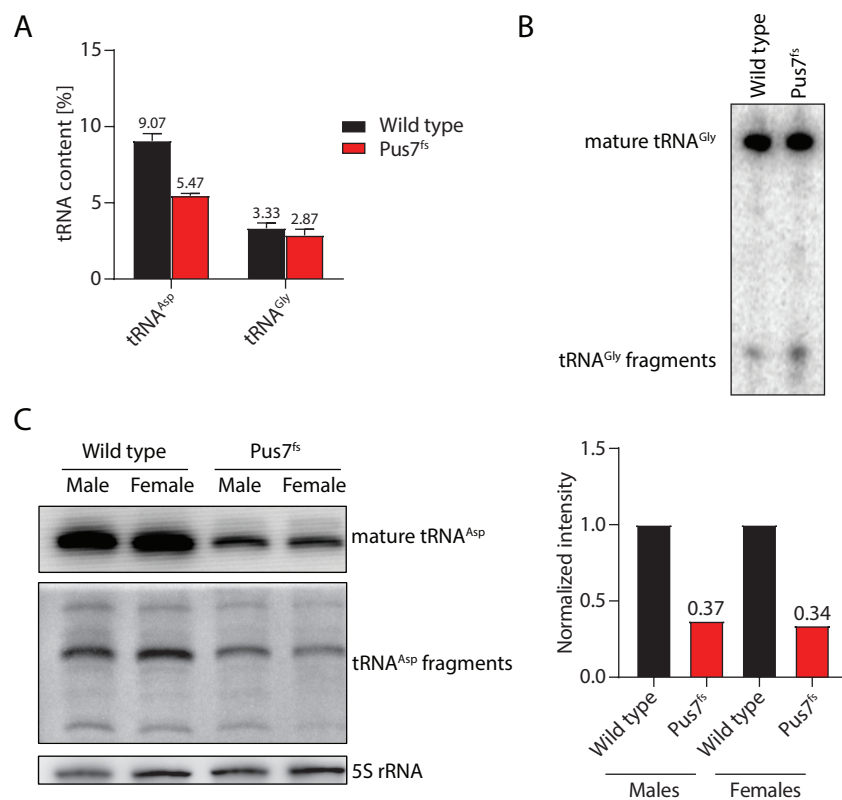


Supplementary Figure S.1: *Pus7* expression is affected in *EGFP-Pus7* and *E3R-Pus7* flies. *Pus7* mRNA levels were quantified by RT-qPCR.

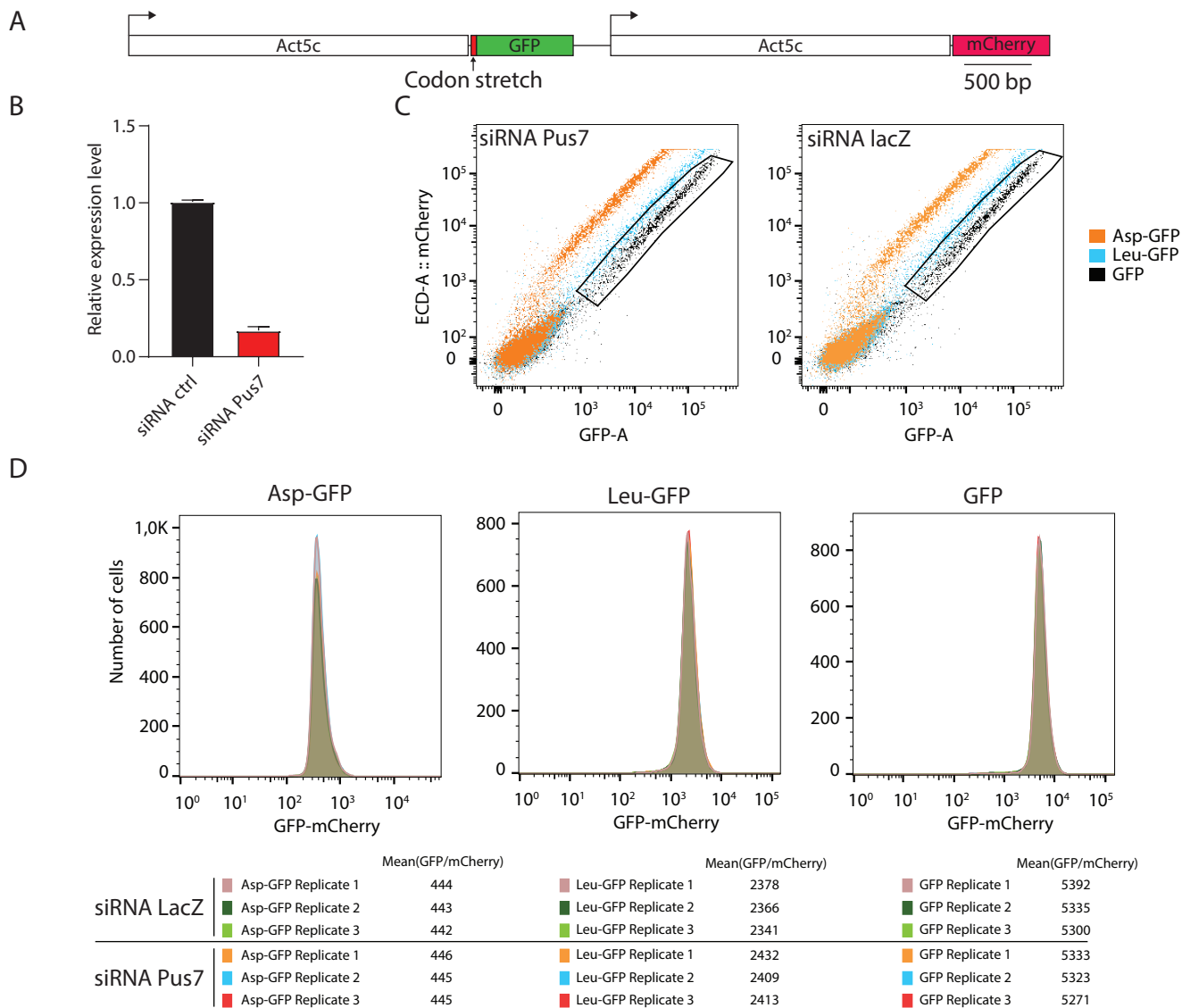
A



Supplementary Figure S.2: Expression analysis of transgenic Flag-Myc-Pus7 in the *Pus7^{fs}* background by western blot. The molecular size is displayed in kDa. β -Tubulin served as loading control.

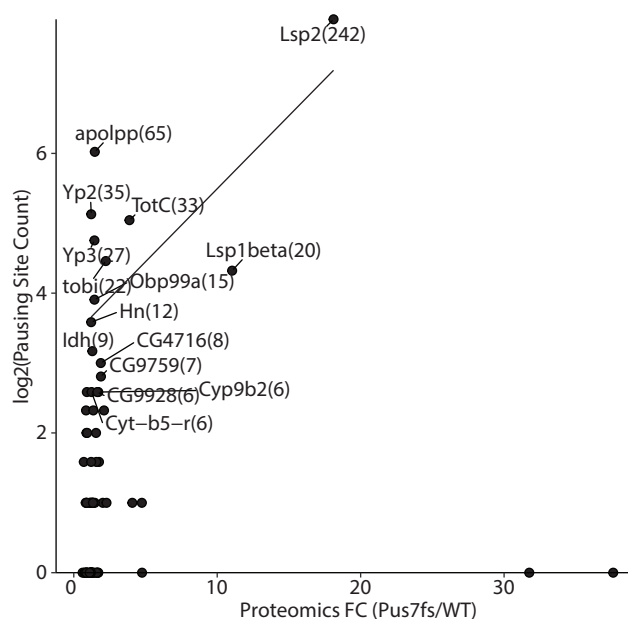


Supplementary Figure S.3: tRNA^{Asp} is systemically downregulated in *Pus7^{fs}* males and females. (A) tRNA^{Asp} and tRNA^{Gly} content in whole flies according to MST. Error bars represent SD of three technical replicates. (B) Northern blot using a probe targeting tRNA^{Gly}. (C) Northern blot and quantification of mature tRNA^{Asp} and tRNA^{Asp} fragments normalized to 5S rRNA.



Supplementary Figure S.4: *Pus7* knockdown in S2R+ cells is not sufficient to trigger translational defects. (A) Schematic of the dual reporter system. The codon stretch represents the stretch of extra codons integrated in the Asp-GFP or Leu-GFP plasmids. (B) Knockdown efficiency of *Pus7* siRNA in S2R+ cells measured by RT-qPCR. (C) Scatterplot with GFP and mCherry intensities of sorted S2R+ cells after knockdown of *Pus7* and transfection with the reporter system. (D). Overlap of GFP/mCherry intensities of all sorted cells in the different samples. Three technical replicates were performed per condition.

A



Supplementary Figure S.5: Genes with ribosome pausing sites show higher protein levels in *Pus7^{fs}*. Genes with significant changes on the protein level are plotted with their amount of ribosome pausing sites indicated in brackets. The regression curve represents upregulated proteins with at least five pausing sites in *Pus7^{fs}*.

Supplementary Table S.1: Proteins in relevant pathways mentioned in this study. Sign.: Significantly dysregulated proteins are marked with a "+". FC: Fold change of *Pus7^{fs}*/WT

FlyBase ID	Gene name	Enzyme / Complex	Pathway	Sign.	FC
FBgn0003748	Treh	Trehalase	Other	+	0.82
FBgn0001186	Hex-A	Hexokinase	Glycolysis		0.96
FBgn0001187	Hex-C	Hexokinase	Glycolysis	+	1.27
FBgn0003074	Pgi	Glocose-6-phosphate isomerase	Glycolysis		1.08
FBgn0003071	Pfk	Phosphofructokinase	Glycolysis		0.92
FBgn0000064	Ald1	Fructose-bisphosphate aldolase	Glycolysis	+	1.1
FBgn0086355	Tpi	Triosephosphate isomerase	Glycolysis	+	1.12
FBgn0001091	Gapdh1	Glyceraldehyde-3-phosphatase dehydrogenase	Glycolysis		0.98
FBgn0001092	Gapdh2	Glyceraldehyde-3-phosphatase dehydrogenase	Glycolysis		0.98
FBgn0250906	Pgk	Phosphoglycerate kinase	Glycolysis	+	1.1
FBgn0023517	Pgam5	Phosphoglycerate mutase	Glycolysis		0.93
FBgn0014869	Pglym78	Phosphoglycerate mutase	Glycolysis		1.08
FBgn0000579	Eno	Enolase	Glycolysis		1.06
FBgn0267385	PyK	Pyruvate kinase	Glycolysis		0.96
FBgn0001258	Ldh	Lactate dehydrogenase	Other	+	1.57
FBgn0027580	PCB	Pyruvate carboxylase	Glycolysis / TCA		1.02
FBgn0028325	Pdha	Pyruvate dehydrogenase	TCA		0.98
FBgn0039635	Pdhb	Pyruvate dehydrogenase	TCA		0.97
FBgn0283658	muc	Pyruvate dehydrogenase	TCA	+	0.91
FBgn0029958	Pdp	Pyruvate dehydrogenase phosphatase	Glycolysis / TCA		0.92
FBgn0010100	mAcon1	Aconitate hydratase	TCA		0.96
FBgn0001248	Idh	Isocitrate dehydrogenase	TCA	+	1.29
FBgn0027291	Idh3a	Isocitrate dehydrogenase	TCA		0.94
FBgn0038922	Idh3b	Isocitrate dehydrogenase	TCA		0.98
FBgn0039358	CG5028	Isocitrate dehydrogenase (Idh3g)	TCA		0.96
FBgn0010352	Nc73EF	α -KG dehydrogenase complex	TCA		0.97
FBgn0037891	CG5214	α -KG dehydrogenase complex	TCA		0.91
FBgn0036762	CG7430	α -KG dehydrogenase complex	TCA		1.03
FBgn0030612	CG5599	α -KG dehydrogenase complex regulator	TCA		0.92

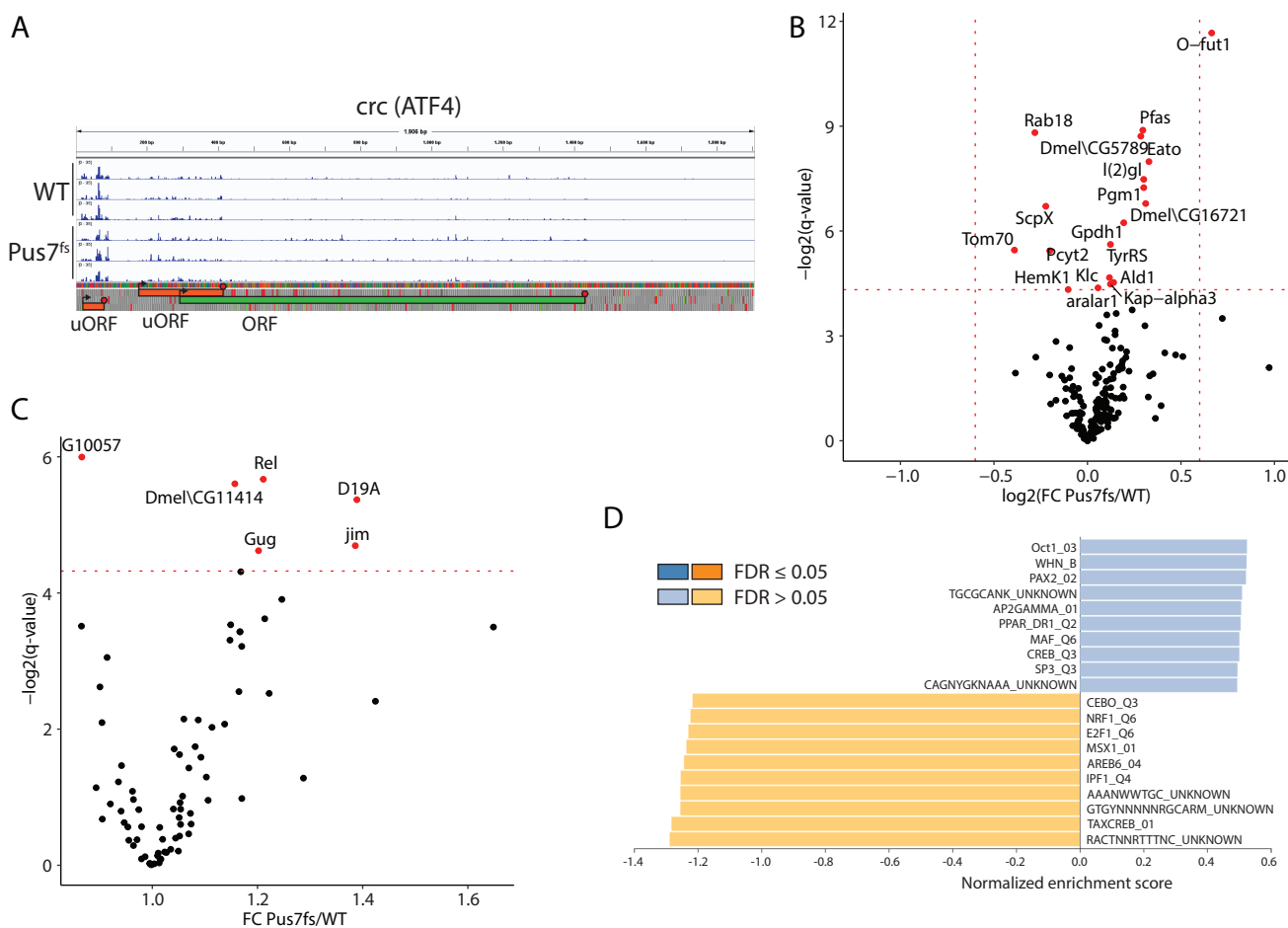
Continued on next page

Supplementary Table S.1 – continued from previous page					
FlyBase ID	Gene name	Enzyme / Complex	Pathway	Sign.	FC
FBgn0004888	Scsalpha1	Succinyl-CoA synthetase	TCA		1.02
FBgn0037643	ScsbetaA	Succinyl-CoA synthetase	TCA	+	0.91
FBgn0029118	ScsbetaG	Succinyl-CoA synthetase	TCA		0.96
FBgn0261439	SdhA	Succinate dehydrogenase	TCA		0.99
FBgn0014028	SdhB	Succinate dehydrogenase	TCA		0.98
FBgn0037873	SdhC	Succinate dehydrogenase	TCA		1.02
FBgn0286222	Fum1	Fumarase	TCA		1.01
FBgn0262559	Mdh2	Malate dehydrogenase	TCA		0.95
FBgn0034356	Pepck2	Phosphoenolpyruvate carboxylase	Glycolysis / TCA	+	1.46
FBgn0261955	kdn	Citrate synthase	TCA	+	0.9
FBgn0263199	Galk	Galactokinase	Leloir pathway	+	1.1
FBgn0263200	Galt	Galactose-1-phosphate uridylyltransferase	Leloir pathway	+	1.39
FBgn0035147	Gale	UDP-galactose 4'-epimerase	Leloir pathway	+	1.16
FBgn0004507	GlyP	Glycogen phosphorylase	Leloir pathway	+	1.19
FBgn0004057	Zw	Glucose-6-phosphate dehydrogenase (G6PD)	PPP	+	1.19
FBgn0030239	CG17333	6-phosphogluconolactonase (PGLS)	PPP		1.02
FBgn0050410	Rpi	Ribose-5-phosphate isomerase (Rpi)	PPP	+	1.12
FBgn0037607	CG8036	Transketolase	PPP		1.14
FBgn0038795	CG4335	Trimethyllysine hydroxylase	Carnitine biosynthesis	+	1.48
FBgn0029823	Shmt	Serine hydroxymethyl transferase	Carnitine biosynthesis	+	1.22
FBgn0039094	CG10184	potential gamma-BBH ortholog	Carnitine biosynthesis	+	1.34
FBgn0012036	Aldh	Aldehyde dehydrogenase	Carnitine biosynthesis		1.1
FBgn0014903	CG14630	potential gamma-BBH ortholog	Carnitine biosynthesis	+	1.22
FBgn0030575	CG5321	potential gamma-BBH ortholog	Carnitine biosynthesis		0.96
FBgn0039543	CROT	Carnitine O-octanoyltransferase	Acyl-Carnitine metabolism	+	0.66
FBgn0261862	whd	Carnitine palmitoyltransferase 1	Acyl-Carnitine metabolism	+	1.48
FBgn0019830	colt	Carnitine Acyl-Carnitine Translocase	Acyl-Carnitine metabolism		0.99
FBgn0035383	CPT2	Carnitine palmitoyltransferase 2	Acyl-Carnitine metabolism		1.02
FBgn0037440	CRAT	Carnitine O-Acetyl-Transferase	Acyl-Carnitine metabolism	+	0.88
FBgn0263120	Acs1	6.2.1.3 KEGG	Fatty acid degradation	+	0.82
FBgn0027572	CG5009	1.3.3.6 KEGG	Fatty acid degradation	+	0.78
FBgn0029969	CG10932	2.3.1.9 KEGG	Fatty acid degradation	+	0.56
FBgn0032161	CG4594	5.3.3.8 KEGG	Fatty acid degradation	+	0.5
FBgn0032775	CG17544	1.3.3.6 KEGG	Fatty acid degradation	+	0.78
FBgn0035203	CG9149	2.3.1.9 KEGG	Fatty acid degradation	+	0.67
FBgn0036824	CG3902	1.3.8.5 KEGG	Fatty acid degradation	+	1.11
FBgn0035811	Mcad	1.3.8.7 KEGG	Fatty acid degradation	+	1.15
FBgn0028479	Mtpalpha	1.1.1.211, 1.1.1.35, 4.2.1.17 KEGG	Fatty acid degradation		0.99
FBgn0025352	Mtpbeta	-	Fatty acid degradation		1.01
FBgn0021765	scu	1.1.1.201, 1.1.1.239, 1.1.1.36, 1.1.1.62 KEGG	Fatty acid degradation		0.99
FBgn0040064	yip2	2.3.1.9 KEGG	Fatty acid degradation	+	1.16
FBgn0035024	CG11414		RQC	+	1.16

We analyzed the protein levels of all predicted TFs in *Drosophila* according to [Hens et al., 2011]. Among 777 predicted TFs, 100 were identified in our mass-spec data with six TFs passing the threshold of FRD ≤ 0.05 (Supplementary figure S.6C). Among those, D19A and jim were upregulated by approximately 40% upon mutation of Pus7. Interestingly, D19A contains Oct1 transcription factor binding sites in its promoter (www.gsea-msigdb.org/gsea/msigdb/cards/OCT1_03) and has itself been proposed as a TF that is maternally deposited. Based on its expression pattern, it might play a role in early embryogenesis and germline cell fate [Jullien, 1998]. jim features high expression levels in the larval CNS (<http://flybase.org/reports/FBgn0027339>) and has been identified as a factor regulating dendrite morphogenesis [Iyer et al., 2013]. G11057 (CG31510) is the only downregulated TF passing the FDR threshold and reduced in abundance by approximately 20%. Like jim and

D19A, its exact targets and function are unknown.

Further, we attempted to identify other transcription factors that might explain the dysregulated proteome in an unbiased manner. Thus, we performed a gene set enrichment analysis (GSEA) to identify targets of transcription factors among all significantly dysregulated proteins upon *Pus7* mutation. The top candidates included Oct1-like transcription factor binding sites (Supplementary figure S.6D). Unfortunately, none of the TF binding sites passed the threshold of the $FDR \leq 0.05$ suggesting that there is no specific transcription factor regulating the genes affected in *Pus7^{fs}* flies.



Supplementary Figure S.6: Potential causes for translational changes in *Pus7^{fs}* flies. (A) Ribosome profiling tracks of *crc* (ATF4). Orange: Regulatory uORFs. Green: *crc* ORF. Arrows: ATGs. Polygons: Stop codons. (B) Protein levels of *Drosophila* dFoxo transcription factor targets. q-value cutoff: 0.05. FC cutoff: $\pm 50\%$. (C) Protein levels of predicted *Drosophila* transcription factors. q-value cutoff: 0.05 (D) Gene set enrichment analysis for transcription factor binding sites around transcription start sites of significantly dysregulated proteins in *Pus7^{fs}*.

Supplementary Table S.2: Dysregulated metabolites in *Pus7^{fs}* flies. FC: Fold change of *Pus7^{fs}*/WT.

Metabolite	p-ValueAdj	FC
Oxalate	0.02	2.61
N,N,N-Trimethyllysine	7.27E-06	2.22
N-Acetylneuraminic acid	1.86E-03	2.08
Phosphoenolpyruvate	5.20E-05	2.04
Stachyose	8.82E-05	2.03
2-Oxobutanoate	1.49E-03	1.99

Continued on next page

Supplementary Table S.2 – continued from previous page

Metabolite	p-ValueAdj	FC
Atp	1.79E-04	1.98
Cytidine 2',3'-Cyclic Phosphate	2.22E-03	1.87
Orotate	3.16E-04	1.74
Oxoproline	2.98E-04	1.73
Uridine 5'-Diphosphate	8.82E-05	1.73
Lactate	6.85E-04	1.72
Uridine Diphosphate-N-Acetylhexosamine	2.09E-03	1.69
Fructose 1,6-Bisphosphate	2.22E-03	1.66
2-Phosphoglycerate/3-Phosphoglycerate	1.32E-04	1.66
Pyruvate	2.45E-03	1.64
Xanthosine	2.09E-03	1.64
Hydroxyphenyllactate	3.80E-03	1.63
Malonate	5.47E-03	1.57
Glycerol 3-Phosphate	2.19E-03	1.57
Uridine Diphosphate Glucuronic Acid	1.32E-03	1.55
Xanthosine-Monophosphate	0.23	1.55
Deoxyribose	1.63E-03	1.53
Pyridoxal	2.65E-03	1.51
Glucose 6-Phosphate	1.04E-03	1.51
Carnosine	7.30E-04	1.50
4-Imidazoleacetate	0.04	1.48
Xanthine	0.02	1.48
Fructose 6-Phosphate	3.80E-03	1.45
Histidine	6.85E-05	1.41
Adipate	2.03E-03	1.39
Allantoin	0.23	1.38
Tryptamine	0.03	1.37
Ophthalmate	3.80E-03	1.37
Asparagine	7.30E-04	1.37
Glycine	3.40E-04	1.37
N-Acetylputrescine	0.08	1.36
P-Hydroxyphenylacetate	0.02	1.36
Sedoheptulose-7-Phosphate	0.01	1.36
1-Methylhistidine	8.82E-05	1.36
Serine	8.45E-05	1.34
Homogentisate	0.07	1.33
Thiamine	0.01	1.31
N-Acetylalanine	0.03	1.30
Glyceraldehyde 3-Phosphate	0.03	1.30
Guanidinosuccinate	4.38E-03	1.29
S-Adenosylmethionine	3.80E-03	1.29
Citrulline	0.01	1.28
Beta-Alanine/Sarcosine	6.60E-04	1.28
Putrescine	0.01	1.28
2-Aminoisobutyrate	3.05E-03	1.27
Methionine	1.47E-04	1.27
3-(4-Hydroxyphenyl)Pyruvate	0.13	1.26
Uridine	7.99E-04	1.26
Myristoylcarnitine (Tetradecanoylcarnitine)	0.14	1.25
Biotin	0.36	1.24
3-Hydroxyphenylacetate	0.33	1.23
N-Acetylleucine	1.42E-03	1.23
Ureidopropionate	0.16	1.22
Cystathionine	0.03	1.21
Cytosine	0.16	1.20
Ribose 5-Phosphate	0.03	1.19
Creatine	0.13	1.18
Uracil	0.11	1.17
Guanosine Diphosphate Mannose	0.38	1.17

Continued on next page

Supplementary Table S.2 – continued from previous page

Metabolite	p-ValueAdj	FC
Nicotinamide	0.36	1.17
Glutathione Oxidized	0.12	1.17
Uridine Monophosphate	0.36	1.16
Acetyl-Coa	0.41	1.16
Nicotinic Acid Adenine Dinucleotide Phosphate	0.02	1.16
Riboflavin	0.08	1.15
N-Methylaspartate	0.12	1.12
Cystine	0.61	1.11
Methylthioadenosine	0.30	1.10
Nadp	0.05	1.10
Tryptophan	0.05	1.10
Glycerol	0.33	1.10
2-Hydroxyglutaric Acid	0.24	1.10
6-Hydroxynicotinate	0.84	1.10
1-Methyladenosine	0.22	1.10
Alpha-Ketoglutarate	0.40	1.10
Tryptophanamide	0.57	1.09
Adp	0.31	1.09
Acetylcarnitine	0.04	1.08
Alanine	0.12	1.07
Melatonin	0.83	1.06
Ribulose 1,5-Bisphosphate	0.91	1.06
Deoxycarnitine	0.74	1.06
S-Adenosylhomocysteine	0.42	1.06
4-Guanidinobutanoate	0.62	1.05
Uridine Diphosphate Hexose	0.62	1.05
Arginine	0.28	1.05
Urate	0.54	1.05
Glutamine	0.58	1.04
Histamine	0.34	1.04
Tyrosine	0.89	1.03
Dimethylglycine	0.61	1.03
Hexose Including Alpha-Glucose	0.77	1.03
N-Formylmethionine	0.72	1.03
Deoxyadenosine	0.80	1.03
5-Hydroxyindoleacetate	0.77	1.02
Isovalerylcarnitine	0.94	1.02
2-Hydroxybutyrate	0.91	1.02
Dimethylarginine (Sdma/Adma)	0.83	1.02
Gamma-Aminobutyrate	0.81	1.01
Galactarate	0.94	1.01
4-Acetamidobutanoate	0.98	1.00
Nicotinate	0.91	1.00
Ethanolamine	0.97	1.00
Malate	0.99	0.99
Stearoylcarnitine	0.73	0.99
Salicylate	0.83	0.98
Proline	0.58	0.98
Acetylcholine	0.95	0.98
Trimethylamine	0.13	0.98
Choline	0.11	0.98
N-Acetylphenylalanine	0.71	0.97
6-Hydroxymelatonin	0.66	0.96
Camp	0.47	0.94
Guanosine Monophosphate	0.42	0.94
Fad	0.30	0.94
Valine	0.25	0.94
Carnitine	0.28	0.93
Betaine	0.25	0.93

Continued on next page

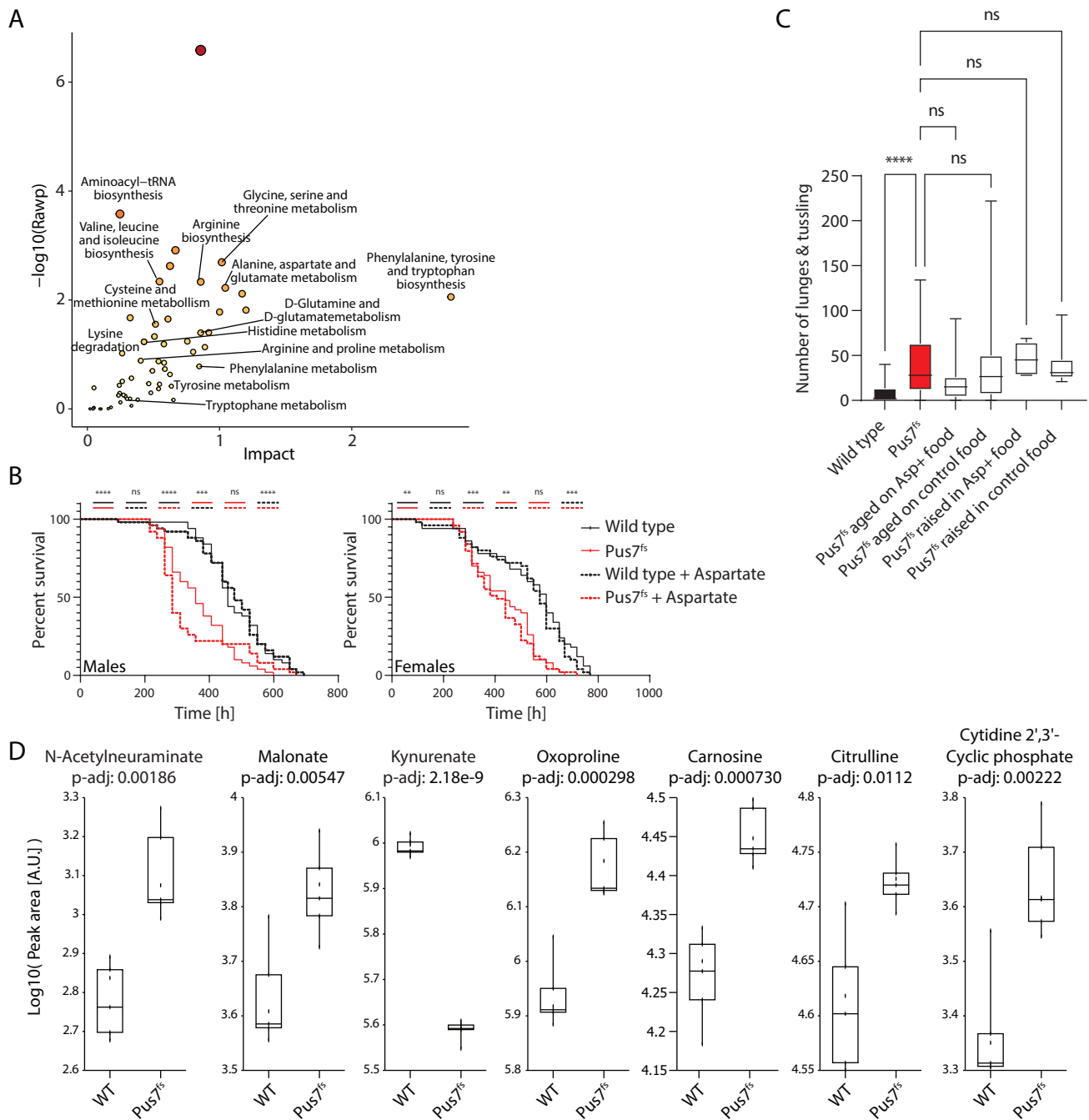
Supplementary Table S.2 – continued from previous page

Metabolite	p-ValueAdj	FC
Tartarate	0.48	0.93
Glucosaminat	0.77	0.92
5'-Deoxyadenosine	0.33	0.91
Propioylcarnitine	0.39	0.91
P-Octopamine	0.67	0.90
3-Dehydroshikimate	0.43	0.90
Xanthurenate	4.08E-03	0.89
Nad	0.09	0.89
Citrate	7.30E-04	0.89
Glutamate	0.08	0.88
4-Hydroxybenzoate	0.40	0.88
Cytidine	0.19	0.88
Lysine	0.13	0.88
Hypoxanthine	0.94	0.88
Citicoline	0.19	0.87
Isocitrate	0.06	0.87
Gluconate	0.20	0.87
Dopa	0.35	0.87
Adenosine 2',3'-Cyclic Phosphate/Adenosine 3',5'-Cyclic Phosphate	0.37	0.87
Palmitoylcarnitine	0.04	0.87
Succinate	0.01	0.86
N-Acetylglutamate	0.13	0.86
Urocanate	0.28	0.86
Taurine	0.01	0.86
N-Acetylaspartate	5.78E-03	0.86
Dethiobiotin	0.16	0.85
Isoleucine	0.03	0.85
Guanosine	0.11	0.85
Inosine Monophosphate	0.16	0.84
Adenosine 3',5'-Cyclic Phosphate	0.07	0.84
N-Methylglutamate	0.05	0.84
Hydroxykynurenine	2.91E-03	0.84
Cdp-Ethanolamine	0.08	0.83
Trigonelline	0.04	0.83
Amp	0.02	0.83
Phenylalanine	0.04	0.82
3-Methoxytyramine	7.74E-03	0.81
Suberate	0.16	0.81
Deoxyguanosine	3.08E-03	0.79
Glycerate	0.04	0.78
N-Acetylproline	0.09	0.78
Cis-Aconitate	1.04E-03	0.78
N-Alpha-Acetyllysine	0.01	0.77
3-(2-Hydroxyphenyl)Propanoate	0.14	0.76
Histidinol	0.02	0.76
Gluconolactone	0.19	0.75
Oxaloacetate	0.02	0.74
Kynurenine	0.01	0.74
Leucine	2.04E-03	0.74
Guanine	0.01	0.73
Pantothenate	1.79E-04	0.72
Butyrylcarnitine	9.80E-03	0.71
Ethylmalonate	0.01	0.71
Glutarate	0.12	0.69
Epinephrine	0.08	0.68
Phosphoserine	1.31E-03	0.66
Pipecolate	6.60E-04	0.66
Lauroylcarnitine	7.11E-03	0.66
Threonine	3.43E-04	0.66

Continued on next page

Supplementary Table S.2 – continued from previous page

Metabolite	p-ValueAdj	FC
Homoserine	0.03	0.62
Aspartate	6.31E-03	0.61
1-Aminocyclopropanecarboxylate	1.29E-04	0.60
Inosine	5.98E-04	0.59
4-Hydroxy-Proline	0.04	0.57
1-Methylnicotinamide	0.35	0.54
Glutaryl carnitine	0.01	0.53
Decanoyl carnitine	7.06E-04	0.51
Hexanoyl carnitine	7.16E-05	0.42
Kynurenate	2.18E-09	0.40
Adenosine	2.90E-05	0.26



Supplementary Figure S.7: Amino acids including aspartate are dysregulated in *Pus7^{fs}* flies. (A) Joint-pathway analysis combining the proteomics and metabolomics datasets revealed pathways related to amino acid synthesis and processing to be dysregulated in *Pus7^{fs}* flies. (B) Lifespan assay with *Pus7^{fs}* flies on 5% sucrose solution supplemented with or without aspartate. (C) Aggression assay with *Pus7^{fs}* flies either aged on or raised in and aged on food supplemented with or without aspartate. (D) Multiple metabolites with implications in neuronal disease in human are dysregulated in *Pus7^{fs}* flies.

Supplementary Table S.3: Protein levels of genes involved in the UPR, JNK, ISR and RQC. Proteins significantly changed on the protein level are marked in bold. ND: not detected.

Pathway	FlyBase ID	Gene symbol	FC (<i>Pus7^{fs}</i> /WT)
UPR, mt. UPR	FBgn0015245	Hsp60A	0.98
UPR, mt. UPR	FBgn0026761	Trap1	0.98

Continued on next page

Supplementary Table S.3 – continued from previous page

Pathway	FlyBase ID	Gene symbol	FC (Pus7 ^{fs} /WT)
UPR	FBgn0261984	Ire1	2.04
UPR	FBgn0037327	PEK	1.43
UPR	FBgn0031260	Spp	1.33
ERAD, UPR	FBgn0035593	CG4603	1.02
ERAD, UPR	FBgn0032398	CG6766	0.99
ERAD, UPR	FBgn0023511	Edem1	1.09
ERAD, UPR	FBgn0032480	Edem2	1.01
ERAD, UPR	FBgn0001218	Hsc70-3	1.02
ERAD	FBgn0259170	alpha-Man-Ia	1.05
ERAD	FBgn0039634	alpha-Man-Ib	1.02
ERAD	FBgn0005585	Calr	0.99
ERAD	FBgn0034068	casp	1.02
ERAD	FBgn0028467	CG11070	1.02
ERAD	FBgn0052640	CG32640	1.32
ERAD	FBgn0035793	CG7546	0.93
ERAD	FBgn0027554	CG8042	1.09
ERAD	FBgn0034071	CG8405	1.09
ERAD	FBgn0033698	CG8858	0.97
ERAD	FBgn0032467	CG9934	1.06
ERAD	FBgn0015622	Cnx99A	1.04
ERAD	FBgn0025608	Faf2	0.94
ERAD	FBgn0039562	Gp93	1.06
ERAD	FBgn0028475	Hrd3	0.97
ERAD	FBgn0028685	Rpt4	0.96
ERAD	FBgn0286784	TER94	0.99
ERAD	FBgn0267384	Ubc7	1.11
ERAD	FBgn0036136	Ufd1-like	1.13
ERAD	FBgn0014075	Uggt	1.01
JNK	FBgn0010909	msn	1.03
JNK	FBgn0000229	bsk	0.92
JNK	FBgn0010333	Rac1	1.02
JNK	FBgn0000499	dsh	0.99
JNK	FBgn0032006	Pvr	0.96
JNK	FBgn0010380	AP-1-2 β	0.89
JNK	FBgn0024833	AP-1 μ	0.99
JNK	FBgn0030089	AP-1 γ	0.97
ISR	FBgn0000370	crc (ATF4)	ND
RQC	FBgn0035024	CG11414 (ZNF598)	1.16